VOL. 22 NO. 1 JULY 1969
PUBLISHED MONTHLY

of 94

JOURNAL OF ELECTROANALYTICAL CHEMISTRY

AND INTERFACIAL ELECTROCHEMISTRY

International Journal devoted to all Aspects of Electroanalytical Chemistry, Double Layer Studies, Electrokinetics, Colloid Stability, and Electrode Kinetics.

ELSEVIER

GENERAL INFORMATION

Types of contributions

(a) Original research work not previously published in other periodicals.
(b) Reviews on recent developments in various fields.
(c) Short communications.
(d) Preliminary notes.

Languages

Papers will be published in English, French or German.

Submission of papers

Papers should be sent to one of the following Editors:
Professor J. O'M. Bockris, John Harrison Laboratory of Chemistry, University of Pennsylvania, Philadelphia 4, Pa. 19104, U.S.A.
Dr. R. H. Ottewill, Department of Chemistry, The University, Bristol 8, England.
Dr. R. Parsons, Department of Chemistry, The University, Bristol 8, England.
Professor C. N. Reilley, Department of Chemistry, University of North Carolina, Chapel Hill, N.C. 27515, U.S.A.

Authors should preferably submit two copies in double-spaced typing on pages of uniform size. Legends for figures should be typed on a separate page. The figures should be in a form suitable for reproduction, drawn in Indian ink on drawing paper or tracing paper, with lettering etc. in thin pencil. The sheets of drawing or tracing paper should preferably be of the same dimensions as those on which the article is typed. Photographs should be submitted as clear black and white prints on glossy paper. Standard symbols should be used in line drawings, the following are available to the printers:

All references should be given at the end of the paper. They should be numbered and the numbers should appear in the text at the appropriate places.
A summary of 50 to 200 words should be included.

Reprints

Fifty reprints will be supplied free of charge. Additional reprints (minimum 100) can be ordered at quoted prices. They must be ordered on order forms which are sent together with the proofs.

Publication

The *Journal of Electroanalytical Chemistry and Interfacial Electrochemistry* appears monthly. For 1969, each volume has 3 issues and 4 volumes will appear.
Subscription price: Sfr. 316.— (U.S. $ 74.60) per year incl. postage. Additional cost for copies by air mail available on request. For subscribers in the U.S.A. and Canada, 2nd class postage paid at Jamaica, N.Y. For advertising rates apply to the publishers.

Subscriptions

Subscriptions should be sent to:

ELSEVIER SEQUOIA S.A., P.O. Box 851, 1001 Lausanne 1, Switzerland

JOURNAL OF ELECTROANALYTICAL CHEMISTRY AND INTERFACIAL ELECTROCHEMISTRY

VOL. 22 (1969)

JOURNAL
of
ELECTROANALYTICAL CHEMISTRY
and
INTERFACIAL ELECTROCHEMISTRY

AN INTERNATIONAL JOURNAL DEVOTED TO ALL ASPECTS OF ELECTROANALYTICAL CHEMISTRY, DOUBLE LAYER STUDIES, ELECTROKINETICS, COLLOID STABILITY AND ELECTRODE KINETICS

VOL. 22 1969

ELSEVIER SEQUOIA S.A.

LAUSANNE

PRINTED IN THE NETHERLANDS

ELECTROANALYTICAL CHEMISTRY AND INTERFACIAL ELECTROCHEMISTRY
Elsevier Sequoia S.A., Lausanne – Printed in The Netherlands

THE ELECTRICAL DOUBLE LAYER ON SILICA IN THE PRESENCE OF BIVALENT COUNTER-IONS

TH. F. TADROS AND J. LYKLEMA
Laboratory for Physical and Colloid Chemistry, Agricultural University, Wageningen (The Netherlands)
(Received October 12th, 1968)

A comparison of double layers on oxidic substances with those on relatively "simple" systems, such as mercury or silver iodide, has revealed a number of striking differences[1,2]. Probably the most important difference is the high surface charge density on oxides[3-7], especially when they are porous. The most recent data[1] on a porous silica sample showed that at high pH and high salt content, the specific surface charge density can reach values beyond the surface density of dissociated silanol groups. Notwithstanding the considerable surface charge, the electrokinetic potentials of silica are not particularly high[8,9], neither are silica sols extremely stable[10]. These facts could be accounted for by postulating cation and OH^- penetration into the sub-surface structure of the porous oxide. The extent of penetration depends upon the nature, valence and concentration of the counter-ion and on the porosity of the surface. A quantitative theory has been developed[2].

These ideas on the double-layer structure on porous surfaces were developed mainly on the basis of studies of the interface between porous silica and solutions containing monovalent counter-ions. The work is now extended to bivalent counter ions (Mg^{2+}, Ca^{2+}, Sr^{2+} and Ba^{2+}). At a given ion-size and specific adsorption potential, the theory predicts an increase in surface charge with counter-ion valency. A second factor is that cations such as Mg^{2+}, Ca^{2+}, Sr^{2+} and Ba^{2+} tend to be chemisorbed on silica[11]. Finally, a study of this type could throw some light onto the reasons for the poor response of glass electrodes to bivalent ions, in contrast to their satisfactory response to H^+ or monovalent cations[12].

EXPERIMENTAL

Materials

The silica sample is the same (precipitated B.D.H.) as described in the previous study[1] with particles of diameter between 500 and 1000 Å and a BET nitrogen surface area of 56 m^2/g. A *t*-plot according to de Boer *et al.*[13] indicated the presence of pores with an average radius below 20 Å and an outer surface of about 40 m^2/g. The value for the outer surface was confirmed to within 10% by negative adsorption.

Alkaline-earth chlorides were of AnalaR grade and were used without further purification. Standard solutions were checked gravimetrically. Distilled water was boiled to expel CO_2.

The point of zero charge (p.z.c.)

In order to obtain absolute surface charge (σ_0) *vs.* pH curves, the point of

zero charge should be known. The precise value accepted for the p.z.c. of the silica system is not critical for the calculated surface charge density, since around the p.z.c. the isotherms are almost horizontal. In the previous study[1] with monovalent counter-ions, pH 3 was accepted as the p.z.c. for all cations from the point of intersection of the adsorption isotherms in 10^{-2} and 10^{-1} N KCl. However, in the presence of bivalent salts the intersection points are indistinct and make it difficult to determine the exact location of the p.z.c. Gaudin and Fuerstenau[14] observed a point of zero zeta-potential at pH 4 for quartz in 10^{-1} N $Ba(NO_3)_2$ solution. However, the iso-electric point does not necessarily coincide with the p.z.c. Another possible method for estimating the location of the p.z.c. is the analytical determination of counter-ion adsorption. The surface excess of, for example, calcium ($\Gamma_{Ca^{2+}}$) is high at high pH, decreases with decreasing pH and becomes negative below the p.z.c. However, the pH at which $\Gamma_{Ca^{2+}} = 0$ may not exactly be identified with the p.z.c. because of specific adsorption and the interference of small amounts of Na^+ and Ca^{2+} present in the solid. Nevertheless, the method gives a good indication of the p.z.c. In this way we found the p.z.c. at pH 3.5 ± 0.5. Another assessment can be obtained from the following indirect method. Careful investigation of the OH^- adsorption isotherms in the presence of monovalent salts showed that the accepted p.z.c. at *ca.* pH 3 coincided with the beginning of the horizontal portion of the isotherms; hence, applying the same criterion to bivalent salts, a p.z.c. of *ca.* 4 was found. However, if there is specific adsorption of bivalent cations at the p.z.c. one would expect a shift to lower pH-values compared to the p.z.c. of 3 found with monovalent salts. We have therefore accepted pH 3 as the p.z.c. for all the σ_0–pH curves since, as in the monovalent case, the precise establishment of the p.z.c. is not critical.

Determination of charge vs. pH curves

The basic technique is essentially a potentiometric titration of suspended SiO_2 with acid or alkali as described previously[1]. The establishment of true equilibrium in the case of the adsorption of H^+ or OH^- on oxides, *i.e.*, to obtain a constant pH with time, is very slow. Readings were taken when the potential of the cell used to determine the pH shifted by less than 0.2 mV in the acid range, 0.5 mV in the neutral and slightly alkaline range, and 1 mV in the alkaline range during 15 min. In this manner we observed that, in general, the time required to reach this quasi-equilibrium state was longer when using bivalent counter-ions than when using monovalent cations. Because of the probable formation of bivalent hydroxo species at high pH-values which might have interfered with the OH^- uptake, the titration was not extended much beyond pH 9.

Counter-ion adsorption determination

In order to check the charge balance of the double layer, the surface charge and counter charge (Ca^{2+}) were measured simultaneously. The adsorption of Ca^{2+} ions was determined analytically using an Eppendorf flame photometer (with an accuracy of $\pm 2\%$). Dissolution of silica during the titration process which also produces pH-changes and hence suggests an apparent change in surface charge, was controlled with the molybdate method of Mullin and Riley[15].

In addition to the Ca^{2+} adsorption measurements used to verify the double layer charge balance, some Ca^{2+} adsorption isotherms have also been measured, both

in the absence and presence of carrier electrolyte (0.1 *N* LiCl). As adsorption of Ca^{2+} tends to lower the pH of the solutions, alkali has to be added during the adsorption process in order to keep the pH constant.

RESULTS

Reversibility of σ_0–pH curves

Unlike the case of monovalent counter-ions, the adsorption shows hysteresis when titrating from low to high pH and back. The extent of hysteresis depends on the pH-range and on the speed of the titration. Below pH $\sim$7.5, hysteresis is absent or negligible provided that the equilibrium criteria set forth in the experimental section are applied. At higher pH-values, hysteresis increases progressively. However, hysteresis is suppressed when the silica sample has been titrated several times back and forth. This is illustrated by the following typical experiments in which the potential was measured 15 min after each addition of acid or alkali. In one experiment a silica suspension at pH 2.87 was titrated with alkali to pH 7.96. When the titration was reversed, using the equivalent amount of acid, the final pH of the sol was 2.81; the two curves did not coincide fully having differences in surface charge of 2–4 $\mu C/cm^2$ depending upon the pH. However, when after completion of this run the sol was left for 16 h, the pH returned to its initial value. When at this stage the suspension was titrated again with alkali, the OH^- adsorption agreed within 1–2 $\mu C/cm^2$ with that in the first titration. In another experiment, a silica sol at pH 3.35 was titrated with alkali to pH 9.26 and then titrated back with an equivalent amount of acid. The final pH of the sol was 3.17 and a large hysteresis in the isotherms was observed with differences in surface charge of 7–32 $\mu C/cm^2$ depending upon the pH. When this sol was left for 16 h, the pH returned to 3.36 and after carrying out the titration three times successively with equivalent amounts of alkali, acid, and alkali, the hysteresis finally disappeared. The final σ_0–pH curve lies within 3–19 $\mu C/cm^2$ above the initial curve.

Adsorption isotherms

Examples of σ_0–pH curves at various concentrations of $CaCl_2$ are shown in Fig. 1. These isotherms represent quasi-equilibrium titrations from low to high pH in the sense described in the experimental section. Plots with other bivalent salts are of the same nature. In general, the shape of the OH^- adsorption isotherms is similar to that obtained with monovalent ions, one of the main differences being that the surface charge rises more steeply at high pH-values. The influence of the nature of the bivalent counter-ion on the specific charge density is given in Fig. 2 for 0.1 *N* concentrations. For comparison the specific charge density for 0.1 *N* KCl is shown in the same Figure. Below pH 8 (the region of little hysteresis) the OH^- adsorption for bivalent counter-ions is either of the same order of magnitude as that for K^+, or slightly higher. At pH >8 (*i.e.*, the region of strong hysteresis) the surface charge in the presence of bivalent counter-ions grows progressively over that of K^+. In this region, σ_0 increases in the order: $Mg^{2+} < Sr^{2+} < Ca^{2+} < Ba^{2+}$. This sequence differs slightly from the sequence: $Ca^{2+} < Sr^{2+} < Ba^{2+}$ obtained by Malati and Estafan[16] on quartz at pH 10.5. It is in qualitative agreement with the calculations of Dugger *et al.*[17] for the affinity of these cations to silicate sites ($Ba^{2+} \sim Ca^{2+} > Sr^{2+} > Mg^{2+}$). However, the sequence: $Mg^{2+} > Ca^{2+} > Ba^{2+} \simeq Sr^{2+}$ has been found on haematite[18].

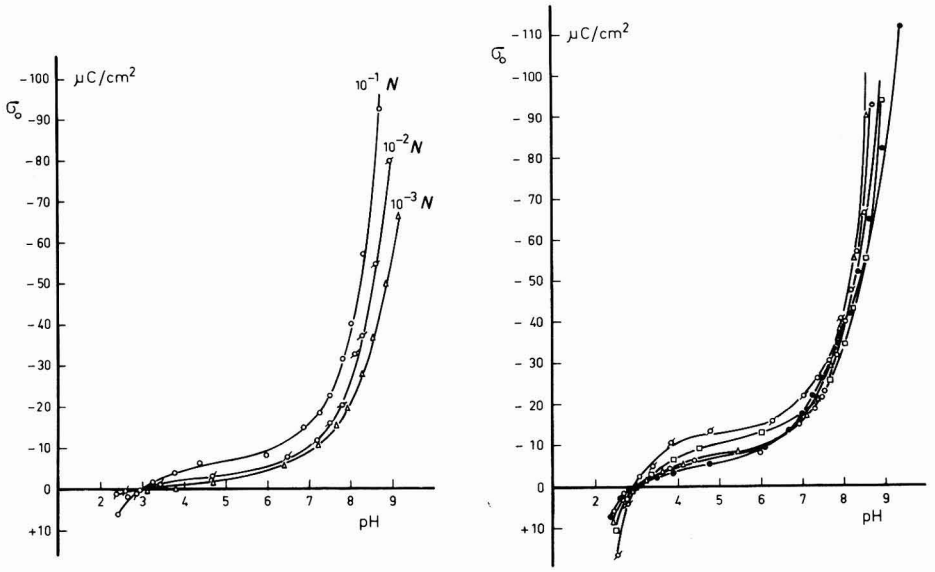

Figs. 1–2. Surface charge as a function of pH for silica; (Fig. 1), in the presence of three concns. of $CaCl_2$; (Fig. 2), in the presence of 0.1 *N* solns. of bivalent chlorides. (△), $BaCl_2$; (-○-), $SrCl_2$; (○), $CaCl_2$; (□), $MgCl_2$; (●), KCl.

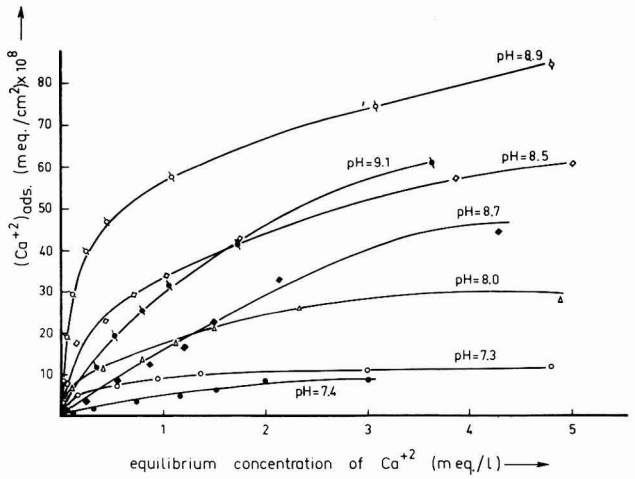

Fig. 3. Calcium adsorption isotherms in presence (black points) and absence (open points) of 0.1 *N* LiCl.

Figure 3 shows Ca^{2+} adsorption isotherms at various constant pH-values in the absence and in the presence of 10^{-1} *N* LiCl. In both cases the surface charge varies very little with calcium concentration: (a) in the absence of LiCl because the ionic strength is low; in this region σ_0 increases only slightly with $c_{Ca^{2+}}$ as long as the latter remains below $5 \cdot 10^{-3}$ equiv./l; (b) in the presence of excess LiCl because now LiCl determines the surface charge. As the number of adsorbed OH^- ions can

be identified with the number of adsorption sites, the curves of Fig. 3 are real adsorption isotherms. The results show that even a 200-fold excess of Li^+ reduces the Ca^{2+} adsorption by not more than 10–50%. In other words, there is a great preference for Ca^{2+} adsorption over Li^+ at a given σ_0.

DISCUSSION

Inspection of the adsorption behaviour of monovalent and bivalent cations on silica shows that whereas the former adsorb physically over the whole pH-range and produce reversible σ_0–pH curves, the latter adsorb partly chemically (or at least specifically) producing only partly reversible σ_0–pH curves. The arguments and considerations are as follows:

(a) Below pH ~ 7.5, both monovalent and bivalent cations adsorb physically, producing reversible σ_0–pH curves. In this region the surface charge is still predominantly confined to the surface and no pronounced preference of Ca^{2+} over K^+ must be expected (Fig. 2). Nevertheless, the adsorption of Mg^{2+} and Sr^{2+} is surprisingly high in this region.

(b) At high pH, monovalent ions still adsorb physically and produce reversible σ_0–pH curves, but bivalent counter-ions are chemisorbed and not easily desorbed, leading to hysteresis in the σ_0–pH curves. After three or four successive runs, all specific adsorption sites are covered and further adsorption is physical. This explains the disappearance of hysteresis after a few titrations.

(c) The Ca^{2+} adsorption isotherms of Fig. 3 (open points) show at low $c_{Ca^{2+}}$ a tendency to change with increasing pH from a Langmuir-type isotherm (indicative of physical adsorption) to a high-affinity isotherm with steep initial rise (indicative of strong specific adsorption).

(d) In Ca^{2+}–Li^+ mixtures there is an enormous preference for Ca^{2+} over Li^+ much more than would be expected solely on the basis of the valence ratio (Fig. 3).

The marked difference between monovalent and bivalent cations has already been demonstrated by Gaudin and Fuerstenau[14] from their streaming potential measurements on quartz. Na^+ ions did not affect the sign of ζ, and reduced its value only at high salt concentrations. On the other hand, Ba^{2+} ions reduced ζ at concentrations as low as 10^{-6} equiv./l and caused charge reversal at concentrations of 0.02 equiv./l. The possibility of super-equivalent adsorption of counter-ions can be checked from a consideration of the counter charge–surface charge balance as illustrated in Table 1. This Table shows the adsorption of OH^- and Ca^{2+} measured under identical conditions at various pH-values in 10^{-3} N $CaCl_2$, together with the amount of silicate dissolved (calculated on the assumption of formation of monosilicic acid and taking the equilibrium value for its dissociation, $K = 10^{-9.8}$ according to Roller and Ervin[19]). As already demonstrated[1], the negative adsorption of Cl^- is a small quantity especially in 10^{-3} N electrolyte concentration, and can therefore be neglected. The data in Table 1 show that the sum of $[Ca^{2+}]_{ads}$ and [silicate] compares well with the OH^- adsorption and there is no indication of Ca^{2+} adsorption in excess of OH^- adsorption. We conclude that, although there are definite indications of strong specific adsorption of Ca^{2+}, there is no evidence that it is so strong as to become super-equivalent. This conclusion is not necessarily in conflict with the findings of Gaudin and Fuerstenau of super-equivalent Ba^{2+} adsorption on quartz[14],

TABLE I

CHARGE BALANCE OF THE ELECTRICAL DOUBLE LAYER IN 10^{-3} N $CaCl_2$
All quantities expressed in (meq/g SiO_2) · 10^2

pH	$[OH^-]$ *ads.*	$[Ca^{2+}]$ *ads.*	$[HSiO_3^-]$ *diss.*	$[Ca^{2+} + HSiO_3^-]$
8.00	5.1	4.6	0.1	4.7
8.42	10.2	8.8	0.4	9.2
8.58	15.4	13.5	0.7	14.2
8.67	20.5	18.0	1.0	19.0
8.92	30.8	28.5	1.9	30.4
9.13	41.0	38.0	2.7	40.7

because in that case $c_{Ba^{2+}}$ had to be as high as $2 \cdot 10^{-2}$ N, which is beyond the range of concentration studied by us. Moreover, Ba^{2+} adsorbs more strongly than Ca^{2+} (Fig. 2) at high pH. A marked difference in the stability of silica sols in the presence of monovalent or bivalent salts was observed by Kruyt and Postma[20]. These authors found that the amount of NaCl required to gelatinize a SiO_2-sol increased with pH, but with $BaCl_2$ this was reversed apparently because the effect of the increasing surface charge is counteracted by specific adsorption of Ba^{2+} ions.

The present study suggests an explanation for the poor response of glass electrodes to bivalent cations. An investigation of the ionic double layer at the glass/aqueous electrolyte interface[21] for some cation-responsive glass powders, showed that a high mobility of cations in the gel layer is essential for good cation response. In view of the strong binding of bivalent cations to the surface silicate sites and their slow release upon changing conditions, their mobility in the surface gel layer is low. Thus, the major problem in designing a bivalent cation-selective glass electrode is to develop a glass with a high surface mobility for the bivalent ion. Owing to the practical difficulties of this requirement on aluminosilicate glasses, a number of authors[22,23] have recommended the use of liquid exchangers in the development of electrodes for bivalent cations.

ACKNOWLEDGEMENT

The authors are indebted to the Netherlands Organization for Development of Pure Scientific Research Z.W.O. for financial support to Th.F.T. during the course of this study.

SUMMARY

The surface charge density of silica in the presence of the chlorides of Mg^{2+}, Ca^{2+}, Sr^{2+} or Ba^{2+} was measured as a function of salt concentration, pH and history of the sample. Below pH ~ 7.5, bivalent counter-ions are physically adsorbed; this region is in many ways analogous to the double layer in the presence of monovalent cations. Above pH ~ 7.5, bivalent cations are partly specifically adsorbed although there is no evidence for super-equivalent adsorption. In this region the surface charge decreases in the order: $Ba^{2+} > Ca^{2+} > Sr^{2+} > Mg^{2+}$.

REFERENCES

1 TH. F. TADROS AND J. LYKLEMA, *J. Electroanal. Chem.*, 17 (1968) 267.
2 J. LYKLEMA, *J. Electroanal. Chem.*, 18 (1968) 341.
3 G. Y. ONODA AND P. L. DE BRUYN, *Surface Sci.*, 4 (1966) 48.
4 R. J. ATKINSON, A. M. POSNER AND J. M. QUIRK, *J. Phys. Chem.*, 71 (1967) 550.
5 G. W. SEARS, *Anal. Chem.*, 28 (1956) 1981.
6 G. H. BOLT, *J. Phys. Chem.*, 61 (1967) 1166.
7 H. G. LI AND P. L. DE BRUYN, *Surface Sci.*, 5 (1966) 203.
8 D. P. BENTON AND G. A. H. ELTON, *Trans. Faraday Soc.*, 49 (1953) 1213.
9 V. PRAVDIĆ AND M. MIRNIK, *Croat. Chim. Acta*, 30 (1958) 113.
10 R. K. ILER, *The Colloid Chemistry of Silica and Silicates*, Cornell University Press, Ithaca, New York, 1955, chap. V.
11 S. A. GREENBERG, *J. Phys. Chem.*, 60 (1956) 325.
12 *Glass Electrodes for Hydrogen and other Cations*, edited by G. EISENMAN, Marcel Dekker, Inc., New York, 1967.
13 J. H. DE BOER, B. C. LIPPENS, B. G. LINSEN, J. C. P. BROEKHOFF, A. VAN DEN HEUVEL AND TH. J. OSINGA, *J. Colloid Interface Sci.*, 21 (1966) 405.
14 A. M. GAUDIN AND D. W. FUERSTENAU, *Trans. AIME*, 202 (1955) 66.
15 J. B. MULLIN AND J. P. RILEY, *Anal. Chim. Acta*, 21 (1955) 162.
16 M. MALATI AND S. F. ESTAFAN, *J. Colloid Sci.*, 22 (1966) 306.
17 D. L. DUGGER, J. H. STANTON, B. N. IRBY, B. L. MCCONNELL, W. W. CUMMINGS AND E. W. MAATMAN, *J. Phys. Chem.*, 68 (1964) 757.
18 A. BREEUWSMA, private communication.
19 P. S. ROLLER AND G. ERVIN, *J. Am. Chem. Soc.*, 62 (1940) 461.
20 H. R. KRUYT AND J. POSTMA, *Rec. Trav. Chim.*, 44 (1925) 765; J. POSTMA, *Rec. Trav. Chim.*, 51 (1932) 726.
21 TH. F. TADROS AND J. LYKLEMA, *J. Electroanal. Chem.*, 22 (1969) 9.
22 J. W. ROSS, JR., *Science*, 155 (1967) 1278.
23 G. EISENMAN, *Anal. Chem.*, 40 (1968) 310.

ELECTROANALYTICAL CHEMISTRY AND INTERFACIAL ELECTROCHEMISTRY
Elsevier Sequoia S.A., Lausanne – Printed in The Netherlands

THE OPERATIVE MECHANISM OF GLASS ELECTRODES AND THE STRUCTURE OF THE ELECTRICAL DOUBLE LAYER ON GLASS

TH. F. TADROS AND J. LYKLEMA
Laboratory for Physical and Colloid Chemistry, Agricultural University, Wageningen (The Netherlands)
(Received November 19th, 1968)

Since the discovery of H^+ selective glass electrodes in the late thirties and the advent of glass electrodes selective for other univalent cations in the fifties, the problem of the operative mechanism of glass electrodes has been the subject of a number of opinions and studies[1-12]. Current ideas can be roughly classified into two groups. In the first approach, the glass is considered to select from a mixture the cation i with the highest affinity for the surface gel layer sites, and in consequence responds to that ion. This "ion-exchange" theory has been advocated by Eisenman[5], Lengyel[13], Nikolskii *et al.*[14-17] and Tendeloo[18]. In this representation, in principle a static equilibrium is attained at the glass–solution interface with the chemical potential difference $(\mu_i^{glass} - \mu_i^{solution})$ as the driving force for the generation of the electric potential difference, the electrochemical potential, η_i, being equal throughout. In the second approach, the glass electrode potential is treated as essentially a diffusion potential, *i.e.* as a typical non-equilibrium phenomenon. In the latter representation, differences in mobility generate a steady-state potential (*e.g.* Nagasawa and Kobatake[19], Teorell[20-22], Meyer and Sievers[23], Sollner[24,25], Doremus[26,27], Altug and Hair[28]). It must be re-emphasized[29] that the glass electrode potential is not a "simple" membrane potential in the sense that it responds only to the ion to which it is permeable, because the experiments by Schwabe and Dahms[30] showed that the conductance of glasses responding to H^+-ions was almost exclusively governed by transport of Na^+-ions.

Both mechanisms proposed can explain a number of experimental facts. However, a detailed experimental check of the merits and demerits of the two approaches is not yet generally possible in view of the lack of data on the ionic mobilities, ionic distributions, activity coefficients, etc., in the surface layer of the glasses. It cannot yet be stated, therefore, which of the two approaches should be preferred, if any. In principle, both mechanisms could be operative at the same time. This possibility led Eisenman[3] to formulate a "compromise" equation accounting for diffusion and specific adsorption at the same time:

$$E^g = \text{const.} + (nRT/F) \ln \left[a_i^{1/n} + (K_{ij}^{pot} a_j)^{1/n}\right] \quad (1)$$

In this equation a_i and a_j are the activities in solution of the two cations to which the glass under consideration can respond, R, T and F have their usual meaning and n is essentially an empirical constant that is perhaps related to the activity coefficient of cations in the glass phase. K_{ij}^{pot} follows from

$$K_{ij}^{pot} = (u_j^g/u_i^g) K_{ij} \quad (2)$$

in which u^g is the mobility of the ion named in the glass phase and K_{ij} is the ion exchange constant of the equilibrium:

$$j^{bulk} + i^g \rightleftarrows j^g + i^{bulk} \tag{3}$$

Equation (1) predicts a gradual transition from response to ions i towards response to ions j if a_j is increased with respect to a_i. The activity range where this transition occurs is determined by K_{ij}^{pot}. The higher K_{ij}^{pot}, the better the electrode responds to j. However, from eqn. (2) it is impossible to decide at a glance whether a high K_{ij}^{pot} must be attributed to a high u_j/u_i ratio or to a high ion-exchange constant, or perhaps to both. A definite answer is possible only if cation mobilities and activities in the glass are known. Unfortunately reliable data are not generally available. Moreover, such an analysis has the disadvantage that it presupposes the correctness of eqn. (1).

A typical property of most glass electrodes is their short response time, suggesting that the potential-determining process requires no extensive diffusion into the solid phase but takes place close to the glass–solution interface in the sub-surface gel layer. This region is at the same time the region of the electrical double layer existing at the phase boundary. Based upon this consideration, a new approach to distinguish between the two mechanisms is explored below. This treatment rests upon recently accumulated knowledge of the double-layer structure on porous silicate-like substrates[31-33]. The essential points of this representation (applied to glass) are as follows.

The surface region of glass has, after prolonged swelling in aqueous solution, a porous swollen structure with dissociable silicate, aluminosilicate and, depending on the nature of the glass, other groups, for which the proton is potential-determining. Depending on the conditions, these groups can be positively charged (at low pH), uncharged (at the point of zero charge, p.z.c.) or negatively charged (at high pH). The surface charge, σ_0, can be defined and determined using

$$\sigma_0 = F(\Gamma_{H^+} - \Gamma_{OH^-}) \tag{4}$$

in which Γ is the surface excess in mole cm^{-2} of the ion named. On closer analysis[31,33] it appears that the surface charge is not confined to the two-dimensional interface proper, but may extend to considerable depth into the surface gel layer. The extent of this penetration depends, for example, on the porosity of the sub-surface phase. The majority of the compensating counter-ions are also adsorbed in this surface gel layer, only a minor part being present in the solution part of the double layer. As the electrical double layer as a whole is electro-neutral, this implies that σ_0 can be identified with $F\Gamma_i$ if Γ_i is the surface excess of the compensating ion. In other words, this surface excess can conveniently be assessed using eqn. (4). The greater the adsorbability of a given counter-ion in the gel layer, the higher the surface charge[33]. If the idea is correct that good response of a glass to a given cation is due to preferential uptake of this ion in the sub-surface gel layer, it must be expected that the surface charge on this glass is higher in a solution of that cation than in solutions of other cations of the same concentration and the same pH.

Although attractive in principle, this approach introduces an experimental difficulty. In order to provide for a sizeable interface, the electrode glass should be ground. However, the constituents of most glasses have a finite solubility. As a result of the leaching of alkaline products, the pH of the solution is increased, obscuring

the analytical determination of C_{H^+} and C_{OH^-} *i.e.*, the basis of the surface charge determination *via* eqn. (4). We have finally succeeded in minimising this difficulty by using two glass samples of relatively low solubility. These glasses respond at high pH to Na^+ and K^+, respectively. They are used for the study of σ_0 in solutions of NaCl, KCl and other salts at various pH-values.

EXPERIMENTAL

Materials

Two samples of glass powders were supplied by Electrofact N.V., Amersfoort, Netherlands. Their approximate composition, as provided by the manufacturer, is shown in Table 1. The first glass responds to Na^+, the second to K^+. At pH 8 the

TABLE 1

COMPOSITION OF GLASS SAMPLES

	Na^+-responsive glass		*K^+-responsive glass*	
	(*wt %*)	(*mole %*)	(*wt %*)	(*mole %*)
SiO_2	66	68.7	66	73.0
GeO_2	2	1.19	2	1.26
Al_2O_3	2	1.22	2	1.30
B_2O_3	13	11.7	13	12.4
Na_2O	17	17.1	—	—
K_2O	—	—	17	12.0

response is ideal over the concentration range, 10^{-4}–1 *N*. The glass was ground in alcoholic suspension in an agate mill, sieved and dried at $\sim 100°$. Before use it was suspended in acid solution for at least one night in order to provide the same surface properties as those of the electrodes.

All salts were of AnalaR grade and used without further purification. Distilled water was boiled in a nitrogen atmosphere before use in order to expel CO_2.

Surface area

The specific surface areas have been determined by the BET (N_2) technique before and after soaking. The results (see Table 2) show that swelling occurs on

TABLE 2

SURFACE AREAS OF GLASS SAMPLES ($m^2\ g^{-1}$)

	Na^+-responsive glass	*K^+-responsive glass*
Area before treatment	7.6 ± 0.2	3.5 ± 0.1
Treatment	1 g in 100 ml 10^{-2} *N* $HClO_4$ during 1 night	0.5 g in 100 ml $1.5 \cdot 10^{-2}$ *N* $HClO_4$ during 1 night
Area after treatment	13.8 ± 0.2	27.3 ± 0.5

soaking. Owing to the presence of many very narrow pores, the effective area of the suspended particles after soaking could still be higher than the BET area.

Information on the porosity of acid-treated samples has been obtained from *t*-plots according to De Boer *et al.*[34], see Fig. 1. The Na^+-responsive glass shows a

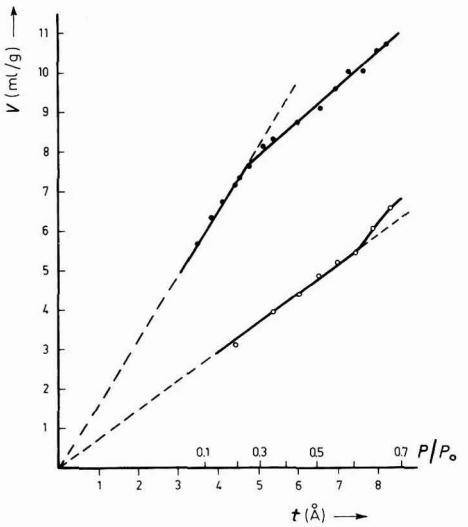

Fig. 1. *t*-Plots for Na^+- and K^+-responsive glass powders, (●), K-; (○), Na-responsive glass.

positive deviation from the linear *t*-plot at relative pressures, $PP_0^{-1} > 0.6$, which is indicative of the presence of wide pores >20 Å with capillary condensation. The surface area, S_t, is 11.3 $m^2\ g^{-1}$ compared with $S_{BET} = 13.8\ m^2\ g^{-1}$. The K^+-responsive glass shows a negative deviation above $PP_0^{-1} \sim 0.3$, which is indicative of the presence of narrow (< 20 Å) slit-shaped pores[34,35] without capillary condensation. For this sample, $S_t = 25.1\ m^2\ g^{-1}$ compared with $S_{BET} = 27.3\ m^2\ g^{-1}$. The question of which of the two areas should be preferred[36] is academic because the effective areas in suspension are much higher than the gas adsorption areas. For the sake of comparison and discussion our results are based upon S_{BET}.

The point of zero charge (p.z.c.)

Since glass consists of a mixture of oxides one would expect the p.z.c. to be located between that of silica (pH ~3) and that of the other oxides. At present, the most reliable method for locating the p.z.c. of glass is from the intersection point of σ_0–pH curves (see below) at various salt levels. This approach gives reliable results if specific adsorption at the p.z.c. is absent. However, this method could not be applied because of the insignificant dependence of σ_0 on c_{salt}. The inflection point in the σ_0–pH curves (pH ~6) was therefore taken as the p.z.c. Fortunately, neither the general trends of our experimental results nor our conclusions are affected by the choice of the p.z.c.

Determination of σ_0–pH isotherms

The basic technique for determining σ_0 using eqn. (4) is essentially a poten-

tiometric titration of glass powder with acid or alkali, as already described[31]. Readings were taken when the potential of the cell used to measure the pH shifted by < 1 mV at pH < 4, by < 2 mV in the pH-range 4–8 and by < 0.2 mV at pH > 8 during 5 min. If the titration is carried out more rapidly, the establishment of adsorption equilibrium is not ensured; if it is carried out more slowly, leaching of the alkaline components of the glass* creates a difficulty. In this way a reproducibility of better than 1% was obtained; under these conditions the isotherms were free of hysteresis.

RESULTS AND INTERPRETATION

An example of σ_0–pH isotherms for Na^+-responsive glass is shown in Fig. 2. Comparison of this figure with the corresponding figures obtained with silica[31]

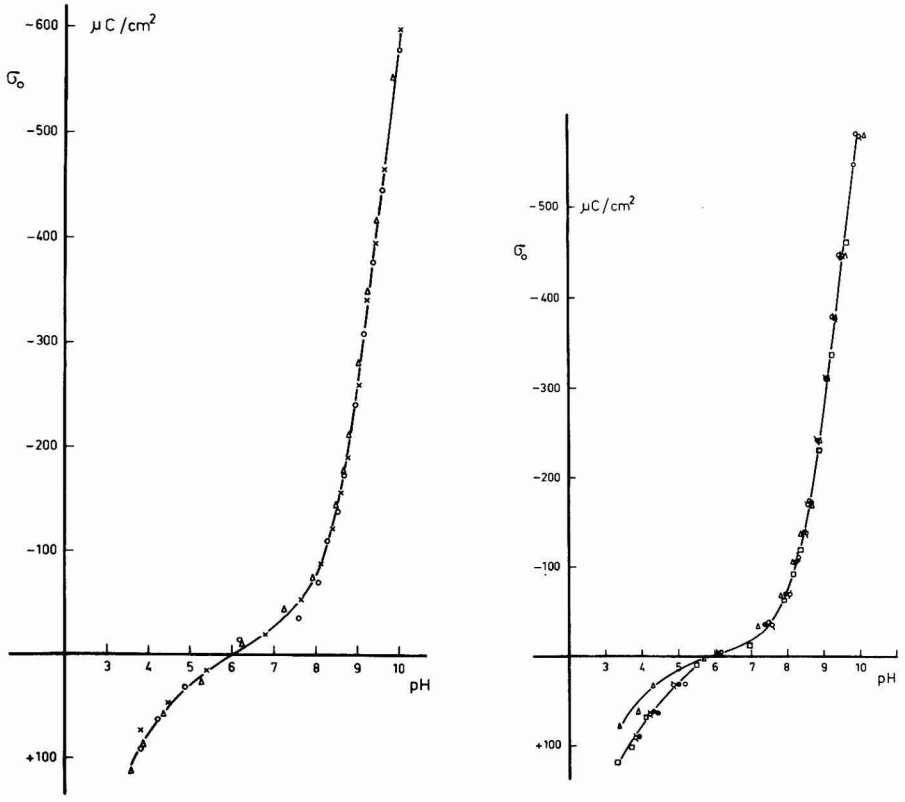

Figs. 2-3. Surface charge as a function of pH for Na^+-responsive glass: (Fig. 2), in the three different concns. of NaCl: (○), 10^{-1}; (×), 10^{-2}; (△), 10^{-3} *M*. (Fig. 3), effect of the nature of the cations. Salt concn., 10^{-1} *N*. (○), LiCl; (-○-), NaCl; (□), KCl; (△), CsCl; (●), $(C_2H_5)_4NCl$.

shows a qualitative similarity which could be expected in view of the similarity in surface structure. Two quantitative differences are worthy of note: the very high surface charge (several times higher than on silica) and the absence of any salt con-

* Chemical analysis of the solution showed that the silica network was not dissolved during this leaching.

centration effect. The first observation is obviously due to the extensive swelling which provides for may dissociable groups in the surface gel layer. If considerable penetration of potential-determining and counter-ions occurs, theory[33] predicts only a slight influence of c_{salt}, in agreement with our second experimental finding. A number of auxiliary experiments corroborate this picture. The presence of many charge carriers in the surface gel layer of glass (although it has not yet been confirmed on our sample) has been revealed by surface conductance studies[37]. Provisional microelectrophoresis experiments with our glass powder lead to electrokinetic charges that are less than 1 % of σ_0, indicating that the solution part of the double layer is not significant. Hence for σ_0 more than 99 % of the charge may be identified with counter ions adsorbed, or absorbed in the surface gel layer.

In the study of the effect of the nature of the counter-ion, the region at high pH

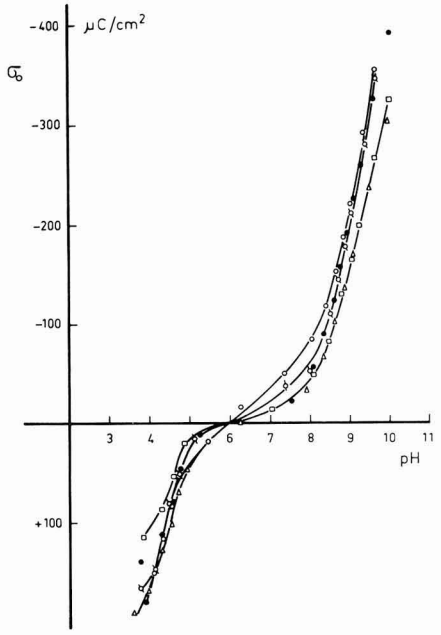

Fig. 4. Surface charge as a function of pH for K^+-responsive glass. Effect of the nature of the cation. Salt concn., 10^{-1} *N*. (○), LiCl; (◐), NaCl, (□), KCl; (△), CsCl; (●), $(C_2H_5)_4NCl$.

is of most interest. In this range the counter-ions are cations (Na^+, K^+, etc.) and it is also in this range that the glasses respond to Na^+ and K^+, respectively.

The effect of the nature of the counter-ion on σ_0 is shown in Figs. 3 and 4 for Na^+-glass and K^+-glass, respectively. Figure 3 shows that for the Na^+-responsive glass there is no detectable effect of the nature of the cation (Li^+, Na^+, K^+, Cs^+ and $(C_2H_5)_4N^+$). This can, in the first instance, be attributed to the relative width of the pores, as the theory[33] showed that discrimination can only be expected when the radii of the pores in the surface layer are comparable to the ionic radii. In the case of K^+-responsive glass, small but measurable differences are observed with different cations. The affinity to the surface gel layer (as judged from σ_0 at high pH) decreases in the order: $Li^+ > Na^+ > K^+ \sim Cs^+$, which is the reverse of the order found on

mercury[38], silver iodide[39] and silica[31], but agrees with results by Altug and Hair on porous glass[46]. The specific effects that occur in this case are apparently due to the narrow pore widths. However, a preference for Li^+ over Cs^+ can only be accounted for if it is assumed that these cations are partially dehydrated.

DISCUSSION

The results described above are surprising. Figure 3 shows that Na^+-responsive glass has no preference for Na^+ over other cations under the conditions where it responds ideally. Figure 4 shows that K^+-responsive glass, also under conditions of ideal response to K^+, has an even lower affinity for K^+ than for Na^+ and Li^+. The glass does not respond to Li^+ or Na^+. We conclude that *there is no relation whatsoever between the response of these glass electrodes towards a given cation and the affinity of that cation for the glass.*

If this conclusion can be generalized, it is of the uttermost importance to the understanding of glass electrode behaviour, because it automatically excludes those theories in which selectivity is interpreted as solely due to preferential uptake. At the same time it gives preference to the theories that emphasize that the cation mobility in the gel layer is the dominant factor.

This conclusion is the quintessence of this work. It gives rise to a number of considerations and suggestions for further study, the most important of which are discussed below.

(1) In view of our conclusion that ionic mobility in the surface gel layer is the dominant factor controlling response and since this quantity is also reflected in surface conductance, the existence of a correlation between surface conductivity and response behaviour of a given type of glass must be expected. As far as we are aware, such a study has not yet been published. A correlation between tangential and normal mobility is presupposed.

(2) In almost all glass electrode theories—of both categories—the assumption is (either tacitly or not) made, that the space charge density of the fixed negative groups is constant. This may hold for the bulk of a glass membrane but is not correct for the surface gel layer. Hence, as far as the potential-determining process takes place in the vicinity of the interface (short response time!) these theories need improvement.

(3) Although (alumino) silicate groups show noticeable selectivity of Ca^{2+} over Na^+ in the high pH range[32], this does not lead to Ca^{2+}-response because we have now seen that it is the mobility that counts, and the mobility of Ca^{2+} in this type of structure is quite low[40]. This explains why attempts to construct glass electrodes for bivalent ions have been largely unsuccessful.

(4) Our results are at variance with the direct measurement of the uptake of $^{24}Na^+$ by Na^+-responsive glass[30,41]. In the experiments by Trebge *et al.*, reported by Eisenman[41], Na^+-sorption was observed at the moment the electrode began to respond to Na^+. We are inclined to consider our measurements as more sensitive because of the large total area (20–30 $m^2\ g^{-1}$ compared to only a few cm^2 in ref. 41).

(5) An important consequence of our representation is, that there is no more than an indirect relationship between electrode response and the chemical composition of the glass; it is porosity that counts and the chemical constitution is only of relevance in that during the leaching process a given network of pores with given radii

is formed. In earlier studies a direct relationship between constitution and response was sought[3,5,16,17,42,44].

(6) Owing to lack of reliable mobility and concentration data no definitive experiments have been reported to check the theoretical equations of the earlier theories, although recently some examples have been reported[11,12]. A very recent experiment by Altug and Hair[45] seems to support our ideas. These authors observed a change in response behaviour due to sintering, *i.e.*, due to a change in pore properties, at unaltered chemical composition.

The question remains whether our results and interpretation may be generalized. If this is the case, a new approach is indicated for further developments in glass electrode theory and practice.

ACKNOWLEDGEMENTS

The authors are indebted to Electrofact (Netherlands) for providing and grinding the glass, to Mr. A. E. Mans for preparing the glass melts and to the Netherlands Organisation for the Development of Pure Scientific Research (Z.W.O.) for financial help to Th.F.T. during the course of this study.

SUMMARY

The problem of the interpretation of glass electrode potentials is approached from the point of view of interfacial electrochemistry. Surface charge *versus* pH curves are obtained for Na^+- and K^+-responsive glasses in the presence of the chlorides of Li^+, Na^+, K^+, Cs^+ and $(C_2H_5)_4N^+$. It has been found that there is no relation between the affinity of a given cation and the glass surface and the tendency of the glass to respond to that cation. It is concluded that the mobility of the ions in the surface gel layer is the primary factor in determining response.

REFERENCES

1 M. DOLE, *The Glass Electrode Methods, Applications and Theory*, J. Wiley and Sons, New York, 1941.
2 M. DOLE, *J. Am. Chem. Soc.*, 53 (1931) 4260.
3 *Glass Electrodes for Hydrogen and other Cations*, edited by G. EISENMAN, Marcel Dekker Inc., New York, 1967.
4 G. EISENMAN, D. O. RUDIN AND J. U. CASBY, *Science*, 126 (1957) 831.
5 G. EISENMAN, *Biophys. J.*, 2 (1962) 259.
6 G. EISENMAN, *Ann. N.Y. Acad. Sci.*, 148 (1968) 5.
7 F. CONTI AND G. EISENMAN, *Biophys. J.*, 5 (1965) 247, 511.
8 V. V. MOISEEV, *Vestn. Leningr. Univ.*, 15 No. 22, *Ser. Fiz. i Khim.*, No. 4 (1960) 49.
9 G. A. RECHNITZ, *J. Chem. Educ.*, 41 (1964) 385.
10 K. SCHWABE AND H. D. SUSCHKE, *Angew. Chem.*, 76 (1964) 39.
11 K. H. STERN, *J. Phys. Chem.*, 72 (1968) 1963.
12 R. H. DOREMUS, *J. Phys. Chem.*, 72 (1968) 2877.
13 B. V. LENGYEL, *Z. Physik. Chem. Leipzig*, 153A (1931) 425.
14 B. P. NIKOLSKII, *Acta Physicochim. U.R.S.S.*, 7 (1937) 597.
15 B. P. NIKOLSKII AND T. A. TOLMACHEVA, *Zh. Fiz. Khim.*, 10 (1937) 513.
16 B. P. NIKOLSKII AND M. M. SHULTS, *Zh. Fiz. Khim.*, 36 (1962) 1327.
17 M. M. SHULTS, *Vestn. Leningr. Univ.*, 15 No. 22, *Ser. Fiz. i Khim.*, No. 4 (1960) 40.
18 H. J. C. TENDELOO, *Discussions Faraday Soc.*, 1 (1947) 293.

19 M. NAGASAWA AND Y. KOBATAKE, *J. Phys. Chem.*, 56 (1952) 1017.
20 T. TEORELL, *Proc. Soc. Exptl. Biol. Med.*, 33 (1935) 282.
21 T. TEORELL, *Trans. Faraday Soc.*, 33 (1937) 1086.
22 T. TEORELL, *Z. Elektrochem.*, 55 (1951) 460.
23 K. H. MEYER AND J. F. SIEVERS, *Helv. Chim. Acta*, 19 (1936) 649, 665, 987.
24 K. SOLLNER, *J. Phys. Chem.*, 49 (1945) 47.
25 K. SOLLNER, *Svensk Kem. Tidskr.*, 70 (1958) 267.
26 R. H. DOREMUS, see ref. 3 pp. 101–132.
27 R. H. DOREMUS, *J. Phys. Chem.*, 72 (1968) 2877.
28 I. ALTUG AND M. L. HAIR, *J. Phys. Chem.*, 72 (1968) 599.
29 J. LYKLEMA, *Med. Electron. Biol. Eng.*, 2 (1964) 265.
30 K. SCHWABE AND H. DAHMS, *Z. Elektrochem.*, 65 (1961) 518.
31 TH. F. TADROS AND J. LYKLEMA, *J. Electroanal. Chem.*, 17 (1968) 267.
32 TH. F. TADROS AND J. LYKLEMA, *J. Electroanal. Chem.*, 22 (1969) 1.
33 J. LYKLEMA, *J. Electroanal. Chem.*, 18 (1968) 341.
34 J. H. DE BOER, B. C. LIPPENS, B. G. LINSEN, J. C. P. BROEKHOFF, A. VAN DEN HEUVEL AND TH. J. OSINGA, *J. Colloid Interface Sci.*, 21 (1966) 405.
35 J. H. DE BOER, B. G. LINSEN, TH. VAN DER PLAS AND G. J. ZONDERVAN, *J. Catalysis*, 4 (1965) 649.
36 K. S. W. SING, private communication.
37 A. WATILLON AND R. DE BACKER, *Vth Intern. Congr. Surface Active Substances, Barcelona, 1968*, Preprints B/0 (195).
38 D. C. GRAHAME, *J. Electrochem. Soc.*, 98 (1951) 343; 99 (1952) 273.
39 J. LYKLEMA, *Trans. Faraday Soc.*, 59 (1963) 418.
40 P. M. SUTTON, *J. Am. Ceram. Soc.*, 47 (1964) 188.
41 Ref. 3, Chap. V.
42 R. M. GARRELS, M. SATO, M. E. THOMPSON AND A. H. TRUESDELL, *Science*, 135 (1962) 1045.
43 B. P. NIKOLSKII, M. M. SHULTS AND A. A. BELYUSTIN, *Dokl. Akad. Nauk SSSR*, 144 (1962) 844.
44 A. L. BUDD, *J. Electroanal. Chem.*, 5 (1963) 35.
45 I. ALTUG AND M. L. HAIR, *J. Phys. Chem.*, 72 (1968) 2976.
46 I. ALTUG AND M. L. HAIR, *J. Phys. Chem.*, 71 (1967) 4260.

ELECTROANALYTICAL CHEMISTRY AND INTERFACIAL ELECTROCHEMISTRY
Elsevier Sequoia S.A., Lausanne – Printed in The Netherlands

THE EFFECT OF IONIC SIZE IN THE DOUBLE LAYER ON THE KINETICS OF ELECTRODE REACTIONS

W. R. FAWCETT
Department of Chemistry, University of Guelph, Guelph, Ontario (Canada)
(Received February 3rd, 1969)

INTRODUCTION

It is well known that the kinetics of charge transfer processes occurring at potentials cathodic of the electrocapillary maximum are markedly affected by the cation present in the double layer. Thus, in a series of experimental investigations[1], it was found that the rate of reduction at constant potential of a particular cation decreased with increase in the crystallographic radius of the base electrolyte cation, whereas that of an anion increased. Frumkin[2] attributed the effect of alkali-metal cations on hydrogen ion reduction to cationic specific adsorption but stated that this effect could also be ascribed to a variation in the distance of closest approach with the cation, and thus, in the potential distribution in the double layer. Additional factors have been considered in the reduction of anions, namely, specific interaction between the reacting anion and cations in the double layer[3,4] and change in the charge on the reacting species with potential and ionic strength[5]. Imperfections in the simple Gouy–Chapman theory normally used to calculate the potential drop in the diffuse layer have been cited as possible causes of abnormal corrected Tafel plots[6,7]. However, when this potential difference was calculated by a more detailed model which took into account specific ionic effects[8], no significant difference in kinetic parameters or in the shape of differential Tafel plots was found[9]. A possible cause of non-linearity in corrected Tafel plots which has not been considered is the change in the position of the outer Helmholtz plane with electrode potential due to electrostriction[10]. Modified kinetic equations that take into account the effects of cation size and electrostriction are presented in this paper. The predictions of the theory are examined with data for the reduction of the peroxydisulphate anion.

THEORY

A simple electron transfer process at a mercury electrode will be considered, namely

$$a0 + ne \rightleftharpoons bR \tag{1}$$

for which the rate-determining step involves n electrons; the species 0 and R with charges z and $(az-n)/b$, respectively, are both soluble, R being soluble in either the solution or the electrode. At potentials sufficiently cathodic of the equilibrium poten-

tial, the dependence of the rate constant for the forward process, k, on potential is given by[1]:

$$\ln k = \ln k_e + (\alpha n - z) f(\phi_r - \phi_r^e) - \alpha n f(\phi_m - \phi_m^e) \quad (2)$$

where ϕ_m is the electrode potential on the rational scale, ϕ_r the potential at the charge centre of the reacting species in the transition state, k_e, ϕ_m^e and ϕ_r^e the values of k, ϕ_m, and ϕ_r at the equilibrium potential, α, the transfer coefficient, and $f = F/RT$. For processes the equilibrium potential of which is too anodic to be observed on a mercury electrode, a more convenient form of eqn. (2) is:

$$\ln k = \ln k_o + (\alpha n - z) f(\phi_r - \phi_r^o) - \alpha n f \phi_m \quad (3)$$

where k_o and ϕ_r^o are the values of k and ϕ_r at the electrocapillary maximum (e.c.m.). In cases where the base electrolyte is not specifically adsorbed, $\phi_r^o = 0$.

In a consideration of the position of the centre of charge of the reacting particle in the transition state, and of the potential at that point, three cases may be distinguished: (i) the particle is at the outer Helmholtz plane (O.H.P.); (ii) the particle is in the inner layer; (iii) the particle is in the diffuse layer. It has been customary to assume that Case (i) holds; then ϕ_r becomes ϕ_2, the potential at the O.H.P., and eqn. (2) reduces to the familiar Frumkin equation. The distance of the O.H.P. from the geometrical electrode–solution interface, x_2, is the average distance of closest approach of the non-specifically adsorbed ions. Mott, Parsons and Watts-Tobin[11] have proposed that this distance depends on the solvated radius of the predominant cation at cathodic potentials. Thus, for the alkali–metal cations, x_2 should decrease with increase in crystallographic radius. Evidence from capacity measurements for this variation is obtained from Grahame's observation[12] that the integral capacity of the inner layer increases with increase in cation atomic number, being about 10% higher for CsCl than for LiCl. However, calculation of relative values of x_2 from these data would be difficult owing to the probable variation of inner layer dielectric constant with the predominant species at the O.H.P. Monk[13] estimated hydrated radii for the series Li–Cs from ionic molar volume data and obtained values of 2.50 Å for Li^+, 2.17 Å for Na^+, 1.75 Å for K^+, and 1.47 Å for Cs^+. With such a large variation in ionic size, and thus in the position of the O.H.P., it is not probable that the distance from the centre of charge of the reacting species in the transition state to the electrode, x_r, will always equal x_2.

The effect of the variation in O.H.P. position with potential may be estimated according to Macdonald's theory of the inner layer[10]. He proposed that x_2 decreases with increase in E, the field in the inner layer, in the following manner:

$$x_2 = x_{2o}/(1 + \beta q E/2) \quad (4)$$

x_{2o} is the value of x_2 at the e.c.m., q the charge on the electrode, and β a compressibility constant dependent on the solvent and its structure in the inner layer. According to his calculations with capacity data for NaF, the inner layer is compressed by approximately 20% when the field reaches its maximum cathodic value. In order for Case (i) to remain valid, x_r would be required to change with potential. It seems unlikely that the compressibility of the inner layer in the region of the reacting species would equal that in the region of the double layer cation. Thus, the position of the reacting species with respect to the O.H.P. would be expected to change with potential.

A knowledge of the potential distribution in the inner layer is needed to calculate ϕ_r in Case (ii). It is generally agreed[14] that the electric displacement in the inner layer is constant when the charge density within it is low. Then, if the dielectric constant within this region does not change with distance, the potential drop is linear so that

$$\phi_r = \phi_2 + \lambda(\phi_m - \phi_2) \tag{5}$$

where

$$\lambda = (x_2 - x_r)/x_2$$

When the reacting species is in the inner layer in the transition state, it is probably valid to assume that its distance to the electrode does not change with potential.

On combining eqns. (4) and (5) with the assumption that the electrostriction effect is small (*i.e.*, $\beta q(\phi_m - \phi_2)/2x_2 \ll 1$), the following expression is obtained for ϕ_r:

$$\phi_r = \phi_2 + \lambda_o(\phi_m - \phi_2) - \sigma q(\phi_m - \phi_2)^2 \tag{6}$$

where

$$\lambda_o = (x_{2o} - x_{ro})/x_{2o} \tag{7}$$

and

$$\sigma = \beta x_{ro}/2x_{2o}^2 \tag{8}$$

It has been postulated by two groups of authors[11,15] that the dielectric constant in the inner layer rises sharply from its low field saturation value in the inner region to a value closer to that in the bulk of the solution at x_1, a distance less than x_2. Then two regions in the inner layer must be considered, one adjacent to the electrode in which the potential varies linearly from ϕ_m to a value close to ϕ_2, and a second region in which the potential is approximately constant and equal to ϕ_2. If this model is correct then x_2 should be replaced by x_1, in eqn. (5). The conclusions drawn above regarding the variation of x_2 with ionic size and potential would also apply to x_1, since these were made on the basis of capacity data. Although the equations presented are based on the simple model with a constant dielectric constant, they could easily be applied to the more detailed model. As Parsons has noted[16], it is important to remember that the simple model involves a discontinuity in the field at the O.H.P., so that when ϕ_r is close to ϕ_2 it is no longer valid to assume a linear potential drop.

An expression for the rate constant valid for Case (ii) in the absence of specific adsorption is obtained by combining eqns. (3) and (5).

$$(\ln k)/f = (\ln k_o)/f - z\phi_2 + [\alpha n - \lambda(\alpha n - z)](\phi_2 - \phi_m) \tag{9}$$

Frumkin derived a similar equation previously[2], but did not consider electrostriction. From eqn. (9), it can be seen that the slope of a corrected Tafel plot of kinetic data ($(\ln k)/f + z\phi_2$ *vs.* $\phi_2 - \phi_m$) depends on the parameter, λ, and on the charge on the reacting particle. As ϕ_m increases cathodically, λ decreases, so that the slope of the above plot increases when $\alpha n - z$ is positive and decreases when it is negative (Fig. 1). In addition, the value of λ depends on the radius of the cation at the O.H.P. such that λ increases with increase in cation size. Thus, the departure of the Tafel slope, $\alpha n - \lambda(\alpha n - z)$, from the "true" Tafel slope, αn, will increase with increase in cation size.

When the particle is in the diffuse layer in the transition state, ϕ_2 may be calculated to a first approximation from the Gouy–Chapman theory. The relationship

between ϕ_r and ϕ_2 in this region for a simple 1–1 electrolyte is

$$\ln \tanh (f\phi_r/4) = \ln \tanh (f\phi_2/4) - \kappa(x_r - x_2) \tag{10}$$

where κ, the reciprocal Debye–Hückel length, equals $(8\pi Ffc/\varepsilon)^{\frac{1}{2}}$, c being the electrolyte concentration, and ε the dielectric constant of the solvent. The above expression may

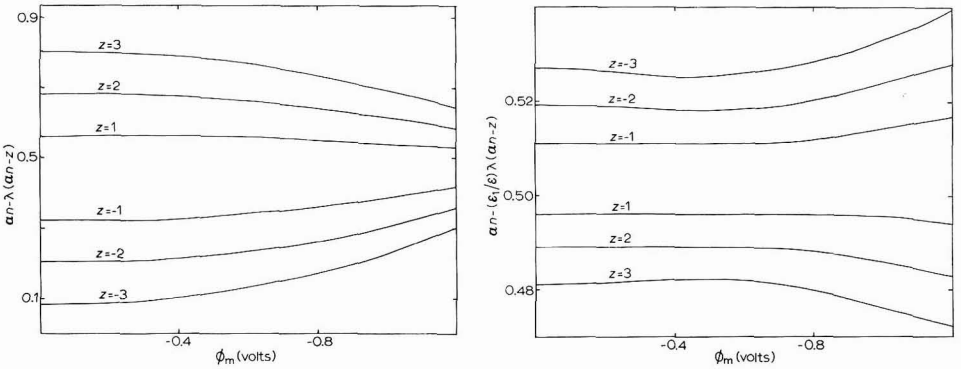

Figs. 1–2. Variation of the Tafel slope with charge on the reacting particle and electrode potential, (Fig. 1) for the case that the particle is in the inner layer in the transition state (x_{ro}=2.2 Å) and (Fig. 2) for the case that the particle is in the diffuse layer in the transition state (x_{ro}=2.6 Å). αn=0.5, x_{2o}=2.5 Å, β=$1.7 \cdot 10^{-10}$ cm^3 μJ^{-1}.

In Fig. 2, ε=78.3. ε_1 is calcd. from the equation[17]:

$$\varepsilon_1 = 1 + 5.0\lambda + 8.9 \tan^{-1} (1.5 \cdot 10^{-7}E)/(1.5 \cdot 10^{-7}E)$$

where $E=(\phi_m - \phi_2)/x_2 - 1.52 \cdot 10^6$. Double-layer data are those for NaF.

be simplified by replacing the function, ln tanh $(f\phi/4)$, by its Taylor's series expansion about $\phi = \phi_2$.

$$\ln \tanh (f\phi_r/4) = \ln \tanh (f\phi_2/4) + (f/2) \operatorname{csch} (f\phi_2/2)(\phi_r - \phi_2) - (f^2/8) \operatorname{csch} (f\phi_2/2) \coth (f\phi_2/2)(\phi_r - \phi_2)^2 + \ldots \tag{11}$$

When $(\phi_r - \phi_2) \ll (4/f) \tanh (f\phi_2/2)$, the function may be represented by the first two terms of the series, and eqn. (10) becomes:

$$\phi_r = \phi_2 - (2\kappa/f) \sinh (f\phi_2/2)(x_r - x_2) \tag{12}$$

The above condition will be fulfilled when ϕ_2 is greater than 100 mV and ϕ_r is close to ϕ_2. By the Gouy–Chapman theory, $\sinh (f\phi_2/2) = (\pi/2RT\varepsilon c)^{\frac{1}{2}} q$; furthermore, when the field in the inner layer is constant the charge on the electrode is given by the relationship, $q = \varepsilon_1(\phi_m - \phi_2)/4\pi x_2$ where ε_1 is the dielectric constant of the solvent in the inner layer. Equation (12) may then be written as

$$\phi_r = \phi_2 + (\varepsilon_1/\varepsilon)\lambda(\phi_m - \phi_2) \tag{13}$$

From the above, the rate constant expression valid in Case (iii) is

$$(\ln k)/f = (\ln k_o)/f - z\phi_2 + [\alpha n - (\varepsilon_1/\varepsilon)\lambda(\alpha n - z)](\phi_2 - \phi_m) \tag{14}$$

Thus, the slope of the corrected Tafel plot depends on the parameter, λ, the charge on the reacting species, and the ratio of the inner layer dielectric constant to that in the

bulk. When the reacting particle is in the diffuse layer in the transition state, it is probably strongly solvated so that its position with respect to the electrode as well as that of the double-layer cation will vary with electrode potential because of electrostriction. The expression for λ becomes:

$$\lambda = \lambda_o - (\beta_2 - \beta_r)(x_{ro}/2x_{2o}^2)q(\phi_m - \phi_2) \quad (15)$$

where β_2 and β_r are the compressibility constants of the inner region in the vicinities of the double-layer cation and reacting species, respectively. The parameter λ is negative as long as the reacting particle is in the diffuse layer. Its change in magnitude with potential depends on the sign of $\beta_2 - \beta_r$. The ratio $\varepsilon_1/\varepsilon$ decreases with increase in field in the inner layer[17]. Thus, the changes in the slope of the corrected Tafel plot with potential are reduced in magnitude but are much more complex than those found in Case (ii). The calculated variation in Tafel slope is shown in Fig. 2 for ε_1 calculated from the equations and parameters given by Macdonald and Barlow and β_r set equal to zero. The effect of ionic size is such that the smaller the ion, the larger is λ. Thus the departure of the Tafel slope from the "true" Tafel slope will increase with decrease in ionic size.

It has been assumed above that the transfer coefficient, α, is potential-independent. Current theories[18,19] predict that α depends on potential for simple electron transfer processes. Unfortunately, this effect cannot be included quantitatively in the case to be discussed since the electrode reaction involves the breaking of chemical bonds. However, it must be considered in drawing conclusions about the potential-dependence of the Tafel slope.

EXPERIMENTAL

Current–voltage curves for the reduction of peroxydisulphate anion in 0.01 *M* solutions of several alkali-metal fluorides and hydroxides were measured at a dropping mercury electrode. The apparatus, methods of reagent purification, and experimental technique were described previously[9]. The rate of charge transfer was calculated from the measured currents and drop times at 50-mV intervals using Koutecký's theory with corrections for electrode sphericity[9]. Double-layer data for the base electrolytes, NaF, CsF, and NaOH were taken from the tabulated results of Grahame and Payne*. Values of q as a function of ϕ_m for KF were estimated from the data of Grahame and Parsons[20] for KCl by using their calculated values of the potential drop across the inner layer in the absence of anion specific adsorption. In the case of LiF, similar data were calculated for values of electrode charge less than $-6\ \mu C\ cm^{-2}$ from Grahame's data[12] for the integral capacity of the inner layer for LiCl.

DISCUSSION

The effect of cation size on the kinetics of peroxydisulphate anion reduction was studied previously by Frumkin *et al.*[3]. The present results are in qualitative agreement with those obtained earlier. In the case where the base electrolyte was the same (NaF), good quantitative agreement was found. The results may be summarized as

* The author wishes to thank Dr. R. Parsons for supplying these data.

follows: (1) the rate of anion reduction at a given electrode potential increases with increase in cation atomic number; (2) the slope of corrected Tafel plots is not constant except when Cs^+ is the base electrolyte cation; (3) the curvature of these plots decreases with increase in cation atomic number; (4) for low values of $\phi_2 - \phi_m$, the Tafel slope increases with increase in cation atomic number; (5) at high values of $\phi_2 - \phi_m$, the slope of the corrected Tafel plots is constant and does not depend on cation size.

The above results are in agreement with the predictions of the model proposed for the case that the reacting particle is in the inner layer. The increase in rate of reduction and Tafel slope with cation atomic number are attributed to a corresponding decrease in the thickness of the inner layer. The large change in Tafel slope with $\phi_2 - \phi_m$ observed when Li^+, Na^+ and K^+ are the base electrolyte cations can be explained by a corresponding change in the inner layer thickness with field in this region, so that as the field increases the O.H.P. approaches the position of the reacting particle in the transition state. Furthermore, the constancy of the Tafel slope at high values of $\phi_2 - \phi_m$ is consistent with the model of the inner layer in which two regions are proposed, one of low dielectric constant adjacent to the electrode, and a region with a higher dielectric constant adjacent to the O.H.P. Thus, for this potential range, although the position of the reacting particle is changing with respect to the O.H.P., ϕ_r is approximately constant and equal to ϕ_2. In the case where Cs^+ is the base electrolyte cation, the reacting particle is in the region of high dielectric constant over the potential range considered. The slope of corrected Tafel plots in the limit of high $\phi_2 - \phi_m$ was 0.34 ± 0.02. This is in fair agreement with the value 0.30 ± 0.02 reported by Frumkin *et al.*[3].

The effect of electrostriction is clearly seen from the differential plots used to determine particle charge[9]. From eqn. (9), the following relationship holds for first differences:

$$\Delta[(\ln k)/f]/\Delta(\phi_2 - \phi_m) = [\alpha n - \lambda(\alpha n - z)] - z\,\Delta\phi_2/\Delta(\phi_2 - \phi_m) \qquad (15)$$

Plots of $\Delta[(\ln k)/f]/\Delta(\phi_2 - \phi_m)$ *vs.* $\Delta\phi_2/\Delta(\phi_2 - \phi_m)$ for kinetic data with the various base electrolyte cations are shown in Fig. 3. In the case of Cs^+, the plots are linear with a slope of 2 and y-intercept of 0.34 ± 0.02. For cations with lower atomic number the slope is 2 in the limit of low $\phi_2 - \phi_m$ but increases steadily as $\phi_2 - \phi_m$ increases. The y-intercept obtained from the straight lines drawn with slope 2 (Fig. 3) gives the value of the Tafel slope at the e.c.m., $\alpha n - \lambda_o(\alpha n - z)$. This intercept increases with increase in cation atomic number thus confirming that λ_o increases, *i.e.*, the inner layer thickness decreases with increase in cation atomic number.

Frumkin *et al.* accounted for the cation effect by assuming that alkali-metal cations are specifically adsorbed at cathodic potentials in the order, $Cs^+ > K^+ > Na^+ > Li^+$. The curvature in the corrected Tafel plots was attributed to specific adsorption of $S_2O_8^{2-}$ at low cathodic potentials. These proposals do not seem to be substantiated by the differential plots. In the presence of specific adsorption the specifically adsorbed charge, q_{sa}, must be known[21] in order to calculate ϕ_2; q_{sa} does not vary simply with the charge on the metal so that if this fact is ignored in estimating ϕ_2, the calculated ϕ_2 will not be simply related to the true value. Thus, in the case of Cs^+ where it is proposed that the greatest amount of cation specific adsorption occurs, the above differential plot would not be expected to the linear since ϕ_2 was calculated with the assumption that no specific adsorption was present. Furthermore, the appro-

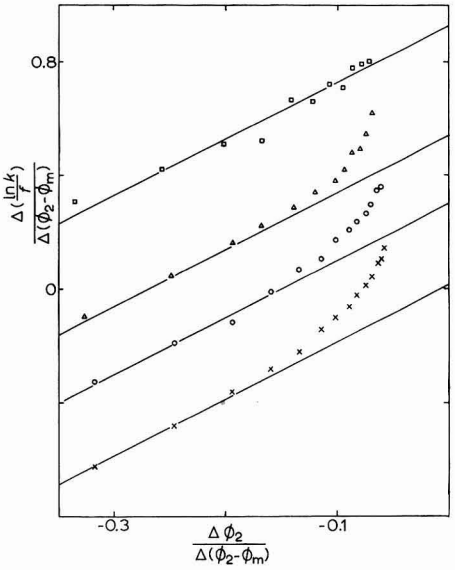

Fig. 3. Differential plots of kinetic data for the reduction of $5 \cdot 10^{-4}$ *M* peroxydisulphate anion on mercury with 0.01 *M* base electrolytes: (×), LiF; (○), NaOH; (△), KF; (□), CsF. The ordinate scale is correct for LiF; for the sake of clarity it has been shifted vertically for the NaOH, KF, and CsF data by 0.2, 0.4 and 0.6 units, respectively.

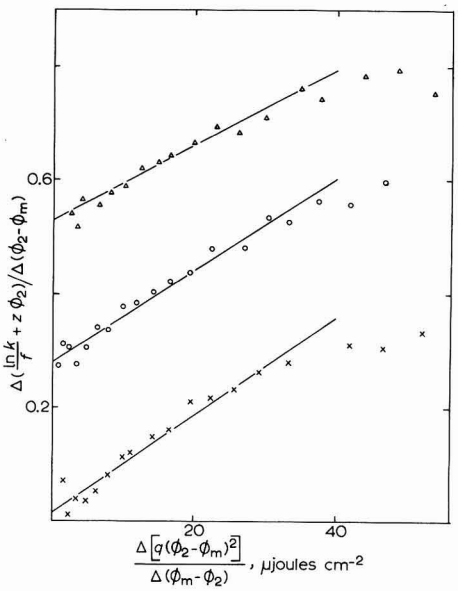

Fig. 4. Plot of change in Tafel slope *vs.* change in electrostrictive pressure in the inner layer for peroxydisulphate kinetic data with 0.01 *M* base electrolytes: (×), LiF; (○), NaOH; (△), KF. The ordinate scale is correct for LiF; for the sake of clarity it has been shifted vertically for the NaOH and KF data by 0.2 and 0.4 units, respectively.

ximate linearity of the differential plots for low cathodic potentials would indicate that specific adsorption of $S_2O_8^{2-}$ is not important; if it were important, the kinetic parameters would be expected to change in this region where the amount of specifically adsorbed reactant is changing with potential. Frumkin *et al.* presented arguments that the reacting particle is at, or very close to, the O.H.P. in the transition state; these arguments were based on a comparison of kinetic data obtained at a dropping thallium amalgam electrode with those for a dropping mercury electrode with KCl as base electrolyte. Corrected Tafel plots of the two sets of data were almost coincident when the electrode potential was expressed with respect to a constant reference electrode; however, the slope of the corrected Tafel plot for the data on the thallium amalgam electrode was lower than that for the mercury electrode at the same potential. Near coincidence of the corrected Tafel plots would indicate that the reacting particle is at, or very near, the O.H.P. if it is assumed that the position of the reacting particle with respect to the O.H.P. does not change with potential. By the model presented here this assumption is not valid. In terms of this model, when the electrode potential is expressed on the rational scale, corrected Tafel plots for the first system would be shifted vertically from those for mercury by a constant equal to the difference in $(\ln k_0)/f$ for the two systems. Examination of the data of Frumkin *et al.* shows that these predictions appear to be fulfilled.

According to the above model, the double-layer parameters, x_{2o} and x_{ro}, may be determined by relating the curvature of the corrected Tafel plots to the electrostrictive pressure in the inner layer. From eqns. (6) and (9), the following relationship holds for first differences:

$$\Delta[(\ln k)/f + z\phi_2]/\Delta(\phi_2 - \phi_m) = \alpha n - \lambda_o(\alpha n - z) + (\alpha n - z)\sigma\,\Delta[q(\phi_2 - \phi_m)^2]/\Delta(\phi_m - \phi_2) \quad (17)$$

Plots of the change in Tafel slope *versus* the change in electrostrictive pressure are shown in Fig. 4. The relationship between these variables appears to be linear for values of $\Delta[q(\phi_2 - \phi_m)^2]/\Delta(\phi_m - \phi_2)$ less than 40 μJ cm^{-2}. The best straight line was drawn through these points in the following fashion. The slope and intercept together with the correlation coefficient, r, were calculated by the method of least squares[22] for the first 10 values of the abscissa and ordinate variables

$$\Delta[q(\phi_2 - \phi_m)^2]/\Delta(\phi_m - \phi_2) < 20\ \mu\text{J cm}^{-2}.$$

This calculation was repeated adding one point at a time. The parameters of the best straight line were chosen for the condition that r be a maximum. The results are summarized in Table 1.

TABLE 1

Double layer cation	$\alpha n - \lambda_o(\alpha n - z)$	$\sigma(\alpha n - z)\cdot 10^3$ ($cm^2\ \mu J^{-1}$)	x_{ro}/x_{2o}	x_{2o} (Å)	$\beta \cdot 10^{10}$ ($cm^3\ \mu J^{-1}$)
Li^+	0.011 ± 0.007	9.1 ± 0.3	0.859	2.20	2.0
Na^+	0.077 ± 0.008	8.3 ± 0.1	0.888	2.13	1.7
K^+	0.140 ± 0.010	6.2 ± 0.3	0.915	2.07	1.2

Using the value of the limiting Tafel slope, αn, the ratio of the distance of closest approach of the reacting species to that of the double-layer cation at the e.c.m. may be calculated. Furthermore, if the compressibility constant for the inner layer is known, these distances may be determined individually. From their detailed analysis of the cathodic properties of the inner layer for aqueous NaF solutions, Macdonald and Barlow[17] assigned a value to β of $1.7 \cdot 10^{10}$ cm^3 μJ^{-1}. Using this value, x_{ro} and x_{2o} for Na^+ were calculated. Assuming that x_{ro} does not vary with the nature of the cation at the O.H.P., values of x_{2o} and β for the other cations were calculated using eqns. (18) and (19). The values of x_{2o} given in Table 1 are low in comparison with other estimates of the thickness of the inner layer[23,24] which assign to it a value of the order of 5 Å. This is interpreted as further evidence for an inner layer model with two different dielectric regions; x_{2o} is then a measure of the thickness of the region of low dielectric

$$\alpha n + \lambda_o(\alpha n - z) - z = (\alpha n - z)x_{ro}/x_{2o} \quad (18)$$

$$(1 - \lambda_o)/\sigma = 2x_{2o}/\beta \quad (19)$$

constant (x_{1o} as defined above). It is evident from the reported values of the ratio, x_{ro}/x_{2o}, and of x_{2o} itself, that small differences in the distances of closest approach lead to large differences in reaction rates. It is interesting to note that the compressibility constant for the inner layer decreases with increase in cation atomic number. This undoubtedly reflects the differences in packing of the water molecules adjacent to the electrode and those in the primary solvation sheath of the cation, and the change in the number of water molecules in the inner layer due to the change in cation solvation.

The quantitative relationship between the corrected Tafel plot curvature and the electrostriction effect is further demonstrated in Fig. 5. The values of $(\alpha n - z)\sigma$

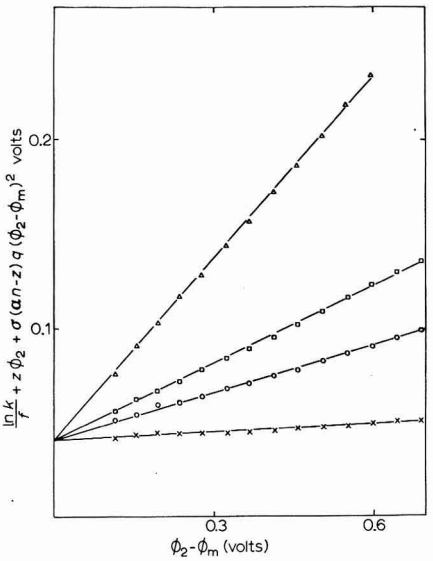

Fig. 5. Tafel plots for peroxydisulphate kinetic data corrected for the double effects described in the text. Base electrolytes: (×), 0.01 *M* LiF; (○), 0.01 *M* NaOH; (□), 0.01 *M* KF; (△), 0.01 *M* CsCl.

used in calculating the ordinate variable were those recorded in Table 1 with a value of 0 assigned for Cs^+. The rate constant at the e.c.m. is thereby determined to be 4.7 ± 0.7 cm sec^{-1} $((\ln k_o)/f = 0.040 \pm 0.004$ volts).

The quantitative aspects of the above analysis are somewhat tentative in that variation of the transfer coefficient, α, with potential cannot be included in the calculations. According to the theory of Marcus[18], α is a linear function of the overpotential for simple electrode reactions. This prediction was confirmed by Parsons and Passeron[26] for the reaction, $Cr^{3+} + e \rightleftharpoons Cr^{2+}$. The variation of the relative distances of closest approach of the reacting species and the double-layer cation (in this case, Na^+) was not considered by these authors. It is probably unimportant here since the strongly solvated ion Cr^{3+} would be expected to be in the inner layer region of high dielectric constant or in the diffuse layer during electron transfer. Thus, variation in Tafel slope due to electrostriction would be negligible. The fact that the Tafel slope is constant over part of the potential range in the case of peroxydisulphate anion reduction suggests that variation of the transfer coefficient with potential is unimportant for this type of reaction.

ACKNOWLEDGEMENTS

The author wishes to thank Mr. Y. C. Kuo Lee for his assistance with the experimental work and the Institute of Computer Science, University of Guelph for the use of their facilities. The financial assistance of the National Research Council of Canada is gratefully acknowledged.

SUMMARY

A model is proposed to account for the anomalous effect of cations on the kinetics of electrode reactions. This phenomenon is attributed to variation in the distance of closest approach to the electrode for the predominate cation in the double layer with both the cation's solvated radius and the field in the inner layer. It is shown that the predictions of the model quantitatively account for the cation effect observed in the reduction of peroxydisulphate anion.

REFERENCES

1 For a review see P. DELAHAY, *Double Layer and Electrode Kinetics*, Wiley–Interscience, New York, 1965, chap. 9.
2 A. N. FRUMKIN, *Advan. Electrochem. Electrochem. Eng.* 1 (1961) 65.
3 A. N. FRUMKIN, O. A. PETRY AND N. V. NIKOLAEVA-FEDOROVICH, *Electrochim. Acta*, 8 (1963) 177.
4 L. GIERST, L. VANDENBERGEN, E. NICOLAS AND A. FRABONI, *J. Electrochem. Soc.*, 113 (1966) 1025.
5 L. GIERST, *Transactions of the Symposium on Electrode Processes, Philadelphia, May 1959*, edited by E. YEAGER, Wiley, New York, 1961, p. 109.
6 K. ASADA, P. DELAHAY AND A. K. SUNDARAM, *J. Am. Chem. Soc.*, 83 (1961) 3396.
7 A. ARAMATA AND P. DELAHAY, *J. Phys. Chem.*, 68 (1964) 880.
8 H. D. HURWITZ, A. SANFELD AND A. STEINCHEN-SANFELD, *Electrochim. Acta*, 9 (1964) 929.
9 W. R. FAWCETT, J. E. KENT AND Y. C. KUO LEE, *J. Electroanal. Chem.*, 20 (1969) 357.
10 J. R. MACDONALD, *J. Chem. Phys.*, 22 (1954) 1857.
11 N. F. MOTT, R. PARSONS AND R. J. WATTS-TOBIN, *Phil. Mag.*, 7 (1962) 483.
12 D. C. GRAHAME, *J. Electrochem. Soc.*, 98 (1951) 343.
13 C. B. MONK, *Electrolytic Dissociation*, Academic Press, New York, 1961, p. 271.
14 R. PARSONS, *Ann. Rep. Progr. Chem. (Chem. Soc. London)*, 61 (1964) 80.
15 J. O'M. BOCKRIS, M. A. V. DEVANATHAN AND K. MULLER, *Proc. Roy. Soc. London, Ser. A*, 274 (1963) 55.
16 R. PARSONS, *Advan. Electrochem. Electrochem. Eng.*, 1 (1961) p. 1.
17 J. R. MACDONALD AND C. A. BARLOW, *J. Chem. Phys.*, 36 (1962) 3062.
18 R. A. MARCUS, *Ann. Rev. Phys. Chem.*, 15 (1964) 155.
19 V. G. LEVICH, *Advan. Electrochem. Electrochem. Eng.*, 4, (1966) 249.
20 D. C. GRAHAME AND R. PARSONS, *J. Am. Chem. Soc.*, 83 (1961) 1291.
21 Ref. 1, chap. 4.
22 J. F. KENNEY AND E. S. KEEPING, *Mathematics of Statistics*, Part 1, Van Nostrand, Princeton, 3rd ed. 1954, chap. XV.
23 J. R. MACDONALD AND C. A. BARLOW, *Proc. First Australian Conference on Electrochemistry, Sydney, February 1963*, Pergamon Press, London, 1964, p. 199.
24 R. PARSONS AND F. G. R. ZOBEL, *J. Electroanal. Chem.*, 9 (1965) 333.
25 R. PARSONS AND E. PASSERON, *J. Electroanal. Chem.*, 12 (1966) 524.

ELECTROANALYTICAL CHEMISTRY AND INTERFACIAL ELECTROCHEMISTRY
Elsevier Sequoia S.A., Lausanne – Printed in The Netherlands

ON THE NEGATIVE FARADAIC ADMITTANCE IN THE REGION OF THE POLAROGRAPHIC MINIMUM OF In(III) IN AQUEOUS NaSCN SOLUTION

R. DE LEVIE AND A. A. HUSOVSKY
Chemistry Department, Georgetown University, Washington, D.C. 20007 (U.S.A.)
(Received January 25th, 1969)

1. INTRODUCTION

The polarographic wave of In(III) exhibits a curious minimum in several aqueous electrolyte solutions. The occurrence of such a minimum was first reported by Lingane[1], and was confirmed subsequently by several authors[2,3]. This minimum has been the subject of some recent papers[4-14]. It is observed with halides[1-3], tartrate[2], oxalate[3], thiocyanate[4,5,7] as well as with several organic sulphur and nitrogen compounds[12]. The minimum cannot be ascribed to electrostatic repulsion in the double layer, since it is observed even in concentrated solutions.

Cozzi and Vivarelli[2] concluded that the minimum resulted from the gradual desorption of anions at increasingly negative electrode potentials. Bulovová[3] invoked electron conduction by polarizable anions in conjunction with an assumed one-electron reduction of In(III) followed by stepwise dismutation of the resulting In(II). Brainina[6] also suggested that ligand bridging was involved in the reversible polarographic wave of In(III) in the presence of halides. However, in a subsequent paper[7], she apparently abandoned that interpretation in favor of a model involving specific adsorption in two different orientations. We have found no evidence for adsorption of any In(III) species in the potential region of the minimum.

Shirai[4,5] noted that the corresponding a.c. polarogram shows a negative admittance. Tanaka *et al.*[8,9] indicated how such a negative faradaic admittance could be understood as a result of a decrease in reduction rate with increasingly negative potentials.

In the present paper we report on the quantitative correlation between faradaic admittance and polarographic current, which confirms the qualitative considerations of Tanaka *et al.*[8,9] as to the origin of the negative faradaic impedance. To this end, we will first derive the necessary mathematical relations. An unsuccessful attempt in the latter direction has recently been made by Sluyters *et al.*[13], whose derivation is needlessly complicated by the *a priori* introduction of parameters like k_{sh} and α, of which the physical significance in the present case is even more vague than usual.

2. GENERAL EXPRESSION FOR THE FARADAIC ADMITTANCE

It is often convenient first to derive a relation between local concentrations at the electrode surface and the resulting mass fluxes. Such a relation depends only

on the laws of mass transport, not on the specific boundary conditions imposed by the kinetics of the electrode reactions. The results so obtained can subsequently be plugged into relations between surface properties only, directly yielding the electrode admittance. This procedure, and also the specific result derived below, does not apply in the case of appreciable coupling[15] between mass transport and thermodynamics, *i.e.*, whenever one or more surface excesses of reacting species are strongly time-dependent, as in the case of strong specific adsorption of reactants or products. We will assume that such a complication is absent.

The theoretical investigations of Matsuda[16] indicate that the expansion of a growing mercury droplet has a much smaller effect on the electrode admittance than it has on the polarographic current, and that the drop expansion may be neglected for all but the lowest frequencies. The calculations of Gerischer[17] show that, under these same circumstances, the curvature of the dropping mercury electrode has a negligible effect on the admittance. Thus we will use laws of plane diffusion for the frequency-dependent part of mass transport. We will make the related assumption that all transient terms containing the fundamental frequency have died out sufficiently near the end of drop life so as to be negligible. Thus we have:

$$\frac{\partial c}{\partial t} = D\,\frac{\partial^2 c}{\partial x^2} \tag{1}$$

$$c(0, t) = c' + c'' \sin \omega t \tag{2}$$

$$c(\infty, t) = c^* \tag{3}$$

where the average surface concentration, c', may still be a function of time, t, but not at the angular frequency, ω. Writing $u \equiv c - c^*$ and applying the Laplace transform yields:

$$p\bar{u} = D\,\frac{\mathrm{d}^2 \bar{u}}{\mathrm{d}x^2} \tag{4}$$

$$\bar{u}(0, p) = (c' - c^*)/p + c''\omega/(p^2 + \omega^2) \tag{5}$$

where

$$\bar{u} \equiv \int_0^\infty u \exp[-pt]\,\mathrm{d}t \tag{6}$$

Thus we find the Laplace-transformed solution

$$\bar{u}(x, p) = \bar{u}(0, p) \exp\left[-x(p/D)^{\frac{1}{2}}\right] \tag{7}$$

$$-D\left(\frac{\mathrm{d}\bar{u}}{\mathrm{d}x}\right)_{x=0} = (c' - c^*)\left(\frac{D}{p}\right)^{\frac{1}{2}} + \frac{c''\omega(pD)^{\frac{1}{2}}}{p^2 + \omega^2} \tag{8}$$

Inverse transformation of the first term on the right-hand side of eqn. (8) yields the transient term, $(c' - c^*)(D/\pi t)^{\frac{1}{2}}$, which does not contain any components of frequency, ω. Inverse transformation of the second term on the right-hand side of eqn. (8) is much more involved. However, the steady-state harmonic components of $D(\partial u/\partial x)_{x=0}$ at the frequency, ω, are simply given[18] by the sum of the residues of eqn. (8) at the poles, $p = \pm j\omega$. We obtain for the residue at $p = j\omega$:

$$c''\omega D^{\frac{1}{2}}\left\{\frac{(p-j\omega)p^{\frac{1}{2}}\exp[pt]}{(p+j\omega)(p-j\omega)}\right\}_{p=j\omega} = c''(\omega D)^{\frac{1}{2}}\frac{j^{\frac{1}{2}}\exp[j\omega t]}{2j} =$$

$$= c''(\tfrac{1}{2}\omega D)^{\frac{1}{2}}\frac{(j+1)\exp[j\omega t]}{2j} \tag{9}$$

The residue at $p=-j\omega$ yields likewise

$$c''(\tfrac{1}{2}\omega D)^{\frac{1}{2}}(j-1)\exp[-j\omega t]/2j \tag{10}$$

so that

$$-D\left(\frac{\partial c}{\partial x}\right)_{x=0} = -D\left(\frac{\partial u}{\partial x}\right)_{x=0} = c''(\tfrac{1}{2}\omega D)^{\frac{1}{2}}\left\{\frac{(j+1)\exp[j\omega t]}{2j} + \right.$$

$$\left. + \frac{(j-1)\exp[-j\omega t]}{2j}\right\} + \text{transient terms} = \tag{11}$$

$$= c''(\tfrac{1}{2}\omega D)^{\frac{1}{2}}\{\sin\omega t+\cos\omega t\} + \text{transient terms}$$

Equation (11) is the required relation* between mass flux and surface concentrations. We must now consider the additional requirements imposed by the electrode kinetics. For a redox reaction of the type:

$$O \rightleftharpoons R + ne^- \tag{12}$$

we have for the mass flux at the electrode surface, $x=0$,

$$D_R\left(\frac{\partial c_R}{\partial x}\right)_{x=0} = -D_O\left(\frac{\partial c_O}{\partial x}\right)_{x=0} = \vec{k}c_R(0,t) - \overleftarrow{k}c_O(0,t) \tag{13}$$

where $\vec{k}$ and $\overleftarrow{k}$ are the rate constants for oxidation and reduction, respectively. Furthermore, we have for plane or expanding plane diffusion[19,20]:

$$c_R(0,t) + \delta c_O(0,t) = c_R^* + \delta c_O^* \equiv c^* \tag{14}$$

$$\delta \equiv (D_O/D_R)^{\frac{1}{2}} \tag{15}$$

so that eqn. (13) can be rewritten in terms of either c_R or c_O, *e.g.*,

$$-D_O\left(\frac{\partial c_O}{\partial x}\right)_{x=0} = \vec{k}c^* - (\vec{k}\delta + \overleftarrow{k})c_O(0,t) \tag{16}$$

For an applied potential

$$E+\varepsilon\sin\omega t \tag{17}$$

with sufficiently small amplitude, ε, of its sinusoidal component, the rate constants can be linearised over the small interval, $E-\varepsilon$ to $E+\varepsilon$, as

$$k+(\partial k/\partial E)\varepsilon\sin\omega t\,. \tag{18}$$

We now rewrite eqns. (2) and (11) with the inclusion of an arbitrary phase angle, φ

$$c_O(0,t) = c_O' + c_O''\sin(\omega t-\varphi) \tag{19}$$

$$-D_O(\partial c_O/\partial x)_{x=0} = c_O''(\tfrac{1}{2}\omega D_O)^{\frac{1}{2}}\{\sin(\omega t-\varphi)+\cos(\omega t-\varphi)\} \tag{20}$$

* See E. Warburg, *Ann. Physik. Chem.*, (3) 67 (1899) 493. The complete solution, including the transient term, is given in ref. 18 for the equivalent heat conduction problem.

Substituting eqns. (18)–(20) into eqn. (16) and collecting terms in ω yields:

$$c''_{\mathrm{O}}(\tfrac{1}{2}\omega D_{\mathrm{O}})^{\frac{1}{2}}\{\sin(\omega t-\varphi)+\cos(\omega t-\varphi)\} = \frac{\partial \vec{k}}{\partial E}c^{*}\varepsilon \sin \omega t +$$

$$-(\vec{k}\delta+\overleftarrow{k})c''_{\mathrm{O}}\sin(\omega t-\varphi) - \frac{\partial(\vec{k}\delta+\overleftarrow{k})}{\partial E}c'_{\mathrm{O}}\varepsilon \sin \omega t \tag{21}$$

Using the trigonometric relations:

$$\sin(\alpha \pm \arctan \beta) = (\beta^2+1)^{-\frac{1}{2}}(\sin \alpha \pm \beta \cos \alpha) \tag{22}$$

$$\cos(\alpha \pm \arctan \beta) = (\beta^2+1)^{-\frac{1}{2}}(\cos \alpha \mp \beta \sin \alpha) \tag{23}$$

and collecting terms in $\sin \omega t$ and $\cos \omega t$ separately, we obtain

$$c''_{\mathrm{O}}(\tfrac{1}{2}\omega D_{\mathrm{O}})^{\frac{1}{2}}\frac{1+\tan\varphi}{(1+\tan^2\varphi)^{\frac{1}{2}}} = \frac{\partial \vec{k}}{\partial E}c^{*}\varepsilon - \frac{\partial(\vec{k}\delta+\overleftarrow{k})}{\partial E}c'_{\mathrm{O}}\varepsilon - \frac{(\vec{k}\delta+\overleftarrow{k})c''_{\mathrm{O}}}{(1+\tan^2\varphi)^{\frac{1}{2}}} \tag{24}$$

$$c''_{\mathrm{O}}(\tfrac{1}{2}\omega D_{\mathrm{O}})^{\frac{1}{2}}\frac{1-\tan\varphi}{(1+\tan^2\varphi)^{\frac{1}{2}}} = (\vec{k}\delta+\overleftarrow{k})\,c''_{\mathrm{O}}\frac{\tan\varphi}{(1+\tan^2\varphi)^{\frac{1}{2}}} \tag{25}$$

Excluding the trivial solution, $c''_{\mathrm{O}}=0$, eqn. (25) yields

$$\tan\varphi = (1+2\zeta)^{-1} \tag{26}$$

$$\zeta \equiv \vec{k}/(2\omega D_{\mathrm{R}})^{\frac{1}{2}} + \overleftarrow{k}/(2\omega D_{\mathrm{O}})^{\frac{1}{2}} \tag{27}$$

and substitution of eqn. (26) into eqn. (24) yields:

$$c''_{\mathrm{O}} = \frac{\varepsilon\left\{(c^{*}-c'_{\mathrm{O}}\delta)\dfrac{\partial\vec{k}}{\partial E} - c'_{\mathrm{O}}\dfrac{\partial\overleftarrow{k}}{\partial E}\right\}}{(2\zeta^2+2\zeta+1)^{\frac{1}{2}}(\omega D_{\mathrm{O}})^{\frac{1}{2}}} = \frac{\varepsilon\left\{c'_{\mathrm{R}}\dfrac{\partial\vec{k}}{\partial E} - c'_{\mathrm{O}}\dfrac{\partial\overleftarrow{k}}{\partial E}\right\}}{(2\zeta^2+2\zeta+1)^{\frac{1}{2}}(\omega D_{\mathrm{O}})^{\frac{1}{2}}} \tag{28}$$

Thus, we find for the component of the faradaic current at the frequency, ω

$$-nFAD_{\mathrm{O}}\left(\frac{\partial c_{\mathrm{O}}}{\partial x}\right)_{x=0} = nFAc''_{\mathrm{O}}(\tfrac{1}{2}\omega D_{\mathrm{O}})^{\frac{1}{2}}\{\sin(\omega t-\varphi)+\cos(\omega t-\varphi)\}$$

$$= nFA\varepsilon\frac{(\zeta+1)\sin\omega t+\zeta\cos\omega t}{2\zeta^2+2\zeta+1}\left\{c'_{\mathrm{R}}\frac{\partial\vec{k}}{\partial E} - c'_{\mathrm{O}}\frac{\partial\overleftarrow{k}}{\partial E}\right\} \tag{29}$$

so that the in-phase and quadrature components of the faradaic admittance, Y'_{F} and Y''_{F}, are given by:

$$Y'_{\mathrm{F}} = nFA\frac{\zeta+1}{2\zeta^2+2\zeta+1}\left\{c'_{\mathrm{R}}\frac{\partial\vec{k}}{\partial E} - c'_{\mathrm{O}}\frac{\partial\overleftarrow{k}}{\partial E}\right\} \tag{30}$$

$$Y''_{\mathrm{F}} = nFA\frac{\zeta}{2\zeta^2+2\zeta+1}\left\{c'_{\mathrm{R}}\frac{\partial\vec{k}}{\partial E} - c'_{\mathrm{O}}\frac{\partial\overleftarrow{k}}{\partial E}\right\} \tag{31}$$

Alternatively, we can express the faradaic admittance in terms of its amplitude, $|Y_{\mathrm{F}}|$, and phase angle, ϕ

$$|Y_{\mathrm{F}}| = \{|Y'_{\mathrm{F}}|^2+|Y''_{\mathrm{F}}|^2\}^{\frac{1}{2}} = \frac{nFA}{(2\zeta^2+2\zeta+1)^{\frac{1}{2}}}\left\{c'_{\mathrm{R}}\frac{\partial\vec{k}}{\partial E} - c'_{\mathrm{O}}\frac{\partial\overleftarrow{k}}{\partial E}\right\} \tag{32}$$

$$\tan \phi = Y''_F/Y'_F = \zeta/(\zeta+1) \tag{33}$$

Note that eqns. (30)–(33) do not pre-suppose any specific dependence of rate constants on potential, and that the amplitude, but not the phase angle, depends on the "d.c." surface concentrations, c'_R and c'_O. To calculate the latter, one can use, for example, the theory of expanding plane diffusion according to the Ilkovič differential equation[21], as given by Meiman[22], Koutecký[23] and Matsuda and Ayabe[24], or one of several approximate analytical expressions[24-26] for the latter. We will use here the simple approximation:

$$\frac{i}{i_{rev}} = F(\chi) \approx \frac{\chi}{1+\chi} \tag{34}$$

$$\chi \equiv \left(\frac{\vec{k}}{(D_R)^{\frac{1}{2}}} + \frac{\overleftarrow{k}}{(D_O)^{\frac{1}{2}}}\right)\left(\frac{12t}{7}\right)^{\frac{1}{2}} = \zeta\left(\frac{24\omega t}{7}\right)^{\frac{1}{2}} \tag{35}$$

which is sufficiently accurate for most purposes, since $\chi/(1+\chi)$ tracks $F(\chi)$ to within ± 0.025, see Fig. 1. Furthermore, we will restrict the application of eqns. (30)–(33) to

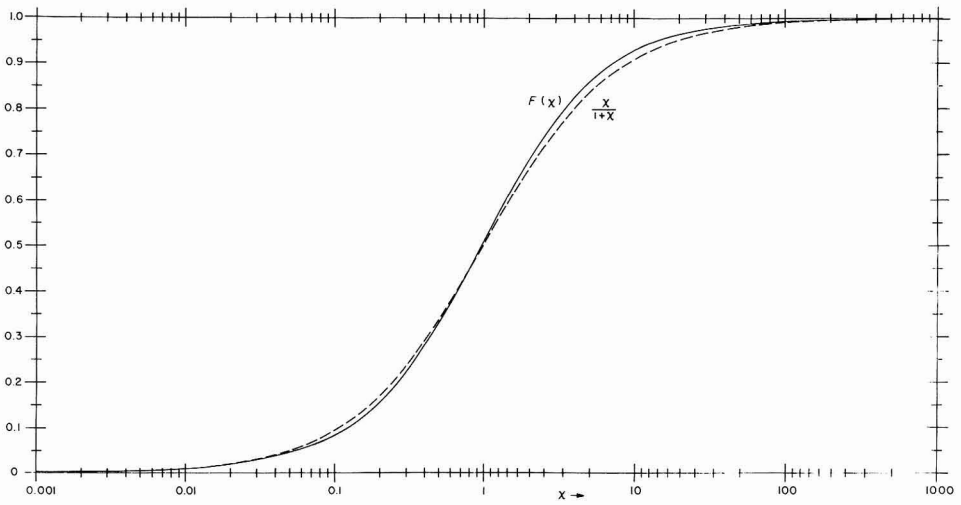

Fig. 1. The Koutecký function, $F(\chi)$, and its approximation by $\chi/(1+\chi)$, eqn. (34), both plotted as a function of log χ. For any given value of χ, the value for i/i_l from $\chi/(1+\chi)$ does not differ by more than ± 0.025 from that calcd. from $F(\chi)$. The reverse process, the calcn. of χ from i/i_l using the approximation eqn. (34) is less precise: for $i/i_l \leqslant 0.7$, the resulting error in χ is at most $\pm 10\%$. For $i/i_l > 0.7$, the error is even larger, up to about 30% near $i/i_l = 0.95$. However, there even the use of $F(\chi)$ does not lead to very precise values of χ in view of the exptl. inaccuracies in i and i_l.

the special case discussed in this paper, *viz*, the faradaic admittance in the region of the polarographic minimum of In(III) in aqueous solutions containing thiocyanate ions.

At potentials where the minimum occurs, there is no difference between a polarogram of mercury in 1 *M* NaSCN or that of indium amalgam in the same solution, see Fig. 2, showing unambiguously that the oxidation reaction rate at these potentials is completely negligible: $\vec{k} = 0$. Thus, eqns. (27), (30) and (31) reduce to:

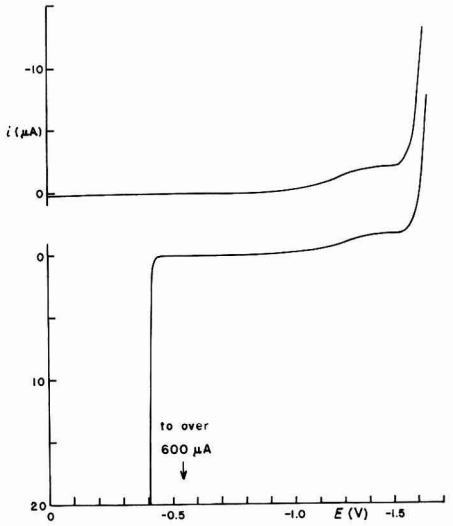

Fig. 2. Polarogram of 1 *M* NaSCN on mercury (top) and that of the same soln. on about 1% (w/w) of indium amalgam (bottom). The curves clearly demonstrate that there is no measurable oxidation in the region of the polarographic minimum, between −0.8 and −1.3 V *vs.* internal Ag/AgSCN, used in this and all subsequent Figures.

$$\zeta = \overleftarrow{k}/(2\omega D_O)^{\frac{1}{2}} \tag{36}$$

$$Y'_F = -nFAc'_O \frac{\zeta+1}{2\zeta^2+2\zeta+1} \frac{\partial \overleftarrow{k}}{\partial E} = -nFAc'_O(2\omega D_O)^{\frac{1}{2}} \frac{\zeta+1}{2\zeta^2+2\zeta+1} \frac{\partial \zeta}{\partial E} \tag{37}$$

$$Y''_F = -nFAc'_O \frac{\zeta}{2\zeta^2+2\zeta+1} \frac{\partial \overleftarrow{k}}{\partial E} = -nFAc'_O(2\omega D_O)^{\frac{1}{2}} \frac{\zeta}{2\zeta^2+2\zeta+1} \frac{\partial \zeta}{\partial E} \tag{38}$$

Furthermore, we have

$$i = nFA(c'_R \overrightarrow{k} - c'_O \overleftarrow{k}) = -nFAc'_O \overleftarrow{k} = -nFAc'_O \zeta (2\omega D_O)^{\frac{1}{2}} \tag{39}$$

$$i_{rev} = i_l = -nFAc^*_O(7D_O/3\pi t)^{\frac{1}{2}} \tag{40}$$

where i_l is the limiting reduction current. Equation (39) enables us to eliminate c'_O from eqns. (37) and (38):

$$Y'_F = \{i(\zeta+1)/\zeta(2\zeta^2+2\zeta+1)\}(\partial\zeta/\partial E) \tag{41}$$

$$Y''_F = \{i/(2\zeta^2+2\zeta+1)\}(\partial\zeta/\partial E) \tag{42}$$

and eqns. (34) and (40) finally lead to

$$Y'_F \approx \frac{i_l(\zeta+1)}{\{\zeta+(7/24\omega t)^{\frac{1}{2}}\}\{2\zeta^2+2\zeta+1\}} \frac{\partial \zeta}{\partial E} \tag{43}$$

$$Y''_F \approx \frac{i_l \zeta}{\{\zeta+(7/24\omega t)^{\frac{1}{2}}\}\{2\zeta^2+2\zeta+1\}} \frac{\partial \zeta}{\partial E} \tag{44}$$

3. ANALYSIS OF EXPERIMENTAL DATA

We must first make sure that our calculations are applicable to the chemical

system studied. We have already demonstrated that the oxidation reaction can be neglected, and we will now show that no In(III) species is specifically adsorbed at the potentials of interest, *i.e.*, for $E \ll E_{\frac{1}{2}}$.

At frequencies of 300 Hz and higher, the quadrature component of the double-layer admittance of 1 *M* NaSCN is virtually independent of the presence or absence of 1 m*M* $In(SCN)_3$.

With 4.5 m*M* $In(SCN)_3$, the measured electrode capacitance at 500 Hz is actually slightly higher than that of 1 *M* NaSCN, see Fig. 6, as a result of the difference in surface tension of mercury and indium amalgam[27,28] formed upon the reduction of In(III). Thus, we conclude that there is no measurable specific adsorption of In(III) at potentials negative of the polarographic wave. For $E > E_{\frac{1}{2}}$, the double-layer capacitance is significantly lowered by specific adsorption of In(III), as has already been reported by Sluyters *et al.*[14,29].

Drop-time measurements in up to 8.5 m*M* $In(SCN)_3$ solutions (again in 1 *M* NaSCN, pH $\approx$ 3.1) also exhibited the lowering of surface tension at potentials positive of $E_{\frac{1}{2}}$, as reported by Takahashi and Shirai[5], but failed to show any abrupt change in the region of the polarographic minimum (we have repeated these measurements many times, sometimes replacing $In(SCN)_3$ by $In(NO_3)_3$ and acidifying with HNO_3 instead of with HSCN, in order to make the solutions identical with those used by Takahashi and Shirai[5]). The measurements were made on an automatic drop-time meter built in this laboratory[30]. The solutions had been treated with activated charcoal, which does not remove any appreciable amount of In(III).

Again, we conclude that there is no indication of specific adsorption at $E \ll E_{\frac{1}{2}}$, so that we need not consider any coupling between faradaic and double-layer parameters. Thus we may write

$$Y''_{el} = Y''_{dl} + Y''_{F} \tag{45}$$

where el, dl and F denote electrode, double layer and faradaic, respectively. We will neglect the small effect of the presence of In(III) on the double-layer capacitance resulting from the formation of indium amalgam, and take Y''_{dl} from the double-layer capacitance data of the inert electrolyte in the absence of In(III) measured at the same low frequency. Using high-frequency data to obtain Y''_{dl} leads to virtually identical results.

In principle, ζ can be determined from the d.c. polarogram *via* eqns. (34), (35) and (40), which combine to

$$\frac{i}{i_l} = \frac{\zeta}{\zeta + (7/24\omega t)^{\frac{1}{2}}} \quad \text{or} \quad \zeta = \frac{i}{i_l - i}\left(\frac{7}{24\omega t}\right)^{\frac{1}{2}} \tag{46}$$

so that Y'_F and Y''_F can be computed directly from eqns. (43) and (44), respectively. Although eqn. (46) yields fairly precise values of ζ for $i/i_l \lesssim 0.7$, the calculation of the first derivative, $\partial\zeta/\partial E$, leads to rather large experimental uncertainty. We have, therefore, used an inverse procedure, which is less direct but involves an integration rather than a differentiation of experimental data. This procedure starts with the measured faradaic admittance and derives from it the shape of the d.c. polarogram. It uses the relation:

$$\zeta_2 = \zeta_1 + \int_1^2 \mathrm{d}\zeta = \zeta_1 + \int_{E_1}^{E_2} \frac{\partial\zeta}{\partial E}\,\mathrm{d}E = \zeta_1 + \frac{1}{i_l}\int_{E_1}^{E_2} b\,Y'_F\,\mathrm{d}E \tag{47}$$

$$b \equiv \frac{\{\zeta + (7/24\omega t)^{\frac{1}{2}}\}(2\zeta^2 + 2\zeta + 1)}{\zeta + 1} \tag{48}$$

As integration constant we have chosen the value of ζ derived from the d.c. polarogram (*via* eqn. (46)) at -1.06 V, *i.e.*, at the lowest point of the minimum. Using this

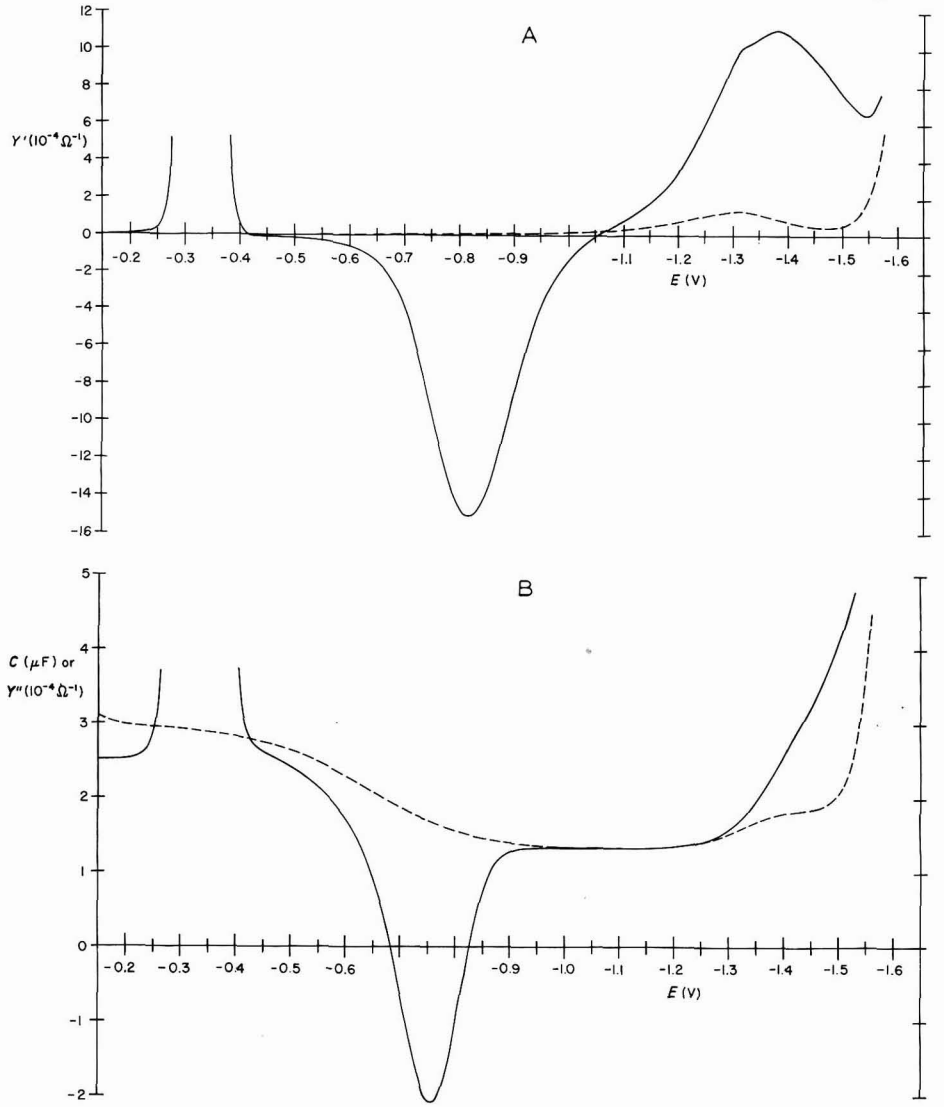

Fig. 3. The in-phase (a) and quadrature (b) components of the electrode admittance of 4.5 m*M* $In(SCN)_3$ in 1 *M* NaSCN acidified with HSCN to pH 3.22, measured at 16.4 Hz and 20 mV top-to-top (10 mV amplitude). The dashed line indicates the same components measured in the absence of In(III). Note the 4 times higher sensitivity used in (b). One of the common features of the faradaic admittance of irreversible processes is clearly visible, namely that the in-phase and quadrature components attain maximum values at different potentials. This can be noted for the hydrogen wave as well as for the negative and positive faradaic admittances of In(III) on either side of the polarographic minimum.

value as ζ_1, one can calculate a corresponding value b, and obtain ζ_2 by graphical or numerical integration. The value obtained for ζ_2 is then used to calculate a second estimate of b, leading to an improved estimate of ζ_2, etc. This iteration cycle was repeated until the successive calculations of ζ_2 did not differ by more than 0.00005, at which point ζ_2 was used to calculate ζ_3 by the same technique, etc. Calculations were initially performed by hand and later verified by computer. Usually, only two or three iterations were needed (and never more than ten) for integration intervals of 10 mV.

Figure 3 shows the measured electrode admittance of 4.5 m*M* $In(SCN)_3$ in 1 *M* NaSCN, acidified with HSCN to pH 3.22, at 25.0° and 16.4 Hz. Figure 4 gives the

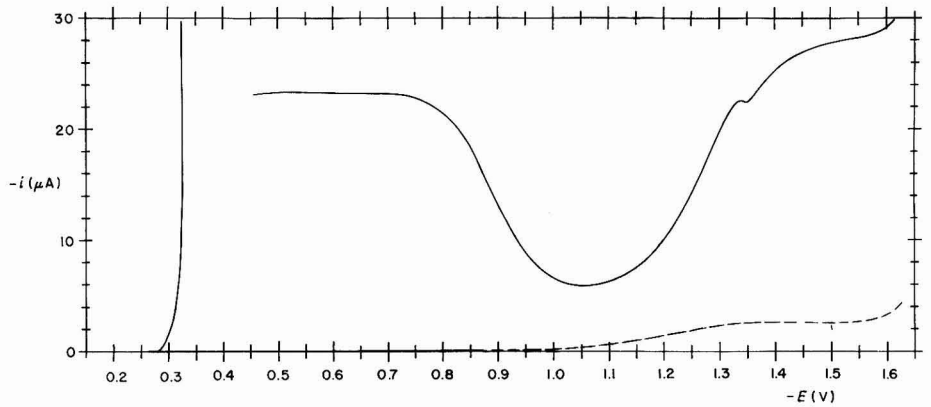

Fig. 4. Polarogram of 4.5 m*M* $In(SCN)_3$ in 1 *M* NaSCN acidified with HSCN to pH 3.22, measured in the same cell and with the same instrument as the admittance shown in Fig. 3. The data of Figs. 3 and 4 were used in the calcns. for Figs. 5 and 6.

d.c. polarogram, obtained on the same solution in the same cell and on the same instrument[31], using the same, mechanically controlled current sampling and drop-times.

From the in-phase component of the electrode admittance, Y'_F, values of ζ were calculated by the procedure outlined above for potentials between -0.78 and -1.42 V, see Fig. 5. All data used had been corrected first for the contributions of the hydrogen reduction to i and Y'_F. These contributions were only appreciable at potentials negative of -1.0 V. Subtraction is simply algebraic since our instrument directly yields the vector components of the electrode admittance. For the calculation of ζ we used $\zeta_1 = 0.0067_5$ at $E = -1.06$ V, and $i_1 = 23.2_4$ μA, both of which data had been taken from the d.c. polarogram. From the values of ζ so calculated over a rather wide range of potentials, the d.c. polarogram was reconstructed *via* eqn. (46). The result is shown in Fig. 6, and indicates agreement (certainly within the limits of validity of the approximate equation (46) used, *cf.* Fig. 1) between observed and calculated values for the d.c. polarographic current, i.

The only significant disagreement between the experimental and the calculated d.c. polarograms is at rather negative potentials. In this region, the d.c. polarogram exhibits a slight maximum, which the computer calculations do not reproduce since our mathematical model does not allow for convective mass transport. However, not all of the disagreement around -1.3 V appears to be caused by this maximum. The

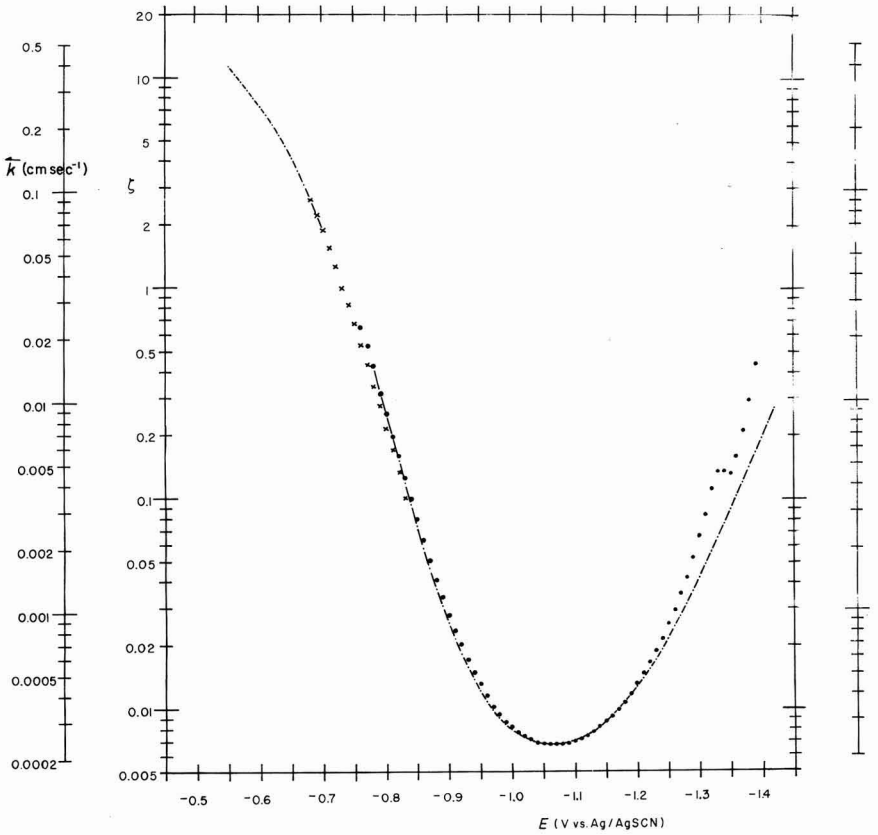

Fig. 5. Values of ζ calcd. from the data shown in Figs. 3 and 4. Corresponding values for the reduction rate constant, $\tilde{k}$, were obtained from eqn. (36) using $\omega = 104$ sec^{-1} and $D_O = 6 \cdot 10^{-6}$ cm^2 sec^{-1}. The following techniques were used: (●) from the d.c. polarogram using eqn. (46); (×) from the phase angle of the faradaic admittance, using eqn. (33); (----), from Y'_{el}, using an integration. From -0.55 to -0.70 V, eqn. (50) was used, and the integration constant was obtained from phase angle measurements (×) as $\zeta = 1.90$ at -0.70 V. From -0.78 to -1.42 V, eqn. (47) was used, and the integration constant was obtained from the d.c. polarogram *via* eqn. (46) as $\zeta = 0.0067_5$ at -1.06 V.

limiting current of the d.c. polarogram in that region is somewhat higher than one would expect on the basis of the limiting current between -0.50 and -0.65 V plus the hydrogen reduction current of the inert electrolyte. The reason for this slight discrepancy is not yet quite understood. It may possibly be related to the simultaneous reduction of hydrogen ions and the consequent increase in the local pH at the electrode surface and/or to the effect of amalgamated indium on the kinetics of the hydrogen reduction, making our baseline corrections inadequate. However, the computer calculations were based on the limiting current around -0.6 V and consequently cannot possibly reproduce a higher current.

It might be noted here that there is only a practical, not a fundamental reason for obtaining the integration constant for the calculation of ζ *via* eqn. (47) from the d.c. polarogram. In principle, ζ could be obtained from the ratio, Y''_F/Y'_F, around -0.8 V, see below, and the integration carried out from there. Such a procedure would

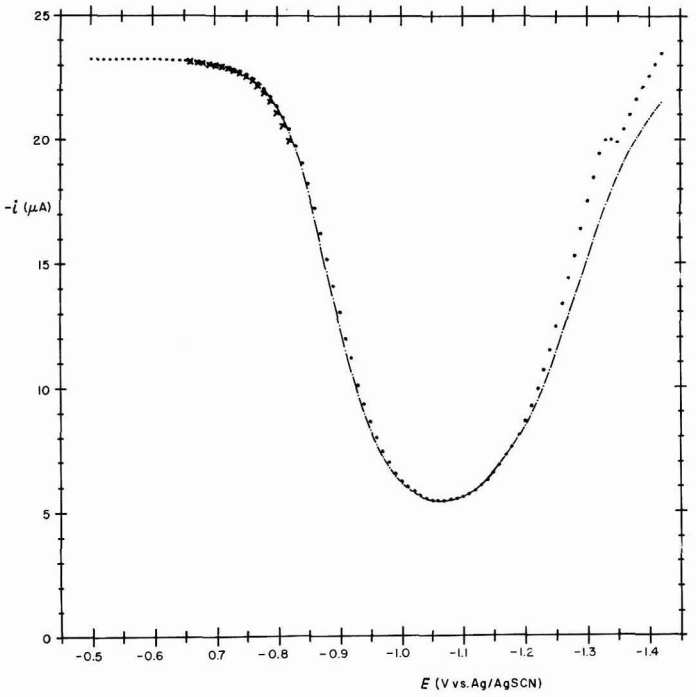

Fig. 6. The polarogram of 4.5 m*M* $In(SCN)_3$ in 1 *M* NaSCN at pH 3.22, corrected for charging and hydrogen reduction current. (●), exptl; (×), from the phase angle of the faradaic admittance; (----), from the in-phase component of the faradaic admittance.

have the advantage that the whole d.c. polarogram would be calculated solely from the faradaic admittance and the value of the limiting current. However, in the present case ζ can be estimated from Y_F''/Y_F' with a precision of at best $\pm 5\%$, since Y_F'' is obtained by subtraction of two large numbers. Starting with, for example, $\zeta = 0.217 \pm 0.011$ at -0.80 V, and subtracting the contribution of $(1/i_l)\int Y_F' dE$ to obtain $\zeta = 0.00675$ at -1.06 V is clearly beyond the possibilities of sound data handling.

We would like to stress here that the values calculated from Y_F' are essentially independent of the integration constant used over most of the potential range. For example, at -0.86 V, the value of ζ at -1.06 V contributes only 10% to the calculated value of ζ, and less than 1% at -0.78 V.

In the region between -0.68 and -0.82 V, the quadrature component of the electrode admittance, Y_F'', is sufficiently large to allow a determination of ζ solely on the basis of the phase angle of the faradaic admittance, eqn. (33). Data so obtained are shown in Fig. 5, and values calculated from them, *via* eqn. (46), for the d.c. polarographic current are indicated in Fig. 6. Finally, for potentials positive of -0.68 V, one has $i \approx i_l$ and eqn. (41) can be used to calculate ζ from Y_F'. Moreover, in this region

$$2\zeta^2 + 2\zeta + 1 = \zeta(\zeta+1)(2+\Delta) \quad \text{where} \quad \Delta \equiv 1/\zeta(\zeta+1) \ll 2$$

so that

$$Y_F' \approx \{i_l/\zeta^2(2+\Delta)\}(\partial\zeta/\partial E) \tag{49}$$

which can be integrated directly when the small correction term, Δ, is treated as a constant,

$$\frac{1}{\zeta_2} \approx \frac{1}{\zeta_1} - \frac{2+\Delta}{i_1} \int_1^2 Y_F' \, dE \tag{50}$$

Starting from the ζ value at -0.70 V as obtained from the phase angle measurements, and again using an iteration cycle (only one iteration was needed between -0.70 and -0.65 V, and none at potentials positive of -0.65 V) to subsequently improve our estimate of Δ, we obtained values for ζ up to -0.55 V. The correctness of these last values cannot be verified by comparison with d.c. polarographic data, since the d.c. currents are completely mass-transfer controlled in this range of potentials. However, the fact that the plot of ζ *vs.* E, Fig. 5, continues with the same slope, gives us confidence in the correctness of this procedure.

Use of eqn. (50) extends the range of obtainable values of ζ by at least a factor of 4. In principle, data for ζ could be obtained all the way to -0.50 V, but very close to $E_{\frac{1}{2}}$ the precision is poor because the value of Y_F' becomes comparable to the uncertainty in the baseline. The integration procedure of eqn. (50), though not overly sensitive to noise, is very sensitive to a slight systematic under- or over-estimate of the baseline. On the basis of an assumed maximum systematic error of $\pm 3 \cdot 10^{-6}\ \Omega^{-1}$ in the baseline (corresponding in our measurements to ± 1 mm on the recorder chart paper), we estimate that the values of ζ and $\hat{k}$ obtained at -0.65, -0.60 and -0.55 V are reliable to within $\pm 10\%$, $\pm 25\%$ and $\pm 50\%$, respectively.

EXPERIMENTAL

All measurements were made on an instrument described previously[31]. Water used was triply-distilled. Baker "Analyzed" NaSCN was used as such. A 0.233 *M* HSCN stock solution was made by first preparing[32] $Ba(SCN)_2(H_2O)_3$ and subsequently exchanging Ba^{2+} for H^+ on a Dowex 50W-X8 column. Thereafter, treatment with activated charcoal was necessary to remove soluble resin components. In the final stock solution, H^+ was determined by titration with NaOH, and SCN^- by titration with $AgNO_3$. Conversion efficiency of the ion exchange was found to be 100%. NaSCN could be used instead of $Ba(SCN)_2$ with only slightly decreased efficiency. The $In(SCN)_3$ stock solution was prepared by dissolution of indium metal in HSCN. Dissolution is reasonably fast when a piece of platinized platinum, also immersed in the same HSCN solution, touches the indium. The In(III) concentration of the resulting acidic stock solution was determined by amperometric titration with $K_4Fe(CN)_6$ or polarographically. The pH of the final solution was adjusted with NaOH. Shortly before use, all solutions were treated with activated charcoal. Commercial tank nitrogen was de-oxygenated by passage over copper turnings at 450° and was saturated with the inert electrolyte used. N_2 was passed over the cell during measurements. The solution contacted only glass, Teflon and the electrodes. Dropping mercury electrode: Corning marine barometer tubing 210–170 (similar to that used in standard Sargent capillaries), Hg height 85 cm, mercury mass flow rate 0.609 mg/sec, mechanically regulated drop-time 6.00 sec, sampling age of drop 5.86 sec, temperature 25.0° unless indicated otherwise. All potentials were measured and are reported *vs.* an internal Ag/AgSCN electrode.

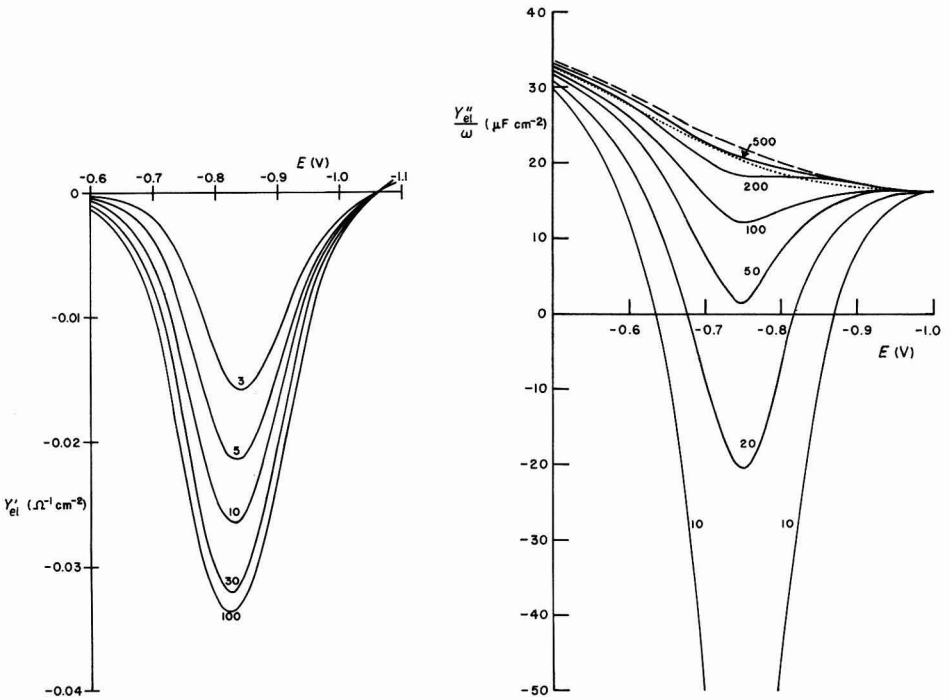

Fig. 7. The in-phase component of the electrode admittance of about 5 m*M* $In(SCN)_3$ in 1 *M* NaSCN, acidified with HSCN to pH 3.1, in the region of the negative faradaic admittance. Frequencies indicated in Hz, amplitude in all cases 10 mV. In the absence of In(III), the baseline is at zero.

Fig. 8. The quadrature component of the electrode admittance of about 5 m*M* $In(SCN)_3$ in 1 *M* NaSCN, acidified with HSCN to pH 3.1, in the region of the negative faradaic admittance. Data are plotted as capacitance, *i.e.*, as Y''_{el}/ω, so as to render the contribution of the double-layer capacitance constant. Frequencies indicated in Hz, amplitude 10 mV. (---), double-layer capacitance estimated by extrapolation of data to $\omega \rightarrow \infty$; (····), double-layer capacitance in absence of In(III), so that the electrode is mercury rather than *in situ*-generated indium amalgam.

The effects of variation of frequency, temperature, pH and concentration are illustrated in Figs. 7–11. Note in Fig. 10 that the faradaic admittance at pH 4 still reveals the presence of the polarographic minimum, even though it is masked completely in the d.c. polarogram by the reduction of hydrogen ions. An apparent dependence of the measured admittance on the amplitude of the sine wave[4] could be generated but was shown to be an instrumental artifact and was absent when the instrument was operated properly.

DISCUSSION

1. The theoretical derivation presented here does not pre-suppose a Volmer-type dependence of rate constants superimposed on a potential-dependence of the standard rate constant[13,14], which seems to us a circuitous way of representing an

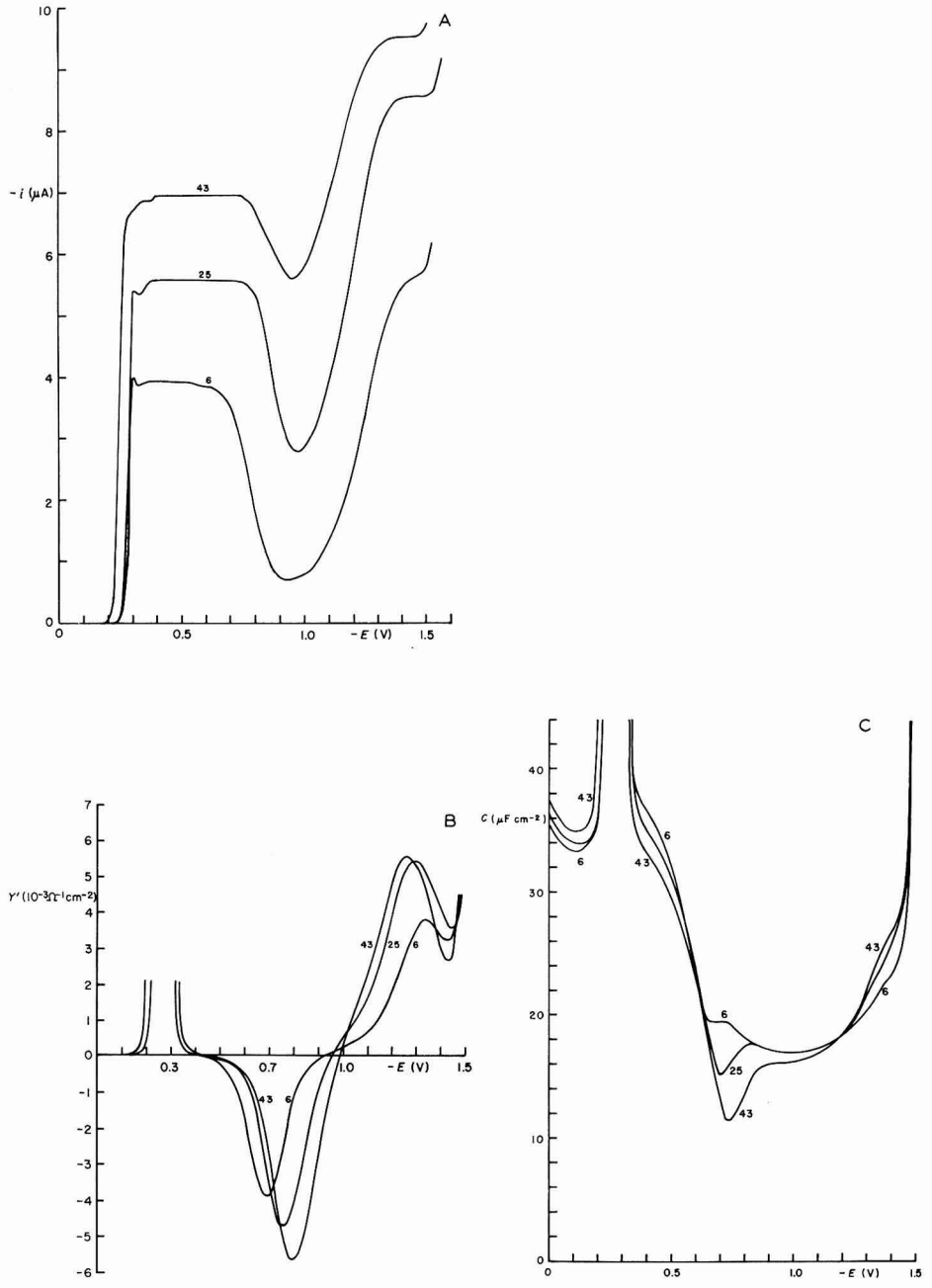

Fig. 9. Temperature-dependence of the d.c. and a.c. polarograms of 1 mM $In(SCN)_3$ in 1 M NaSCN acidified with HSCN to pH 3.1. Temps. indicated in °C. Both the d.c. and a.c. polarograms show the increase of rate constant with increasing temp. The components of the electrode admittance were measured with 31.8 Hz, 10 mV amplitude. The differences between the quadrature curves around −0.45 V are due to similar differences in the double-layer capacitance of 1 M NaSCN at the same temp.

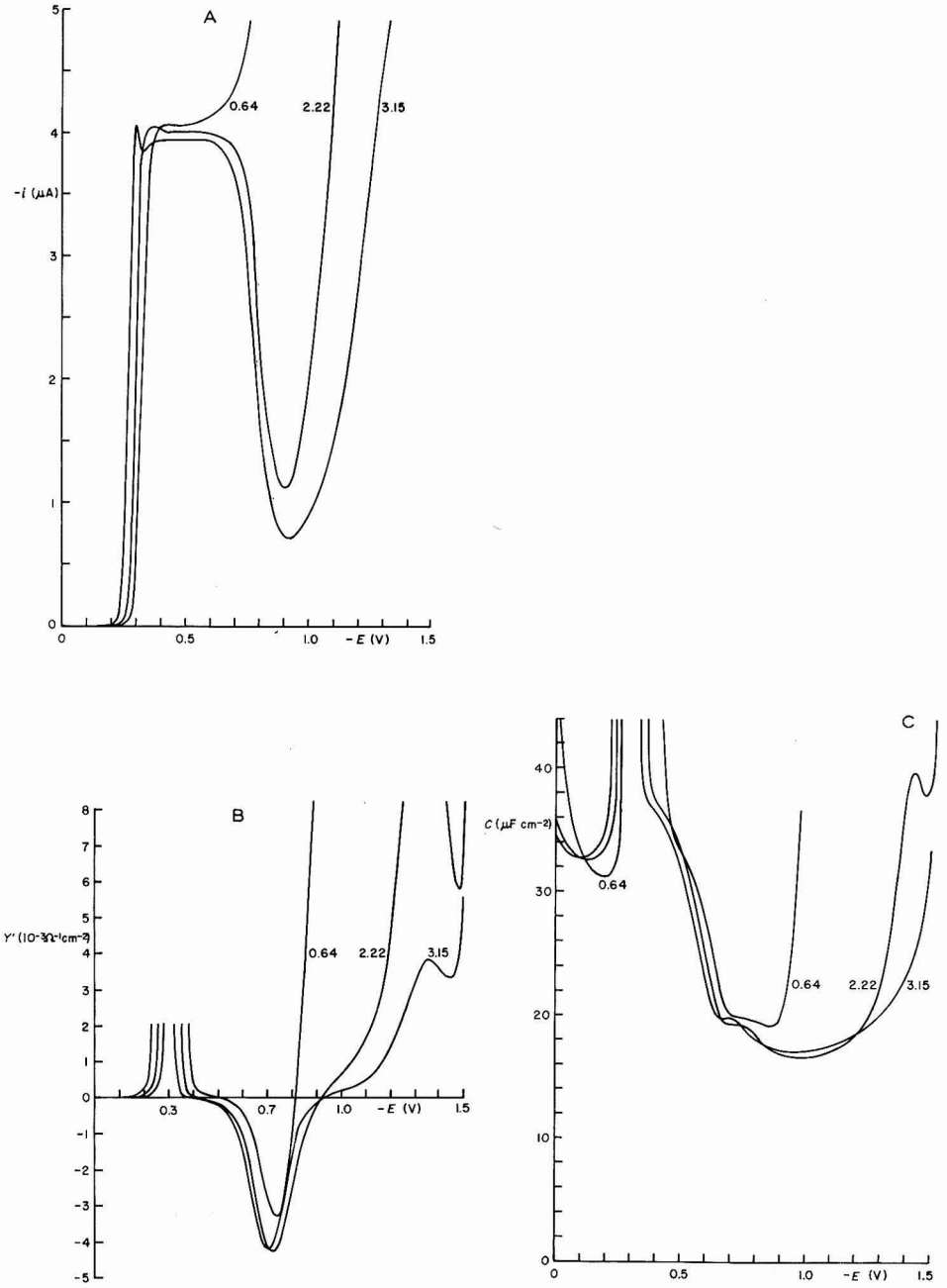

Fig. 10. Dependence on pH of the d.c. and a.c. polarograms of 1 m*M* $In(SCN)_3$ in 1 *M* NaSCN acidified with HSCN to the pH indicated. Temp.: 5.5°, a.c. measurements at 31.8 Hz, 10 mV amplitude. The d.c. polarographic minimum is completely obscured at pH 0.64 by the reduction of hydrogen ions, but the corresponding a.c. polarograms still show the negative faradaic admittance. Note that the specific adsorption of In(III) around −0.2 V appears to be pH-dependent.

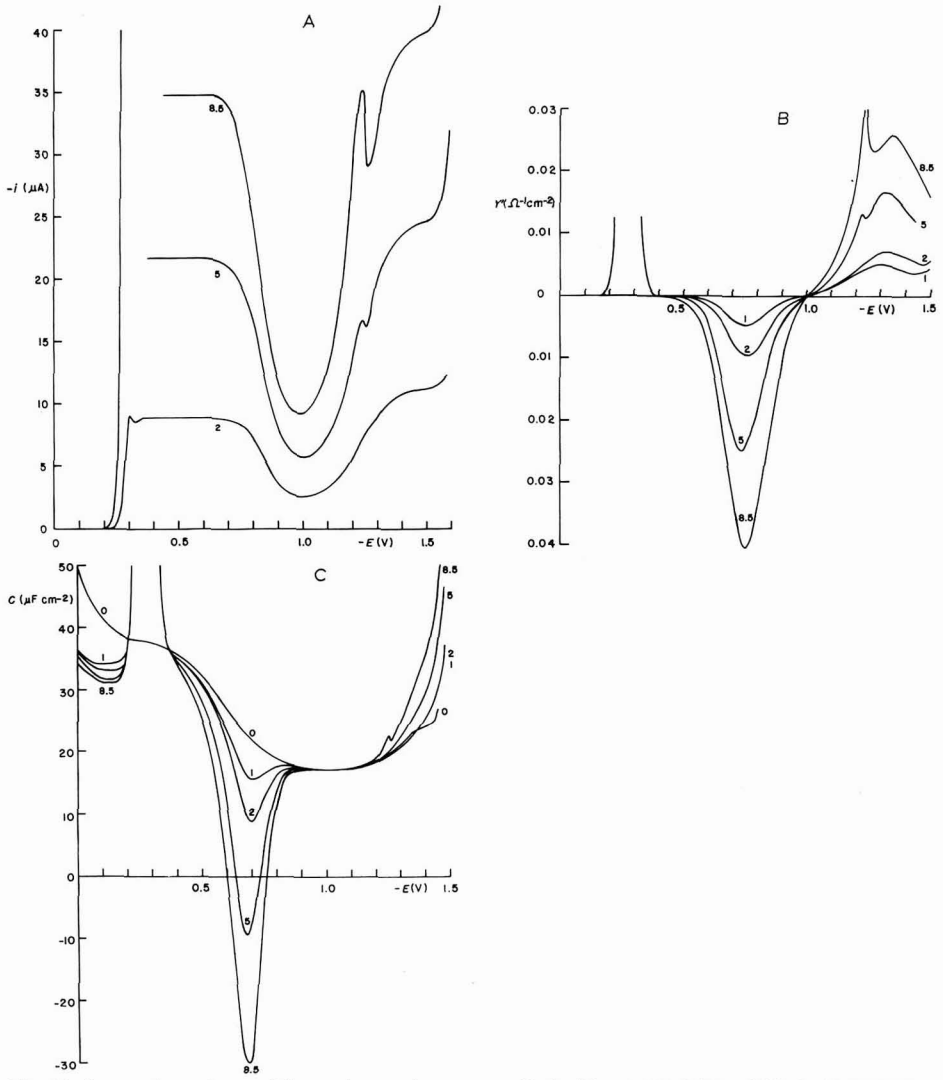

Fig. 11. Concn.-dependence of d.c. and a.c. polarograms of In(III) in 1 *M* NaSCN acidified with HSCN to pH 3.2. A.c. data at 31.8 Hz, 10 mV amplitude. A very pronounced maximum is observed near $E_{\frac{1}{2}}$ in the more concd. solns., clearly a consequence of the abrupt change in specific adsorption of In(III). A second, much smaller maximum is observed on the negative side of the minimum, again especially in the more concd. solns, and probably results from the formation of sparingly soluble indium hydroxides at the potential where hydrogen ions are reduced and the local pH is consequently increased.

arbitrary dependence of rate constant on potential. The very concept of a standard rate constant, k_{sh}, seems to be inapplicable to the present case, since there is no measurable rate of oxidation even at potentials where the rate of reduction drops to very low levels. By the same token, the concept of a charge transfer coefficient, α, is inapplicable since it implies a model of charge transfer which is clearly not valid in the present case. Staying within the narrow framework of k_{sh} and α may lead to demonstrably in-

PUBLISHED MONTHLY

International Journal of Mass Spectrometry and Ion Physics

ELSEVIER PUBLISHING COMPANY

SCOPE

The journal is devoted to the fundamental aspects of mass spectrometry and ion physics and to the study of the application of mass spectrometric techniques to specific problems. The following topics are considered to fall within the scope of the journal:

Theoretical and experimental studies of ion formation, ion separation and ion detection processes.

Interpretation of mass spectrometric data.

Theoretical computation; the design and performance of instruments (or their parts) and accessories.

Measurements such as natural isotope abundances, precise isotope mass measurements; ionization, appearance and excitation potentials; ionization cross sections.

Development of techniques in relation to structural determination, geological ageing, thermodynamic studies, chemical kinetics studies, surface phenomena studies, chemical analysis.

The journal publishes research papers, review articles, book reviews and short communications.

LANGUAGES

The main language of the journal is English, although papers in French or German are also published.

SUBMISSION OF PAPERS

Papers should be submitted to one of the following:

J. FRANZEN
Institut für Spektrochemie und angewandte Spektroskopie
Postfach 778, 46 DORTMUND (Germany)

A. QUAYLE
"Shell" Research Ltd., Thornton Research Centre
P.O. Box No. 1, CHESTER (England)

H.J. SVEC
Department of Chemistry, Iowa State University
AMES, Iowa 50010 (U.S.A.)

They should be submitted in three copies, in double-spaced type with adequate margins. Figures should be drawn in Indian ink on drawing or tracing paper and be in a form ready for the blockmaker. Standard symbols should be used in line drawings. Photographs should be submitted as clear black and white glossy prints. Legends to illustrations should be typed on a separate page. There are no page charges for publication. Further details are available on request.

FREQUENCY AND SUBSCRIPTION INFORMATION

Publication is monthly. One volume appeared in 1968. Volumes 2 and 3 will be published in 1969. Volumes 4 and 5 are scheduled for publication in 1970. The subscription price for 1969 is Dfl. 180.00 plus Dfl. 6.00 postage or equivalent (US$50.00 plus US$1.70; £20.19.0 plus 14s. at April 1, 1969).

A specimen copy will be sent on request.

Vol. 1 (1968); Vols. 2 and 3 (1969); Vols. 4 and 5 (1970).

OF INTEREST TO: physical, analytical, organic, inorganic and organometallic chemists; university libraries, research laboratories of the petroleum and chemical industries (e.g. pharmaceuticals, flavors, dyestuffs, polymers, carbohydrates), nuclear research centres, some of the larger geological institutes.

CONTENTS OF VOLUME 2

International Journal of Mass Spectrometry and Ion Physics

VOL. 2, NO. 1

VOL. 2, NO. 2

Papers on field ionization, presented at the 16th Annual Conference on Mass Spectrometry and Allied Subjects of ASTM Committee E-14 on Mass Spectrometry, May 13, 1968, at Pittsburgh, Pa. (U.S.A.)

VOL. 2, NO. 3

PAPERS RECEIVED

Photoelectron spectra of conjugated hydrocarbons and heteromolecules
J.H.D. Eland (Oxford, Great Britain)

Intramolecular kinetic isotope effect in the acid decomposition of carbonates
S.K. Sharma and T. Sharma (Kanpur, India)

Kinetic energy distributions of fragment ions in the mass spectrum of isocyanic acid
C.G. Rowland, J.H.D. Eland and C.J. Danby (Oxford, Great Britain)

The use of Koopmans' theorem in the interpretation of photoelectron spectra
W.G. Richards (Oxford, Great Britain)

Mass spectrometric study of dissociative attachment in diatomic molecules. I. CO and H_2
R. Locht and J. Momigny (Liège, Belgium)

Ion cyclotron resonance mass spectra of fluoroalkenes. I. Ion-molecule reactions of ethylene and vinyl fluoride
R.M. O'Malley and K.R. Jennings (Sheffield, Great Britain)

CONTENTS OF VOLUME 2 (continued)

International Journal of Mass Spectrometry and Ion Physics

VOL. 2, NO. 4/5

correct conclusions such as the statement[14] that the surface concentration of In(III) will be very low at the negative potentials at which the minimum occurs.

In fact, the d.c. surface concentration, c'_O, of In(III) follows from eqns. (39) and (40) as:

$$\frac{c'_O}{c^*_O} = \frac{i}{i_l}\frac{1}{\zeta}\left(\frac{7}{6\pi\omega t}\right)^{\frac{1}{2}} = \frac{i}{i_l}\frac{1}{\bar{k}}\left(\frac{7D_O}{3\pi t}\right)^{\frac{1}{2}} \tag{51}$$

which leads in our example ($c^*_O = 4.5$ mM, $i/i_l = 0.235$ and $\zeta = 0.0067_5$ at $E = -1.06$ V, $\omega = 103$ sec^{-1} and $t = 5.86$ sec) to $c'_O = 3.89$ mM, which is not at all negligible and is only 13.6% less than the bulk concentration. Thus, there is strong In(III) adsorption at $E > E_{\frac{1}{4}}$ (≈ -0.33 V) but no detectable In(III) adsorption, for a comparable surface concentration, c'_O, in the potential region of the minimum. This suggests the adsorption of a neutral or negatively charged indium–thiocyanate complex[33-35] at $E > E_{\frac{1}{4}}$, the bulk concentration of which need not be high since it can be formed close to, or at, the adsorbing surface.

2. Equation (14) has been derived[19,20] for plane diffusion only. It can easily be shown that eqn. (14) still holds for expanding plane diffusion as represented by the Ilkovič differential equation[21]. Equation (14) no longer applies when electrode curvature is taken into account, a refinement seldom justified in experiments with a dropping mercury electrode in view of the many other, unaccounted for effects of similar order of magnitude like solution transfer from preceding drops[36-38], shielding due to the bottom end of commonly used blunt capillaries[39], uneven current distribution resulting from eccentric drop growth[40], etc.

3. Even with the rather approximate eqn. (34) used here for the sake of simplicity, our results are more accurate than those employing a diffusion layer model[13,41], which can be shown to correspond in the present case to the approximation

$$F(\chi) \approx \chi/(\tfrac{1}{2}\pi^{\frac{1}{2}} + \chi) = \chi/(1.128 + \chi) \tag{52}$$

In fact, the diffusion layer model is only correct for plane or expanding plane diffusion with infinitely fast (Nernstian) electrode reactions. In the case of "irreversible" reactions, it is neither the simplest nor the most accurate approximation available.

4. The agreement obtained between rate constants calculated from the a.c. and d.c. polarograms (one might properly call our vector-resolved admittance recording an a.c. polarogram) is quite satisfactory. In our experiments, the two methods differ in effective frequency by about two orders of magnitude, which is as wide a frequency range as can be obtained in the present case with a.c. polarographic measurements alone. However, a comparison between a.c. and d.c. polarographic data is more useful than a comparison of a.c. polarographic data at various frequencies, because the d.c. polarographic current depends only on $\bar{k}$ whereas the faradaic admittance also depends on $\partial\bar{k}/\partial E$.

5. The integration procedure followed here, especially that represented by eqn. (50), is capable of yielding rate constants up to quite high values (in the present case, well beyond 0.1 cm sec^{-1}) from low-frequency measurements. Paradoxically, high-frequency measurements would not have been more powerful in this case in view of the constancy of Y'_F and the rapid decrease of Y''_F with increasing frequency. The use of low frequencies is especially advantageous since it minimizes instrumental artifacts resulting from stray capacitance and component inductance, as well as any

error introduced by incomplete compensation of solution resistance[42]. The use of a dropping mercury electrode, of course, sets a practical lower limit to the frequencies used for a number of reasons: the theory of faradaic admittance is much simplified after the attainment of a steady state, drop oscillations and their principal harmonics should not interfere, and the rise-time of the final filter should not cause distortion of the signal while retaining a high over-all quality factor, Q, of the synchronous rectifier for optimum noise suppression. With the usual drop-times of 3–8 sec this sets a practical lower limit of 3–5 Hz for reliable measurements on a normal dropping mercury electrode.

6. The present technique enables us to obtain reduction rate constants over a wide range of potentials, including that range for which reliable surface excess data are available for specific adsorption of thiocyanate on Hg[43–46]. Thus a correlation between $\overleftarrow{k}$ and Γ_{SCN^-} is feasible. Data so obtained do not support a direct proportionality between rate constant and surface excess of specifically adsorbed catalyst as suggested earlier by Tanaka *et al.*[8,9], but rather a proportionality of $\overleftarrow{k}$ with $(\Gamma_{SCN^-})^n$ where $n \geqslant 4$ or, possibly, an exponential relationship[47]. We will report on such correlations between k and the surface excesses of SCN^- and various halides in a separate communication.

7. One might notice that, at least in principle, the problem of the so-called electrochemical oscillator[10,11] of In(III) in NaSCN has been solved, since eqns. (41) and (42) or their approximate counterparts, eqns. (43) and (44), describe the faradaic admittance of the electrode as a function of the potential-dependent parameter, ζ. Thus, one can derive the transfer function of the cell and its external circuit, bearing in mind that the electrode admittance is in parallel with the frequency-independent double-layer capacitance, and that the changing surface area of a dropping mercury electrode renders both the electrode impedance and the solution resistance time-dependent. The mathematical formulation of this problem will be reported elsewhere.

8. The present work clearly illustrates the need for consistency in the signs of currents and potentials. We have observed both positive and negative faradaic admittances, and we want to emphasize that the signs of these are not arbitrary: the existence of an electrochemical oscillator[10,11] attests to the physical reality of the negative sign of Y in the range of potentials between $E_{\frac{1}{2}}$ and the lowest point of the polarographic minimum. Since admittance has the physical meaning

$$Y = \partial i/\partial E \tag{53}$$

it follows that a reduction current *must* be given a negative sign if the internationally agreed-upon Stockholm convention of electrode potentials[48] is used, *i.e.*, if reduction is ordinarily favored by an increasingly negative potential. We have made this point before[49], and it appears to be the only logical choice of the sign of i consistent with the Stockholm convention and physical reality.

9. The negative faradaic admittance discussed in the present paper is not necessarily tied to a polarographic minimum. The latter is observable only when the reduction rate constant drops below about 0.01 cm sec^{-1}. In 0.1 M NaSCN, virtually no minimum is observed[3], yet the corresponding electrode admittance exhibits both a negative and a positive faradaic contribution at potentials more negative than the half-wave potential. Indeed, we have measured reduction rate constants in this potential range, using eqns. (33) and (50), and we have found values for $\overleftarrow{k}$ varying be-

tween a highest reliably measurable value of 0.3 cm sec^{-1} to a minimum value of 0.01 cm sec^{-1}. Note that we can still measure the reduction rate constants in this case. In the present paper, we have considered only a concentrated NaSCN solution in order to verify our calculations by comparison with well-established polarographic theory.

10. The present communication has dealt only with the formal aspects of the reduction of In(III), but has not discussed any of its mechanistic features. We have shown that there is, in fact, nothing extraordinary in the formal behavior, once the conclusion[8,9] is accepted that the charge transfer resistance (and consequently the Warburg impedance) can be a negative quantity. We have shown that the current can be described by the simple formalism of eqn. (13), which implies that the rate-limiting process occurs at, or very close to, the electrode surface. The dependence of the reduction rate constant on the surface excess of thiocyanate turns out to be more complicated than had been anticipated earlier[8,9].

11. Several previous workers have ascribed the undeniably electrocatalytic aspects of the reduction of In(III) to the presence of adsorbed ions which would be capable of assisting electron transfer. Thus, Brainina[6] mentioned ligand bridging, and Tanaka *et al.*[8,9] assumed that the rate constant would be higher on that "fraction" of the surface which is "covered" with adsorbed anions. At present, we tend to interpret our and previous observations on In(III) more in terms of a heterogenous reaction with adsorbed ligands, generating transient species which can subsequently accept electrons from the electrode. We hope to present more conclusive evidence for such a mechanism in the near future.

ACKNOWLEDGEMENT

Our most sincere thanks are due to Miss Joyce C. Kreuser for writing and operating the computer program, and to Dr. Lubomír Pospíšil for verifying many of our experimental data. This research was supported by the National Science Foundation under grants GP 5432 and GP 8575.

SUMMARY

A general relation between the faradaic admittance and the d.c. polarographic current has been derived. Its applicability is demonstrated in the case of the negative faradaic admittance of In(III) in 1 *M* NaSCN, by calculating the d.c. polarogram from the measured faradaic admittance. The inverse process, the calculation of the faradaic admittance from the d.c. polarogram, is equally feasible in principle, but is less precise. Rate constants for the reduction of In(III) in 1 *M* NaSCN have been obtained over a 0.8 V wide range of potentials. The procedure used makes it possible to obtain rate constants of fast processes (k of the order of 0.1 cm sec^{-1}) from low-frequency measurements where instrumental errors can be kept to a minimum.

REFERENCES

1 J. J. LINGANE, Thesis, University of Minnesota, 1938; I. M. KOLTHOFF AND J. J. LINGANE, *Polarography*, Interscience, New York, 1941, p. 275.
2 D. COZZI AND S. VIVARELLI, *Z. Elektrochem.*, 57 (1953) 408; 58 (1954) 907.

3 M. BULOVOVÁ, *Collection Czech. Chem. Commun.*, 19 (1954) 1123.
4 H. SHIRAI, *J. Chem. Soc., Japan, Pure Chem. Sect.*, 81 (1960) 1248.
5 T. TAKAHASHI AND H. SHIRAI, *Rev. Polarog. Kyoto*, 11 (1963) 155.
6 K. Z. BRAININA, *Dokl. Akad. Nauk SSSR*, 130 (1960) 797.
7 A. G. STROMBERG AND K. Z. BRAININA, *Zh. Fiz. Khim.*, 35 (1961) 2016.
8 N. TANAKA AND R. TAMAMUSHI, *Proc. Australian Conf. Electrochem., 1963*, p. 248.
9 N. TANAKA, T. TAKEUCHI AND R. TAMAMUSHI, *Bull. Chem. Soc. Japan*, 37 (1964) 1435.
10 R. TAMAMUSHI, *J. Electroanal. Chem.*, 11 (1966) 65.
11 R. TAMAMUSHI AND K. MATSUDA, *J. Electroanal. Chem.*, 12 (1966) 436.
12 A. J. ENGEL, J. LAWSON AND D. A. AIKENS, *Anal. Chem.*, 37 (1965) 203.
13 M. SLUYTERS-REHBACH, B. TIMMER AND J. H. SLUYTERS, *Z. Physik. Chem. Frankfurt*, 52 (1967) 89.
14 B. TIMMER, M. SLUYTERS-REHBACH AND J. H. SLUYTERS, *J. Electroanal. Chem.*, 19 (1968) 73.
15 P. DELAHAY, *J. Phys. Chem.*, 70 (1966) 2069, 2373.
16 H. MATSUDA, *Z. Elektrochem.*, 62 (1958) 977.
17 H. GERISCHER, *Z. Physik. Chem.* 198 (1951) 286.
18 H. S. CARSLAW AND J. C. JAEGER, *Conductivity of Heat in Solids*, Oxford University Press, 2nd ed., 1959, p. 317.
19 Y. P. GOKHSHTEIN AND A. Y. GOKHSHTEIN, *Advan. Polarog.*, 2 (1960) 465.
20 W. H. REINMUTH, *Anal. Chem.*, 34 (1962) 1446.
21 D. ILKOVIČ, *J. Chim. Phys.*, 35 (1938) 129.
22 N. MEIMAN, *Zh. Fiz. Khim.*, 22 (1948) 1454.
23 J. KOUTECKÝ, *Collection Czech. Chem. Commun.*, 18 (1953) 597.
24 H. MATSUDA AND Y. AYABE, *Bull. Chem. Soc. Japan*, 28 (1955) 422.
25 D. E. SMITH, T. G. MCCORD AND H. L. HUNG, *Anal. Chem.*, 39 (1967) 1149.
26 K. B. OLDHAM AND E. P. PARRY, *Anal. Chem.*, 40 (1968) 65.
27 J. N. BUTLER, M. L. MEEHAN AND A. C. MAKRIDES, *J. Electroanal. Chem.*, 9 (1965) 237.
28 J. N. BUTLER, *J. Phys. Chem.*, 69 (1965) 3817.
29 B. TIMMER, M. SLUYTERS-REHBACH AND J. H. SLUYTERS, *J. Electroanal. Chem.*, 15 (1967) 343.
30 R. DE LEVIE AND A. A. HUSOVSKY, unpublished work.
31 R. DE LEVIE AND A. A. HUSOVSKY, *J. Electroanal. Chem.*, 20 (1969) 181.
32 K. H. HERSTEIN, *Inorg. Syn.*, 3 (1950) 24.
33 N. SUNDEN, *Svensk Kem. Tidskr.*, 66 (1954) 50.
34 T. P. RADHAKRISHNAN AND A. K. SUNDARAM, *J. Electroanal. Chem.*, 5 (1963) 124.
35 Y. NARUSAWA, J. HASHIMOTO AND H. HAMAGUCHI, *Bull. Chem. Soc. Japan*, 38 (1965) 234.
36 L. AIREY AND A. A. SMALES, *Analyst*, 75 (1950) 287.
37 W. HENNE AND W. HANS, *Naturwissenschaften*, 40 (1953) 524.
38 W. HANS, W. HENNE AND E. MEURER, *Z. Elektrochem.*, 58 (1954) 836.
39 H. MATSUDA, *Bull. Chem. Soc. Japan*, 26 (1953) 342.
40 R. DE LEVIE, *J. Electroanal. Chem.*, 9 (1965) 311.
41 B. TIMMER, M. SLUYTERS-REHBACH AND J. H. SLUYTERS, *J. Electroanal. Chem.*, 14 (1967) 169.
42 R. DE LEVIE AND J. C. KREUSER, *J. Electroanal. Chem.*, 21 (1969) 221.
43 N. TANAKA, T. TAKEUCHI AND R. TAMAMUSHI, *J. Chem. Soc. Japan, Pure Chem. Sect.*, 85 (1964) 846.
44 H. WROBLOWA, Z. KOVAC AND J.O'M. BOCKRIS, *Trans. Faraday Soc.*, 61 (1965) 1523.
45 S. MINC AND J. ANDRZEJCZAK, *J. Electroanal. Chem.*, 17 (1968) 101.
46 R. PARSONS AND P. C. SYMONS, *Trans. Faraday Soc.*, 64 (1968) 1077.
47 P. TEPPEMA, M. SLUYTERS-REHBACH AND J. H. SLUYTERS, *J. Electroanal. Chem.*, 16 (1968) 165.
48 J. A. CHRISTIANSEN AND M. POURBAIX, *Proc. 17th IUPAC Meeting, Stockholm 1953*, p. 83.
49 R. DE LEVIE, *Advan. Electrochem. Electrochem. Eng.*, 6 (1967) 329.

ELECTROANALYTICAL CHEMISTRY AND INTERFACIAL ELECTROCHEMISTRY
Elsevier Sequoia S.A., Lausanne – Printed in The Netherlands

RELAXATION TIMES FOR ADSORPTION COUPLED WITH A HOMOGENEOUS REACTION IN SOLUTION

R. D. ARMSTRONG

Electrochemistry Research Laboratory, Department of Physical Chemistry, The University of Newcastle upon Tyne, Newcastle upon Tyne, NE1 7RU (England)

(Received January 17th, 1969)

INTRODUCTION

It has been shown recently[1,2] that the diffusion-controlled adsorption of a substance at an electrode for sinusoidal perturbations of the electrode potential can be described by a distribution of relaxation times about a mean time $(\partial\Gamma/\partial C_0)_\phi^2/D$. The form of the distribution is represented by the Cole–Cole[3] formula with $\alpha = 0.5$. In this communication this concept is extended to the case where adsorption is coupled with a homogeneous reaction in solution.

THE DIFFUSION EQUATIONS

We consider a species, S_1 (bulk concentration, C_0) which is always in equilibrium with S_1 adsorbed molecules at the electrode surface ($x = 0$). This species reacts in solution as:

$$S_1 \underset{k'}{\overset{k}{\rightleftharpoons}} S_2 \tag{1}$$

For a sinusoidal potential perturbation

$$\phi = \phi_0 + P \exp(j\omega t) \tag{2}$$

The diffusion equations are (S_1 and S_2 are assumed to have identical diffusion coefficients):

$$\frac{\partial C}{\partial t} = D\frac{\partial^2 C}{\partial x^2} + k'C' - kC \tag{3}$$

$$\frac{\partial C'}{\partial t} = D\frac{\partial^2 C'}{\partial x^2} + kC - k'C' \tag{4}$$

with the boundary conditions:

$$C \to C_0, \quad C' \to C_0' \qquad x \to \infty \tag{5}$$

$$\left(\frac{\partial C'}{\partial x}\right)_{x=0} = 0 \tag{6}$$

$$D\left(\frac{\partial C}{\partial x}\right)_{x=0} = \left(\frac{\partial \Gamma}{\partial C_0}\right)_{\phi}\left(\frac{\partial C}{\partial t}\right)_{x=0} + \left(\frac{\partial \Gamma}{\partial \phi}\right)_{C_0}\frac{\mathrm{d}\phi}{\mathrm{d}t} \tag{7}$$

The steady state solutions are:

$$C = C_0 + \frac{C_2 C_0}{C_0'}\left(\frac{k_0+j\omega}{j\omega}\right)^{\frac{1}{2}} \exp\left[-\left(\frac{j\omega}{D}\right)^{\frac{1}{2}}x\right]\exp(j\omega t) + C_2 \exp\left[-\left(\frac{k_0+j\omega}{D}\right)^{\frac{1}{2}}x\right]\exp(j\omega t) \tag{8}$$

$$C' = C_0' + C_2\left(\frac{k_0+j\omega}{j\omega}\right)^{\frac{1}{2}} \exp\left[-\left(\frac{j\omega}{D}\right)^{\frac{1}{2}}x\right]\exp(j\omega t) - C_2 \exp\left[-\left(\frac{k_0+j\omega}{D}\right)^{\frac{1}{2}}x\right]\exp(j\omega t) \tag{9}$$

where

$$C_2 = \frac{-\left(\frac{\partial \Gamma}{\partial \phi}\right)_{C_0} Pj\omega}{D^{\frac{1}{2}}(k_0+j\omega)^{\frac{1}{2}}\left(1+\frac{C_0}{C_0'}\right)+\left(\frac{\partial \Gamma}{\partial C_0}\right)_{\phi} j\omega\left[1+\frac{C_0}{C_0'}\left(\frac{k_0+j\omega}{j\omega}\right)^{\frac{1}{2}}\right]} \tag{10}$$

and $k_0 = k(1+C_0/C_0')$ (11)

These solutions reduce to those given previously[4] for the restriction that

$$C_0' \gg C_0$$

THE ELECTRODE IMPEDANCE

Since

$$\frac{\mathrm{d}\Gamma}{\mathrm{d}t} = D\left(\frac{\partial C}{\partial x}\right)_{x=0} = \frac{\left(\frac{\partial \Gamma}{\partial \phi}\right)_{C_0} Pj\omega D^{\frac{1}{2}}(k_0+j\omega)^{\frac{1}{2}}\exp(j\omega t)\left(1+\frac{C_0}{C_0'}\right)}{D^{\frac{1}{2}}(k_0+j\omega)^{\frac{1}{2}}\left(1+\frac{C_0}{C_0'}\right)+\left(\frac{\partial \Gamma}{\partial C_0}\right)_{\phi} j\omega\left[1+\frac{C_0}{C_0'}\left(\frac{k_0+j\omega}{j\omega}\right)^{\frac{1}{2}}\right]} \tag{12}$$

and the electrode impedance is given by:

$$\frac{1}{Z} = j\omega\,{}_{\infty}C_{\mathrm{p}} + \left(\frac{\partial q_{\mathrm{M}}}{\partial \Gamma}\right)_{\phi}\frac{\mathrm{d}\Gamma}{\mathrm{d}t}\frac{1}{P\exp(j\omega t)} \tag{13}$$

where

$${}_{\infty}C_{\mathrm{p}} = \left(\frac{\partial q_{\mathrm{M}}}{\partial \phi}\right)_{\Gamma}$$

we can write

$$\frac{1}{Z} = j\omega\,{}_{\infty}C_{\mathrm{p}} + \frac{\left(\frac{\partial q_{\mathrm{M}}}{\partial \Gamma}\right)_{\phi}\left(\frac{\partial \Gamma}{\partial \phi}\right)_{C_0} j\omega D^{\frac{1}{2}}(k_0+j\omega)^{\frac{1}{2}}\left(1+\frac{C_0}{C_0'}\right)}{D^{\frac{1}{2}}(k_0+j\omega)^{\frac{1}{2}}\left(1+\frac{C_0}{C_0'}\right)+\left(\frac{\partial \Gamma}{\partial C_0}\right)_{\phi} j\omega\left[1+\frac{C_0}{C_0'}\left(\frac{k_0+j\omega}{j\omega}\right)^{\frac{1}{2}}\right]} \tag{14}$$

RELAXATION TIMES

Equations (12) and (14) represent a relaxation process where there are three coupled relaxation times. These are:

$$\tau_{\mathrm{D1}} = \left(\frac{\partial \Gamma}{\partial C_0}\right)^2 \Big/ D$$

$$\tau_{\mathrm{D2}} = \left(\frac{\partial \Gamma}{\partial C_0}\right)^2 \left(\frac{C_0}{C_0'+C_0}\right)^2 \Big/ D$$

$$\tau_{\mathrm{R}} = \left(\frac{\partial \Gamma}{\partial C_0}\right) \Big/ k_0^{\frac{1}{2}} D^{\frac{1}{2}}$$

where τ_{D1} and τ_{D2} are mean times with a distribution of times around them described by the function:

$$f(\tau) = \tau_{\mathrm{D}}^{\frac{1}{2}} / \{\pi\tau^{\frac{1}{2}}(\tau_{\mathrm{D}}+\tau)\}$$

whilst τ_{R}, the reaction relaxation time, is a single time.

LIMITING CASES

Most experimental investigations will be likely to involve a frequency range such that only one or two of the relaxation times are detectable. Below, we consider in detail two of the most important possibilities. Other limiting situations are tabulated in Table 1.

TABLE 1

OBSERVABLE RELAXATION TIMES FOR SPANNING THE RELAXATION PROCESS UNDER VARIOUS CONDITIONS

Conditions	*Times*
$\omega \gg k_0$	τ_{D1}
ω comparable with k_0 $\quad C_0 \ll C_0'$	$\tau_{\mathrm{D1}}+\tau_{\mathrm{R}}$
$\omega \ll k_0 \quad k_0^{\frac{1}{2}} C_0 \ll \omega^{\frac{1}{2}} C_0'$	τ_{R}
$\omega \ll k_0 \quad k_0^{\frac{1}{2}} C_0$ comparable with $\omega^{\frac{1}{2}} C_0'$	$\tau_{\mathrm{R}}+\tau_{\mathrm{D2}}$
$\omega \ll k_0 \quad k_0^{\frac{1}{2}} C_0 \gg \omega^{\frac{1}{2}} C_0'$	τ_{D2}

(i) $\omega \ll k_0$ such that $C_0 k_0^{\frac{1}{2}}$ and $C_0' \omega^{\frac{1}{2}}$ are comparable

Here we have:

$$\frac{d\Gamma}{dt} = \frac{D^{\frac{1}{2}}\left(\frac{\partial\Gamma}{\partial\phi}\right)_{C_0} Pj\omega \exp(j\omega t)}{D^{\frac{1}{2}} + \left(\frac{\partial\Gamma}{\partial C_0}\right) j\omega\left[k_0^{-\frac{1}{2}} + \frac{C_0}{C_0'}(j\omega)^{-\frac{1}{2}}\right]} \tag{15}$$

Equation (15) represents the coupling of τ_{D2} and τ_R in exactly the same way as that found for the coupling of diffusion with a slow heterogeneous step[5] and physically corresponds to a reaction layer which is thin compared with the diffusion layer. The Lorenz[5] function is then given by:

$$\omega(C_p - {}_\infty C_p)R_p = \omega C_p^* R_p = \{1 + (2/\omega\tau_{D2})^{\frac{1}{2}}\}/\{1 + (2\omega/\tau_{D2})^{\frac{1}{2}}\tau_R\} \tag{16}$$

(*ii*) *ω and k comparable but $C_0 \ll C_0'$*

In this case

$$\frac{d\Gamma}{dt} = \frac{D^{\frac{1}{2}}(\partial\Gamma/\partial\phi)_{C_0} Pj\omega \exp(j\omega t)}{D^{\frac{1}{2}} + (\partial\Gamma/\partial C_0)_\phi\, j\omega(k_0 + j\omega)^{-\frac{1}{2}}} \tag{17}$$

which represents the coupling of a single time, τ_R, with τ_{D1} in such a way that τ_R dominates for $\omega < k$ and τ_{D1} at $\omega > k$.

The corresponding value of $\omega C_p^* R_p$ is:

$$\omega C_p^* R_p = \frac{D^{\frac{1}{2}}(k_0^2 + \omega^2)^{\frac{1}{2}} + (\partial\Gamma/\partial C_0)_\phi \omega[\frac{1}{2}(k_0^2 + \omega^2) - \frac{1}{2}k_0]^{\frac{1}{2}}}{(\partial\Gamma/\partial C_0)_\phi \dfrac{\omega^2}{2^{\frac{1}{2}}[(k_0^2 + \omega^2)^{\frac{1}{2}} - k_0]^{\frac{1}{2}}}} \tag{18}$$

When considered as a function of $\omega^{-\frac{1}{2}}$, $\omega C_p^* R_p$ can show a minimum as shown earlier[4].

For $k > \omega$ $\quad \omega C_p^* R_p \to 1/\omega\tau_R$

and for $k < \omega$ $\quad \omega C_p^* R_p \to 1 + (2/\omega\tau_{D1})^{\frac{1}{2}}$

CONCLUSION

A homogeneous reaction in solution coupled with adsorption leads to a relaxation process which is in part characterised by a reaction relaxation time, τ_R. However, unless τ_R lies between τ_{D1} and τ_{D2}, the rate of the homogeneous reaction will be only slightly reflected in the observed impedance–frequency spectrum.

SUMMARY

The problem of adsorption coupled with a homogeneous reaction has been solved for a sinusoidal perturbation of the electrode potential. The impedance–frequency spectrum can be described by the use of three relaxation times.

NOTATION

C Concentration of species S_1 (mole cm^{-3})
C' Concentration of species S_2 (mole cm^{-3})
C_0 $= C$ as $x \to \infty$

C'_0 $= C'$ as $x \to \infty$
C_p Parallel interfacial capacity (μF cm^{-2})
${}_\infty C_p = C_p$ as $\omega \to \infty = \left(\frac{\partial q_M}{\partial \phi}\right)_\Gamma$
C_p^* $= C_p - {}_\infty C_p$
D Diffusion coefficients of S_1, S_2 (cm^2 sec^{-1})
j $= \sqrt{-1}$
kk' First-order homogeneous rate constants (sec^{-1})
k_0 $= k(1 + C_0/C'_0)$
P Amplitude of sinusoidal perturbation (V)
q_M Charge on metal (μC cm^{-2})
R_p Parallel interfacial resistance (Ω cm^2)
t Time (sec)
x Distance from electrode (cm)
Z Electrode impedance (Ω cm^2)
α Parameter $0 \leqslant \alpha \leqslant 1$ determining the distribution of relaxation times
Γ Surface concentration of adsorbed molecules (mole cm^{-2})
ϕ Potential of metal (V)
ϕ_0 D.c. component of ϕ (V)
τ Relaxation time (sec)

REFERENCES

1 R. D. Armstrong, W. P. Race and H. R. Thirsk, *J. Electroanal. Chem.*, 16 (1968) 517.
2 K. Takahashi, *Electrochim. Acta*, 13 (1968) 1609.
3 K. S. Cole and R. H. Cole, *J. Chem. Phys.*, 9 (1941) 341.
4 R. D. Armstrong, D. F. Porter and H. R. Thirsk, *J. Electroanal. Chem.*, 16 (1968) 219.
5 W. Lorenz and F. Möckel, *Z. Elektrochem.*, 60 (1956) 507.

ELECTROANALYTICAL CHEMISTRY AND INTERFACIAL ELECTROCHEMISTRY
Elsevier Sequoia S.A., Lausanne – Printed in The Netherlands

THE PASSIVATION OF ZINC AMALGAM IN ALKALINE SOLUTIONS

R. D. ARMSTRONG, G. M. BULMAN AND H. R. THIRSK

Electrochemistry Research Laboratory, Department of Physical Chemistry, University of Newcastle upon Tyne, Newcastle upon Tyne, NE1 7RU (England)

(Received February 19th, 1969)

INTRODUCTION

The mechanism of dissolution of zinc amalgam in alkaline solutions was investigated by Gerischer[1] who showed that although the overall reaction was

$$Zn + 4\ OH^- = [Zn(OH)_4]^{2-} + 2\ e \quad (1)$$

the rate-determining step was

$$Zn + 2\ OH^- \rightarrow Zn(OH)_2 + 2\ e \quad (2)$$

At more anodic potentials, passivation occurs. The kinetics of the related active–passive transition for zinc metal have been extensively investigated[1-8] and it has been generally found that the formation of a surface layer of ZnO or $Zn(OH)_2$ is in some way associated with passivity, although the exact mechanism for the formation of this layer is not clear (for a short review see ref. 8). There has also been some controversy over the role of OH^- transport[3,5-7].

The present investigation was undertaken in order to determine the mechanism of passivation on a zinc amalgam electrode where the uniformity of the surface allows measurements at short times and null techniques to be used with advantage.

EXPERIMENTAL

Zinc amalgams (1 at. %) were prepared by direct combination of the elements (5N Zn wire, twice-distilled Hg) under an atmosphere of nitrogen. The solutions investigated were 0.1 *M* NaOH + 3 *M* NaCl, and 0.01 *M* NaOH + 3 M NaCl (AR-grade reagents). Some additional experiments were carried out using $NaNO_3$ and $NaSO_4$ as alternative supporting electrolytes. All solutions were deoxygenated with nitrogen. Saturated calomel reference electrodes (to which all potentials are referred) were used.

Square pulse potentiostatic measurements were made on a sitting drop electrode (area $\sim 10^{-1}$ cm^2). For short times, the *i–t* transients were recorded using an oscilloscope and at longer times, a chart recorder. Impedance measurements were made using: (a) a potentiostat in conjunction with a phase sensitive detector[9] and (b) a hanging drop electrode and a conventional Wien bridge[10].

For various potentials in the passive region, samples of the surface film were removed from a pool electrode and examined by electron microscopy and transmission electron diffraction. All measurements were made at room temperature, 25 ± 2°C,

except when control to 0.1°C was necessary, when an air thermostat was used. A determination of the e.m.f. of the cell:

$$\text{Zn 1 at. \% (Hg)} \left| \text{ZnO} \right| \begin{matrix} 0.1\ M\ \text{NaOH} \\ \\ 3\ M\ \text{NaCl} \end{matrix} \Bigg| \Bigg| \begin{matrix} \text{Satd.} \\ \text{KCl} \end{matrix} \Bigg| \text{Hg}_2\text{Cl}_2 \Bigg| \text{Hg}$$

gave $E = 1.375$ V.

RESULTS

(i) *Potentiostatic measurements*

Anodic square pulse potentiostatic measurements with $E_1 = -1.4$ V gave transients of two types. Thus, for 0.1 M NaOH + 3 M NaCl at $E_2 < -1.36$ V, a pseudo steady state current was observed (Fig. 1a) due to the active dissolution of zinc as

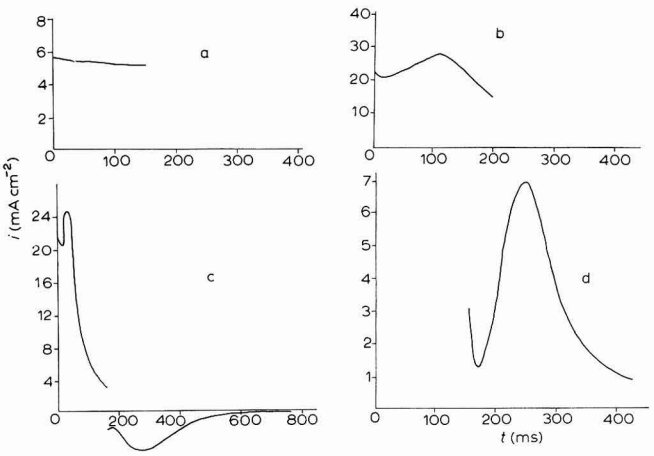

Fig. 1. Current–time transients for 0.1 M NaOH + 3 M NaCl. $E_1 = -1.40$ V; E_2: (a), −1.34; (b), −1.32; (c), −1.30 (anodic transients); (d), −1.20 V (cathodic transient on returning to E_1).

zincate, whereas for $E_2 > -1.36$ V a knee was observed in the i–t curve after which the current fell to a low value (Fig. 1b). For increasingly anodic potentials, this feature was observed to occur at shorter times (Fig. 2) and eventually a clear maximum was found (Fig. 1c). In more dilute OH^- solutions the basic features were the same, except that the effect of depletion of OH^- was more apparent in the active branch. The use of SO_4^{2-} and NO_3^- instead of Cl^- as supporting electrolytes, produced no significant change. The cathodic transient on returning to the potential, E_1, showed a peak, provided that the potential change was made after the knee had occurred. The integrated charge under this peak was approximately constant at 500 ± 100 μC cm^{-2} (Fig. 1d).

(ii) *Impedance measurements*

Measurements were made using 0.1 M NaOH + 3 M NaCl. The electrode impedance was found to be capacitative at potentials cathodic to −1.45 V. At more anodic

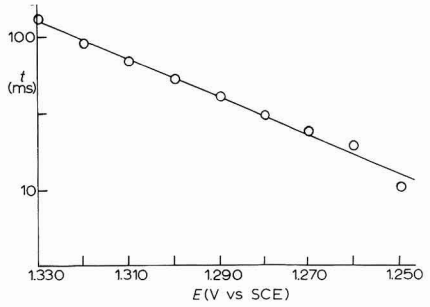

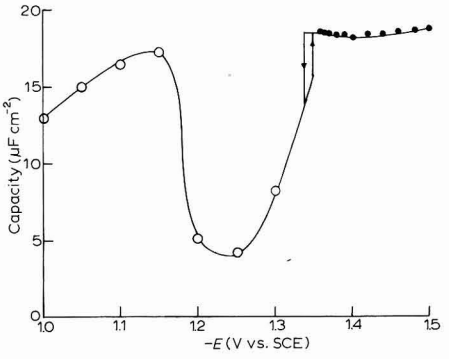

Fig. 2. Potential-dependence of the time to passivation for 0.1 *M* NaOH + 3 *M* NaCl.

Fig. 3. Potential-dependence of the double-layer capacity for 0.1 *M* NaOH + 3 *M* NaCl. (●), Measured at 25 kHz; (○), at 1 kHz, $t \rightarrow \infty$.

potentials a pseudo capacity was found which was attributed to reaction (1). The electrode impedance was analysed assuming that a "Randles circuit" was the appropriate analogue. The value of C_{dl} used was that measured at 25 kHz. Figure 4 shows that R_{sf} and $(\omega C_{sf})^{-1}$ are linear functions of $\omega^{-\frac{1}{2}}$ confirming that a Randles circuit describes the data within experimental error. The intercepts of R_{sf} at $\omega \rightarrow \infty$ were used to obtain the exchange current for reaction (1) as a function of potential (the surface concentration of $Zn(OH)_4^{2-}$ at $E = -1.360$ was estimated as 10^{-3} *M* from the slopes of the Randles plots, which is sufficiently small that the surface and bulk concentrations of Zn(Hg) and OH^- can be considered the same). These i_0-values together with steady state currents obtained potentiostatically enabled a composite current–voltage curve to be drawn (Fig. 5) which clearly shows the active–passive transition. In the active region, a Tafel line can be drawn with a slope of 60 ± 1 mV/decade which should be compared with that obtained by Gerischer[1], 57 mV/decade. In the passive region the current is almost independent of potential.

At potentials more anodic than -1.36 V, the impedance was found to be time-dependent. For times >1 min the impedance at these potentials was purely capacitative (to 2%). C_{dl} is shown as a function of time in Fig. 6, whilst C_{dl} as $t \rightarrow \infty$ is shown in Fig. 3. Visible observation of the surface showed a thick white film to be present at

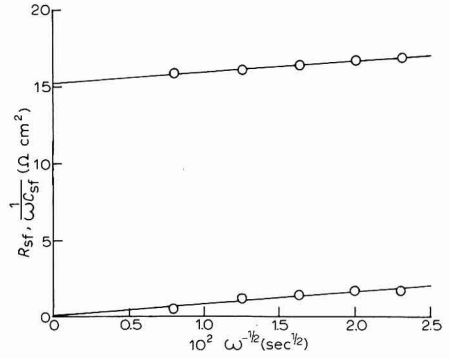

Fig. 4. Dependence of R_{sf}, $1/\omega C_{sf}$ on $\omega^{-\frac{1}{2}}$; 0.1 *M* NaOH + 3 *M* NaCl; $E = -1.4$ V.

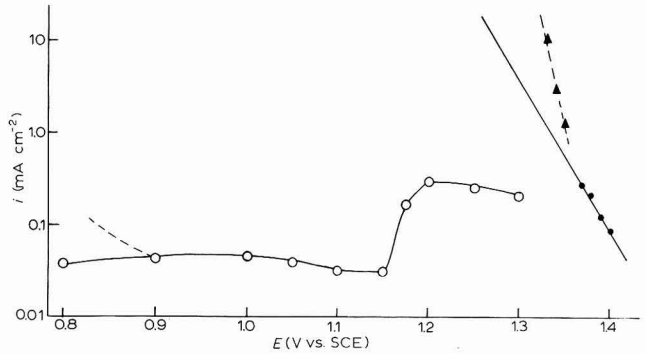

Fig. 5. Composite current–voltage curve. (○), Steady state; (●), a.c. impedance; (▲), transient potentiostatic measurements.

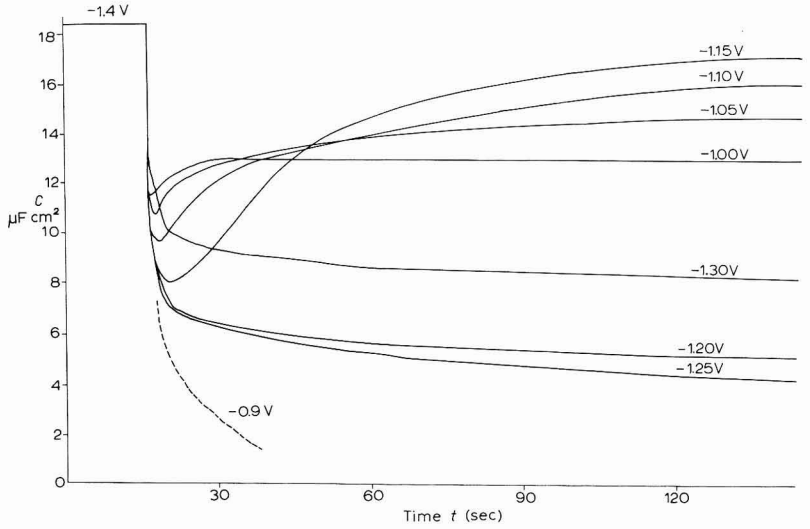

Fig. 6. Time-dependence of C_{dl} in the passive region: 0.1 *M* NaOH + 3 NaCl.

potentials more anodic than −0.9 V, which accords with the sharp change in C_{dl} at this potential.

(iii) Electron diffraction

Electron diffraction patterns were obtained from deposits formed at −1.2 V, −1.0 V and −0.7 V (region of thick deposit) for the 0.1 *M* NaOH + 3 *M* NaCl solution. Ring patterns were obtained (Fig. 7, a and b) which were identified as zinc oxide (ASTM card 5-0664), one degree oriented with the (0001) plane parallel to the electrode surface. For films formed at −0.7 V there was also some evidence for zinc hydroxides. Diffraction patterns from a tilted specimen (Fig. 7d) showed arcing which was also consistent with ZnO in the (0001) orientation.

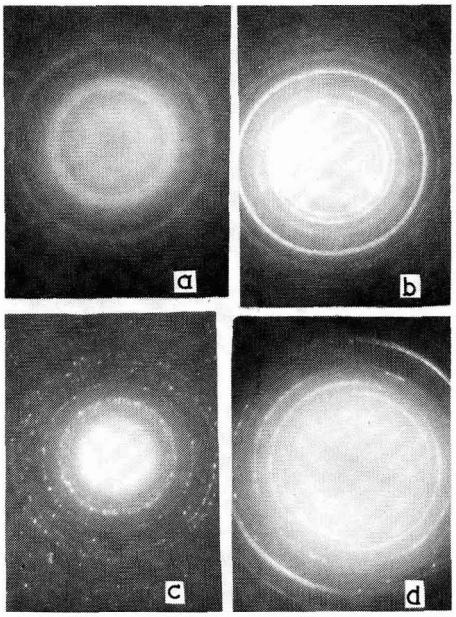

Fig. 7. Electron diffraction patterns for: (a), film formed at −1.2 V; (b), −0.7 V; (c), random ZnO for comparison; (d), as (b) but tilted at 45°.

DISCUSSION

(i) *The mechanism of passivation*

The experimental results obtained can be accounted for if it is assumed that passivation is due to the formation of a phase monolayer on the electrode surface by a mechanism involving two-dimensional nucleation and growth. It is tempting to identify this monolayer as a layer plane of ZnO, although this is doubtful because of the use of a *non in situ* technique. The calculated charge for a layer plane of ZnO is 350.4 μC cm^{-2} which is reasonably near that found by cathodic reduction. The anodic current–time transients can be interpreted as suggested earlier[11], *i.e.*, at any one potential there are three component currents:

$$i_1 = q_{\text{mon}}\, \pi v^2 A t^2 \exp\left(-\tfrac{1}{3}\pi v^2 A t^3\right) \tag{3}$$

due to formation of the phase layer;

$$i_2 = i'_0 \exp\left(-\tfrac{1}{3}\pi v^2 A t^3\right) \tag{4}$$

due to reaction (1) occurring on the "bare" metal surface ($i_2 \to 0$ as $t \to \infty$);

$$i_3 = i''_0\left[1 - \exp\left(-\tfrac{1}{3}\pi v^2 A t^3\right)\right] \tag{5}$$

due to reaction (1) occurring on the "covered" surface ($i_3 \to i''_0$ as $t \to \infty$).

The present results can be simulated reasonably well by assuming that i_3 is too small to be observed under the experimental conditions (Fig. 8). The cathodic reduction transient would be expected to follow eqn. (3) and this is tested in reduced variable form in Fig. 9.

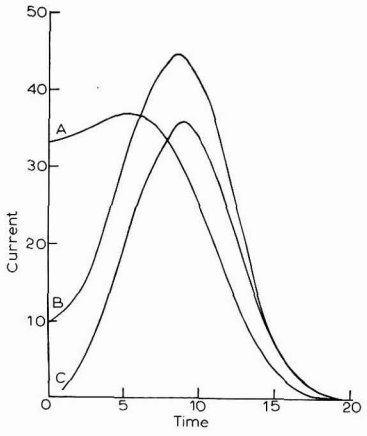

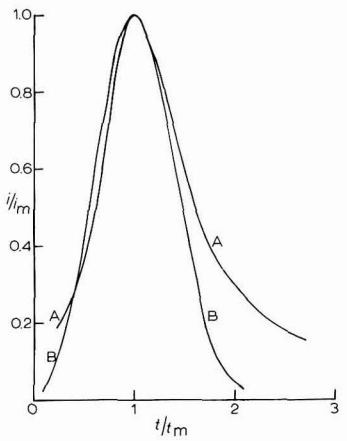

Fig. 8. Simulated current–time transients for $i_1 + i_2$ (eqns. (3), (4)) with (A), i_2 or (C), i_1 the dominant component.

Fig. 9. Test of cathodic reduction transient (Fig. 1d) for a fit to eqn. (3). (A) Experimental, (B) theoretical.

Information on the role of OH^- adsorption in passivation can be obtained from the C_{dl}-values. Since these do not show any marked change as the active–passive transition is approached, we conclude that there is no measurable adsorption of OH^- or indeed any reactant. It must therefore be concluded that OH^- adsorption is not responsible for the passive behaviour and that the experimentally distinguishable formation of the phase monolayer is all important.

The steady state current–voltage relationship obtained in the passive region requires some further comment. In the case of iron, Vetter[12] has suggested that the constant current arises from a constant field across the film, *i.e.*, the film thickness varies linearly with potential. In the present situation this explanation does not seem appropriate since the potentiostatic experiments and the C_{dl}-values lead us to conclude that there is only a monolayer film present on the electrode between $E = -1.36$ V and $E = -0.9$ V. The appropriate constancy of the current must therefore arise from modifications of the phase layer which are induced by the field across it.

(*ii*) *Comparison with related work*

The explanation of the passivation of zinc amalgam given here is similar to that proposed for zinc by Kabanov *et al.*[3] who suggested that a quantity of oxygen or oxide is present on the electrode equivalent to 1 mC cm^{-2}. We have found no evidence that the passivating layer is formed by "precipitation"[6,7] in the solution as has been suggested by some authors and we consider that relationships[6,7] of the type

$$i\tau^{\frac{1}{2}} = \text{constant} \tag{6}$$

are not particularly significant.

It should be noted that the formation of a thin layer of oxide on Zn(Hg) which does not appreciably thicken over a considerable range of potential has certain similarities with the anodic behaviour of Pt[13], and differs from that of Cd(Hg)[14] and Hg[15] in alkaline solution (see Table 1).

TABLE 1

COMPARISON OF THE ANODIC BEHAVIOUR OF Hg, Cd(Hg), Zn(Hg) IN ALKALINE SOLUTIONS

Metal	Zn(Hg)	Cd(Hg)	Hg
Solution	0.1 *M* NaOH + 3 *M* NaCl	1 *M* NaOH	1 *M* NaOH
Principal dissolved species	$[Zn(OH)_4]^{2-}$	$[Cd(OH)_4]^{2-}$	$Hg(OH)_2$
Passivating phase	ZnO	β–$Cd(OH)_2$	HgO(orthorhombic)
OH^- adsorption prior to phase formation	too small to measure		18% coverage
Difference between monolayer and bulk reversible potential	+9 mV	+15 mV	+15 mV
Effect of monolayer phase on dissolution reaction	discontinuous decrease in dissolution rate		reversible before and after phase formation
Behaviour subsequent to monolayer formation	Film does not thicken for 400 mV	2nd and 3rd monolayers formed on further 10 mV polarisation	Multilayer formed on further 10 mV polarisation, discontinuous decrease in dissolution rate

SUMMARY

It has been shown that the passivation of zinc amalgam in alkaline solutions is due to the formation of a phase monolayer on the electrode surface. This layer is formed by a mechanism involving 2D nucleation. No specific OH^- adsorption can be detected at potentials prior to the active–passive transition.

NOTATION

A Rate of nucleation of two-dimensional centres (nuclei cm^{-2} sec^{-1})
C_{dl} Double-layer capacity (μF cm^{-2})
C_{sf} Series component of the interfacial capacity due to a faradaic reaction (μF cm^{-2})
i'_0 Exchange current for dissolution reaction occurring on bare metal surface (A cm^{-2})
i''_0 Exchange current for dissolution reaction occurring on covered metal surface (A cm^{-2})
q_{MON} Charge associated with phase monolayer (μC cm^{-2})
R_{sf} Series component of the interfacial resistance due to a faradaic reaction (Ωcm^2)
V Rate of advance of the edge of a two-dimentional centre (cm sec^{-1})

REFERENCES

1 H. GERISCHER, *Z. Physik. Chem. Leipzig*, 202 (1953) 302.
2 I. SANGHI AND M. FLEISCHMANN, *Electrochim. Acta*, 1 (1959) 161.
3 T. I. POPOVA, V. S. BAGOTSKII AND B. N. KABANOV, *Zhr. Fiz. Khim.*, 36 (1962) 1433, 1440.

4 T. I. POPOVA, N. A. SIMONOVA AND B. N. KABANOV, *Elektrokhimiya*, 2 (1966) 1476.
5 T. P. DIRKSE, *J. Electrochem. Soc.*, 101 (1954) 328.
T. P. DIRKSE, D. DE WIT AND R. SHOEMAKER, *J. Electrochem. Soc.*, 115 (1968) 442.
T. P. DIRKSE, preprint from International Power Sources Symposium, Brighton, 1968.
6 M. A. V. DEVANATHAN AND S. LAKSHMANAN, *Electrochim. Acta*, 13 (1968) 667.
7 N. A. HAMPSON AND M. J. TARBOX, *J. Electrochem. Soc.*, 110 (1963) 95.
8 F. JOLAS, *Electrochim. Acta*, 13 (1968) 2207.
9 R. D. ARMSTRONG AND E. BARR, *J. Electroanal. Chem.*, 20 (1969) 173.
10 R. D. ARMSTRONG, W. P. RACE AND H. R. THIRSK, *Electrochim. Acta*, 13 (1968) 245.
11 R. D. ARMSTRONG, D. F. PORTER AND H. R. THIRSK, *J. Phys. Chem.*, 72 (1968) 2300.
12 K. J. VETTER, *Electrochemical Kinetics*, Academic Press, New York, 1967, p. 761.
13 S. GILMAN, *Electroanalytical Chemistry*, Vol. 2, edited by A. J. BARD, Marcel Dekker Inc., New York, 1967.
14 R. D. ARMSTRONG, J. D. MILEWSKI, W. P. RACE AND H. R. THIRSK, *J. Electroanal. Chem.*, 21 (1969) 517.
15 R. D. ARMSTRONG, W. P. RACE AND H. R. THIRSK, *J. Electroanal. Chem.*, 19 (1968) 233.

ELECTROANALYTICAL CHEMISTRY AND INTERFACIAL ELECTROCHEMISTRY
Elsevier Sequoia S.A., Lausanne – Printed in The Netherlands

POLAROGRAPHIC INVESTIGATIONS OF ORGANIC PEROXIDES

S. MOLNÁR AND F. PÉTER
Industrial Department for Plastics and Rubber, Technical University, Budapest (Hungary)

(Received October 21st, 1968; in revised form January 1st, 1969)

Reduction of organic peroxides at the dropping mercury electrode has received some interest[1-9], in particular with respect to structural effects and practical applications. This study considers the influence of different types of solvents (benzene, dichloroethane, dioxan, ethyl acetate, methanol, acetic acid) on the polarographic properties of diacyl peroxides of type:

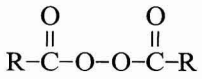

where R is:

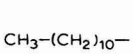

(Lauroyl peroxide)

(Benzoyl peroxide)

(Furoyl peroxide)

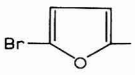

5-Bromofuroyl peroxide)

(Nicotinoyl peroxide)

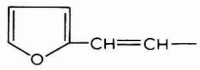

(Furilacrylic acid peroxide)

EXPERIMENTAL

Experiments were carried out using a Radelkis type 7-77-4/b polarograph. A dropping mercury electrode was used as cathode, and a mercury pool as anode. Oxygen was expelled from the solutions investigated by oxygen-free nitrogen gas. Because the commonly used conducting salts are insoluble in apolar solvents, solvent mixtures were used where one of the components was always methanol. The most satisfactory waves were obtained in 1 : 1 solvent mixtures.

The compounds investigated in organic solvent medium were polarographically active giving a single cathodic (reduction) wave. At the beginning of the limiting current there is a large maximum of first-order and, subsequently, a small one of second-order, their size being dependent on the nature and quantity of the depolarizer and the base electrolyte used, as well as the solvent. The maxima can be suppressed under the investigating conditions. The most suitable waves for evaluation were obtained with LiCl as conducting salt and this salt was used, therefore, for the investigations described.

RESULTS

1. *Change of the limiting current as a function of peroxide concentration*

Starting from 0.0 V, the polarograms of the peroxides have no base current. The polarograms pass the zero line of the galvanometer from the anodic side. In the presence of peroxides a wave is formed on the anodic side, its height being always the same and independent of the peroxide concentration (Fig. 1). In this study this wave is not discussed: it is most likely caused by anodic oxidation due to the presence of the peroxide. The cathodic peroxide wave follows this anodic wave in the negative voltage range.

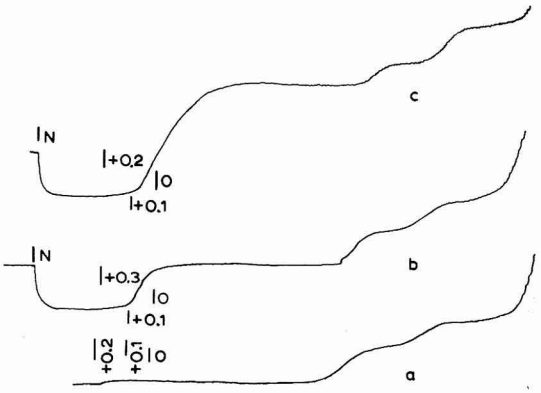

Fig. 1. Polarogram of benzoyl peroxide in potential range, +0.2 to −2 V. Depolarizer concn.: (a), 0; (b), $1 \cdot 10^{-4}$; (c), $1 \cdot 10^{-3}$ *M*. Solvent: 1:1 benzene–methanol mixture; base electrolyte: 0.1 *M* NH_4NO_3; maximum suppressor: $2.96 \cdot 10^{-3}$ *M* fuchsine; sensitivity: $3 \cdot 10^{-7}$ A/mm.

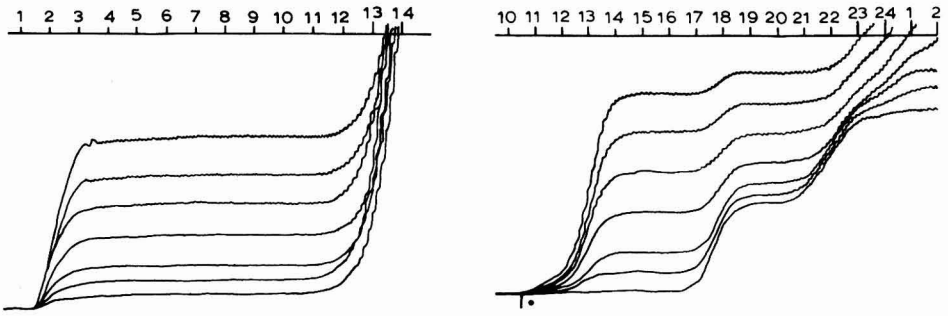

Fig. 2. Lauroyl peroxide concn. series in the presence of methylene blue as maximum suppressor. Solvent: 1:1 acetic acid–methanol mixture; base electrolyte: 0.1 *M* LiCl; sensitivity: $1 \cdot 10^{-7}$ A/mm; maximum suppressor: $3.13 \cdot 10^{-5}$ *M* methylene blue. Curves, bottom to top: 0; 1; 2; 4; 6; 8; $10 \cdot 10^{-4}$ *M* lauroyl peroxide.

Fig. 3. Lauroyl peroxide concn. series in presence of fuchsine as maximum suppressor. Solvent: 1:1 dioxan–methanol mixture; base electrolyte: 0.1 *M* LiCl; sensitivity: $1 \cdot 10^{-7}$ A/mm; maximum suppressor: $1.25 \cdot 10^{-3}$ *M* fuchsine. Curves, bottom to top: 0; 1; 2; 4; 6; 8; $10 \cdot 10^{-4}$ *M* lauroyl peroxide.

With each peroxide, there is a linear relation between the depolarizer concentration ($1 \cdot 10^{-4}$–$1 \cdot 10^{-3}$ *M*) and the cathodic wave height in the solvents studies (Figs. 2 and 3). The values of i_d/c are shown in Table 1.

In the case of lauroyl peroxide the half-wave potential remains the same with increase in peroxide concentration whereas with the other peroxides it is shifted slightly towards more negative potentials. More detailed results are to be found in the literature[10–13].

TABLE 1

VALUES OF POLAROGRAPHIC PARAMETERS IN DIFFERENT SOLVENT MIXTURES

Solvent: 1 : 1 mixture of solvent and methanol; base electrolyte: 0.1 *M* LiCl; maximum suppressor: fuchsine

Peroxide (*m.p.*)		*Ethyl acetate*	*Methanol*	*Benzene*	*Dichloro-ethane*	*Dioxan*	*Acetic acid*
Lauroyl	i_d/c	8.9	8.8	7.7	7.1	7.3	5.63
(54.5–55°)	I	3.67	3.72	3.14	2.92	3.01	2.31
	$I\eta^{\frac{1}{2}}$	2.64	2.76	2.48	2.47	3.93	2.24
	α	0.23	0.24	0.50	0.34	0.31	0.22
	n		1.91	1.76			
Benzoyl	i_d/c	12.0	11.2	10.6	11.1	9.35	8.5
(108.5–109°)	I	5.03	4.63	4.44	4.65	3.92	3.56
				3.67*			
	$I\eta^{\frac{1}{2}}$	3.61	3.56	3.50	3.93	3.81	3.45
				2.89*			
	α	0.23	0.33	0.22	0.27	0.23	0.29
	n		2.19	2.04			
Furoyl	i_d/c	11.8	11.2	11.1	10.1	10.7	8.6
(86–87°)	I	4.84	4.61	4.56	4.17	4.39	3.55
	$I\eta^{\frac{1}{2}}$	3.47	3.54	3.59	3.59	4.27	3.43
	α	0.20	0.25	0.22	0.21	0.18	0.27
	n		2.11	2.08			
Bromofuroyl	i_d/c	9.6	6.3	9.3	8.5	6.9	4.9
(125–126°)	I	4.02	2.64	3.88	3.56	2.89	2.05
	$I\eta^{\frac{1}{2}}$	2.89	2.03	3.07	3.01	2.81	1.99
	α	0.26	0.27	0.26	0.27	0.26	0.25
	n		1.67	2.03			
Nicotinoyl	i_d/c	12.3	7.9	10.3	11.1	9.5	—
(87–89°)	I	5.15	3.31	4.31	4.65	3.87	—
	$I\eta^{\frac{1}{2}}$	3.70	1.95	3.39	3.93	3.76	—
	α	0.27	0.26	0.25	0.27	0.26	—
	n		1.55	2.02			
Furilacrylic	i_d/c	6.2	—	8.4	5.2	3.8	—
acid	I	2.46	—	3.32	2.06	1.51	—
(97–99°)	$I\eta^{\frac{1}{2}}$	1.77	—	2.52	1.74	1.47	—
	α	0.28	—	0.24	0.31	0.32	—
	n			1.60			

* Base electrolyte: 0.1 *M* NH_4NO_3.

2. *The character of the electrode process and the mechanism of the reaction*

The wave height depends linearly on the square root of the height of the mercury column. The temperature coefficient is as follows: lauroyl peroxide, 0.97%/°C; benzoyl peroxide, 1.09%/°C; furoyl peroxide, 0.60%/°C nicotinoyl peroxide, 0.90%/°C; 5-bromofuroyl peroxide, negative.

With furilacrylic acid peroxide it exponentially decreases. Since in the case of organic solvents, the temperature coefficient of the viscosity, η, is about -1.6% compared with $d\eta/dT = -2.4\%$, the value for water, the temperature coefficient of value 1.0%/°C indicates a diffusion current. In the case of peroxides, however, to verify the character of the electrode process the temperature coefficient can only be used together with some other factors, because the decomposition of peroxides at higher temperatures may result in errors.

The linear relation between the wave height and the depolarizer concentration and the square root of the mercury column height indicates the diffusion nature of the limiting current.

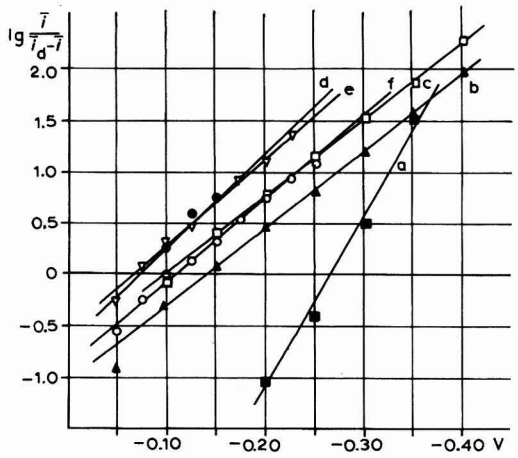

Fig. 4. Logarithmic analysis of current waves. Depolarizer concn.: $1 \cdot 10^{-3}$ *M*; solvent: 1:1 benzene–methanol mixture; base electrolyte: 0.1 *M* LiCl. Depolarizer: (a), lauroyl; (b), benzoyl; (c), furoyl; (d), bromofuroyl; (e), nicotinoyl; (f), furilacrylic acid peroxide.

The small values of α, the transfer coefficient (Table 1, Fig. 4), and the concentration-dependency of the half-wave potentials prove the irreversibility of the electrode process.

The character of the electrode process during the reduction was studied also by determining the electron number (n) on the basis of Ilkovič's equation (Table 1). It can be seen that two electrons participate in the reduction of one peroxide molecule. Reduction therefore takes place as follows:

$$\mathrm{R{-}\overset{\overset{O}{\|}}{C}{-}O{-}O{-}\overset{\overset{O}{\|}}{C}{-}R} + 2\,e^- + 2\,H^+ \longrightarrow 2\,\mathrm{R{-}\overset{\overset{O}{\|}}{C}{-}OH}$$

3. *The effect of organic solvents on the polarographic properties*

The values of I, $I\eta^{\frac{1}{2}}$ and α of the diffusion constant in different solvents are given in Table 1. The values of $I\eta^{\frac{1}{2}}$ are the same (within 10%) with a few exceptions. The small variations found by more careful investigation are not dealt with in the present paper.

Different solvents also slightly affect the half-wave potential values (for more details, see refs. 1–4). Because of the absence of regular polarograms (that start with a base current) and the gradual shift of the half-wave potentials within one concentration series, the values of the change of half-wave potential in different solvent mixtures could not be related to any one solvent characteristic (*e.g.*, dielectric constant).

The change in the value of α for different solvents (Fig. 5) did not show any regularity and thus cannot be attributed to changes of reversibility of the electrode process.

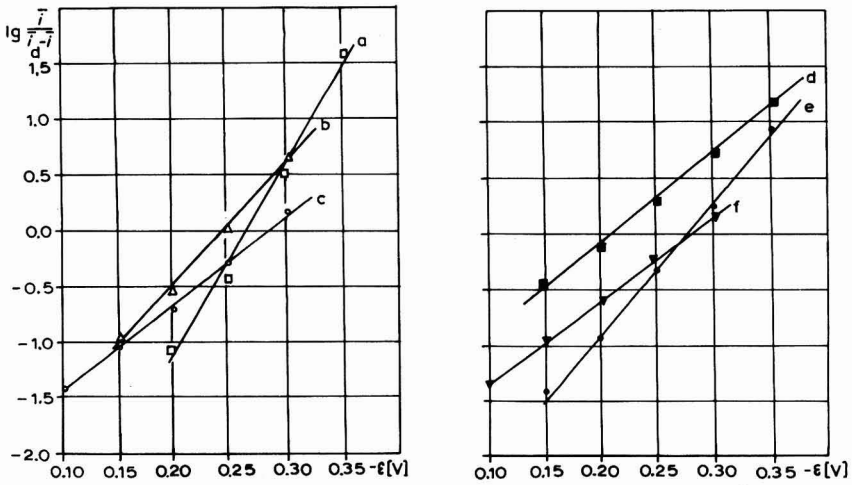

Fig. 5. Logarithmic analysis of lauroyl peroxide wave. Depolarizer concn.: $1 \cdot 10^{-3}$ M; base electrolyte: 0.1 M LiCl; maximum suppressor: $1.25 \cdot 10^{-3}$ M fuchsine. Solvent in 1 : 1 mixture with methanol: (a), benzene; (b), dioxan; (c), ethyl acetate; (d), methanol; (e), dichloroethane; (f), acetic acid.

Although there are slight differences in the half-wave potentials of the individual peroxides, the precise evaluation and investigation of the correlation between the peroxide structure and the half-wave potential are restricted by the concentration-dependency of the half-wave potentials and by the fact that the diffusion wave of peroxide reduction coincides with the anodic wave.

SUMMARY

The R–C(=O)–O–O–C(=O)–R-type diacyl peroxides investigated (lauroyl, benzoyl, furoyl, 5-bromofuroyl, nicotinoyl and furilacrylic acid peroxide) in 1 : 1 by volume

mixtures of methanol with benzene, dichloroethane, dioxan, ethyl acetate, and acetic acid, are polarographically active providing an anodic and a cathodic wave. The height of the anodic wave is not dependent on the peroxide concentration, but the concentration of the cathodic wave changes with variations in the depolarizer concentration.

In the case of the cathodic wave, the limiting current is diffusion-controlled. The electrode process is irreversible and the value of the transfer coefficient is low. The electron number of the electrode process is 2. In different solvents, the values of $I\eta^{\frac{1}{2}}$ are the same within 10%. The effect of the solvents and the structure on the half-wave potentials of the peroxides is not at present explicable.

REFERENCES

1 V. STERN AND S. POLJAK, *Acta Physicochim. U.R.S.S.*, 10 (1939) 797.
2 M. B. NEIMAN AND M. I. GERBER, *Zh. Anal. Khim.*, 1 (1946) 211.
3 C. O. WILLITS, C. RICCIUTI, C. C. KNIGHT AND D. SWERN, *Anal. Chem.*, 24 (1952) 785.
4 P. H. GIGUÈRE AND D. LAMONTAGNE, *Canad. J. Chem.*, 29 (1951) 54.
5 D. SWERN AND L. S. SILBERT, *Anal. Chem.*, 35 (1963) 880.
6 D. A. SKOOG AND B. H. LAUWZECHA, *Anal. Chem.*, 28 (1956) 825.
7 H. BRÜSCHWEILER AND G. J. MINKOFF, *Anal. Chim. Acta*, 12 (1955) 186.
8 V. L. ANTONOVSKII AND Z. S. FROLOVA, *Zh. Obshch. Khim.*, 35 (1965) 954.
9 E. S. LEVINE, *Elektrokhimiya*, 2 (1966) 955.
10 S. MOLNÁR, F. PÉTER AND S. PATYI, *Magy. Kem. Folyoirat*, 73 (1967) 341.
11 S. MOLNÁR, F. PÉTER AND A. TÓTH, *Magy, Kem. Folyoirat*, 74 (1968) 422.
12 S. MOLNÁR AND F. PÉTER, *Periodica Polytech.*, 12 (1968) 113.
13 S. MOLNÁR AND F. PÉTER, *Periodica Polytech.*, in press.

ELECTROANALYTICAL CHEMISTRY AND INTERFACIAL ELECTROCHEMISTRY
Elsevier Sequoia S.A., Lausanne – Printed in The Netherlands

PHYSICO-CHEMICAL STUDIES ON THE BINDING OF DYES WITH SURFACTANTS

II. POLAROGRAPHY OF SURFACTANT–DYE MIXTURES

WAHID U. MALIK AND PURAN CHAND
Chemical Laboratories, University of Roorkee, Roorkee (India)
(Received December 10th, 1968)

Recently, Buchanan and Griffith[1] have made a brief investigation of the applicability of the polarographic method to the estimation of anionic surfactants. This method (with slight modifications) can be used not only for estimating the surfactant concentration but also for determining quantitatively the binding of the dyes to the surfactant. The present communication describes the polarographic investigation of the binding of acidic dyes to cationic surfactants and basic dyes to anionic surfactants and is an extension of our earlier spectrophotometric study[2].

EXPERIMENTAL

Reagents

Dioctyl sodium sulphosuccinate (Manoxol OT), cetyltrimethylammonium bromide (CTMAB) and cetylpyridinium bromide (CPB) were all BDH products and were used without further purification.

Methylene blue, congo red and alizarin red S were BDH products and were purified by further recrystallization.

Buffers (Robinson–Britton, glycine and acetate) were prepared in doubly-distilled water by the usual method[3]. The pH was checked with a Beckman pH-meter, model H.

Apparatus

Polarographic measurements were carried out using a Heyrovský polarograph, model Lp 55A operated manually using a Scalamp Pye galvanometer. All measurements were made at $25 \pm 0.1°$ by immersing the H-cell in a thermostatic water bath. Purified hydrogen was used to maintain an inert atmosphere.

Procedure

The method proposed by Buchanan and Griffith[1] is analogous to amperometric titrations between the surfactant and the dye. It was found that sufficient time for complete reaction and settling of the precipitate should be allowed before polarographic analysis. Also, in some dye–surfactant mixtures, *e.g.*, methylene blue and Manoxol OT, the reaction product is sticky and likely to damage the polarographic capillary. For accurate determinations the following modified procedure was, therefore, employed.

Working solutions were prepared by taking a known amount of dye solution (10^{-3} *M*) and mixing it with a constant amount of the appropriate buffer solution (4.0 ml). Varying amounts of the surfactant solution (10^{-2} *M*) were then added, and the total volume was adjusted to 10.0 ml with doubly-distilled water. The solutions were allowed to stand overnight to complete the reaction. The polarograms of the supernatant solutions were carried out after passing purified hydrogen through the solution for about 10 min.

RESULTS AND DISCUSSION

Behaviour of dyes at the DME

Congo red gives a reversible polarographic wave with a half-wave potential ($E_{\frac{1}{2}}$) = −0.48 V in glycine buffer at pH 6.0 (Fig. 1, curve 1). The reduction of the dye could not be studied at low pH-values because of change in colour (blue) in acidic medium due to transformation into the quinonoid form[4].

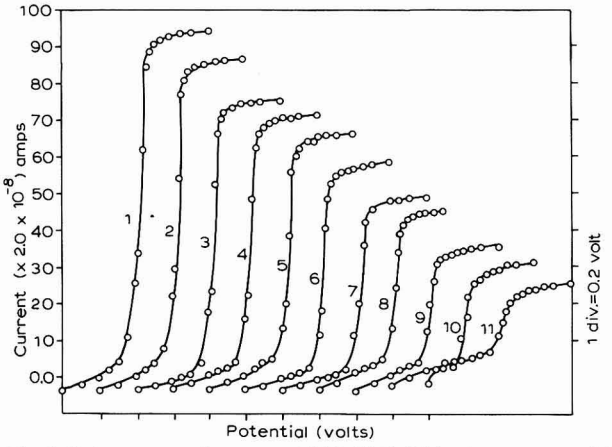

Fig. 1. Polarograms of congo red ($2.0 \cdot 10^{-4}$ *M*) in the presence of different concns. of CTMAB: (1), 0.0; (2), 0.2; (3), 0.6; (4), 1.0; (5), 1.2; (6), 1.6; (7), 2.0; (8), 2.2; (9), 2.6; (10), 3.0; (11), $3.4 \cdot 10^{-4}$ *M*. Each curve starts at −0.1 V.

The reduction of alizarin red S was possible over a wider pH-range. The $E_{\frac{1}{2}}$-values of the waves (which were reversible) were as follows:

	Acetate buffer			*Robinson–Britton buffer*
pH	3.09	4.00	5.00	7.00
$E_{\frac{1}{2}}$ (V)	−0.28	−0.40	−0.48	−0.50

A well-defined reversible polarographic wave with $E_{\frac{1}{2}} = -0.26$ V was obtained for methylene blue in glycine buffer, pH 6.0.

Polarography of surfactant–dye mixtures

In order to determine polarographically the binding of dye to surfactant, the

optimum conditions for the precipitation of the surfactant–dye complex were first ascertained. Mixtures containing varying proportions of the two reactants were prepared; those containing a large excess of dye did not give well-defined waves owing to the partial dissolution of the precipitate. On the other hand, the surfactant–dye complex was dispersed in excess of surfactant with the result that no reduction step could be realised. Between these two limits lay the zone of complete precipitation from which the concentration range for carrying out the polarographic analysis could be chosen.

The polarography of congo red and CTMAB and CPB mixtures was carried out at pH 6.0, while corresponding studies with alizarin red S could be carried out at pH 3.09, 4.0, 5.0 and 7.0. In all cases, a decrease in the limiting current of the dye was observed on the gradual addition of surfactant (Fig. 1) and a linear relationship was realised on plotting the decrease in wave-height, $(i_d)_0 - i_d$, against surfactant concentration (Fig. 2). A slight deviation from linearity was observed at low concentrations of the surfactant as it appears that the flocculation zone is not reached at low surfactant concentrations.

Polarographic reduction of methylene blue was carried out in glycine buffer at pH 6.0 in the presence of varying amounts of Manoxol OT (Fig. 3). As with cationic surfactants, a decrease in wave height was observed. However, a slight shift in $E_{\frac{1}{2}}$

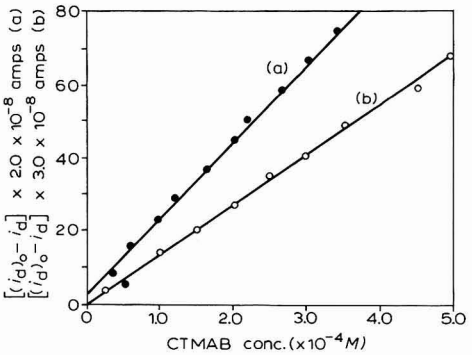

Fig. 2. Plots of CTMAB concn. *vs.* decrease in wave height. Congo red concn.: (a), 2.0; (b), $3.0 \cdot 10^{-4}$ *M*.

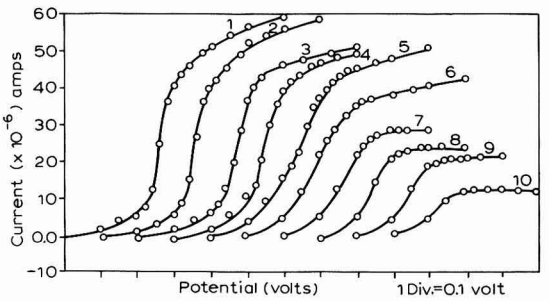

Fig. 3. Polarograms of methylene blue ($2.0 \cdot 10^{-3}$ *M*) in the presence of different concns. of Manoxol OT: (1), 0.0; (2), 0.4; (3), 0.8; (4), 1.0; (5), 1.4; (6), 1.6; (7), 1.8; (8), 2.0; (9), 2.2; (10), $3.0 \cdot 10^{-3}$ *M*. Each curve starts at 0.0 V.

towards more positive potentials (from -0.26 to -0.14 V), which was not found in cationic surfactant–acid dye mixtures, was observed.

The plots between decrease in wave height and surfactant concentration can be used as calibration curves for determining surfactant concentration. The polarographic method has the advantage over existing methods (spectrophotometry, conductometry, potentiometry, etc.) in that it can be used over a wide concentration range, *i.e.*, above the critical micelle concentration (c.m.c.), and also that it can be employed in a very small volume of reaction mixture, say, less than 1.0 ml.

The polarographic data indicate that cationic surfactants can be estimated more accurately (even at lower concentrations) than anionic surfactants. This may be due to the fact that the flocculation zone is reached at very small concentrations in the case of cationic surfactants.

Binding of dyes with surfactants

The polarographic data of surfactant–dye mixtures were used to determine the binding of the dye with surfactants at various concentrations.

Cationic surfactants–acidic dyes. The results on the binding of congo red ($2.0 \cdot 10^{-4}$ *M*) with CTMAB and CBP are given in Table 1.

Table 1 shows that one molecule of dye is bound to two molecules of surfactant. This ratio is not reached at lower surfactant concentrations owing to the dispersion of the insoluble dye–surfactant complex in excess of the dye.

The binding data for alizarin red S are shown in Table 2.

It is evident that the binding of the dye is extremely small in the case of CPB (dye : surfactant = 1 : 10), but quite large for CTMAB (dye : surfactant = 2 : 1). The

TABLE 1

BINDING OF CONGO RED WITH SURFACTANTS

Surfactant concn. ($\cdot 10^{-4}$ *M*)	i_d ($\cdot 2.0 \cdot 10^{-8}$ A)	$(i_d)_0 - i_d$ ($\cdot 2.0 \cdot 10^{-8}$ A)	$i_d/(i_d)_0$	*Free dye* ($\cdot 10^{-4}$ *M*)	*Bound dye* ($\cdot 10^{-4}$ *M*)	*Surfactant concn./ bound dye concn.*
CTMAB						
$(i_d)_0 = 90.0 \times 2 \cdot 10^{-8}$ A; dye concn. $= 2.0 \cdot 10^{-4}$ *M*						
1.00	67.0	23.0	0.74	1.48	0.52	1.92
1.60	53.0	37.0	0.59	1.18	0.82	1.95
2.00	45.0	45.0	0.50	1.00	1.00	2.00
2.60	31.0	59.0	0.34	0.68	1.32	1.97
3.00	23.0	67.0	0.25	0.50	1.50	2.00
3.40	15.0	75.0	0.17	0.34	1.66	2.05
CPB						
$(i_d)_0 = 93.0 \times 2 \cdot 10^{-8}$ A; dye concn. $= 2.0 \cdot 10^{-4}$ *M*						
0.80	74.0	19.0	0.80	1.60	0.40	2.00
1.00	70.0	23.0	0.75	1.50	0.50	2.00
1.60	56.0	37.0	0.60	1.20	0.80	2.00
2.00	45.0	48.0	0.48	0.96	1.04	1.92
2.40	40.0	53.0	0.43	0.86	1.14	2.10
3.00	23.0	70.0	0.25	0.50	1.50	2.00

TABLE 2

BINDING OF ALIZARIN RED S WITH SURFACTANT AT pH 4.00

Surfactant concn. ($\cdot 10^{-5}$ *M*)	i_d ($\cdot 10^{-8}$ *A*)	$(i_d)_0 - i_d$	$i_d/(i_d)_0$	*Free dye* ($\cdot 10^{-4}$ *M*)	*Bound dye*	*Surfactant concn./ bound dye concn.*
CTMAB						
$(i_d)_0 = 70.0 \cdot 10^{-8}$ A; dye concn. $= 15.0 \cdot 10^{-4}$ *M*						
5.0	65.0	5.0	0.93	13.95	1.05	0.48
10.0	60.0	10.0	0.86	12.90	2.10	0.48
25.0	46.0	24.0	0.66	9.90	5.10	0.49
37.5	36.0	34.0	0.50	7.50	7.50	0.50
50.0	25.0	45.0	0.36	5.40	9.60	0.52
62.5	13.0	57.0	0.19	2.85	12.15	0.51
CPB						
$(i_d)_0 = 44.0 \cdot 10^{-8}$ A; dye concn. $= 10.0 \cdot 10^{-4}$ *M*						
5.0	42.0	2.0	0.95	9.5	0.5	10.0
20.0	35.0	9.0	0.80	8.0	2.0	10.0
25.0	33.0	11.0	0.75	7.5	2.5	10.0
30.0	30.0	14.0	0.68	6.8	3.2	9.4
50.0	23.0	21.0	0.52	5.2	4.8	10.4
60.0	17.0	27.0	0.40	4.0	6.0	10.0
70.0	12.0	32.0	0.27	2.7	7.3	9.6

TABLE 3

BINDING OF METHYLENE BLUE WITH MANOXOL OT AT pH 6.0
$(i_d)_0 = 46.0 \cdot 10^{-6}$ A; dye concn. $= 2.0 \cdot 10^{-3}$ *M*

Manoxol OT concn. ($\cdot 10^{-4}$ *M*)	(i_d) ($\cdot 10^{-6}$ *A*)	$(i_d)_0 - i_d$	$i_d/(i_d)_0$	*Free dye* ($\cdot 10^{-3}$ *M*)	*Bound dye*	*Manoxol concn./ bound dye concn.*
0.4	42.0	4.0	0.91	1.82	0.18	0.22
1.0	36.0	10.0	0.78	1.56	0.44	0.23
1.40	31.0	15.0	0.67	1.34	0.66	0.21
1.80	26.0	20.0	0.57	1.14	0.86	0.21
2.00	23.0	23.0	0.50	1.00	1.00	0.20
2.20	21.0	25.0	0.46	0.92	1.08	0.20

binding of alizarin red S with CTMAB and CPB was also determined at different pH-values, *viz*, 3.09, 5.00 and 7.0 and in all cases the combining ratio was not influenced by change in pH of the reaction mixture.

Anionic surfactant–basic dye. The results on the binding of methylene blue to Manoxol OT are given in Table 3.

It is evident from the above table that the binding ratio does not change with Manoxol OT concentration. Unlike cationic surfactants, the amount of dye bound is much higher, the dye-surfactant binding ratio being 5 : 1.

ACKNOWLEDGEMENT

The authors are grateful to C.S.I.R. (India) for the award of a fellowship to one of us (P.C.) in support of this work.

SUMMARY

The polarographic method has been used to determine the binding of the acidic dyes, congo red and alizarin red S, to cationic surfactants (cetylpyridinium bromide—CPB, and cetyltrimethylammonium bromide—CTMAB) and that of the basic dye, methylene blue, to the anionic surfactant, dioctyl sodium sulphosuccinate (Manoxol OT). The surfactant concentration did not affect the combining ratio of dye to surfactant. Similarly, the pH of the reaction mixture had no influence on the combining ratio of dye to surfactant in the case of alizarin red S. A slight positive shift in $E_{\frac{1}{2}}$ of methylene blue in the presence of Manoxol OT was realized at higher surfactant concentration. The calibration curve of surfactant concentration *vs.* decrease in wave height was used to determine the concentration of anionic and cationic surfactants.

REFERENCES

1 G. S. BUCHANAN AND J. C. GRIFFITH, *J. Electroanal. Chem.*, 5 (1963) 204.
2 W. U. MALIK AND S. P. VERMA, *J. Phys. Chem.*, 70 (1966) 26.
3 H. T. S. BRITTON, *Hydrogen Ions*, Vol. 1, D. Van Nostrand Co., Inc. Princeton, New Jersey, 1956.
4 W. U. MALIK AND R. HAQUE, *J. Phys. Chem.*, 67 (1963) 2082.

ELECTROANALYTICAL CHEMISTRY AND INTERFACIAL ELECTROCHEMISTRY
Elsevier Sequoia S.A., Lausanne – Printed in The Netherlands

THE FORMATION OF TETRAETHYLLEAD BY ELECTROCHEMICAL REDUCTION OF ETHYL BROMIDE

R. GALLI
Montecatini Edison S.p.A., "G. Donegani" Research Institute, Novara (Italy)
(Received December 10th, 1968)

INTRODUCTION

Recent developments in organo-electrochemistry have given particular importance to studies on the preparation of metal–alkyl derivatives—particularly lead–alkyl derivatives. In effect, the possibility of generating radicals electrochemically has greatly increased interest in the study of the interactions of such radicals with electrodic materials[1]. In this field, the Nalco and Ziegler processes—using as alkylating agents organometallic compounds of an auxiliary metal (MgRCl in the Nalco process; $NaAlR_4$ in the Ziegler process)—are well known.

Moreover it should be appreciated that the present industrial synthesis of tetraethyllead ($PbEt_4$) by ethylation of PbNa alloy with EtCl may be considered formally as an electrochemical process like the reductions with amalgam. The alloy is a galvanic element where Pb represents the cathodic area and Na the anodic area. Thus, the overall reaction:

$$4\ PbNa + 4\ EtCl \rightarrow PbEt_4 + 4\ NaCl + 3\ Pb$$

can be considered as the sum of the partial electrodic reactions:

$$\tfrac{1}{4}\ Pb + EtCl + e \rightarrow \tfrac{1}{4}\ PbEt_4 + Cl^-$$
$$Na \rightarrow Na^+ + e$$

In spite of the industrial importance of lead–alkyls, only a little information is available on their formation[2].

We have, therefore, carried out a study on the formation of lead alkyls by reduction of alkyl halides at Pb cathodes. The reduction of alkyl halides, RX, has been thoroughly investigated mainly by polarographic studies on the complete reduction to hydrocarbons. Less attention has been paid to the one-electron reduction[3-6], *i.e.*:

$$RX + e \rightarrow R^{\cdot} + X^- \qquad (1)$$

and to the interactions of the radicals produced with the electrode material.

We have studied in particular the formation of $PbEt_4$ by reduction at Pb cathodes of ethyl bromide (EtBr) in propylene carbonate (PC) solutions with Et_4NBr as supporting electrolyte. We examined together with the electrochemical process, the static potentials of Pb, to determine the relevant reactions, the effect of proton-donors in solution and of noble metal impurities in Pb.

The form in which EtBr is present in solution was examined from a consider-

ation of its partial dissociation in PC through interactions, causing fission of the carbon–halogen bond.

The cell reaction is as follows:

$$\tfrac{1}{4}\,Pb + EtBr \rightarrow \tfrac{1}{4}\,PbEt_4 + \tfrac{1}{2}\,Br_2 \qquad (2)$$

Considering each electrode reaction: the formation of the organometallic compound takes place at the cathode

$$\tfrac{1}{4}\,Pb + EtBr + e \rightarrow \tfrac{1}{4}\,PbEt_4 + Br^- \qquad (3)$$

and the discharge of the halide ions at the Pt or graphite anode:

$$Br^- - e \rightarrow \tfrac{1}{2}\,Br_2 \qquad (4)$$

EtBr is reported to be stable to anodic oxidation[7].

EXPERIMENTAL

Materials

The materials used were as follows: lead (Carlo Erba, $>99\%$); ethyl bromide (Carlo Erba, 99.5 %); lithium perchlorate (British Drug Houses); tetraethylammonium bromide (Carlo Erba); propylene carbonate (Jefferson Chemical Co., $>99.6\%$); tetraethyllead (Montecatini-Edison, 98%). EtBr and PC were stored in the presence of molecular sieves 4A-1/16′ (Union Carbide) to minimize the water content (usually about 100 p.p.m.). Before each test, the Pb electrodes were mechanically treated to remove the surface layer of oxide.

Conductivity

Measurements were carried out with a conductivity bridge, LKB type 3216 B, equipped with Wagner earth (accuracy: 0.1 %), and using LKB measurement cells. All measurements were made in a water thermostat controlled to $\pm 0.1°$.

Reference electrodes in PC

The following half-cell was used as reference electrode to measure the electrode potentials:

$$Pt|Hg|Hg_2Br_2|Et_4NBr \text{ satd.}, Hg_2Br_2 \text{ satd.}, PC$$

Tetraethylammonium halides were used as supporting electrolytes as they are more soluble and dissociated in PC than the potassium salts usually used in aqueous solution. The stability of these half-cells was satisfactory: after suitable ageing, two electrodes prepared in the same way showed differences of less than 1 mV.

Static potentials

In order to determine the Pb static potentials, the mechanically deoxidized electrodes were dipped in the solution to be examined while stirring; the variation of the potential with time, referred to the reference electrode, at constant temperature ($25 \pm 0.1°$), was followed until stabilization was achieved.

The value of the potential was measured with a type 610 B Keithley electrometer, with an input impedance of $10^{14}\ \Omega$, and an accuracy of 1% full scale.

Polarization curves

The experimental cathode polarization η_c is equal to the electrode potential with current flow, less its value in the absence of current[8].

The potentiostatic polarization curves have been obtained point by point. In each test, for each polarization the values of current density chosen were those having a variation lower than 1% in 2 min (generally attained in 5–20 min).

The solution was renewed after each test for two reasons:

(a) to avoid diffusion of Br_2 into the catholyte and of $PbEt_4$ into the anolyte;

(b) to avoid accumulation of the $PbEt_4$ formed, which could have modified the experimental conditions.

Diaphragm

Fritted glass or polypropylene fabric were used as diaphragms. Of several samples tested, this fabric appeared to be the most efficient and corrosion resistant in the solutions used.

Material yields and current efficiency

Tests were carried out in a conventional H-cell, with a capacity of 250 ml and a sintered glass diaphragm using Pb cathodes and Pt anodes.

The duration of the tests was usually 5–30 h, with a continuous reading of cathodic polarization, cell tension and current density; the quantity of electricity was measured by a Lingane-type H_2–O_2 coulometer or by a copper coulometer.

The amount of Pb dissolved at the cathode and of $PbEt_4$ present in the solution were determined at the end of each test.

On the basis of the electrodic reaction (3), 4 faradays are required to dissolve 1 mole of Pb at the cathode and form 1 mole of $PbEt_4$. The current yields referring to the loss of weight of Pb and to the amount of $PbEt_4$ in the solution were determined and compared. The Pb dissolved is not completely converted to $PbEt_4$; the yield percent of the transformation, Pb $\rightarrow$ $PbEt_4$, was calculated from the ratio of the two yields.

Analysis

The quantitative determination of $PbEt_4$ in solution was carried out by vapour phase chromatography with a stainless steel column, with a stable phase of 20% Carbowax 4000 on Chromosorb W ($T=150°$; injector 210°; helium carrier gas; pressure 0.7 atm) and hot wire detector. When the total amount of Pb in solution was required—independently of the type of compound—it was determined with an atomic absorption spectrophotometer (Perkin Elmer 303).

PC–EtBr interactions

EtBr is a weakly polar compound ($\mu=1.9$, $D=9.2$ at 25°), and a weak Lewis acid as, in general, alkyl halides are. These compounds can interact with polar compounds having donor-electron centres. Kornblum and Blackwood[9] found a slow reaction between alkyl halides and dimethylformamide.

We examined the possibility of a similar behaviour with PC by conductivity measurements in PC–EtBr mixtures. The results are shown in Fig. 1, together with those of mixtures of PC + PrBr (Pr = *n*-propyl) and PC + BuBr (Bu = *n*-butyl). The

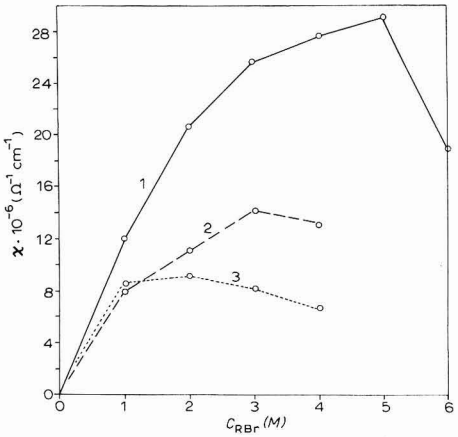

Fig. 1. Variation of specific conductivity, χ, of PC–RBr mixtures with RBr concn. at 26°. (1) RBr = ethyl bromide, (2) RBr = *n*-propyl bromide, (3) RBr = *n*-butyl bromide.

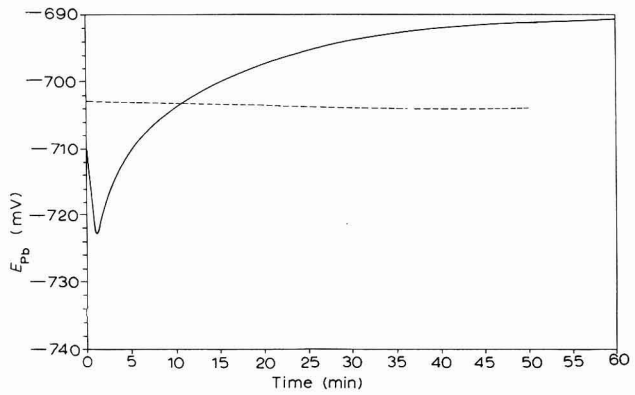

Fig. 2. Pb static potentials (E_{Pb}) *vs.* time plot, for two electrolytic systems. Temp. 25°. (——), PC, Et_4NBr 0.05 *M*, EtBr 2 *M*, $PbEt_4$ 0.015 *M*; (-------), PC, Et_4NBr 0.05 *M*, EtBr 0.2 *M*, $PbEt_4$ 0.015 *M*, CH_3COOH 0.1 *M*.

values reported refer to the measurements carried out a month after the preparation of the solutions, which was necessary in order to obtain stable enough values: the interaction rate is very low causing the conductivity to vary continuously with time. There is a sharp increase in conductivity, with respect to that of the pure components, up to maximum above which a rapid drop is observed due to the prevalence in the solution of the weakly polar halogenated hydrocarbon. This phenomenon increases in the order, $C_2 > C_3 > C_4$, and the maximum is reached first by the C_4-compound and then by the C_3- and C_2-compounds.

These results may be attributed to an interaction between EtBr and the oxygen atoms of PC, which are the donor-electron centres. This may occur either with ester-type oxygen atoms (A) or with carboxylic oxygen atoms (B), and an equilibrium between the two forms is probable.

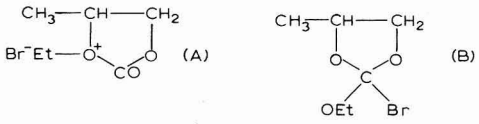

However, these interactions between PC and EtBr, indicated by the conductivity measurements, are not relevant (the conductivity values attain low levels, just above $10^{-5}\ \Omega^{-1}\ cm^{-1}$), although the hypothesized species can play an important rôle in the mechanism. The decrease of the phenomenon observed at increasing length of the aliphatic chains, may be attributed to the lower Lewis acidity of these compounds.

Static potentials of Pb electrodes

The static potentials of Pb electrodes in the PC–EtBr–Et_4NBr–$PbEt_4$ system have been examined, by following their variation with time until stabilization takes place. The data reported were measured in non-deaerated solutions; O_2, however, influences the value of the potentials; by bubbling O_2 in deaerated solutions, shifts of about 100 mV towards more positive values were observed.

TABLE 1

Pb STATIC POTENTIALS (E_{Pb})

Effect of the components of the system, PC–EtBr–$PbEt_4$–Et_4NBr, and of other compounds involved

Components	*Concn. range* (*M*)	$dE_{Pb}/d\log c$ (*mV*)
Et_4NBr	10^{-2}–1	−60
EtBr	10^{-5}–1	no effect
$PbEt_4$ (neutral soln.)	10^{-3}–$7\cdot10^{-2}$ (satd.)	no effect
$PtEt_4$* (acid soln.)	10^{-3}–$7\cdot10^{-2}$ (satd.)	no effect
O_2	bubbling	towards positive value
Acetic acid and	up to 10^{-2}	no effect
Propionic acid	$>10^{-2}$	+60
Ethane	bubbling	no effect

The potential *vs.* time plots are of similar shape in almost all the tests (Fig. 2). Just after the immersion of the electrode, a short period of instability is observed with an irregular and erratic shape of the curve; then the potential tends to more positive values, until it reaches a steady state value.

In the presence of acids, at increasing concentrations, the potential change with time is less noticeable; above 10^{-2} *M*, the potential is practically constant just after the immersion.

The effect of the components of the system on the Pb static potential is shown in Table 1. Only Et_4NBr has any effect: the potential shift towards negative values, at increasing Et_4NBr concentration indicates that bromide ion acts as reduced species, *i.e.*, the Pb electrode in the mixtures examined behaves as a bromide half-cell:

$$Pb + 2\ Br^- \rightarrow PbBr_2 + 2\ e \qquad (5)$$

* In presence of 0.05 *M* acetic acid.

The electrode, therefore, tends to be coated with a layer of bromides since the solubility of $PbBr_2$ in PC is very low (0.42 g/l or $2 \cdot 10^{-3}$ *M*). From galvanostatic measurements, a charge of about 500–600 $\mu C/cm^2$ is needed to reduce the surface layer suggesting the presence of a $PbBr_2$ layer.

The scattering of our data (± 15 mV) led us to investigate other equilibria which could take place at the electrode to give it a partial character of mixed potential.

(*a*) *Oxygen equilibria.* In Table 1 are reported the effects of oxygen and of two acids; the results suggests that the reaction

$$\tfrac{1}{2}\, O_2 + 2\, H^+ + 2\, e \rightarrow H_2O \qquad (6)$$

contributes to the Pb static potential.

(*b*) *Static potentials at platinum electrodes.* We have examined the tendency of EtBr and $PbEt_4$ to attain hydrogenation and dehydrogenation equilibria, by studying the static potentials in solutions of $PC + LiClO_4 + EtBr$ or $PbEt_4$ at electrodes of smooth Pt, which is a catalyst for these phenomena. The results are reported in Table 2. Only $PbEt_4$ seems to have any effect, and acts as oxidized species. This behaviour may be attributed to the equilibria initiated by ethyl radicals, released by the Pt-catalyzed dissociation of $PbEt_4$ at the electrode; these are probably hydrogenation and de-

TABLE 2

Pt STATIC POTENTIALS (E_{Pt})
Effect of $PbEt_4$, EtBr, C_2H_6

Components	*Concn. range* (*M*)	$dE_{Pt}/d\log c$ (*mV*)
$PbEt_4$	10^{-3}–$7 \cdot 10^{-2}$ (satd.)	+60
EtBr	10^{-5}–1	no effect
Ethane	bubbling	towards negative value

hydrogenation equilibria to ethane and ethylene, respectively. The electrode potential then assumes the characteristics of a mixed potential, determined by the competition between the two processes:

$$PbEt_4 - ne - nH^+ \rightarrow PbEt_{4-n} + n\, C_2H_4 \qquad (7)$$

$$PbEt_4 + ne + nH^+ \rightarrow PbEt_{4-n} + n\, C_2H_6 \qquad (8)$$

$$2\, PbEt_4 \rightarrow 2\, PbEt_{4-n} + n\, C_2H_4 + n\, C_2H_6$$

Process (8) is faster than process (7) because of the presence of water traces, and also because hydrogenation processes are usually faster than dehydrogenation processes. Moreover, in this case the formation of ethylene, mostly adsorbed on platinum, would further slow down the process because of the probable occupation of the active centres. Therefore, the electrode potential is close to that determined by (8). The action of C_2H_6 as reduced species, as well as the experimental value of the slope of $dE_{Pt}/d\log [PbEt_4] = 60$ mV, confirm this hypothesis for $n = 1$.

We conclude, therefore, that, beside the fundamental equilibrium (5), the following side equilibria may take place at Pb electrodes:

(a) equilibria involving oxygen and H^+ ions, due to traces of water or other proton-donors;

(b) equilibria involving $PbEt_4$ dissociation, locally catalyzed by impurities of hydrogenation–dehydrogenation catalyst metals in Pb.

This would give a partial character of mixed potential to the static potential of Pb in the mixtures examined, and may be related to the reproducibility of our data.

Cathode process

Figure 3 is a typical potentiostatic current/time plot for our system. An initial current transient is observed, followed by a sharp decrease of the current, which slowly tends to a steady state value (attained in 5–20 min, depending on the polarization imposed). The current transient is explained by the reduction of the $PbBr_2$ film at the electrode surface. After switching on, the film starts reducing, and consequently the surface ohmic resistance decreases and the current increases; then the reduction of the electroactive species starts at the clean Pb surface.

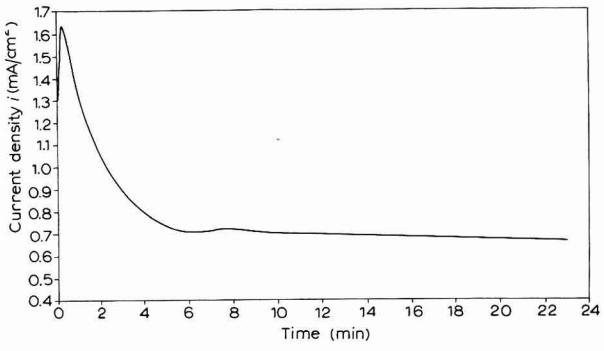

Fig. 3. Potentiostatic current density *vs.* time plot, at Pb cathode. $\eta_c = 1200$ mV; temp. 25°. Electrolyte: PC, Et_4NBr 0.1 *M*, EtBr 0.1 *M*, $PbEt_4$ 0.01 *M*.

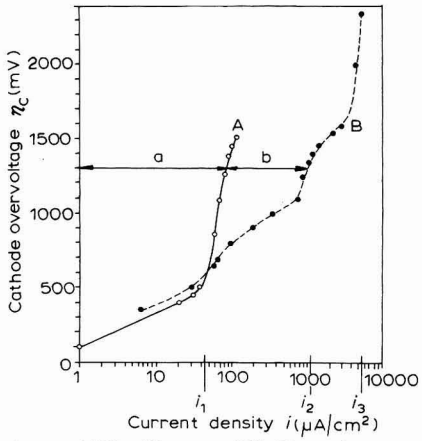

Fig. 4. Potentiostatic polarization curves at Pb cathodes, at 25°. (A) PC, Et_4NBr 0.1 *M*; (B) PC, Et_4NBr 0.1 *M*, EtBr 0.1 *M*.

The reduction of EtBr at Pb electrodes to form $PbEt_4$ takes place when the cathodic polarization, η_c, is higher than 500 mV. Figure 4 shows the polarization curves for cathodes immersed in a solution containing the solvent and the supporting electrolyte only (PC, Et_4NBr 0.1 *M*—Curve A), and in a solution containing the reagent EtBr (PC, Et_4NBr 0.1 *M*, EtBr 0.1 *M*—curve B). Curve B is characterized by three limiting currents (i_1, i_2, i_3) for polarizations of 500, 1400 and 2000 mV. Curves A and B are practically coincident for polarizations up to 500 mV; above this value, they deviate because EtBr reduction starts.

The sections of Fig. 4 marked with (a) and (b) indicate the different utilisation of the current. Section (a) represents the background current for the discharge of the oxygen dissolved in the solvent and of the impurities of the solvent and electrolyte. Section (b) refers to the discharge processes of EtBr.

To illustrate the phenomena occurring at different polarizations, Fig. 5 shows the plot of current utilisation *vs.* cathodic polarization, where R_A, R_B, R_C, R_D indicate

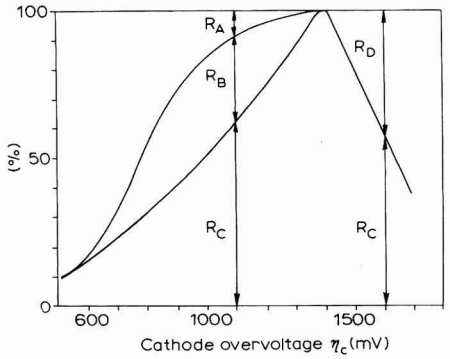

Fig. 5. Current utilization *vs.* cathode polarization.

the current percentage used for processes A, B, C and D, respectively:

A. Side processes due to impurities and dissolved oxygen.

B+C. One-electron reduction of EtBr, with dissolution of the cathodic Pb as metal alkyl. Since all the dissolved Pb is not found as $PbEt_4$, B indicates the processes causing the dissolution of Pb, forming compounds different from $PbEt_4$, and C the process forming $PbEt_4$. R_B+R_C was calculated from the decrease of weight of the cathode, while R_C was obtained from the amount of $PbEt_4$ in the solution.

D. Side reactions taking place at high polarizations: two-electron reduction of EtBr to ethane; decomposition of radicals to hydrocarbons, C_2–C_4; processes due to the presence of H_2O (H_2 discharge), and discharge of the supporting electrolyte.

Thus curve B of Fig. 3 may be divided into the following sections:

(a) $\eta_c < 500$ mV; $i < i_1$; $R_A = 1$; $R_B + R_C + R_D = 0$

All current is used for side processes A.

(b) $500 < \eta_c < 1400$ mV; $i_1 < i < i_2$; $R_B + R_C = 1 - R_A$; $R_D = 0$.

In this polarization range, there is a decrease in weight of Pb cathodes greater than that calculated from the amount of $PbEt_4$ found in solution. For polarization up to 900 mV, less than 60% of the Pb lost is transformed into $PbEt_4$; however, at increasing polarizations, the ratio mole $PbEt_4$ found/mole Pb dissolved increases up to 1 ($R_B=0$) at $\eta_c \simeq 1400$ mV; at this polarization, the current efficiency for the formation of $PbEt_4$ reaches maximum selectivity ($R_C=1$).

(c) $1400 < \eta_c < 2000$ mV; $i_2 < i < i_3$; $R_C + R_D = 1$; $R_A + R_B \rightarrow 0$ (the current percentage used for these processes is negligible).

Above 1400 mV, the yield of $PbEt_4$ decreases sharply and reaches 60% when $\eta_c = 1600$ mV, while remaining current produces gases: ethane, with small amounts ($\sim 10\%$) of ethylene and butane.

The formation of the hydrocarbons is due to side reactions of ethyl radicals:

$$\text{Dismutation } 2\,C_2H_5^{\cdot} \rightarrow C_2H_4 + C_2H_6 \qquad (9)$$

$$\text{Dimerization } 2\,C_2H_5^{\cdot} \rightarrow C_4H_{10} \qquad (10)$$

and chiefly to the two-electron process, which takes place at high polarizations:

$$C_2H_5Br + H^+ + 2\,e \rightarrow C_2H_6 + Br^- \qquad (11)$$

This determines the predominance of ethane in the cathodic gases.

(d) $\eta_c > 2000$ mV; $i > i_3$; $R_D \rightarrow 1$; $R_A + R_B + R_C \rightarrow 0$.

All current is now used to reduce ethyl bromide to ethane and for side reactions; the quantity of electricity used for the formation of $PbEt_4$ is negligible.

DISCUSSION

The $PbEt_4$ formation reaction can be divided formally into two main steps: (1) the formation of ethyl radicals by one-electron discharge of EtBr; (2) the chemical surface reaction between the radicals formed and the electrode material, yielding the metal alkyl.

The electrochemical step has been discussed thoroughly in various polarographic studies[10-13] on the reduction of alkyl halides, in which hydrogen replaces halogen (see reaction (11)). These publications discuss the problems relating to the intimate mechanism of this step, such as the orientation and the elongation of the carbon–halogen bond of the alkyl halide molecule in the double layer, due to the action of the electrostatic field, the transition state and the charge transfer.

As a basis for discussing the surface chemical step, we will consider the plot: current utilization *vs.* polarization. For various η_c up to 1400 mV, the solubilized Pb is only partially transformed into $PbEt_4$. This is probably due to the formation of other metal alkyls, such as $PbEt_2$ and $PbEt_3$ (in equilibrium with the dimeric form, Pb_2Et_6). In solution, these compounds tend to dismutate to Pb and $PbEt_4$:

$$2\ PbEt_2 \rightarrow Pb + PbEt_4 \quad (12)$$

$$2\ Pb_2Et_6 \rightarrow Pb + 3\ PbEt_4 \quad (13)$$

or to add EtBr, yielding halo-derivatives; these compounds also tend to decompose into Pb, $PbEt_4$, $PbBr_2$ and C_2–C_4 hydrocarbons[14]. After each electrolysis the presence of $PbBr_2$ and of extremely fine lead powder has always been noted. Brownish-yellow colours have also often been observed at the cathodes (disappearing on air bubbling), typical of the lower alkylated lead alkyls.

The incomplete transformation, Pb $\rightarrow$ $PbEt_4$, observed for $500 < \eta_c < 1400$ mV is explained by the side reactions described above; the percent yield of this transformation increases with the polarization up to 1400 mV. For $\eta_c \simeq 1400$ mV, all dissolved Pb is found as $PbEt_4$. At higher polarizations, this process takes place together with the two-electron reduction to ethane.

CONCLUSIONS

The electrochemical formation of metal alkyls is well known[1]. Depending on the alkylating agent, the attacking radicals can be formed at the anode or at the cathode: Grignard compounds and various alkyl complexes (*e.g.*, $NaAlR_4$, $NaBR_4$, $NaZnR_3$) have been used in anodic reactions, and alkyl halides, onium salts, ketones in cathodic reactions. However, generally speaking, there are two main steps in the reaction:

(a) an electrochemical step generating the radical, R$^\bullet$, by charge transfer (in an anodic or cathodic way);

(b) a surface chemical step, in which the radical R$^\bullet$ attacks the metal, M, according to the scheme:

$$R^+ \xrightarrow{e} R\cdot \xleftarrow{-e} R^-$$
$$\downarrow M$$
$$MR$$

The radical–electrode interaction is competitive with other possible reactions of radicals: dimerization, dismutation, reaction with the solvent, reduction, oxidation. The type of electrode and of radicals and the electrode potential influence the final reaction products.

In our studies on EtBr reduction at Pb cathodes, we have pointed out the effect of the potential on the transformation of alkyl radicals at the electrodes. It is possible to control the overall electrode reaction acting on the electrode potential, *i.e.*, on the accumulation rate of radicals and on the reducing power of the electrode. Under optimum conditions, a great selectivity can be reached with regard to the formation of completely alkylated metal alkyls.

ACKNOWLEDGEMENTS

The author wishes to express his appreciation to Professor G. Bianchi for his valuable suggestions and his continuous interest in the work. The author is also indebted to Mr. F. Olivani for his contribution in carrying out the experimental work.

SUMMARY

The formation of $PbEt_4$ by reduction of EtBr at Pb cathodes in propylene–carbonate (PC) solutions with tetraalkylammonium salts as supporting electrolyte has been studied.

EtBr–PC interactions, static potentials of Pb, steady state potentiostatic polarization curves, material yields and current efficiency of the main and side reactions as functions of the electrode potential, have been examined.

On the basis of these results, a reaction mechanism has been proposed.

REFERENCES

1 E. M. Marlett, *Ann. N.Y. Acad. Sci.*, 125 (1965) 12.
2 S. Mishima, *Bull. Chem. Soc. Japan*, 40 (1967) 608.
3 General Motors, U.S. Pat. 1.539.297; U.S. Pat. 1.567.159.
4 E. I. du Pont de Nemours & Co., Brit. 949.925; Neth. Appl. 6.508.049.
5 A. P. Tomilov and L. V. Kaabak, *Zh. Prikl. Khim.*, 32 (1959) 2600.
6 L. G. Feoktistov, A. P. Tomilov, Yu. D. Smirnov and M. M. Goldin, *Soviet Electrochem.*, 1 (1966) 791.
7 L. L. Miller and A. K. Hoffmann, *E.C.S. Dallas Meeting, 1967, Electro-organic Division*, Abs. No. 116, p. 20.
8 R. Defay, N. Ibl, E. Levart, G. Milazzo, G. Valensi and P. van Rysselberghe, *J. Electroanal. Chem.*, 7 (1964) 426.
9 N. Kornblum and R. K. Blackwood, *J. Am. Chem. Soc.*, 78 (1956) 4037.
10 J. W. Sease, P. Chang and J. L. Groth, *J. Am. Chem. Soc.*, 86 (1964) 3154.
11 F. L. Lambert, A. H. Albert and J. P. Hardy, *J. Am. Chem. Soc.*, 86 (1964) 3155.
12 P. J. Elving and B. Pullmann, *Advan. Chem. Phy.*, 3 (1960) 1.
13 P. J. Elving, *Record Chem. Progr. Kresge-Hooker Sci. Lib.*, 14 (1953) 99.
14 G. A. Razuvaev, M. S. Vyazankin and Yu. I. Dergonov, *Zh. Obshch. Khim.*, 30 (1960) 1310.

ELECTROANALYTICAL CHEMISTRY AND INTERFACIAL ELECTROCHEMISTRY
Elsevier Sequoia S.A., Lausanne – Printed in The Netherlands

"METAL-COMPLEX" ELECTRODES

IV. THE STABILITY OF SOME COMPLEX COMBINATIONS IN NON-AQUEOUS MEDIA

G. POPA AND V. MAGEARU
The Laboratory of Analytical Chemistry of the University of Bucharest, Bucharest (Rumania)
(Received December 23rd, 1968)

Recently[1,2], a new class of electrodes of the second type, called "metal-complex" in which the role of the difficultly-soluble compound is taken by a stable, soluble complex has been realized and studied:

$$Me/[MeL_p], L \qquad (1)$$

The metal-complex electrodes are reversible to the ligand, L, which forms with the ions of the electrode metal, the complex, $[MeL_p]$, which is slightly dissociated (for simplification the other ions in solution have been neglected). The theory and the method of use of these electrodes have been dealt with previously[1,2].

Since the electrode metal may be varied, and the role of ligand taken by many anions or neutral molecules, these electrodes are diverse, and their applications numerous. Thus, metal-complex electrodes have already been successfully used in the study of the formation equilibria of some complexes in aqueous solution, and in the quantitative determination of some neutral molecules or anions in solution[3-10]. The present paper extends the application of metal-complex electrodes to the study of the formation equilibria of complexes in non-aqueous media. The stability of Zn(II) complexes with diethylamine (Et_2NH) and piperidine (pip) in methanolic solutions has been investigated using the following electrodes:

$$Ag/[Ag(Et_2NH)_2]^+, Et_2NH \qquad (2)$$

$$Ag/[Ag(pip)_2]^+, pip \qquad (3)$$

EXPERIMENTAL AND RESULTS

The formation equilibria of the electrode complexes in methanolic solutions were first studied. Thus, the successive stability constants of the complexes, $[Ag(Et_2NH)_p]^+$ and $[Ag(pip)_p]^+$, have been determined using the method of successive extrapolation[11,12] of the complexation functions, $F(L)$[13], calculated from the e.m.f. of cells of the form:

$$\begin{aligned} &\text{(I)}\ Ag|Ag^+|NH_4NO_3(satd.)|KCl(satd.), Hg_2Cl_2|Hg \\ &\text{(II)}\ Ag|[AgL_p]^+, L|NH_4NO_3(satd.)|KCl(satd.), Hg_2Cl_2|Hg \end{aligned} \qquad (4)$$

the diffusion potential of which is constant. In both elements equal and small quantities of Ag^+ ions ($C_{Ag^+} \simeq 10^{-5}$ M) have been added.

The results of these determinations showed that in solutions of methanol as in water only two complexes are formed with stability constants: Ag^+–Et_2NH, $K_1 = 5 \cdot 10^3$ l mole^{-1}; $K_2 = 4.24 \cdot 10^7$ l^2 mole^{-2}; Ag^+–pip, $K_1 = 4 \cdot 10^3$ l mole^{-1}; $K_2 = 3.2 \cdot 10^7$ l^2 mole^{-2}.

These constants have been used to calculate Bjerrum's function[14]:

$$\bar{n} = (K_1[L] + 2K_2[L]^2)/(1 + K_1[L] + K_2[L]^2) \quad (5)$$

The formation curves of the respective complexes can then be drawn: these indicate the domain of concentration of the ligand at which formation of a given complex takes place.

If cell (4-II) also contains a known quantity of Zn^{2+} ions ($C_{Zn^{2+}}$) that form complexes with the ligand L, then this cell takes a new form:

$$\text{(III) } Ag|[AgL_p]^+, L, Zn^{2+}|NH_4NO_3(\text{satd.})|KCl(\text{satd.}), Hg_2Cl_2|Hg \quad (6)$$

in which a competitive equilibrium[15] is set up; one part of the ligand concentration (C_L) is used to form Zn(II) complexes. The concentration of the free ligand ([L]), released from the complex can be calculated from the difference of e.m.f. between elements (II) and (III) according to the indications already given[1], by using the relation:

$$\ln [L] = \ln C_L + (E_{II} - E_{III})/(2RT/F) \quad (7)$$

From these concentrations Bjerrum's function was calculated[14]:

$$\bar{n} = (C_L - [L])/C_{Zn^{2+}} \quad (8)$$

which gives the average numbers of the coordinated ligands. These can be used to plot the formation curves, $\bar{n}$–$p[L]$, from which the partial stability constants can be determined.

The solutions used were prepared from commercially available materials (p.a. Merck, Serva, Carlo Erba and AnalaR) in doubly-distilled methanol. The ionic strength of all solutions was maintained constant at $\mu = 1$ with NH_4NO_3. The electromotive force (e.m.f.) was measured by means of a VEB-Messtechnik Mellenbach potentiometer with a precision of ± 0.1 mV. The cells were maintained at a constant temperature of $25 \pm 0.1°$, in an Ultrathermostat type U-10.

DISCUSSION

Figures 1 and 2 show the formation curves of the complexes in methanol (MeOH), together with the formation curves of some complexes in aqueous solutions at ionic strength $\mu = 2$ (NH_4NO_3) previously reported[4,5,16].

The formation curves of the Zn^{2+}–L systems, drawn on a large scale, have also been used to determine the approximate successive constants:

$$\log k_n = p[L]_{\bar{n} = n - \frac{1}{2}} \quad (9)$$

These were then corrected according to Bjerrum's method[14]. The results of these calculations are shown in Table 1. It can be seen that the stability of these complexes is higher in MeOH than in water. This can be attributed to an influence of the dielectric constant of the solvent on the dissociation of the complexes, which is in agreement with other workers[17–21] dealing with the same problems.

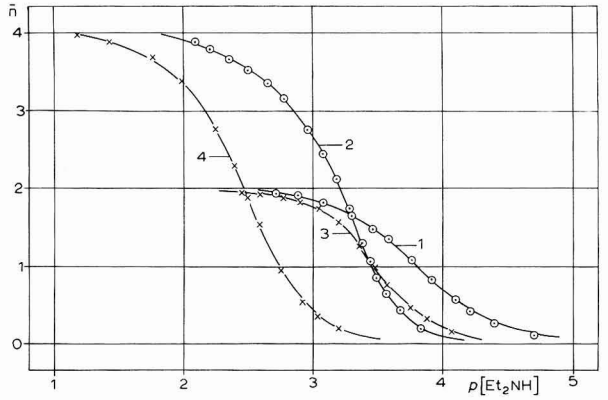

Fig. 1. Formation curves of the systems: (1), Ag^+–Et_2NH–MeOH; (2), Zn^{2+}–Et_2NH–MeOH; (3), Ag^+–Et_2NH–H_2O[16]; (4), Zn^{2+}–Et_2NH–H_2O[4].

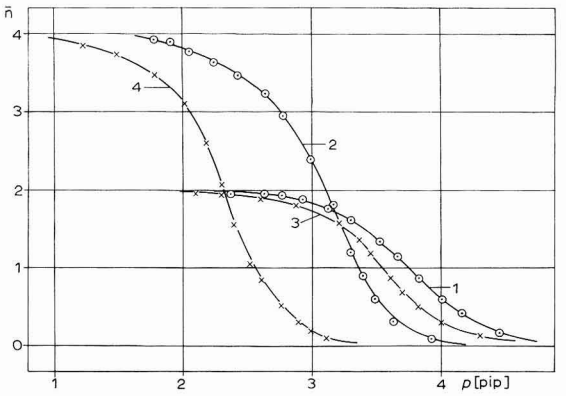

Fig. 2. Formation curves of the systems: (1), Ag^+–pip–MeOH; (2), Zn^{2+}–pip–MeOH; (3), Ag^+–pip–H_2O[16]; (4), Zn^{2+}–pip–H_2O[5].

TABLE I

VALUES OF THE FORMATION CONSTANTS OF THE Zn(II) COMPLEXES WITH DIETHYLAMINE AND PIPERIDINE

n	$[Zn(Et_2NH)_n]^{2+}$				$[Zn(pip)_n]^{2+}$			
	$p[Et_2NH]_{\bar{n}=n-\frac{1}{2}}$		$log\ k_n$		$p[pip]_{\bar{n}=n-\frac{1}{2}}$		$log\ k_n$	
	H_2O[4]	$MeOH$	H_2O[4]	$MeOH$	H_2O[5]	$MeOH$	H_2O[5]	$MeOH$[a]
1	2.965	3.628	2.511	3.085	2.780	3.515	2.313	3.005
2	2.598	3.330	2.448	3.251	2.410	3.218	2.211	3.150
3	2.340	3.058	2.529	3.312	2.210	2.932	2.331	3.171
4	1.921	2.512	2.333	2.832	1.765	2.391	2.171	2.711
log K_4	9.824	15.528	9.821	12.480	9.165	12.066	9.026	12.037

[a] 25°C; $\mu=2$ (H_2O), $\mu=1$ (MeOH) with NH_4NO_3.

SUMMARY

The applications of "metal-complex" electrodes are extended to the study of the formation equilibria of complexes in non-aqueous media. By using the electrodes:

$Ag/[Ag(Et_2NH)_2]^+$, Et_2NH

$Ag/[Ag(pip)_2]^+$, pip

the successive stability constants of Zn(II) complexes with diethylamine (Et_2NH) and piperidine (pip) in methanolic solutions were determined. The results are compared with those already obtained in aqueous solutions.

REFERENCES

1 C. Luca, V. Magearu and Gr. Popa, *J. Electroanal. Chem.*, 12 (1966) 45.
2 C. Luca, *Bull. Soc. Chim. France*, 7 (1967) 2556.
3 Gr. Popa and V. Magearu, *Rev. Roumaine Chim.*, 12 (1967) 1107.
4 Gr. Popa, V. Magearu and C. Luca, *J. Electroanal. Chem.*, 17 (1968) 335.
5 Gr. Popa, V. Magearu and E. Dăscălescu, *Anal. Univ. Bucureşti*, 2 (1967) 67.
6 V. Magearu and Gr. Popa, *Rev. Roumaine Chim.*, in press.
7 Gr. Popa and V. Magearu, *Rev. Roumaine Chim.*, 7 (1969) 14.
8 V. Magearu and Gr. Popa, *Anal. Univ. Bucureşti*, 2 (1968).
9 V. Magearu, C. Luca and M. Teodorescu, *J. Electroanal. Chem.*, 12 (1966) 148.
10 G. Berthon and C. Luca, *Chim. Anal. Paris*, 49 (1967) 6.
11 I. Leden, *Z. Physik. Chem.*, A-188 (1941) 160.
12 H. Olerup, Dissertation, Lund, 1944.
13 K. B. Yatsimirski, *Zh. Neorgan. Khim.*, 1 (1956) 412.
14 J. Bjerrum, *Metal Ammine formation in Aqueous Solution*, Haase, Copenhagen, 1957.
15 F. Rossotti and H. Rossotti, *The Determination of Stability Constants*, McGraw-Hill Book Co, New York, 1961.
16 Gr. Popa and V. Magearu, *Anal. Univ. Bucuresti*, in press.
17 Gr. Popa, C. Luca and V. Magearu, *Anal. Univ. Bucureşti*, 2 (1965) 9.
18 Gr. Popa, C. Luca, V. Magearu and M. Teodorescu, *Anal. Univ. Bucureşti*, 1 (1965) 65.
19 Gr. Popa, E. Iosif and C. Luca, *Rev. Roumaine Chim.*, 12 (1967) 169.
20 A. B. Babko and O. F. Drako, *Zh. Obshch. Khim.*, 20 (1950) 228.
21 K. K. Mead, D. L. Maricle and G. A. Streuli, *Anal. Chem.*, 37 (1965) 237.

ELECTROANALYTICAL CHEMISTRY AND INTERFACIAL ELECTROCHEMISTRY
Elsevier Sequoia S.A., Lausanne – Printed in The Netherlands

THEORY OF FLOODED POROUS ELECTRODES

I. GALVANOSTATIC TRANSIENTS AND GENERALISED IMPEDANCE

S. K. RANGARAJAN
Central Electrochemical Research Institute, Karaikudi-3 (India)
(Received December 17th, 1968)

1. INTRODUCTION

This paper presents an analytical solution to the problem of transient behaviour of flooded porous electrodes under galvanostatic and sinusoidal *perturbations*. All the three types of dynamic polarisation: ohmic, activation and concentration, are considered but the treatment is limited by the idealised model assumed for the porous body. The results given here are therefore valid for what can be termed as "homogeneous, mono-pore models". For an actual matrix, a proper averaging, taking into account the distribution of pore lengths, can be resorted to. In spite of such limitations, a transient analysis of ohmic, concentration and double-layer effects is needed because (i) the devices employing porous electrodes are varied in nature and their operating conditions are widely different, (ii) basic researches with mono-tubular electrodes can be very useful in understanding (the significance of certain non-dimensional parametric groups on) the performance of a "real" porous matrix and (iii) the transient studies provide a method for the evaluation of some of the so-called "effective" parameters.

2. THE MODEL

Many electrochemical devices exploit advantageously the large electrode–electrolyte interface offered by flooded porous electrodes, but this same factor, *viz.* an effective pore wall surface, introduces difficulties in the theoretical formulation of these porous-electrode operations. In particular, before setting up mathematical equations that adequately represent the true behaviour of the porous electrode, the following must be identified/specified and defined:

(a) a model for the capillary porous structure;

(b) the species transported and the mode of mass transfer in the electrolyte in the pores and exterior to the porous electrode;

(c) assumptions concerning the potential distributions in the solid matrix and the electrolyte phases;

(d) the "local" relationship existing between the rate of the electrode process and the potential difference across the pore wall–electrolyte interface.

(a)–(d) are not mutually independent but may to a large extent depend on each other although demanding consistency in themselves.

Some salient features of the model adopted in this paper are as follows:

(a) The specific structure of the porous material is ignored*. Its behaviour is assumed to be equivalent to that of an isotropic, macroscopically homogeneous medium. This helps in restricting the space variations along one dimension, *i.e.*, "the depth" of the electrode only. This hypothesis naively transforms the sources or sinks distributed over the pore walls to "volume" sources or sinks. Such a one-dimensional model has been advocated and justified earlier by several workers**[1-7]. It can be argued that the model is satisfactory if the pore radii are small compared with other dimensions involved in the problem. We examine here the problem of one-dimensional porous electrodes with finite thickness.

(b) In general, the transport of a number of ionic and neutral species is involved in the process. Of the three modes of mass transfer—convection, migration and diffusion—only diffusion is considered in this paper, but migration can be very significant in the operation of porous electrodes since ionic transport also is invariably involved. In the near-equilibrium conditions that alone interest us in the present investigation, if ionic concentrations are sufficiently in excess, and if the concentration changes of reactants and products (assumed inert) alone are significant, it is sufficient to set up equations for the diffusion (without any migration term) of neutral species only***. In other words, the present paper assumes:

(i) diffusion to be the sole mode of mass transfer and

(ii) concentration changes of only the reactant, R, and the product, P, need be considered.

The above hold true also in the exterior of the porous electrode and the diffusion equations written for the interior and the outside of the porous matrix are linked through proper continuity conditions. Also, a constant diffusion layer thickness, δ, is assumed in the exterior.

(c) That the potential distribution is given by a simple enough equation is ensured by the hypothesis that the conductivity of the solution phase is constant and small enough in comparison with that of the solid matrix. Since the one-dimensional model is chosen for the pores, the electrode reaction takes place "all over". Thus, the problem of potential (current) distribution is one involving distributed parameters. To obtain an exact transient behaviour, we confine ourselves to perturbation from equilibrium conditions and hence a linearisation (not neglecting concentration changes) of the local current density–potential relationship is employed. The porous electrode can then be considered equivalent to a transmission line of finite length with the electrolyte resistance in series, shunted by a parallel combination of double-layer and faradaic impedances.

A different way of looking at the transmission line picture is *via* Poisson's equation by writing it in the form:

* Alternatively, to account for the structural details of the porous material, a resort to idealisations as regards both (i) the pore-geometry and (ii) the pore-distribution becomes a *sine qua non*. Obviously, the mathematical descriptions of these are cumbersome.

** The list is not exhaustive since only the references pertaining to non-steady state conditions and those considering concentration polarisation are taken note of in this paper. For a comprehensive bibliography see ref. 3.

*** Even if the study pertains to diffusion of charged species, it is permissible sometimes to neglect the migration term if the charged reactants and products are in the presence of excess supporting electrolyte, *cf.* section 4, 6.

$$\sigma\nabla^2\Phi = -\partial\rho/\partial t$$

Identifying the rate of flow of charge in the volume (with time) with $\partial J/\partial X$ the local current density, and equating this to the sum of double-layer charging ($C\,\partial\Phi/\partial t$) and faradaic $\partial j/\partial X$ we deduce that

$$-\frac{\partial\rho}{\partial t} = \partial J/\partial X = C\frac{\partial\Phi}{\partial t} + \frac{\partial j}{\partial X} = \sigma\nabla^2\Phi$$

(d) Assuming a pseudo-monomolecular reaction (the rate-determining step, $R \rightleftharpoons P$) and denoting the instantaneous and equilibrium concentrations of the reactants and the products as $C_i(x, t)$ and C_i^v (i = R, P), respectively, we use a Volmer-type expression to describe the local faradaic current density:

$$i/i_0 = [(C_r/C_r^v)\exp(\alpha_c F\eta/RT) - (C_p/C_p^v)\exp(\alpha_c - n)F\eta/RT)] \tag{2}$$

Moreover, we assume a quasi-stationary regime between the reactant and the products, expressed through:

$$\Delta C_r(x, t)/C_r^v + \Delta C_p(x, t)/C_p^v = 0 \tag{3}$$

ΔC_r, ΔC_p are the changes in the concentrations from their equilibrium values (it is proposed to relax (3) in a future work).

In (2), we have written $(\alpha_c - n)$ for $(-\alpha_a)$, the anodic transfer coefficient, so that

$$n = \alpha_c + \alpha_a \tag{4}$$

Under near-equilibrium conditions, eqn. (2) can be linearised as:

$$i = i_0\left[\frac{\Delta C_r}{C_r^v} - \frac{\Delta C_p}{C_p^v} + \frac{nF\eta}{RT}\right] = i_0\left[E\frac{\Delta C_r}{C_r^v} + \frac{nF\eta}{RT}\right] \tag{5}$$

—a result used in relaxation methods.

The simplifications proposed above in (a)–(d) introduce certain effective parameters*.

For example, the diffusion coefficients and the specific resistance of the electrolyte need not be the same** in the interior and the exterior of the porous electrode. Two other important parameters are the (internal) specific surface and the exchange current density introduced by the electrochemical step (d).

3. THE PROBLEM

Define the X-axis along the "depth" of the porous electrode and this is also the direction of diffusional flow and $x = L$ denotes the apparent surface in contact with the exterior. The equations to be solved are:

$$\partial C_r/\partial t = D' \cdot \partial^2 C_r/\partial X^2 - v_r\, si/nF \tag{6}$$

$$\partial C_p/\partial t = D' \cdot \partial^2 C_p/\partial X^2 + v_p\, si/nF \tag{7}$$

---

* See, for example, ref. 8 which discusses various models for porous electrodes that transform an inherently "structural medium" into a homogeneous one by introducing simultaneously certain "effective" parameters different from those prevailing in the exterior.

** But, see ref. 5 where no such distinction is made.

and

$$\partial\eta/\partial t = (1/C\rho_e)\,\partial^2\eta/\partial X^2 - si/C \tag{8}$$

with

$$i = i_0[E\Delta C_r/C_r^v + nF\eta/RT] \tag{9}$$

The initial conditions are:

$$C_i(X, 0) = 0, \quad i = r, p; \qquad \eta(X, 0) = 0 \tag{10}$$

Boundary conditions are:

$$\partial C_r/\partial X = \partial C_p/\partial X = \partial\eta/\partial X = 0; \qquad X = 0 \tag{11}$$

We assume a two-sided reactant supply so that the diffusional flux is zero at the central plane of the electrode which is chosen as $X = 0$. (Note: A similar condition holds if the electrode has an inert backing).

$$\partial\eta/\partial X = \rho_e I: \qquad X = L \tag{12}$$

The "continuity-conditions" at the pore mouth provide the remaining boundary conditions. They are:

$$D'(\partial C_r/\partial X)_{X=L-} = D(\partial C_r/\partial X)_{X=L+} \tag{13}$$

$$C_r)_{X=L-} = C_r)_{X=L+} \tag{14}$$

With

$$D\,\partial^2 C_r/\partial X^2 = \partial C_r/\partial t: \qquad L_+ < X < L+\delta \tag{15}$$

$$C_r = C_r^v, \qquad t = 0 \tag{16}$$

4. PREVIOUS WORK

Compared with the theoretical investigations on the steady state, information on the transient response of flooded porous electrodes is scanty. Only the treatments by Ksenzhek[4], Grens and Tobias[5], Guruvich and Bagotskii[1,2] (referred to as G and B) and Winsel[7] account for, partly or wholly, *all* three types of polarisation: concentration, activation and ohmic, *with their time-dependence*. With the exception* of Winsel, all used the one-dimensional model for the porous electrode.

The work of Grens and Tobias[5] is the most general in at least two ways—it neither avoids the effects of migration nor does it confine its scope to perturbations from equilibrium. On the other hand, two of the assumptions made: (i) same values for diffusion constants, etc., inside and exterior to the pores and (ii) $t > \tau$, time constant for double layer charging, are relaxed here. Another deviation is to be found in the equations describing the potential distributions inside the pores.

Also, the method adopted by Tobias[5] to solve the differential equations is *numerical* whereas we consider here an *analytical* solution**.

---

* This exception is to be qualified by the remarks of Grens II and Tobias, ref. 5.

** It is conceded that, ultimately, numerical analysis may be needed for inversion of Laplace Transformation or for computing the equivalent circuit elements, but this is a trivial exception. For standard procedures for inverting, see refs. 9 and 10.

A comparison can be made with the computed results of Grens and Tobias provided that:

(a) the overpotential is not large;
(b) there is "excess" supporting electrolyte;
(c) the double-layer charging is "completed";
(d) the "ohmic" polarisation is absent within the pores.

The constraints (a) and (b) are necessary owing to the approximations inherent in our analysis while (c)–(d) are imposed by the limitations of ref. 5. Such a special case is discussed later in this paper (section 6) and it is shown that an excellent agreement is obtained with the calculated curves (for ferrocyanide–ferricyanide reaction) of ref. 5. The comparison, moreover, indicated that "the linearisation" used here (eqn. (9)), is valid and holds even when $\eta > 5$ mV.

G and B[1] also treated the problem that is dealt with in this paper. The boundary conditions they used and the procedure adopted to solve the problem are critically examined, and modified solutions are presented here.

The linearised form for the i–η relationship used by G and B is:

$$i = i_0[E\Delta C_r/C_r^v + E(n-\alpha_c)F\eta/RT] \tag{17}$$

whereas that adopted in this paper is:

$$i = i_0[E\cdot\Delta C_r/C_r^v + nF\eta/RT] \tag{18}$$

The final calculations for η based on each of these two equations could be very different and cause serious error especially when E is large. Under the assumption that the "perturbation" values, $\Delta C_i/C_i^v$ (i = r, p) and $nF\eta/RT$ are *all* small, the form (18) is the proper linearisation to adopt*.

To illustrate this point, consider the special case, $\alpha_a = \alpha_c - n = 0$. Then, from (12)

$$\begin{aligned} i/i_0 &= [(1+\Delta C_r/C_r^v)\exp(nF\eta/RT) - (1+\Delta C_p/C_p^v)] \\ &= \Delta C_r/C_r^v - \Delta C_p/C_p^v + nF\eta/RT \\ &= E\cdot\Delta C_r/C_r^v + nF\eta/RT \end{aligned} \tag{19}$$

neglecting only terms like $(nF\eta/RT)^2$ and $\{(\Delta C_r/C_r^v)\cdot(nF\eta/RT)\}$. It is obvious that the linearisation of G and B—unlike eqn. (18)—will not result in the above and becomes

$$i = i_0 E\cdot(\Delta C_r/C_r^v) \quad \text{if} \quad \alpha_c = n\,. \tag{20}$$

The error in (17) is due to an inconsistent procedure adopted for linearising but for the sake of brevity detailed arguments are not given here.

Tobias[5] assumes the following boundary condition (A) at $X = L$ for η instead of eqn. (12) ($\partial\eta/\partial X = \rho_e I$) used here, and Bagotskii uses (B) *in addition* to (12):

$$\text{(A)}\; s\int_0^L i\,dx = I \tag{21}$$

* See, for example, ref. 11.

$$\text{(B)} \int_0^{\infty} [D_i'(\partial C_i/\partial X)_{X=L} \mp v_i I/nF]\,dt \tag{22}$$
$$= \int_0^{L} [C_i(x, \infty) - C_i(x, 0)]\,dx$$

(eqn. (3), ref. 1).

Equation (21) shows that all the applied current is faradaic while (B) is "the material balance equation".

An integration of eqn. (8) gives:

$$(CL)\,d\eta_{av}/dt + (sL)i_{av} = (1/\rho_e)(\partial\eta/\partial X)_{X=L} = I \tag{23}$$

where

$$\eta_{av} = (1/L)\int_0^{L} \eta\,dx$$

and (24)

$$i_{av} = (1/L)\int_0^{L} i\,dx$$

Equation (23) expresses the fact that, at any instant, the impressed current is the sum of (double-layer) charging and faradaic currents. It should be noted that (23) is similar to the familiar equation used for planar electrodes:

$$C\,d\eta/dt + i_f = I \tag{25}$$

Thus, eqn. (21) can be a *substitute* for (12) if the charging transient is neglected but not otherwise. A careful examination reveals that the eqn. (22) of G and B is equivalent to (21) in spite of the apparent complexity of (23)! To show this, one need only integrate eqns. (1)–(3) and use the condition (12). Hence, in spite of the involved *form* of (22) (which compelled G and B to resort to various approximations and simplifications the inaccuracies of which could not be estimated), eqns. (21) and (22) are equivalent and for this reason, the validity of the use of (22) by G and B in their analysis (which includes charging transients) is questionable. Moreover, the boundary conditions (12) and (22) of G and B[1] are *not* actually *independent* and only the more general form, (eqn. (12)) is to be retained. The "continuity" conditions linking the interior to the exterior should then supply the "missing" boundary conditions. They are:

$$D'(\partial C_r/\partial X)_{X=L-} = -(D/\delta)\Delta C_{r(X=L-)} \tag{26}$$

("steady state" outside the pores: $Dt \gg \delta^2$)

or eqns. (13)–(14) with the diffusion equations in the region, $X > L$, *viz.*,

$$D\,\partial^2\Delta C_r/\partial X^2 = \partial\Delta C_r/\partial t\,, \tag{27}$$
$$\Delta C_r = 0\,, \qquad t = 0 \tag{28}$$
$$\Delta C_r = 0\,, \qquad X = L + \delta\,. \tag{29}$$

5. THE SOLUTION

Define the following non-dimensional parameters:

$$c = (C_r - C_r^v)/C_r^v \tag{30}$$

$$\phi = (nF\eta/ERT) \tag{31}$$

$$x = X/L \tag{32}$$

$$\tau = D't/L^2 \tag{33}$$

$$\theta_1 = C\rho_e D' \tag{34}$$

$$\theta_2 = si_0\rho_e L^2 nF/RT \tag{35}$$

$$\theta_3 = v_r\, si_0 EL^2/nF C_r^v D' \tag{36}$$

$$\theta_p = pL^2/D \tag{37}$$

$$\theta_4 = \theta_4^\circ \cdot (\theta_p\delta^2/L^2)^{\frac{1}{2}} \cdot \coth(\theta_p\delta^2/L^2)^{\frac{1}{2}} \tag{38}$$

$$\theta_4^\circ = (DL/D'\delta) \tag{38a}$$

$$\Delta i = I/(si_0 L) = I/I_0 \tag{39}$$

$$\bar{c} = p\int_0^\infty \exp(-pt)\, c(x,t)\mathrm{d}t \tag{40}$$

$$\bar{\phi} = p\int_0^\infty \exp(-pt)\,\phi(x,t)\mathrm{d}t \tag{41}$$

and in general

$$\bar{f} = p\int_0^\infty \exp(-pt) f(t)\mathrm{d}t \tag{42}$$

The system of eqns. (6)–(12), (24)–(26) can be recast using only the above parameters. In the non-dimensional form, the problem is as follows:
Solve for $\bar{\phi}(x, p)$ and $\bar{c}(x, p)$ if

$$(\partial^2/\partial x^2 - \theta_p - \theta_3)\bar{c} + \theta_3\bar{\phi} = 0 \tag{43}$$

$$(\partial^2/\partial x^2 - \theta_p\theta_1 - \theta_2)\bar{\phi} + \theta_2\bar{c} = 0 \tag{44}$$

with the boundary conditions:

$$\partial\bar{c}/\partial x = \partial\bar{\phi}/\partial x = 0\,, \qquad \text{at } x = 0 \tag{45}$$

$$\partial\bar{\phi}/\partial x = \theta_2\Delta i, \quad x = 1 \tag{46}$$

and

$$\partial\bar{c}/\partial x = -\theta_4\bar{c} \qquad \text{at } x = 1 \tag{47}$$

The details of the derivation and the complete solutions are not reproduced here. Confining our attention to the potential drop (and the generalised impedance) at the pore mouth, the expression for the Laplace Transform of $\eta(L, t)$, *viz.*, $\bar{\eta}(L, p)$ alone is required. We have

$$\bar{\eta} = L[\eta(L,t)] = p\int_0^\infty \exp(-pt)\eta(L,t)\mathrm{d}t$$

$$= \bar{I}\rho_e L\left\{\frac{f(p,\alpha,\beta)\cosh\alpha - f(p,\beta,\alpha)\cosh\beta}{f(p,\alpha,\beta)\,\alpha\sinh\alpha - f(p,\beta,\alpha)\,\alpha\sinh\beta}\right\} \tag{48}$$

where

$$f(p, \alpha, \beta) = (\alpha^2 - \theta_p - \theta_3)(\cosh \beta + \beta \sinh \beta/\theta_4)$$
$$f(p, \beta, \alpha) = (\beta^2 - \theta_p - \theta_3)(\alpha \sinh \alpha/\theta_4 + \cosh \alpha) \tag{49}$$
$$\alpha^2 + \beta^2 = \theta_p(1 + \theta_1) + \theta_2 + \theta_3$$
$$\alpha^2 \beta^2 = \theta_p(\theta_p \theta_1 + \theta_2 + \theta_3 \theta_1) \tag{50}$$

and

$$\theta_p = pL^2/D' \tag{51}$$

In (48), θ_p, θ_4, α and β are functions of p while θ_1, θ_2, θ_3 and θ_4° are constants. It is obvious that the inversion of (48) is not immediate. The difficulty lies in locating the poles of $\bar{\eta}(L, p)$. But it is easy to show as follows that $\bar{\eta}$ is a meromorphic function; it has no branch points in spite of the complicated irrational dependence of α and β on p (*cf.* eqn. (50)).

Rearranging, we have an alternative form of (48):

$$\begin{aligned}\bar{\eta}(L, p) = \bar{I}\rho_e L\{&[\cosh(\alpha+\beta) + \cosh(\alpha-\beta)] \\ &+ [\alpha\beta(\sinh(\alpha+\beta)/(\alpha+\beta) - \sinh(\alpha-\beta)/(\alpha-\beta))] \\ &+ ((\theta_p+\theta_3)/\theta_4)[\sinh(\alpha+\beta)/(\alpha+\beta) + \sinh(\alpha-\beta)/(\alpha-\beta)]\} \\ \div \{&[\alpha\beta(\sinh(\alpha+\beta)/(\alpha+\beta) - \sinh(\alpha-\beta)/(\alpha-\beta))] \\ &+ (\alpha^2+\beta^2-\theta_p-\theta_3)[\sinh(\alpha+\beta)/(\alpha+\beta) + \sinh(\alpha-\beta)/(\alpha-\beta)] \\ &+ (1/\theta_4)[\alpha\beta(\cosh(\alpha+\beta) - \cosh(\alpha-\beta))]\end{aligned} \tag{52}$$

Each term in square brackets on the right-hand side of (52) is a function of $(\alpha^2 + \beta^2)$ and $\alpha^2\beta^2$ only. Equation (50) ensures that $\alpha^2 + \beta^2$, $\alpha^2\beta^2$ are linear and "quadratic" functions of p, respectively. The coefficients of the square bracket terms also are functions of p. Thus, it is proved that $\bar{\eta}$ has no branch points.

Thus the problem of inversion is one of evaluating all the roots of the transcendental equation:

$$f(p, \alpha, \beta)\, \alpha \sinh \alpha = f(p, \beta, \alpha)\, \beta \sinh \beta \tag{53}$$

No detailed discussion on the nature of the roots of (53) is given here; it is sufficient to say that the poles lie on the negative real axis of the p-plane. It is easy to demonstrate that there are no positive real zeros for (53), for, if $p > 0$, α^2 and β^2 are positive. But $(\alpha^2 - \theta_p - \theta_3)/(\theta_2\theta_3)^{\frac{1}{2}}$ and $(\beta^2 - \theta_p - \theta_3)/(\theta_2\theta_3)^{\frac{1}{2}}$ are of opposite sign since these are the roots of the quadratic:

$$m^2 - mx - 1 = 0 \tag{54}$$

where

$$x = (\theta_p(\theta_1 - 1) + \theta_2 - \theta_3)/(\theta_2\theta_3)^{\frac{1}{2}} \tag{55}$$

Hence the two sides of eqn. (53) are of opposite sign and cannot be equal if $p > 0$.

The inversion is immediate, once the poles and the residues of $\bar{\eta}(L, p)$ are evaluated.

There are infinite number of zeros for eqn. (53). Heuristically, one may relate the "rise time" (or time taken to set up a stationary state) to the zeros of (53). If the zeros of (53) are $p = -\{p_n\}$, $n = 1, 2, 3 \ldots$ such that

$$0 < p_1 < p_2 < p_3 \ldots \tag{56}$$

then

$$\eta(L, t) = \sum_{n=1}^{\infty} a_n \exp(-p_n t) \tag{57}$$

A more detailed discussion on τ is possible only with a thorough evaluation of $\{p_n\}$ and the residues of $\bar{\eta}(L, p)$ at $p = -\{p_n\}$.

An approximate inversion of $\bar{\eta}(L, p)$ and the evaluation of τ for different choices of θ are possible. Further details on the computation of τ and its variation as a function of basic parameters like C, ρ_e, L, E, etc., will be given in a later communication.

6. PARTICULAR CASES

Convenient and simplified expressions for $\alpha^2(p)$, $\beta^2(p)$ and consequently, $\bar{\eta}(L, p)$ result under certain limiting conditions. Table 1 presents some of these degenerate forms:

TABLE 1

Limiting condition	α^2	β^2	$\alpha^2 - \theta_p - \theta_3$	$\beta^2 - \theta_p - \theta_3$
$\theta_p \to 0$	$\theta_2 + \theta_3$	0	θ_2	$-\theta_3$
$\theta_1 \to 1$	$\theta_p + \theta_2 + \theta_3$	θ_p	θ_2	$-\theta_3$
$\theta_2 \to 0$	$\theta_p + \theta_3$	$\theta_p \cdot \theta_1$	0	$\theta_p(\theta_1 - 1) - \theta_3$
$\theta_3 \to 0$	$\theta_p\theta_1 + \theta_2$	θ_p	$\theta_p(\theta_1 - 1) + \theta_2$	0

(a) *Steady state* ($t \to \infty$)

Under steady-state conditions, ($\theta_p \to 0$) (see Table 1)

$$nF\eta(L, t)/RT = (I/si_0L)[(\theta_2 + \theta_3)^{\frac{1}{2}} \coth (\theta_2 + \theta_3)^{\frac{1}{2}} + \theta_3/\theta_4^{\circ}] \tag{62}$$

and

$$\eta(0, \infty) = \eta(L, \infty) - \{I\rho_e L/(\theta_2 + \theta_3)^{\frac{1}{2}}\} \cdot \tanh \{\tfrac{1}{2}(\theta_2 + \theta_3)^{\frac{1}{2}}\} \tag{63}$$

The steady-state impedance can therefore be expressed as:

$$Z = (R_t + R_D + R_m) \tag{64}$$

where the resistance "elements", R_t, R_D and R_m, are defined through:

$$R_t = (RT/nFI_0), \quad (I_0) = si_0L \tag{65}$$

$$R_D = (RT/nFI_{lim}), \quad (I_{lim} = nFC_r^v ED/v_r\delta) \tag{66}$$

and

$$R_m = (RT/nFI_0)[(\theta_2 + \theta_3)^{\frac{1}{2}} \coth (\theta_2 + \theta_3)^{\frac{1}{2}} - 1] \tag{67}$$

In (65)–(67), R_t is the familiar charge transfer resistance, R_D the resistance due to the diffusion in the *exterior* and R_m the impedance due to the *mixed* control of the diffusion *within* the pores, ohmic drop and the activation control.

(*b*) *Double-layer charging regime*

Case (*i*). When θ_2 and t are sufficiently small, the faradaic component of the total current will be small and the potential–time relationship will be controlled by $(\rho_e L) \leftrightarrow (CL)$ combination. Under these conditions

$$\bar{\eta}(L, p) \sim I\rho_e L \coth (C\rho_e pL^2)^{\frac{1}{2}}/(C\rho_e pL^2)^{\frac{1}{2}} \tag{68}$$

It is possible to obtain a parabolic followed by linear $\eta(L, t)$ *vs.* t plots if the conditions, $t \ll C\rho_e L^2$ and $C\rho_e L^2 \ll t \ll \tau$, are obeyed, respectively. τ is the "rise time", *i.e.*, time taken for $\eta(L, t)$ to attain a value close enough to:

$$\eta_\infty = R_t \cdot I[\sqrt{\theta_3} \coth \sqrt{\theta_3} + \theta_3/\theta_4] \tag{69}$$

θ_2 being much less than unity. Inverting eqn. (68), we have the following limits[12]:

$$\eta(L, t \to 0) = 2I(\rho_e t/\pi C)^{\frac{1}{2}} \tag{70}$$

$$\eta(L, t) \to It/Cl + 2I\rho_e L \sum_{n=1}^{\infty} \left(\frac{1 - \exp(-n^2\pi^2 t/C\rho_e L^2)}{n^2\pi^2} \right) \tag{71}$$

Case (*ii*). If $\theta_2 \gg 1$ but t is sufficiently small, the double layer is "charged through" the transfer resistance, R_t, and

$$\eta(L, t) = IR_t(1 - \exp(-t/R_t CL)) \tag{72}$$

We have assumed here that double layer charging precedes the onset of mass transfer control.

The difference in the forms of transient expressions given through (70)–(72) for ohmic and activation controls arises because the former represents "a distributed" impedance while the latter is equivalent to a "lumped" one.

(*c*) *Activation-ohmic polarisation only* ($\theta_3 \to 0$)

This corresponds to the situation where there is no concentration polarisation but the activation impedance is finite. This is realised by making $\theta_3 = 0$ ($D' \to \infty$) in the general expression (48). Then (see Table 1)

$$\bar{\eta}(L, p) \to \bar{I}\rho_e L \cdot \coth (C\rho_e L^2 + \theta_2)^{\frac{1}{2}}/(C\rho_e L^2 + \theta_2)^{\frac{1}{2}} \tag{73}$$

and

$$\eta(L, \infty) \to I\rho_e L \cdot \coth \sqrt{\theta_2}/\sqrt{\theta_2} \tag{74}$$

The time-dependence of $\eta(L, t)$ is given through

$$\eta(L, t) = I\rho_e L \left(1 + 2 \sum_{r=1}^{\infty} \frac{(1 - \exp\{(-\theta_2 - n^2\pi^2)/C\rho_e L^2)t\})}{\theta_2 + n^2\pi^2} \right) \tag{75}$$

Equation (75) is Ksenzhek's result[4] (also, eqn. (23), ref. 1).

Substitution of $\theta_2 = 0$ in (75) gives us the charging transient under ohmic control only (eqn. (71)). Equation (72) is a degenerate case of (75) when $\rho_e \to 0$.

(*d*) *Overvoltage when* $t \gg \tau_{dl}$ ($\theta_1 \to 0$)

If one is concerned with the behaviour after double-layer charging is over, the expression for $\bar{\eta}(L, p)$ to be used is the same as that in (48) except that

$$\alpha^2+\beta^2=\theta_p+\theta_2+\theta_3 \tag{76}$$

and

$$\alpha^2\beta^2=\theta_p\theta_2 \tag{77}$$

The relaxation times are then dependent on the zeros of the transcendental eqn. (53) with α^2, β^2 defined through (76)–(77) instead of (50). In this case, the boundary condition, $\partial\eta/\partial X=\rho_e I$, is equivalent to $I=s\int_0^L i\,dx$.

(*e*) *Ohmic polarisation absent* ($\rho_e \to 0$; $\theta_2, \theta_1 \to 0$)

By allowing $\theta_2, \theta_1 \to 0$ simultaneously, while their ratio (θ_2/θ_1) remains constant and is equal to $(v_r I_0 L/CD')$, the response of the porous electrode valid under negligible ohmic polarisation conditions can be evaluated.

It can be shown that (see Table 1)

$$\underset{\theta_2,\theta_1\to 0}{\text{Lt.}}\ \frac{\alpha^2-\theta_p-\theta_3}{\theta_2}\simeq\frac{\theta_3}{\theta_p+\theta_3} \tag{78}$$

$$\underset{\theta_2,\theta_1\to 0}{\text{Lt.}}\ \frac{\beta^2}{\theta_2}\simeq\frac{\theta_p}{\theta_p+\theta_3} \tag{79}$$

Then

$$\bar{\eta}(L,p)\to(IR_t)\cdot Z(p) \text{ with} \tag{80}$$

$$Z(p)=\frac{(\theta_p+\theta_3)[\cosh(\theta_p+\theta_3)^{\frac{1}{2}}+(\theta_p+\theta_3)^{\frac{1}{2}}\sinh(\theta_p+\theta_3)^{\frac{1}{2}}/\theta_4^\circ]}{(\theta_p+\theta_3)^{\frac{1}{2}}\sinh(\theta_p+\theta_3)^{\frac{1}{2}}\{1/\theta_4^\circ+\theta_3/(\theta_p+\theta_3)\}+\theta_p\cosh(\theta_p+\theta_3)^{\frac{1}{2}}} \tag{81}$$

if "a steady behaviour" in the exterior is assumed, *i.e.*, if t is large enough, then $\theta_4\sim\theta_4^\circ$. There is no loss of generality in doing this since the results given below can easily be extended also to the case, $\theta_4\neq\theta_4^\circ$.

If, in addition, $\theta_4\simeq\theta_4^\circ$ and $\theta_4^\circ\to\infty$,

$$Z\to Z_0(p)=\frac{\theta_p+\theta_3}{\theta_p+\theta_3\cdot\tanh(\theta_p+\theta_3)^{\frac{1}{2}}/(\theta_p+\theta_3)^{\frac{1}{2}}} \tag{82}$$

The poles of $\bar{\eta}(L,p)$, as expressed by (80)–(82), are obtained as $p=-\{p_n\}$ where

$$\tanh(\theta_3-p_nL^2/D')^{\frac{1}{2}}/(\theta_3-p_nL^2/D')^{\frac{1}{2}}=(p_nL^2/D')/\theta_3 \tag{83}$$

It is interesting to observe that the mathematical aspects of this special case are identical with the one developed[13]* for studying galvanostatic transients and impedance characteristics in surface diffusion problems. We may state here, without details, that

$$\tau_g\simeq(3X_0\coth X_0/\theta_3)\cdot(L^2/D') \tag{84}$$

where X_0 is non-zero real root of

$$\tanh X+X(X^2/\theta_3-1)=0 \tag{85}$$

$$|X_0|<\sqrt{\theta_3} \quad \text{and if } \theta_3\gg 1,$$

$$\tau_g\to(3\,L^2/D')(1/\sqrt{\theta_3}) \tag{86}$$

* A more detailed discussion regarding the similarity of porous electrode and surface diffusion phenomena will be presented elsewhere.

For example, if $\theta_3 = 10$, $X_0 = 2.44$; and if $\theta_3 = 100$, $X_0 \sim 9.5$.

The computed results for the ferricyanide–ferrocyanide redox couple obtained by Grens[5] can be compared with those derived in this section. Noting that

$$\theta_3 \text{ (of this paper)} = \nu E\xi/\pi\gamma \text{ of ref. 5} \tag{87}$$

and with[5] $E=2$, $\nu=1$, $\pi=(1/6.4)$, $\xi=80$ and $\nu=0.05$, (see eqns. (17) and (25) of ref. 5) we find $\theta_3 \simeq 2.048 \cdot 10^4$; also

$$(I/si_0l) = (\beta/\xi) \text{ of ref. 5} = 6.25 \cdot 10^{-4}$$

Hence $\Phi_0 = F\eta_{X=0}(t\to\infty)/RT = 8.94 \cdot 10^{-2}$ as calculated from our equations while the value given by Grens is $8.91 \cdot 10^{-2}$—an error less than 0.5%.

TABLE 2

γ	β	Φ_0 (*this paper*)	Φ_0 (*ref.* 5)
0.10	0.05	0.063	0.063
0.05	0.05	0.089	0.089
0.01	0.05	0.200	0.199
0.05	0.15	0.268	0.267
0.10	0.50	0.632	0.638
0.05	0.50	0.894	0.910
0.01	0.50	2.00	2.12
0.10	5.00	6.38	6.00

For further results, see Table 2. The last two columns in Table 2 are given to illustrate the deviations accruing at *large* overpotentials. What is surprising is not that they occur, but that they are *not larger* considering that the potential at the pore mouth exceeds 50 mV! (it may be remembered that we have made use of a linear form (eqn. (5)) here and that Grens has used a rate expression of the form (12) with $\alpha=\frac{1}{2}$ and $n=1$). The agreement could be expected to be even better in the non-stationary states since $\Phi=0$ at $t=0$, and $\Phi(t) \leqslant \Phi_0$ for all $t \geqslant 0$.

We now compare a typical transient curve. Since τ (of ref. 5) $=\tau_g$ (6.4) where τ_g is given by eqn. (86), we calculate $\tau_{90\%}$ through (86) to be approximately $=3(6.4)/\sqrt{\theta_3} \simeq 0.134$ in close agreement with the value reported by Grens. The variation of τ with $\sqrt{\theta_3}$, and hence the initial concentration, is as predicted in our theory.

7. GENERALISED IMPEDANCE: EQUIVALENT CIRCUIT ELEMENTS

The generalised impedance offered by the porous matrix—electrolyte interface is given by

$$Z(p) = \bar{\eta}/\bar{I}$$

$$= (\rho_e L)\left[\frac{f(p,\alpha,\beta)\cosh\alpha - f(p,\beta,\alpha)\cosh\beta}{f(p,\alpha,\beta)\alpha\sinh\alpha + f(p,\beta,\alpha)\beta\sinh\beta}\right]$$

where $f(p,\alpha,\beta)$, $f(p,\beta,\alpha)$ and α, β are defined through (49)–(50).

Under sinusoidal perturbations, the behaviour of the interface can be simulated

by the formal, frequency-dependent series elements, R_s and $1/\omega C_s$, given by

$$Z(j\omega) = R_s - j/\omega C_s$$

where ω is angular frequency and $j = \sqrt{-1}$.

We also note the following limiting behaviour:

$$(a)\ R_s(\omega \to 0) \to (\rho_e L/\theta_2)[(\theta_2+\theta_3)^{\frac{1}{2}} \coth (\theta_2+\theta_3)^{\frac{1}{2}} + \theta_3/\theta_4^\circ]$$

and

$$[\omega C_s(\omega \to 0)]^{-1} \to 0$$

$$(b)\ R_s,\ 1/\omega C_s(\omega \to \infty) \to 0$$

Under certain conditions, a "warburg-impedance like" behaviour results for sufficiently high frequencies and then

$$R_s \to (\rho_e L)/\{2\omega(C\rho_e L^2)\}^{\frac{1}{2}}$$

$$1/\omega C_s \to (\rho_e L)/\{2\omega(C\rho_e L^2)\}^{\frac{1}{2}}$$

(Note that this is not "caused" by diffusion of any species, but by the distributed impedance characteristic of the porous element).

(c) If a wide range of ω can be scanned, a limiting behaviour for R_s and a maximum for $1/\omega C_s$ could be obtained. But, if θ_2, $\theta_3 \gg \theta_1$, and θ_2 and θ_3 are very different, two maxima for $1/\omega C_s$ and two limiting plateaux for R_s are possible. These denote that the regions controlled by activation and diffusion become distinct and well separated. Caution is needed therefore when interpreting a "limiting range" for R_s or a maxima of $1/\omega C_s$ as due to activation or diffusion *alone*. However, such a separation is not always attainable and one has to interpret the mixed effects.

The variation of the equivalent elements with frequencies are plotted as *illustrations* in Figs. 1–4. The values chosen for the parameters are indicated in Table 3. The impedance elements plotted are R_s/R_0 and $(1/\omega C_s)/R_0$ where R_0, the "zero-

TABLE 3

Fig.	θ_1	θ_2	θ_3	θ_4°	R_0
1a			0.10		2.07
b	0.10	0.10	1.00	0.10	11.34
c			10.00		103.19
2a	0.10	1.00	0.10	0.10	2.34
b			1.00		11.59
c			10.00		103.32
3a			0.10		4.19
b	0.10	10.00	1.00	0.10	13.33
c			10.00		104.47
4a	0.10				
b	1.00	10.00	1.00	1.00	4.33
c	10.00				

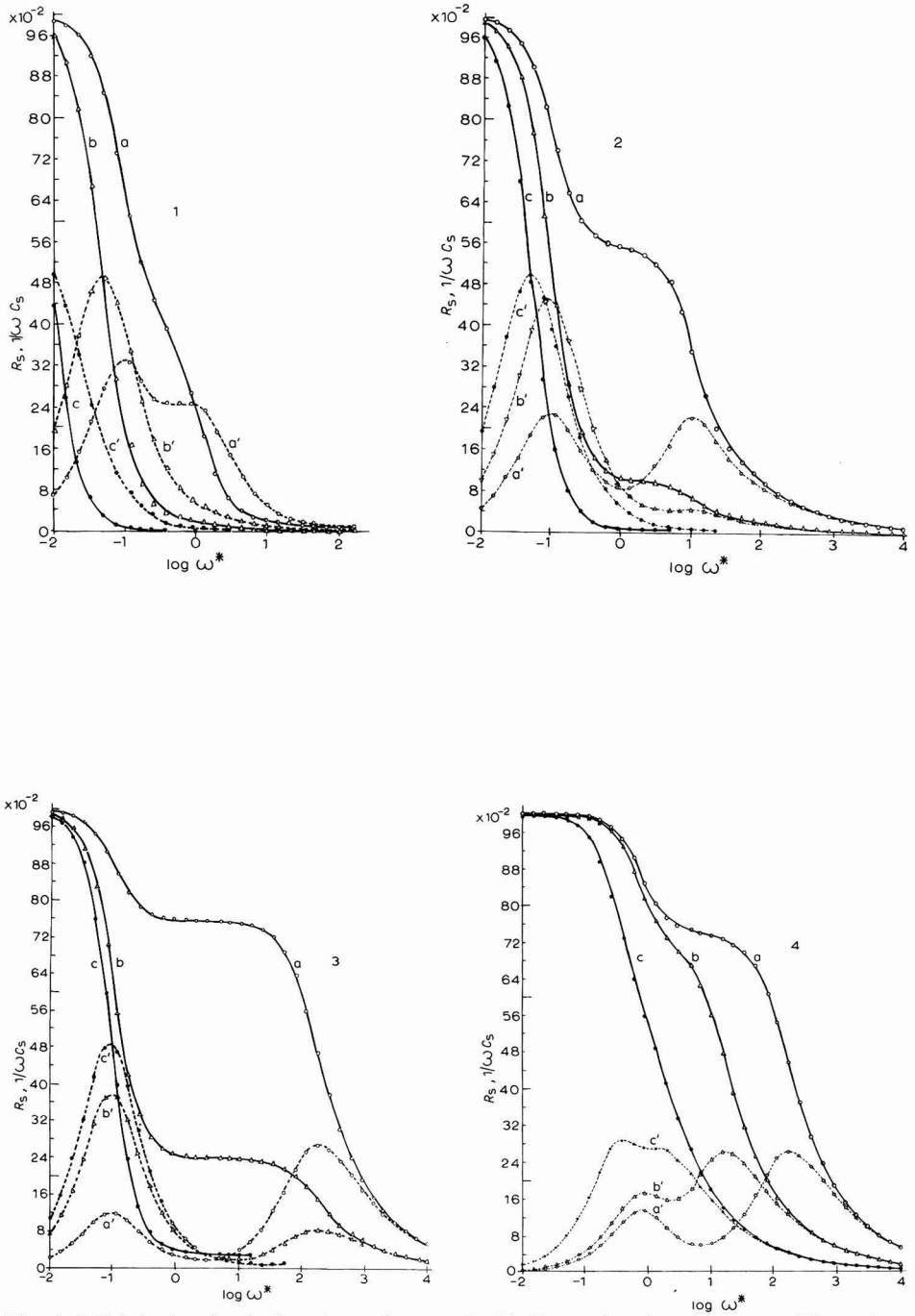

Figs. 1–4. Calcd. plots for the impedance elements, R_s, $1/\omega C_s$, as a function of frequency. The various parameters are listed in Table 2. Note that the plotted values for R_s, $1/\omega C_s$ are normalised with respect to $R_0 = R_s(\omega \rightarrow 0)$. The solid lines denote R_s and the dashed, $1/\omega C_s$; $\omega^* = \omega L^2/D$.

limit" resistance, is equal to $R_s(\omega \to 0)$. The computations were done through CDC-3600 at the Tata Institute of Fundamental Research, Bombay.

The print-out included the values for the equivalent impedance at the "pore-back", $X=0$, and the "reaction-zone" parameters, $\alpha(\omega)$ and $\beta(\omega)$, as functions of frequency and the other parameters. R_0 was also given. Discussions regarding "penetration depths" and concentration variations have been omitted.

(d) We reiterate here the usefulness of a Laplace-transform (or generalised impedance) approach in interpreting transients. The behaviour when $t \to \infty$ corresponds to the behaviour as $\omega \to 0$. A limiting "resistive" behaviour, if it results when $\omega \to 0$, is equivalent to a "steady-state" potential. One could say heuristically that well-defined plateaux in the R_s–ω plot are indicative of the pseudo-steady behaviour in the η–t curves and that the frequencies where the inflexions for R_s occur are related to the relaxation times of the various stages marking the potential rise to the steady value. It is also well known that the following simple integral relationship exists between a original $h(t)$ and the Fourier-cosine (sine) transforms of the imaginary/real parts of $\bar{h}(j\omega)$:

$$\eta(t) = I\left\{R_0 + \frac{2}{\pi}\int_0^\infty \left(\frac{1}{\omega C_s}\right)\frac{\cos \omega t}{\omega}\,\mathrm{d}t\right\}$$

$$= I \cdot \frac{2}{\pi}\int_0^\infty R_s(\omega)\frac{\sin \omega t}{\omega}\,\mathrm{d}\omega$$

ACKNOWLEDGEMENT

The author thanks Dr. H. V. K. Udupa for his interest in this work.

NOTATION

C	Specific capacitance of the double layer in the porous electrode;
$C_i(x, t)$	Instantaneous concentration of the species i; i=r for reactant; i=p for product;
C_i^v	Equilibrium concentrations of the species, i;
ΔC_i	$C_i - C_i^v$;
D	Diffusion coefficient in the exterior;
D'	Effective diffusion coefficient in the pores;
ν_i	Stoichiometric reaction coefficients of the species, i;
E	$1 + \nu_p C_r^v / \nu_r C_p^v$;
i	Faradaic current density (microkinetic);
i_0	Exchange current density for the electrochemical step;
α_i	Transfer coefficient; i=c, cathodic; i=a, anodic;
L	"Semi-thickness" of the porous electrode under "operation from the sides": (thickness of porous electrodes if with inert backing);
s	Specific, internal electrode surface;
I_0	si_0L;
δ	Diffusion layer thickness;
I	"Total" current/unit apparent area;

ρ_e Effective specific resistance of the electrolyte in the pores;
p Laplace transform variable;
$\bar{f}$ Laplace transform of $f = p \int_0^\infty \exp(-pt) \cdot f(t) dt$
(also see (30)–(41), (49)–(50), (65)–(66) in the text).

SUMMARY

(a) A description of the homogeneous one-dimensional model of the porous electrode used in the present analysis is given (section 2),

(b) The time-dependent boundary value problem is posed and a formal analytical solution obtained (section 3, section 5).

(c) The earlier results of Tobias and of Guruvich and Bagotskii are critically examined (section 4, 6); under certain conditions a close agreement with the calculations of Grens and Tobias is established (section 6).

(d) Several special cases of the above analysis discussed are: (i) $t \ll \tau_{dl}$, time-constant for double-layer charging; (ii) the concentration polarisation is negligible and (iii) ohmic-activation control is predominant with mass transfer effects in the exterior taken into consideration (section 6).

The equivalence of "surface diffusion" and "porous" models is indicated (section 6).

(e) The equivalent circuit elements representing the porous matrix–electrolyte interface are derived and the computed values are plotted for various values of the basic parameters (section 7).

Further reports on this problem will discuss the dependence of the rise times and the steady-state values on various parameters under different reactant-supply conditions.

REFERENCES

1 I. G. GURUVICH AND V. S. BAGOTSKII, *Elektrokhimiya*, 1 (1965) 1102; *Electrochim. Acta*, 9 (1964) 1151.
2 A. CHIZMADZHEV, *Elektrokhimiya*, 2 (1966) 1.
3 R. DE LEVIE, *Advan. Electrochem. Electrochem. Eng.*, 4 (1967) 000; *Electrochim. Acta*, 8 (1963) 757.
4 O. S. KSENZHEK, *Zh. Fiz. Khim.*, 36 (1960) 243; 37 (1963) 2007; 38 (1964) 1846.
5 E. A. GRENS II AND C. W. TOBIAS, *Ber. Bunsenges. Physik. Chem.*, 68 (1964) 236; E. A. GRENS II, Thesis, 1963, University of California, U.S.A.
6 M. BONNEMAY, G. BRONOËL, E. LEVART AND A. A. PILLA, *J. Electroanal. Chem.*, 13 (1967) 44.
7 A. WINSEL, *Z. Elektrochem.*, 66 (1962) 287.
8 K. B. OLDHAM AND O. TOPOS, *J. Phys. Chem.*, 71 (1967) 3007.
9 R. E. BELLMAN, R. E. KALABA AND J. A. LOCKETT, *Numerical Inversion of Laplace Transforms*, American Elsevier Publishing Co., New York, 1966.
10 I. W. SNEDDON, *Handbuch der Physik*, Vol. II, edited by S. FLUGGE, Springer Verlag, Berlin, 1955, p. 23.
11 S. K. RANGARAJAN, *Anal. Chem.*, 40 (1968) 1382.
12 P. BRO AND J. EPSTEIN, *Electrochim. Acta*, 10 (1965) 471.
13 S. K. RANGARAJAN, *J. Electroanal. Chem.*, 16 (1968) 485.

ELECTROANALYTICAL CHEMISTRY AND INTERFACIAL ELECTROCHEMISTRY
Elsevier Sequoia S.A., Lausanne – Printed in The Netherlands

ZUR BESTIMMUNG DER AUSTAUSCHSTROMDICHTE AM REDOXSYSTEM $[Co(NH_3)_6]Cl_2/[Co(NH_3)_6]Cl_3$

H. BARTELT UND S. LANDÁZURY
Sektion Chemie der Humboldt-Universität, 108 Berlin, Bunsenstr. 1 (DDR)
(Eingegangen am 13. Januar, 1969)

1. EINLEITENDES

Elektronenübergangsreaktionen zwischen Redoxpartnern gleicher stöchiometrischer Zusammensetzung sind in den vergangenen Jahren mehrfach Gegenstand sowohl theoretischer[1,2] als auch praktischer[3,4] Arbeiten gewesen. Dabei sind Vorstellungen und Modelle diskutiert worden, mit deren Hilfe die Geschwindigkeit des Elektronenüberganges zwischen den beiden Komponenten eines Redoxsystems berechnet werden kann. Danach wird der Elektronenübergang zwischen den beiden Redoxpartnern durch Faktoren, wie z.B. Änderung des Bindungsabstandes Zentralion–Solvathülle, Änderung der elektronischen Struktur des Zentralions und durch die Änderung der Bindungszustände Zentralion–Solvathülle beeinflusst.

Zur Messung der Austauschgeschwindigkeit zwischen beiden Redoxpartnern sind vorwiegend Untersuchungen in homogener Phase durchgeführt worden. Dagegen sind nur wenige elektrochemische Ergebnisse zur Diskussion herangezogen worden[3,5], obgleich in letzter Zeit eine Reihe von Austauschstromdichten und Geschwindigkeitskonstanten zusammengestellt wurden[6,7].

Nach Marcus können die elektrochemischen Austauschstromdichten zu einem direkten Vergleich zwischen Redoxreaktion in homogener und heterogener Phase herangezogen werden[1,5].

Zur Bestimmung der elektrochemischen Parameter einer Durchtrittsreaktion erweist sich die Messung des Durchtrittswiderstandes in Gleichgewichtsnähe, wie sie zuerst von Butler[8] vorgeschlagen und später mehrfach[9,10] angewandt wurde, als besonders vorteilhaft. Danach besteht zwischen der Stromdichte i und der Austauschstromdichte i_0 folgende Beziehung:

$$i = i_0(zF/RT)\eta_D \tag{1}$$

Dabei bedeuten: i=Stromdichte, i_0=Austauschstromdichte, η_D=Durchtrittsüberspannung, $RT/F = 25.6$ mV, $z = 1$.

Damit können wir bereits den wichtigsten elektrochemischen Parameter (i_0) bestimmen. Die Bestimmung der Durchtrittsfaktoren erfolgt aus der Konzentrationsabhängigkeit der Austauschstromdichte[9,10]

$$i_0 = nFk_{el}c_O^{\alpha} \cdot c_R^{1-\alpha} \tag{2}$$

k_{el} ist die elektrochemische Geschwindigkeitskonstante; c_O ist die Konzentration der höheren Wertigkeitsstufe; c_R ist die Konzentration der niedrigen Wertigkeitsstufe.

Durch partielle Differentiation der Austauschstromdichte nach der Konzentration erhält man:

$$\left(\frac{\partial \ln i_0}{\partial \ln c_O}\right)_{c_R} = \alpha; \qquad \left(\frac{\partial \ln i_0}{\partial \ln c_R}\right)_{c_O} = 1-\alpha \tag{3}$$

Diese Methode zur Bestimmung der Austauschstromdichte ist dann anwendbar, wenn es sich um die Bestimmung relativ kleiner Austauschstromdichten handelt, bei denen die Diffusionsüberspannung vernachlässigbar ist. Unter den genannten Bedingungen kann mit einfachen Gleichstrommessungen die Austauschstromdichte eines Redoxsystems relativ leicht berechnet werden.

Mit dieser Methode wurde die Geschwindigkeit des Elektronenaustausches am Redoxsystem

$$[Co(NH_3)_6]^{2+} \rightleftharpoons [Co(NH_3)_6]^{3+} + e \tag{I}$$

bestimmt und mit Daten aus der Literatur für den homogen-kinetischen Elektronenaustausch nach der Theorie von Marcus[1,5] verglichen.

Die Geschwindigkeit des Elektronenaustausches des Redoxvorganges (I) ist in homogener Phase mit Hilfe der Radioisotopenmethode von Lewis[11] und Mitarbeitern sowie von Stranks[12] und Mitarbeitern untersucht worden.

Die relativ kleine Geschwindigkeitskonstante[12] liess auch eine geringe Austauschstromdichte an Platinelektroden erwarten, die die Anwendung einfacher Gleichstrommessungen rechtfertigte. Das Redoxsystem (I) wurde von Laitinen und Kivalo[13] polarografisch untersucht. Die Austauschstromdichte wurde jedoch nicht bestimmt.

Die beiden Komponenten des Redoxsystems (I) weisen unterschiedliche Stabilitätskonstanten auf. Wie den eingehenden Untersuchungen von Bjerrum[14] zu entnehmen ist, liegen in Abhängigkeit von der Konzentration des Ammoniaks als Komplexbildner Co^{2+}-Komplexe unterschiedlicher Koordinationszahl in Lösung vor ($K_{[Co(NH_3)_6]^{2+}} = 10^{5.28}$, $K_{[Co(NH_3)_6]^{3+}} = 10^{34.36}$). Weiterhin sei darauf verwiesen, dass das $[Co(NH_3)_6]^{2+}$-Ion äusserst sauerstoffempfindlich ist[11,12,14].

In der vorliegenden Arbeit wird über die elektrochemische Bestimmung der Geschwindigkeitskonstanten und Durchtrittsfaktoren der Reaktion (I) aus Messungen in Gleichgewichtsnähe und im Tafelbereich berichtet. Der Einfluss der Konzentration des Komplexbildners und des Leitelektrolyten wird nachgewiesen.

2. EXPERIMENTELLES

Der Leitelektrolyt bestand aus NH_4Cl, das zweimal umkristallisiert und dann in bidestilliertem Wasser gelöst wurde.

Das $[Co(NH_3)_6]Cl_3$ wurde nach einer bekannten Vorschrift hergestellt und umkristallisiert[14].

Das $[Co(NH_3)_6]^{2+}$-Ion ist empfindlich gegen Luftsauerstoff und wurde deshalb erst in der Lösung vor Beginn der Messung in einer Reinststickstoffatmosphäre aus $CoCl_2 \cdot 6\,H_2O$ und überschüssigem Ammoniak hergestellt. Die verwendeten Stoffe waren p.a.

Der Reinststickstoff wurde durch einen Turm mit Kupferkatalysator sowie

durch Waschflaschen mit $CrCl_2$-Lösung und danach durch eine Waschflasche mit ammoniakalischer $CoCl_2$-Lösung geleitet.

Die Messzelle enthielt 5 Zuleitungen und war mit einem Temperiermantel versehen. Die Messelektrode (Oberfläche 0.5 cm^2—in Teflon eingebettet) und Gegenelektrode bestanden aus Platin. Das Potential der Messelektrode wurde mit einem Kompensator gegen eine gesättigte Kalomelelektrode gemessen.

Die Messzelle (50 cm^3) wurde zunächst mit 25 cm^3 2 *N* NH_4Cl und 25 cm^3 konzentriertem NH_3 gefüllt, die Elektroden eingesetzt und Stickstoff unter Rühren eingeleitet. Während dieser Zeit wurde die Messelektrode aktiviert, indem einige Minuten je 20 sec abwechselnd anodisch und katodisch polarisiert wurde, zuletzt jedoch 20 sec katodisch. Danach wurde mit einer Mikrobürette die gewünschte Menge $CoCl_2$-Lösung zugegeben. Wie Potentialmessungen zeigen, ist die Komplexbildung des $[Co(NH_3)_6]^{2+}$-Ions nach weiteren 30 min abgeschlossen.

Der grosse Überschuss an Ammoniak (6.8 *N*) ist erforderlich, um die Bildung des $[Co(NH_3)_6]^{2+}$-Ions zu gewährleisten[14].

Die $[Co(NH_3)_6]^{3+}$-Lösung wurde dann 5 min vor Beginn der Messung zugesetzt. Das Potential stellt sich dann relativ schnell ein und bleibt auch unter einem

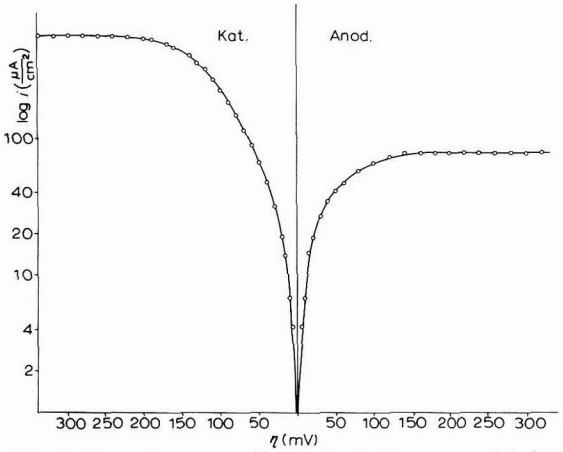

Abb. 1. Strom–Spannungs-Kurve des Redoxsystems $[Co(NH_3)_6]^{2+}/[Co(NH_3)_6]^{3+}$ in 7 *N* NH_3, 1 *N* NH_4Cl; Pt-Elektrode; Rührung, 25 U/sec.

kontinuierlichen Stickstoffstrom über längere Zeit konstant. In Übereinstimmung mit Bjerrum[14] fanden wir für das Redoxsystem $[Co(NH_3)_6]^{2+}/[Co(NH_3)_6]^{3+}$ ein Potential von $E_0 = -183 \pm 2$ mV gegen die gesättigte Kalomelelektrode.

Der Potentialverlauf gehorchte der Nernstschen Gleichung. Die Messungen zur Bestimmung der Austauschstromdichte wurden mit konstantgehaltenem Gleichstrom bei Überspannungen bis zu 5 mV durchgeführt.

Die Untersuchungen wurden an einer rotierenden Scheibenelektrode durchgeführt, obgleich sich zeigte, dass der Polarisationswiderstand im untersuchten Konzentrationsbereich praktisch rührunabhängig ist.

Den allgemeinen Verlauf der Strom–Spannungs-Kurve bei 25 Umdrehungen pro Sekunde zeigt Abb. 1. Die beiden Komponenten des Redoxsystems wurden als

$[Co(NH_3)_6]Cl_3$ ($1 \cdot 10^{-3}$ *M*) und $CoCl_2$ ($1 \cdot 10^{-3}$ *M*) zugegeben. Der katodische Teil der Kurve lässt einen Tafelbereich und ein Grenzstromgebiet erkennen. Der anodische Bereich zeigt einen Grenzstrom, der wesentlich kleiner ist als der katodische, obgleich die Diffusionskoeffizienten der beiden Kobalthexamminionen nicht sehr unterschiedlich sein dürften. Laitinen und Kivalo[13] geben dafür folgende Deutung: Entsprechend dem Verlauf der Bildungsfunktion[14] des $[Co(NH_3)_6]^{2+}$-Ions ist nur ein von der NH_3-Konzentration abhängiger Bruchteil der Gesamtkonzentration an Co^{2+}-Ionen als $[Co(NH_3)_6]^{2+}$-Ion vorhanden. Dieser geringeren Konzentration entspricht ein kleinerer anodischer Grenzstrom.

3. MESSUNGEN IN GLEICHGEWICHTSNÄHE

3.1 *Variation der* $[Co(NH_3)_6]^{3+}$*-Konzentration*

Zur Bestimmung der Austauschstromdichte am Redoxsystem

$$[Co(NH_3)_6]^{2+} \rightleftharpoons [Co(NH_3)_6]^{3+} + e \qquad \text{(I)}$$

aus dem Durchtrittswiderstand wurde die $[Co(NH_3)_6]^{3+}$-Konzentration von etwa $1 \cdot 10^{-4}$–$1 \cdot 10^{-2}$ *M* unter Konstanthaltung der Co^{2+}-Konzentration zu $1 \cdot 10^{-3}$ und $3 \cdot 10^{-3}$ *M* variiert. Erwartungsgemäss steigt die Austauschstromdichte mit der $[Co(NH_3)_6]^{3+}$-Konzentration an, wie es der Verlauf in Abb. 2 zeigt.

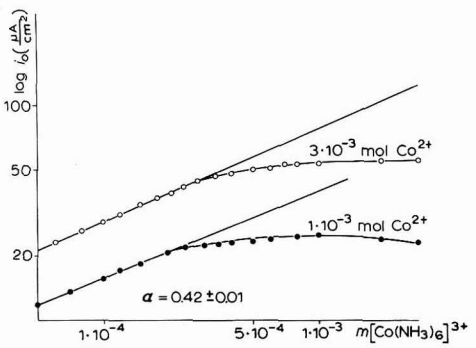

Abb. 2. Änderung der Austauschstromdichte bei Variation von $[Co(NH_3)_6]^{3+}$ und konstantem $[Co(NH_3)_6]^{2+}$.

Aus der Konzentrationsabhängigkeit der $[Co(NH_3)_6]^{3+}$-Ionen lässt sich nach Gl. (3) der Durchtrittsfaktor α bestimmen. Dabei zeigt sich, dass diese Beziehung nur in einem begrenzten Konzentrationsbereich gefunden wird:

$$\left(\frac{\partial \ln i_0}{\partial \ln c_{Co(III)}}\right)_{c_{Co(II)}} = 0.42 \pm 0.01$$

Das Redoxsystem verhält sich bei weiterer Steigerung der $[Co(NH_3)_6]^{3+}$-Konzentration keineswegs ideal, denn die Stromdichte steigt in beiden Messreihen zunächst noch an, durchläuft ein Maximum und fällt danach wieder ab.

Wir haben dieses Verhalten des $[Co(NH_3)_6]^{3+}$-Ions mit den Angaben aus der Literatur[12] für homogen-kinetische Untersuchungen verglichen und fanden auch dort, allerdings bei höheren Konzentrationen (0.01–0.07 *M*) und Temperaturen

(64.5°), eine ähnlich verlaufende Abweichung von der Linearität und werden darauf noch ausführlich eingehen.

Die Extrapolation der Geraden in Abb. 2 auf das Konzentrationsverhältnis $[Co(NH_3)_6]^{3+}$, $c = 1 \cdot 10^{-3}$ *M* und Co^{2+}, $c = 1 \cdot 10^{-3}$ *M* gestattet die Bestimmung einer "idealen" Austauschstromdichte und ergibt einen Wert von $i_0 = 40 \pm 2$ $\mu A/cm^2$. Die gemessene Austauschstromdichte beträgt dagegen nur $i_0 = 25 \pm 1$ $\mu A/cm^2$.

An dieser Stelle sei auf den besonderen Einfluss der Vorbehandlung der Elektrode bei Messungen zur Bestimmung des Polarisationswiderstandes verwiesen. Wie aus der eingangs beschriebenen Darstellung hervorgeht, wurde die Elektrode vor der Messung 20 sec katodisch bei 1 mA reduziert.

Wir haben diese Art der Vorbehandlung dahin abgewandelt, dass wir 20 und 60 sec anodisch bei 1 mA oxidiert haben. Das Ergebnis dieser unterschiedlichen Vorbehandlung zeigt Tabelle 1.

TABELLE 1

	Vorbehandlung	*Austauschstromdichte* ($\mu A/cm^2$)
(1)	20 sec katodisch	40
(2)	20 sec anodisch	26
(3)	60 sec anodisch	8

Die starke Verringerung der Austauschstromdichte ist offensichtlich auf eine Zunahme der Oxidbedeckung der Elektrode zurückzuführen. Wir haben deshalb weiterhin nur mit "reduzierten" Elektroden gearbeitet.

3.2 *Variation der $CoCl_2$-Konzentration*

Die Austauschstromdichte zeigt in Abhängigkeit von der $CoCl_2$-Konzentration einen linearen Anstieg (Abb. 3) mit einem Durchtrittsfaktor von

$$\left(\frac{\partial \ln i_0}{\partial \ln c_{Co(II)}}\right)_{c_{Co(III)}} = 0.52 \pm 0.01$$

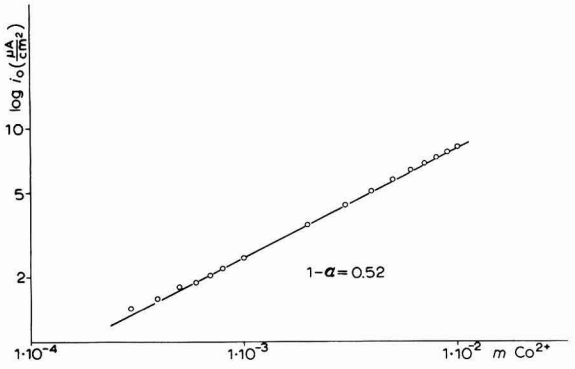

Abb. 3. Konzentrationsabhängigkeit der Austauschstromdichte bei Variation von Co^{2+} und konstantem $[Co(NH_3)_6]^{3+}$, $1 \cdot 10^{-3}$ *M*.

Dabei wurde die $CoCl_2$-Konzentration von $3 \cdot 10^{-4}$–$1 \cdot 10^{-2}$ M variiert, während die Ammoniakkonzentration (6.8 N) sowie die $[Co(NH_3)_6]^{3+}$-Konzentration ($c = 1 \cdot 10^{-3}$ M) konstant gehalten wurde. Die Summe der beiden Durchtrittsfaktoren ergibt 0.94. Die Differenz zu 1 wird von uns folgendermassen gedeutet:

Während die Co^{2+}-Konzentration in der Lösung linear ansteigt, verläuft die Komplexbildung dieses Ions[14] zu $[Co(NH_3)_6]^{2+}$ nicht ganz der Co^{2+}-Konzentration proportional, weil die gesamte NH_3-Konzentration konstant gehalten wird und die freie NH_3-Konzentration sich mit steigender $CoCl_2$-Konzentration verringert. Dadurch sinkt die Austauschstromdichte bei höheren Co^{2+}-Konzentrationen etwas ab und beeinflusst die Bestimmung des Durchtrittsfaktors. Trotz des relativ hohen NH_3-Gehalts der Lösung ist die Komplexbildung des Co^{2+}-Ions keineswegs quantitativ. Aus den Untersuchungen von Bjerrum[14] geht hervor, dass bei dieser NH_3-Konzentration nur 70% oder $7 \cdot 10^{-4}$ M $[Co(NH_3)_6]^{2+}$-Ionen vorliegen. Der Rest besteht aus Kobalt-Pentammin- und Kobalt-Tetramminionen.

Die Abweichung des katodischen Durchtrittsfaktors vom geforderten Wert bewog uns, diesen Parameter nach einer anderen Methode zu bestimmen. Dazu führten wir Messungen im Tafelbereich unter konstanten Konzentrationsverhält-

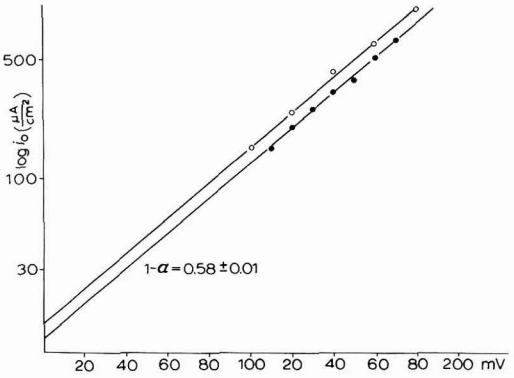

Abb. 4. Bestimmung des katodischen Durchtrittsfaktors $1-\alpha$ im Tafelbereich. (●) $2 \cdot 10^{-4}$; (○), $1 \cdot 10^{-3}$ M $[Co(NH_3)_6]^{3+}$; konstant Co^{2+}, $1 \cdot 10^{-3}$ M.

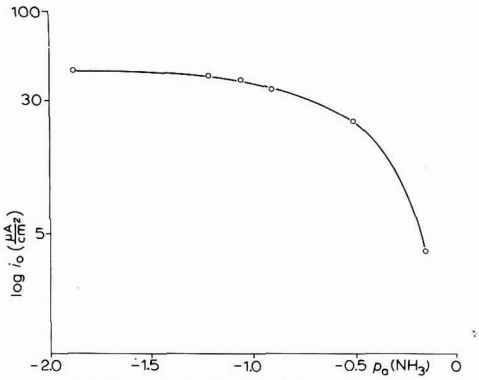

Abb. 5. Verlauf der Austauschstromdichte in Abhängigkeit von der NH_3-Konzentration.

nissen an der rotierenden Scheibenelektrode durch. Wir haben den Durchtrittsfaktor bei zwei $[Co(NH_3)_6]^{3+}$-Konzentrationen ($2 \cdot 10^{-4}$ und $1 \cdot 10^{-3}$ M) unter Konstanthaltung der Co^{2+}-Konzentration ($1 \cdot 10^{-3}$ M) und der NH_3-Konzentration bestimmt. Durch Extrapolation der Stromdichte auf unendliche Rührgeschwindigkeit und Auftragung gegen verschiedene Überspannungen erhielten wir aus der Tafelgeraden (Abb. 4) einen katodischen Durchtrittsfaktor von $1-\alpha = 0.58 \pm 0.01$, der sich nunmehr mit dem anodischen Durchtrittsfaktor zu 1 ergänzt.

Setzt man die gefundenen Parameter und Konzentrationen (Co(III) $= 1 \cdot 10^{-3}$ M, Co(II) $= 7 \cdot 10^{-4}$ M) in die Gl. (2) ein, so erhält man für $i_0 = 40$ $\mu A/cm^2$ die elektrochemische Geschwindigkeitskonstante:

$$k_{el} = 5.25 \cdot 10^{-4} \text{ cm sec}^{-1}$$

3.3 *Variation der NH_3-Konzentration*

Wir haben in einer weiteren Messreihe den Einfluss des Komplexbildners NH_3 auf die Austauschstromdichte untersucht. Die Zusätze an NH_3 wurden von 1.34–13.4 *M* (konzentrierte Lösung) variiert. Einem Vorschlag von Bjerrum[14] folgend, haben wir die Austauschstromdichte gegen $p_a(NH_3)$, dem negativen dekadischen Logarithmus der Aktivität des Ammoniaks* aufgetragen und finden folgenden Kurvenverlauf (Abb. 5).

Die bei fallender NH_3-Aktivität abnehmende Austauschstromdichte entspricht qualitativ dem Verlauf der Bildungsfunktion für das $[Co(NH_3)_6]^{2+}$-Ion in NH_3. Das legt die Annahme nahe, dass die NH_3-Konzentration über das Komplexgleichgewicht die an der Durchtrittsreaktion beteiligte Konzentration der $[Co(NH_3)_6]^{2+}$-Ionen beeinflusst, während die $[Co(NH_3)_6]^{3+}$-Ionen infolge der höheren Bildungskonstanten durch die Änderung der NH_3-Aktivität nicht beeinflusst werden.

Mit Hilfe der Gl. (2), bei Kenntnis von k_{el} und Einsetzen der $[Co(NH_3)_6]^{2+}$-Konzentration, die in Abhängigkeit von der NH_3-Aktivität[14] nach

$$E_R^0 = E_R + 0.059 \log \alpha_6^{**} \quad \text{für} \quad 25°$$

berechnet werden konnte, ergab sich auch durch Berechnung der Verlauf der Kurve in Abb. 5.

Darin ist allerdings die Annahme enthalten, dass an der elektrochemischen Durchtrittsreaktion nur die sechsfach-koordinierten Ionen, $[Co(NH_3)_6]^{2+}$, teilnehmen, während die Komplexionen mit einer geringeren Zahl von NH_3-Liganden ($n < 6$) elektrochemisch inaktiv sind. Ähnliche Beobachtungen wurden auch von Konrad und Vlček[15] am System $[Coen_3]^{2+}/[Coen_3]^{3+}$ gemacht und daraus geschlossen, dass der Elektronenaustausch nur zwischen Ionen mit gleicher stöchiometrischer Zusammensetzung erfolgt.

3.4 *Der Einfluss des Leitelektrolyten*

Schliesslich haben wir noch den Einfluss des Leitelektrolyten NH_4Cl untersucht, da er mit dem Komplexbildner ein Puffersystem bildet. Ausserdem beeinflusst die Konzentration der NH_4^+-Ionen nach Bjerrum[14] auch noch folgendes Gleichgewicht:

$$[Co(NH_3)_6]^{3+} + H_2O \rightleftharpoons [Co(NH_3)_5OH]^{2+} + NH_4^+ \qquad \text{(II)}$$

Danach liegt in 1 *N* NH_4Cl-Lösung mit hinreichendem Überschuss an NH_3 das $[Co(NH_3)_6]^{3+}$-Ion zu etwa 97% vor. Mit abnehmendem NH_4Cl-Gehalt der Lösung steigt jedoch die Konzentration an Pentammin- und Tetrammin-Ionen. Nach den Untersuchungen von Schwarz und Tede[16] sowie Linhard und Flygare[17] hydrolysieren diese Ammine aber relativ leicht gemäss der Gleichung

$$[Co(NH_3)_5OH^-]^{2+} + 2\,H_2O \rightleftharpoons Co(OH)_3 + 2\,NH_4^+ + 3\,NH_3 \qquad \text{(III)}$$

Diese Hydrolysevorgänge wurden durch Leitfähigkeitsmessungen bestätigt[16]. Weiterhin wird angegeben, dass $Co(OH)_3$ an Aktiv-Kohle adsorbiert wird.

---

* Die p_a (NH_3)-Werte für Lösungen mit 1 *N* NH_4Cl entnahmen wir ebenfalls der Monografie von Bjerrum[14].

** α_6 ist dabei der Anteil der Co^{2+}-Ionen, der in der Hexammin-Form vorliegt.

Wir haben deshalb die Konzentration des NH_4Cl im Bereich von 0.25–5 N variiert, um eine qualitative Vorstellung über den Einfluss des Leitelektrolyten zu gewinnen. Das Ergebnis zeigt die Abb. 6. Wir beobachteten einen beachtlichen Abfall der Austauschstromdichte bei steigender Leitelektrolytkonzentration.

Für die Deutung dieses Verhaltens gibt es einen weiteren Faktor, den wir kurz anführen wollen, um die Kompliziertheit des Systems anzudeuten.

Wie die Untersuchungen von Evans und Nancollas[18] sowie Larsson[19] zeigen, nimmt die Ionenpaarbildung zwischen $[Co(NH_3)_6]^{3+}$- und Cl^--Ionen mit steigender Konzentration zu. Dabei werden je nach der Konzentration auch mehrere Cl^--Ionen an ein Komplexion in zweiter Sphäre angelagert. Diese Ionenpaare haben einen grösseren Ionenradius und sollten für den Elektronendurchtritt wegen des grösseren Abstandes zur Elektrode energetisch benachteiligt sein.

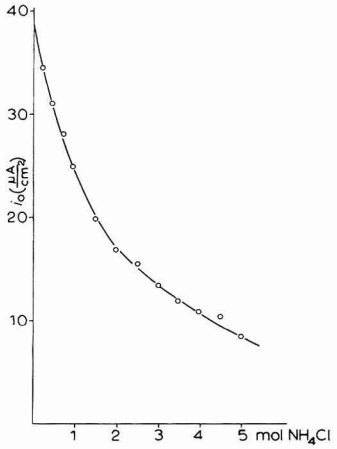

Abb. 6. Abhängigkeit der Austauschstromdichte von der NH_4Cl-Konzentration, 0.25–5 M, $[Co(NH_3)_6]^{2+}$/$[Co(NH_3)_6]^{3+}$, $1 \cdot 10^{-3}$ M.

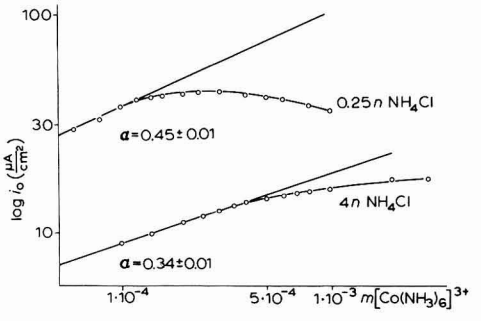

Abb. 7. Verlauf der Austauschstromdichte bei Variation von $[Co(NH_3)_6]^{3+}$ und konstantem Co^{2+} ($1 \cdot 10^{-3}$ M) bei verschiedenen NH_4Cl-Konzentrationen.

Auch an der Elektrodenoberfläche steigt die Chloridionen-Konzentration und wirkt auf den Ladungsdurchtritt. Da sich die Chloridionen sowohl an der Elektrodenoberfläche als auch an der Oberfläche der Komplexionen befinden, sollte eine elektrostatische Abstossung stattfinden, die zu einer Verringerung der Austauschstromdichte führt.

Zum Nachweis, dass nicht nur die Austauschstromdichte sinkt, sondern auch die Durchtrittsfaktoren beeinflusst werden, haben wir bei verschiedenen Leitelektrolytkonzentrationen die Durchtrittsfaktoren aus der Konzentrationsabhängigkeit der Austauschstromdichte bestimmt.

Dabei zeigt sich, dass mit Erhöhung der Leitelektrolytkonzentration auch die Durchtrittsfaktoren beeinflusst werden. Auf eine weitere Besonderheit sei in diesem Zusammenhang noch verwiesen:

Eingangs dieser Untersuchung (3.1) war festgestellt worden, dass eine Abweichung der Austauschstromdichte von der Linearität (Abb. 2) beobachtet wurde.

TABELLE 2

Leitelektrolyt-konzentration (N NH_4Cl)	$1-\alpha$	α
0.25		0.43
1	0.52	0.42
4	0.63	0.34

Es wurde weiterhin festgestellt, dass die NH_4Cl-Konzentration das Gleichgewicht (II) beeinflusst. Demnach sollten mit steigender NH_4Cl-Konzentration die Hydrolysevorgänge zurückgedrängt werden.

Wir haben zur Bestätigung dieser Vorstellung Messungen bei niederen NH_4Cl-Konzentrationen durchgeführt. In 0.1 *N* NH_4Cl sind praktisch keine Messungen möglich, weil der Widerstand der Lösung enorm ansteigt. In 0.25 *N* NH_4Cl-Lösungen wurde wiederum eine Abweichung von der Linearität beobachtet, die bei noch geringeren Konzentrationen beginnt als es in 1 *N* NH_4Cl-Lösung der Fall ist (Abb. 7).

Ebenso geht aus der Darstellung hervor, dass bei Erhöhung der NH_4^+-Ionenkonzentration der Hydrolysevorgang nach Gl. (II) zurückgedrängt werden kann. Auch diese Vorstellung wird durch die Messreihe in 4 *N* NH_4Cl bestätigt.

Bei homogenkinetischen Untersuchungen[12] wurde eine Abhängigkeit der Geschwindigkeitskonstanten der Reaktion (I) vom pH-Wert der Lösung gefunden. Das Puffersystem NH_3/NH_4Cl lässt nur eine geringe Änderung des pH-Wertes zu. Wir haben deshalb die gleiche Messreihe wie in Abb. 6 wiederholt, nur wurde nach Herstellung der Ausgangsbedingungen (6.8 *N* NH_3, 1 *N* NH_4Cl) KCl anstelle von NH_4Cl zugesetzt. Die Ergebnisse lassen keinen Unterschied zwischen beiden Salzen erkennen, obgleich nach den oben zitierten Untersuchungen[12] für den Zusatz von NH_4Cl ein stärkerer Abfall der Austauschstromdichte zu erwarten gewesen wäre, weil hier gleichzeitig der pH-Wert der Lösung fällt.

3.5 *Einfluss der Temperatur*

Um weitere Hinweise über die Durchtrittsreaktion zu erhalten, wurde unter konstanten Konzentrationsbedingungen (Co^{2+}—$1 \cdot 10^{-3}$ *M*, 6.8 *N* NH_3 und 1 *N* NH_4Cl) bei alleiniger Änderung der $[Co(NH_3)_6]^{3+}$-Konzentration der Einfluss der Temperatur untersucht (Abb. 8). Die Aktivierungsenergie wurde nach[10]

$$\frac{\partial \ln i_0}{\partial T^{-1}} = -\frac{\Delta H}{R}$$

zu 7.5 kcal mol^{-1} bestimmt.

Von besonderer Bedeutung ist hier abermals die Abweichung von der Linearität. Wie die Messungen zeigen, wird dieser Einfluss mit steigender Temperatur geringer.

Mit steigender Temperatur werden aus NH_3 und H_2O mehr NH_4^+-Ionen gebildet, die nach Gl. (II) das Gleichgewicht nach links verschieben und dadurch die nachfolgende Hydrolyse nach Gl. (III) verringern.

Deshalb sollte die Bedeckung der Platinelektrode durch $Co(OH)_3$ mit steigen-

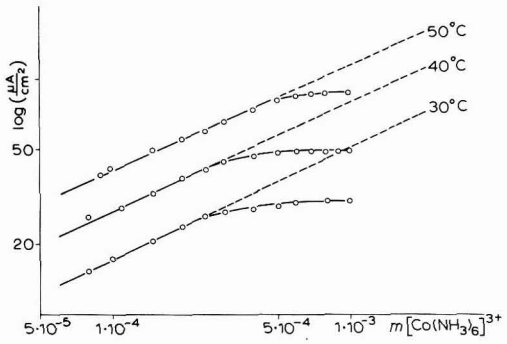

Abb. 8. Temperaturabhängigkeit der Austauschstromdichte.

der Temperatur geringer werden. Dadurch würde der Bedeckungsgrad verringert und sollte sich erst bei höheren $[Co(NH_3)_6]^{3+}$-Konzentrationen bemerkbar machen. Schliesslich sollten auch die Chloridionen bei Temperatursteigerung auf das $Co(OH)_3$ einwirken und damit ebenfalls zu einer Verringerung der Elektrodenbedeckung beitragen.

4. DISKUSSION

Die vorliegenden Untersuchungen zeigen, dass durch Messungen des Polarisationswiderstandes die Bestimmung der elektrochemischen Parameter der Durchtrittsreaktion (I) möglich ist.

Aus den Messungen wurde unter bestimmten Bedingungen (6.8 *N* NH_3, 1 *N* NH_4Cl) die elektrochemische Geschwindigkeitskonstante k_{el} bestimmt.

Mit Hilfe der Theorie von Marcus, wonach

$$(k_{hom}/10^{11})^{\frac{1}{2}} \geqslant k_{el}/10^4$$

gilt, wird ein Vergleich mit den homogenkinetischen Untersuchungen von Stranks[12] und Mitarbeitern möglich, da sowohl die Leitsalzkonzentration ($I = 1$), als auch die Konzentration des Komplexbildners etwa gleich war.

Rechnet man die Geschwindigkeitskonstante, k_{hom}, mit Hilfe der angegebenen Aktivierungsenergie auf 25° um, so erhält man folgende Werte:

$$(k_{hom}/10^{11})^{\frac{1}{2}} = 6.3 \cdot 10^{-8} \qquad k_{el}/10^4 = 5.25 \cdot 10^{-8}$$

Wie schon an anderen Redoxsystemen[3,5], so zeigt sich auch am vorliegenden System eine befriedigende Übereinstimmung.

Während allgemein in der Literatur das $[Co(NH_3)_6]^{3+}$-Ion als sehr stabil angesehen wird, weist Bjerrum[14] in seinen grundlegenden Untersuchungen bereits darauf hin, dass diese Feststellung in ammoniakalischer, ammonsalzhaltiger Lösung eine gewisse Einschränkung erfährt. Die durch die Gln. (II–III) beschriebenen Hydrolysevorgänge werden durch folgende Faktoren beeinflusst.

1. Die Platinelektrode wirkt als Katalysator für die Gleichgewichtseinstellung.

2. Co^{2+}-Salze fördern in Abhängigkeit von der Konzentration ebenfalls die Einstellung der Gleichgewichte.

3. Intensive Rührung in einer Stickstoffatmosphäre fördert eine schnellere Gleichgewichtseinstellung.

Da bis zum Beginn der Messung stets die Einstellung des Gleichgewichtspotentials abgewartet wurde, muss damit gerechnet werden, dass die Hydrolysevorgänge (II–III) abgelaufen sind. Wie aus unseren Untersuchungen hervorgeht, beeinflussen die Vorgänge die Austauschstromdichte. Dabei scheint die Co^{2+}-Konzentration von besonderer Bedeutung zu sein. Es wurde nämlich beobachtet, dass die Abweichung von der Linearität (Abb. 2) unter Normalbedingungen stets beim gleichen Potential erfolgt. Für die Deutung, dass die Abweichung der Austauschstromdichte von der Linearität durch Hydrolyse der $[Co(NH_3)_6]^{3+}$-Ionen hervorgerufen wird, sprechen die Messungen in Abhängigkeit von der NH_4Cl-Konzentration. Der Einfluss der Temperatur steht ebenfalls im Einklang mit diesen Beobachtungen.

Die hier gegebene Deutung für die Abweichung der Austauschstromdichte von der Linearität kann auch zur Deutung des niedrigen anodischen Grenzstromes herangezogen werden, wenn man annimmt, dass durch die Oxidation der $[Co(NH_3)_6]^{2+}$-Ionen nach Gl. (I) zunächst $[Co(NH_3)_6]^{3+}$-Ionen gebildet werden, die aber bereits auf der Elektrodenoberfläche teilweise hydrolysieren und zu einer ständig fortschreitenden Bedeckung führen. Tatsächlich beobachtet man bei Messungen im anodischen Grenzstrombereich, dass die Ströme (i) nicht genau reproduzierbar sind, sondern von Versuch zu Versuch schwanken und (ii) ständig langsam absinken.

Allein die schlechte Reproduzierbarkeit der anodischen Grenzströme deutet auf einen heterogenen Elektrodenvorgang hin. Die Zeitabhängigkeit des Grenzstromes zeigt, dass dieser Prozess der Blockierung der Elektrodenoberfläche bei Stromfluss ständig zunimmt. Damit kann auch die eingangs dargelegte Unsymmetrie der Stromdichte–Potentialkurve (Abb. 1) durch einen Bedeckungsvorgang gedeutet werden.

Die mehrfach diskutierte Irreversibilität[13,15] des Kobalt-Hexammin-Redoxsystems kann auf eine relativ geringe Austauschstromdichte mit einer zusätzlichen Überlagerung durch einen Hydrolysevorgang zurückgeführt werden.

DANKSAGUNG

Herrn Prof. R. Landsberg möchten wir für die Anregungen und Diskussionen recht herzlich danken.

ZUSAMMENFASSUNG

Die Austauschstromdichte i_0 des Redoxsystems $[Co(NH_3)_6]^{2+}/[Co(NH_3)_6]^{3+}$ wurden aus Polarisationswiderstandsmessungen beim Gleichgewichtspotential ermittelt; die Konzentrationsabhängigkeit der Austauschstromdichte ergab die Durchtrittsfaktoren.

Bei höheren Konzentrationen des Co(III)-Komplexes kommt es zu Abweichungen von der Linearität zwischen log i_0 und log c dieses Komplexes. Das wird durch Bedeckung der Elektrode durch das Hydrolyseprodukt des Co(III)-Komplexes verursacht, dafür sprechen die Abhängigkeit dieser Erscheinung von der NH_4Cl-Konzentration und der Temperatur. Die anodische Bildung des Co(III)-Komplexes begünstigt die Bedeckung der Elektrode durch Hydrolyseprodukte, das bewirkt

einen anormalen niedrigen anodischen Grenzstrom. Die Abhängigkeit der Austauschstromdichte von der Ammoniakkonzentration entspricht der Abhängigkeit der $[Co(NH_3)_6]^{2+}$-Konzentration vom Ammoniakgehalt und spricht dafür, dass als Redoxpartner allein die Hexamminkomplexe wirksam sind. Steigender NH_4Cl- und KCl-Gehalt senkt die Austauschstromdichte, das wird mit der Ionenpaarbildung $[Co(NH_3)_6]^{3+}$–Cl^- und Cl^--Adsorption an der Elektrode in Verbindung gebracht.

Die ermittelte heterogene Geschwindigkeitskonstante entspricht dem Literaturwert für die homogene Konstante unter Zugrundelegung einer von Marcus abgeleiteten Beziehung.

SUMMARY

The exchange current i_0 of the redox system $[Co(NH_3)_6]^{2+}/[Co(NH_3)_6]^{3+}$ was determined by measurement of the polarization resistance at the equilibrium potential; the concentration dependence of i_0 gave the transfer coefficient. At higher concentrations of the Co^{III} complex there is a deviation from the linear relation between log i_0 and the log of the concentration of this complex. This is caused by the coverage of the electrode by the hydrolysis product of the Co^{III} complex; hence this phenomenon depends on the NH_4Cl concentration and the temperature. The anodic formation of the Co^{III} complex favours the coverage of the electrode by the hydrolysis product, causing an anomalously low anodic limiting current. The dependence of i_0 on the ammonia concentration corresponds to the dependence of the $[Co(NH_3)_6]^{2+}$ concentration on the ammonia content and shows that the hexamine complex alone takes part in the redox reaction. Increase of NH_4Cl and KCl concentration causes a lowering of i_0 as a result of the formation of the $[Co(NH_3)_6]^{3+}$–Cl^- ion pair and Cl^- adsorption on the electrode.

The heterogeneous rate constant derived here corresponds to the literature value for the homogeneous constant according to the relation proposed by Marcus.

LITERATUR

1 R. A. MARCUS, *J. Chem. Phys.*, 43 (1965) 679.
2 V. G. LEVICH, *Advan. Electrochem. Electrochem. Eng.*, Vol. 4, (1966) 249.
3 Z. GALUS UND R. N. ADAMS, *J. Phys. Chem.*, 67 (1963) 866.
4 A. A. VLČEK, *Progr. Inorg. Chem.*, 5 (1963) 211.
5 R. A. MARCUS, *J. Phys. Chem.*, 67 (1963) 853.
6 N. TANAKA UND R. TAMAMUSHI, *Electrochim. Acta*, 9 (1964) 963.
7 M. SPIRO, *Electrochim. Acta*, 9 (1964) 1531.
8 J. A. V. BUTLER, *Trans. Faraday Soc.*, 28 (1932) 379.
9 H. GERISCHER, *Z. Physik. Chem. Leipzig*, 202 (1953) 292.
10 P. DELAHAY, *Double layer and Electrode Kinetics*, Interscience Publishers, New York, 1965.
11 W. B. LEWIS, C. D. CORYELL UND J. W. IRVINE, *J. Chem. Soc., Suppl. Issue*, 2 (1949) 386.
12 N. S. BIRADAR, D. R. STRANKS UND M. S. VAIDYA, *Trans. Faraday Soc.*, 58 (1962) 2421.
13 H. A. LAITINEN UND P. KIVALO, *J. Am. Chem. Soc.*, 75 (1953) 2198.
14 J. BJERRUM, *Metal Ammine Formation in Aqueous Solution*, Haase and Son, Copenhagen, 1941.
15 D. KONRAD UND A. A. VLČEK, *Collection Czech. Chem. Commun.*, 28 (1963) 808.
16 R. SCHWARZ UND K. TEDE, *Ber. Deut. Chem. Ges.*, 60 (1927) 63.
17 M. LINHARD UND H. FLYGARE, *Z. Anorg. Allgem. Chem.*, 261 (1950) 328.
18 M. G. EVANS UND G. H. NANCOLLAS, *Trans. Faraday Soc.*, 49 (1953) 363.
19 R. LARSSON, *Acta Chem. Scand.*, 16 (1962) 1919.

ELECTROANALYTICAL CHEMISTRY AND INTERFACIAL ELECTROCHEMISTRY
Elsevier Sequoia S.A., Lausanne – Printed in The Netherlands

POTENTIAL SWEEP VOLTAMMETRY WITH UNCOMPENSATED OHMIC POTENTIAL DROP. IRREVERSIBLE CHARGE TRANSFER

SERGIO ROFFIA
Institute of Chemistry 'G. Ciamician' University, Bologna (Italy)
MARINA LAVACCHIELLI
Polarographic Centre, C.N.R., Padova (Italy)
(Received November 18th, 1968; in revised form, February 17th, 1969)

INTRODUCTION

Among the various electrochemical relaxation techniques, linear potential sweep voltammetry has found wide applications in the investigation of the mechanism of electrode processes.

The availability of three-electrode instruments would make the problem of the ohmic drop in the cell seem of little interest. However, under certain conditions, even with three-electrode instruments, the uncompensated ohmic drop can alter the voltammetric curves to such an extent that theoretical equations which do not take this effect into account, are not valid.

The uncompensated cell resistance causes a distortion of the voltammetric curve both because of the displacement along the potential axis, depending upon the current intensity in each single point, and because of the non-linearity of the potential scan.

The effects of this distortion have been considered by Delahay[1], who made an approximate evaluation of the decrease of the peak current due to the ohmic drop. Recently, Nicholson[2] and de Vries and van Dalen[3] presented a rigorous solution in the case of a reversible charge transfer at plane electrodes.

This paper presents the theory of the current/potential curves for totally irreversible processes with uncompensated ohmic potential drop when mass transfer takes place only by semi-infinite linear diffusion.

This class of problem gives rise to non-linear integral equations[2,4]. Other examples of problems in electrochemical theory that result in equations of this type, and their numerical solution, have been recently presented[2,3,5–7].

The theory reported in this paper has been briefly outlined in a preliminary communication[8].

Experimental data obtained for totally irreversible reduction of bromate ions have been examined in terms of this theory and the results obtained have been compared with those reported in the literature[9].

THEORETICAL TREATMENT

The boundary value problem for the totally irreversible reduction of oxidized

species, O, to a reduced species, R, at a plane electrode in the case of linear sweep voltammetry with uncompensated ohmic drop, has already been reported[10], except that the equation defining the potential variation must be suitably modified to account for the ohmic drop. In this case, the electrode potential at any time is defined as:

$$E = E_i - vt + iR_u \tag{1}$$

where E_i is the initial potential, v the voltage sweep rate, R_u the uncompensated resistance, and i the current at time, t. Thus, the last boundary condition (eqn. (38), ref. 10) becomes

$$f(t) = D_O \left(\frac{\delta C_O}{\delta x}\right)_{x=0} = C_O k_i e^{bt} \exp\left[-\left(\frac{\alpha n_\alpha F}{RT}\right) R_u i\right] \tag{2}$$

where

$$k_i = k_s \exp\left[-(\alpha n_\alpha F/RT)(E_i - E^0)\right] \tag{3}$$

and

$$b = \alpha n_\alpha F v/RT \tag{4}$$

The symbols used have the meaning given in ref. 10.

With suitable changes in variables and substitutions[10], it is easy to show that the function

$$\chi(bt) = i/nFAC_O^* \pi D_O b$$

is a solution of the following dimensionless non-linear integral equation:

$$\exp(u - bt)\chi(bt) \exp\left[H\chi(bt)\right] = 1 - \int_0^{bt} \frac{\chi(z)\,dz}{(bt - z)^{\frac{1}{2}}} \tag{5}$$

where

$$u = \ln\left\{(\pi D_O b)^{\frac{1}{2}}/k_i\right\} \tag{6}$$

and

$$H = (\alpha n_\alpha F/RT) n R_u F A C_O^* (\pi D_O b)^{\frac{1}{2}}$$

For specific values of u and H, the solution of eqn. (5) provides values of $\chi(bt)$ as a function of bt, which is related to the applied voltage $V = E - iR_u$ through the equation:

$$bt = (\alpha n_\alpha F/RT)(E_i - V)$$

which is readily obtained from (1) and (4).

In general, current/potential curves depend on u, which is in turn related to the initial potential E_i by means of eqns. (6) and (3). However, our calculations have shown that for u greater than about 7, theoretical current/potential curves become independent of u, within 1%. Experimentally, this mathematical condition corresponds to the fact that the initial potential, E_i, must be made considerably more positive than the half-peak potential in order that experimental current/potential curves are independent of it within the limits of experimental error.

The numerical solution of eqn. (5) has been carried out by us according to Huber's method[11]; an account of its principle has been given recently by de Vries[12]. If δ is the width of the intervals into which the bt-axis is divided and χ_n is the approxi-

mate value of $\chi(bt)$ at $bt=n\delta$, the following equation results from eqn. (5):

$$\tfrac{4}{3}\delta^{\frac{1}{2}}\sum_{i=1}^{n}\{(\chi_i-\chi_{i-1})[(n-i+1)^{\frac{3}{2}}-(n-i)^{\frac{3}{2}}]\}+2\chi_0(\delta n)^{\frac{1}{2}}+$$
$$+\exp(u-\delta n)\,\chi_n\exp(H\chi_n)-1=0$$

from which it is possible to obtain successively the values of χ_n for $n=1, 2, \ldots$. The value of χ_0 is obtained from eqn. (5) for $bt=0$. A bisection method has been used for solving the transcendental equations and the iteration process was interrupted when the relative error was less than 10^{-9}. The values of δ and u used in these calculations were 0.04 and 7, respectively.

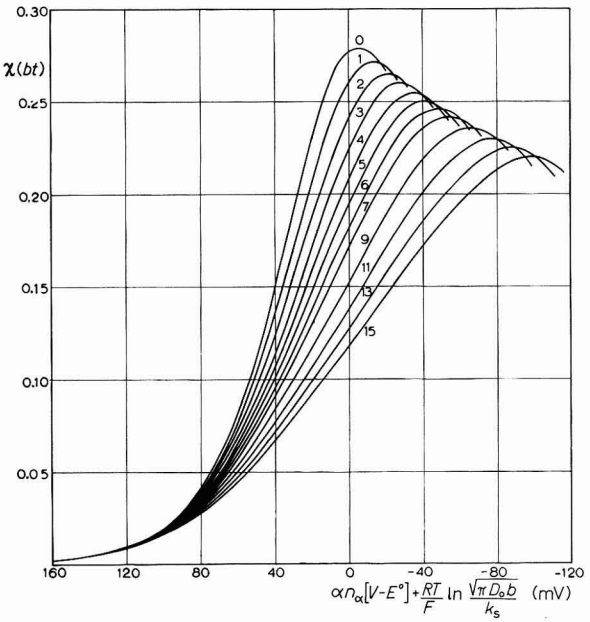

Fig. 1. Calcd. voltammetric curves for totally irreversible charge transfer in presence of uncompensated ohmic potential drop. Values reported on each curve refer to the parameter H. $T=25°$.

The calculated χ-functions for some values of H are plotted in Fig. 1. The following linear function of the applied cell voltage, V,

$$(RT/F)(u-bt)=\alpha n_\alpha[V-E^0]+(RT/F)\ln(\pi D_O b)^{\frac{1}{2}}/k_s \qquad (7)$$

has been used as independent variable, so that the calculated curves have the same shape of the experimental current/voltage curves. Furthermore, their position along the abscissa is independent of the initial potential.

In particular, for $R_u=0$ ($H=0$), the curve is identical with that obtained for the totally irreversible case without ohmic drop[10]. Only in this case does the applied voltage, V, coincide with the electrode potential, E. For other values of H, Fig. 1 shows that with increase in H, the curves become more drawn out and displaced towards more negative potentials.

The calculations were carried out for 25°; values for any other temperature, T (expressed in absolute degrees), can be obtained multiplying the abscissa by the factor $T/298.16$.

In Table 1 are reported the values of the abscissae corresponding, respectively, to half of the maxima $[\frac{1}{2} \max \chi(bt)]$ and to the maxima $[\max \chi(bt)]$ of the curves of Fig. 1 for various values of the parameter, H. The values of the abscissae corresponding to $\max \chi(bt)$ have been computed by quadratic interpolation between the three higher values of the computed χ_n sequence, while those corresponding to $\frac{1}{2} \max \chi(bt)$ have been computed by linear interpolation between the two consecutive values, χ_{k-1}, χ_k, for which $\chi_{k-1} \leqslant \frac{1}{2} \max \chi(bt) \leqslant \chi_k$.

TABLE 1

VALUES OF ABSCISSAE CORRESPONDING TO HALF OF THE MAXIMA [1/2 MAX χ (bt)] AND TO THE MAXIMA [MAX χ (bt)] OF THE CURVES PLOTTED IN FIG. 1

H	*Abscissa corresponding to* $\frac{1}{2}$ *max* $\chi(bt)$ (mV)	*Abscissa corresponding to max* $\chi(bt)$ (mV)	H	*Abscissa corresponding to* $\frac{1}{2}$ *max* $\chi(bt)$ (mV)	*Abscissa corresponding to max* $\chi(bt)$ (mV)
0	42.3	− 5.4	6	26.2	−48.6
1	39.4	−13.6	7	23.7	−54.8
2	36.6	−21.3	9	18.8	−66.8
3	33.9	−28.6	11	14.2	−78.1
4	31.3	−35.5	13	9.7	−89.0
5	28.7	−42.2	15	5.3	−99.5

The potential scale is $\alpha n_\alpha (V - E^0) + (RT/F) \ln \{(\pi D_O b)^{\frac{1}{2}}/k_s\}$

TABLE 2

DEPENDENCE OF PEAK CURRENT ON UNCOMPENSATED OHMIC POTENTIAL DROP AT THE PEAK

H	$\alpha n_\alpha i_p R_u =$ *max* $\chi(bt)(RT/F)H$ (mV)	$i_p/i_{p(R_u=0)}$	H	$\alpha n_\alpha i_p R_u =$ *max* $\chi(bt)(RT/F)H$ (mV)	$i_p/i_{p(R_u=0)}$
1	7.00	0.974	7	43.73	0.870
2	13.67	0.952	9	54.67	0.845
3	20.08	0.932	11	65.15	0.824
4	26.26	0.914	13	75.26	0.806
5	32.25	0.898	15	84.78	0.789
6	38.07	0.883			

Table 2 shows the decrease in the ratio between the peak current obtained experimentally, and that obtained without ohmic drop, as a function of the ohmic drop at the peak current.

EXPERIMENTAL CORRELATIONS

In order to present the data obtained in a convenient form for practical use, the data reported in Table 1 were used to derive diagrams allowing the determination

of electrochimical kinetic parameters from the characteristics of the experimental voltammetric curves. The difference between the values of the abscissae corresponding, respectively, to $\frac{1}{2}$ max $\chi(bt)$ and to max $\chi(bt)$, is reported as a function of H, in Fig. 2. This difference (see eqn. (7)) represents the product of αn_α and the experimental difference between the half-peak and peak voltages. When all the quantities that define the value of H (with exception of αn_α) and the experimental value of $[V_{p/2} - V_p]$ are known, the value of αn_α can be determined from such a diagram. In fact, αn_α must have such a value that the straight lines through the points $\alpha n_\alpha[V_{p/2} - V_p]$ and H (both corresponding to the particular value of αn_α) and parallel to the axes, meet at a point that lies on the curve shown in Fig. 2.

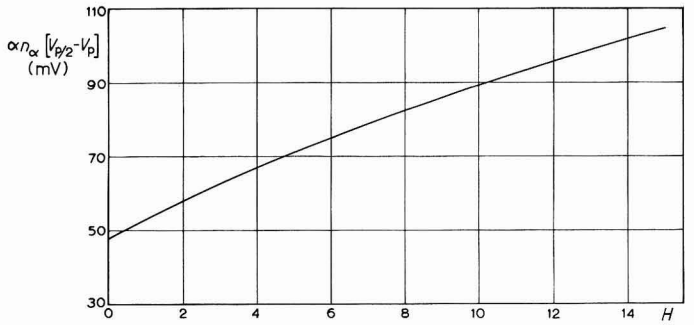

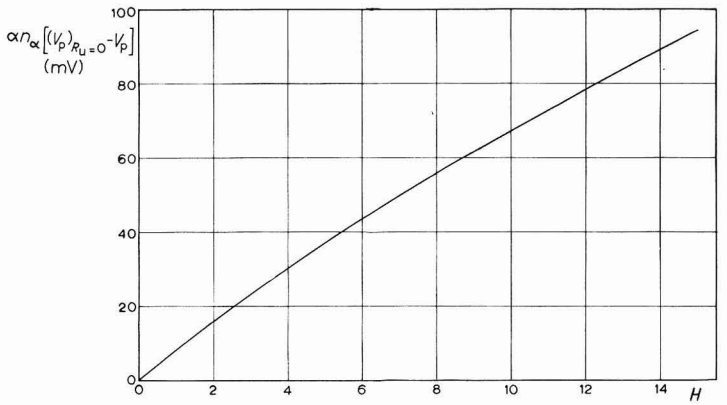

Figs. 2–3. Dependence of (Fig. 2) $\alpha n_\alpha[V_{p/2} - V_p]$ and (Fig. 3) $\alpha n_\alpha[(V_p)_{R_u=0} - V_p]$, on H. $T = 25°$.

The difference between the abscissa corresponding to max $\chi(bt)$ when $H = 0$ and those corresponding to max $\chi(bt)$ for various H-values, is reported as a function of H in Fig. 3. This difference represents the product of αn_α and the difference between the peak potential that would be obtained without ohmic drop and that obtained experimentally.

Thus, when the αn_α- and H-values are known, this diagram can be used to deduce the peak potential, $(V_p)_{R_u=0}$, that would be obtained in the absence of ohmic drop. With this $(V_p)_{R_u=0}$ value, it is possible to calculate the value of $k^0 = k_s \exp[(\alpha n_\alpha / RT) FE^0]$ by means of the following well known equation (eqn. (50) ref. 10)

$$(V_p)_{R_u=0} = \frac{RT}{\alpha n_\alpha F}\left\{-0.78+\ln\frac{k^0}{D_O^{\frac{1}{2}}}-\tfrac{1}{2}\ln\frac{\alpha n_\alpha F v}{RT}\right\} \quad (8)$$

In order to verify the theory presented, experiments have been carried out on a system of known electrochemical kinetic parameters. The system chosen was $1\cdot10^{-3}$ M $NaBrO_3$ in 1 M (NaCl + 1% NaOH) because the corresponding electrode process at a mercury electrode is totally irreversible[9].

CHEMICALS AND APPARATUS

All substances used were reagent-grade chemicals. Solutions were prepared and de-aerated as previously reported[13]. All measurements were performed at 25 ± 0.1°. A SCE was used as a reference electrode and all potentials are referred to it. The hanging mercury drop electrode used was of the type described by Vogel[14]. The electrode area was $3.48\cdot10^{-2}$ cm^2. Potential sweep voltammetric curves were recorded by means of a Model 448 two-electrode instrument (AMEL, Milan).

The cell resistance, measured by means of a Wiss. Techn. Werksstolten conductometer, was 140 Ω.

The bromate diffusion coefficient deduced from the polarographic limiting current, using Ilkovič's equation, was $1.66\cdot10^{-5}$ cm^2 sec^{-1}.

RESULTS AND DISCUSSION

The experimental values of half-peak and peak voltages deduced from voltammetric curves are reported, at various sweep rates, in Table 3.

TABLE 3

HALF-PEAK AND PEAK VOLTAGES AT VARIOUS SWEEP RATES FOR THE TOTALLY IRREVERSIBLE REDUCTION OF BROMATE ION IN 1 M (NaCl + 1% NaOH)

v (V/sec)	$V_{p/2}$ (V)	V_p (V)	v (V/sec)	$V_{p/2}$ (V)	V_p (V)
0.35	−1.699	−1.793	2.62	−1.739	−1.852
0.65	−1.713	−1.814	3.44	−1.758	−1.873
1.10	−1.732	−1.836	5.00	−1.762	−1.884
1.62	−1.739	−1.844	6.00	−1.763	−1.886
1.93	−1.746	−1.855			

Half-peak and peak voltages are referred to satd. calomel electrode.

The αn_α-values, deduced from experimental differences between the half-peak and peak voltages using the well known equation (eqn. (52), ref. 10),

$$\alpha n_\alpha = 0.048/(E_{p/2}-E_p) \qquad \text{(at 25°)} \quad (9)$$

are reported, at various sweep rates, in Fig. 4. Open circles refer to the experimental differences between half-peak and peak voltages as measured on the voltammetric curves, while crosses refer to differences corrected for the ohmic drop in the usual way, *i.e.*, adding to the half-peak and peak voltages the product of the cell resistance and the relative current.

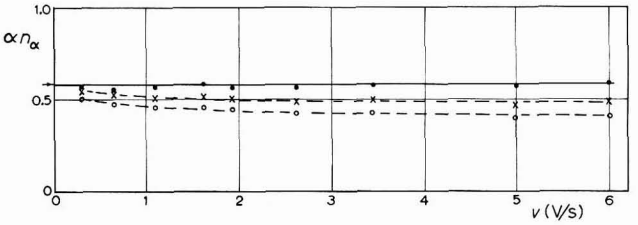

Fig. 4. Dependence of αn_α on potential sweep rate for the reduction of bromate ion ($1 \cdot 10^{-3}$ M) in 1 M (NaCl + 1% NaOH) soln. (●), Values obtained by means of the present theory; (×), (○), αn_α-values deduced by means of eqn. (9), corrected (×) and uncorrected (○) for the ohmic potential drop in the usual way. The arrow indicates the αn_α-value reported in ref. 9.

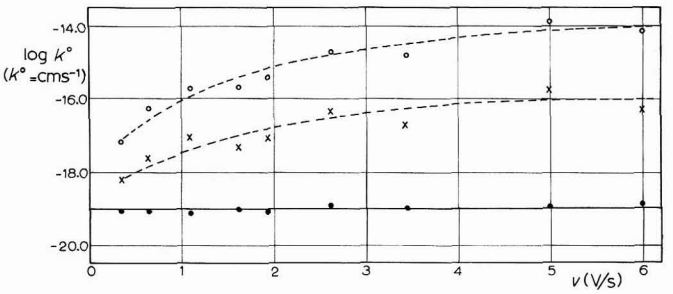

Fig. 5. Dependence of log k^0 on the potential sweep rate; exptl. conditions as in Fig. 4. (●), values obtained by means of the present theory; (×), (○), values deduced by means of eqn. (8), uncorrected (○) and corrected (×) for the ohmic potential drop in the usual way.

The αn_α-values obtained making use of the diagram of Fig. 2 are reported (full circles) in the same Figure.

It can be seen that the αn_α-values deduced from eqn. (9), even when corrected for the ohmic drop decrease with increasing potential sweep rate and are always lower than those reported in the literature[9]. This shows that the uncompensated ohmic drop causes both a shift of the voltammetric curve along the potential axis and a distortion of the potential sweep linearity. The values deduced through the theory reported here are, however, practically constant, and the average value of αn_α is equal, within the limits of experimental error, to the value obtained by Gierst[9].

Successively, the k^0-values were calculated from eqn. (8) using the previously obtained average value of αn_α and the peak voltage values corrected using the diagram of Fig. 3. The log k^0-values are reported, at various sweep rates, in Fig. 5 (full circles).

The log k^0-values obtained by introducing into eqn. (8) αn_α-values and peak voltages relative to each sweep rate without any ohmic drop correction (open circles), and those with the usual correction (iR) (crosses) are reported in the same Figure, for comparison purposes.

It can be seen that the log k^0-values obtained by means of this theory are practically constant within the limits of experimental error, whereas the others although corrected for ohmic drop, show a strong dependence on the potential sweep rate.

The average αn_α- and k^0-values obtained from the present theory were used for

the straight line plot of the dependence of log k on potential, E (eqn. (39), ref. 10)

$$\log k = \log k^0 - (\alpha n_\alpha F/RT)E$$

which, together with a dashed-line representing the data of ref. 9, is shown in Fig. 6.

The agreement between the data obtained from potential sweep voltammetry using the theoretical treatment presented in this paper, and those obtained by Gierst[9] from d.c. polarography is completely satisfactory.

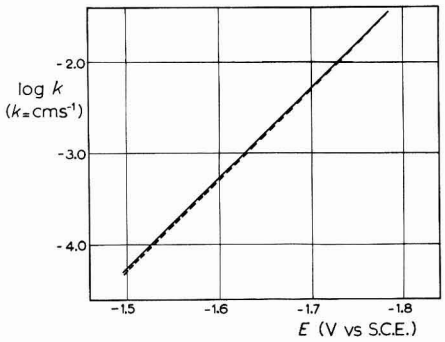

Fig. 6. Dependence of log k on electrode potential. (———), Straight line drawn according to αn_α- and k^0-values obtained by potential sweep voltammetry; (– – – –), straight line obtained by d.c. polarography (see ref. 9).

ACKNOWLEDGEMENT

The authors are indebted to Prof. E. Vianello for valuable suggestions and stimulating discussions. The numerical calculations were carried out at the computing Centre of CNEN, Bologna. The assistance of Prof. G. Casadei and Mr. V. Fedele is gratefully acknowledged.

SUMMARY

Potential sweep voltammetric curves for a totally irreversible electrode process with uncompensated ohmic drop, when mass transfer takes place by semi-infinite linear diffusion, have been calculated. These curves have been used to derive operational diagrams that allow the evaluation of the electrochemical kinetic parameters.

Experimental data obtained for the totally irreversible reduction of bromate ion at a mercury electrode have been examined in terms of the theory. The electrochemical kinetic parameters thus derived are in very good agreement with those reported in the literature.

REFERENCES

1 P. DELAHAY, *New Instrumental Methods in Electrochemistry*, Interscience Publishers New York, 1954, p. 132.

2 R. S. NICHOLSON, *Anal. Chem.*, 37 (1965) 667.
3 W. T. DE VRIES AND E. VAN DALEN, *J. Electroanal. Chem.*, 10 (1965) 183.
4 W. H. REINMUTH, *Anal. Chem.*, 34 (1962) 1446.
5 W. T. DE VRIES AND E. VAN DALEN, *J. Electroanal. Chem.*, 12 (1966) 9; 14 (1967) 315.
6 W. T. DE VRIES, *J. Electroanal. Chem.*, 17 (1968) 31; 19 (1968) 41, 55.
7 M. L. OLMSTEAD AND R. S. NICHOLSON, *J. Phys. Chem.*, 72 (1968) 1650.
8 S. ROFFIA, *Ric. Sci.*, 38 (1968) 1257.
9 L. GIERST, *Transaction of the Symposium on Electrode Processes*, edited by E. YEAGER, J. Wiley and Sons, New York, 1961, p. 109.
10 R. S. NICHOLSON AND I. SHAIN, *Anal. Chem.*, 36 (1964) 706.
11 A. HUBER, *Monatsh. Mathemat. Phys.*, 47 (1939) 240.
12 W. T. DE VRIES, *J. Electroanal. Chem.*, 9 (1965) 448.
13 S. ROFFIA AND E. VIANELLO, *J. Electroanal. Chem.*, 15 (1967) 405.
14 J. VOGEL, *J. Electroanal. Chem.*, 8 (1964) 82.

ELECTROANALYTICAL CHEMISTRY AND INTERFACIAL ELECTROCHEMISTRY
Elsevier Sequoia S.A., Lausanne – Printed in The Netherlands

VOLTAMÉTRIE À TENSION LINÉAIREMENT VARIABLE EN COUCHE MINCE RIGIDE

III. L'EFFET DE LA DIFFUSION DE L'HYDROGÈNE EN PALLADIUM SUR LA CINÉTIQUE DE LA RÉACTION D'OXYDATION ANODIQUE DES ÉLECTRODES MINCES (Pd–H)

R. V. BUCUR
Institut de Physique Atomique, Cluj, (Roumanie)
(Reçu le 10 décembre, 1968)

1. INTRODUCTION

La réaction globale d'oxydation à tension linéairement variable d'une électrode mince (Pd–H) se déroule d'après un mécanisme complexe, dans lequel le poids des processus partiaux est déterminé par les conditions expérimentales[1-4]. Dans les parties I et II de ce travail on a précisé ces conditions et leur influence sur le mécanisme de la réaction globale d'électrode. Il a été possible de délimiter deux domaines différents, selon la valabilité de la relation, $I_p \sim C_1^{0n}$: le domaine de diffusion, $(n=1)$, où la cinétique de la réaction globale est contrôlée par la diffusion de l'hydrogène en Pd, et le domaine mixte, $(n \neq 1)$, dans lequel la cinétique de la réaction globale est contrôlée par l'effet combiné de la diffusin de l'hydrogène en Pd et le transport par diffusion convective et migration, en solution[1,4].

Dans ce travail-ci nous nous sommes proposés de vérifier si les conditions expérimentales pour lesquelles $n=1$ sont suffisantes pour assurer un contrôle effectif de la cinétique de cette réaction basé sur la diffusion, et d'établir—d'une manière plus complète—l'effet des paramètres expérimentaux caractéristiques à l'oxydation anodique par voltamétrie à tension linéairement variable: vitesse de balayage du potentiel, v, l'épaisseur de l'électrode mince, l, la concentration de l'hydrogène dans l'électrode, C_1^0, et la température.

2. MÉTHODE DE TRAVAIL ET CONDITIONS EXPÉRIMENTALES

On a employé des solutions H_2SO_4 et H_3PO_4 (pH = 2.76 à 25°). La technique de travail a été décrite dans la partie II de ce travail. Les électrodes couches minces ont été préparées par dépôt électrolytique dans une solution à phosphates[5], sur un disque de platine dont la surface géométrique totale, $S=1.36$ cm^2. L'épaisseur des films de Pd a été calculée à partir de la pesanteur du dépôt.

Du point de vue expérimental la vérification de l'effet de la diffusion sur la cinétique de la réaction globale d'oxydation dans les conditions de la voltamétrie à tension linéairement variable des électrodes minces (Pd–H) impose, tout d'abord, de réaliser les conditions du contrôle exclusif par diffusion, c'est-à-dire de réduire l'influence des autres processus partiaux.

Si on écrit l'expression de la résistance équivalente globale, R_g, correspondante à la réaction globale d'oxydation, conformément au mécanisme présenté dans la partie II[4,8], nous avons:

$$R_g = R_d + R_t + R_\delta + R_s \tag{1}$$

où on a noté:

R_d = la résistance équivalente à la diffusion de l'hydrogène en Pd,
R_t = la résistance équivalente au transfert de l'hydrogène à travers l'interface,
R_s = la résistance de la solution électrolytique,
$R_\delta = R_m \cdot R_{dc}/(R_m + R_{dc})$—la résistance équivalente au transfert de substance à travers la couche de transfert de substance d'épaisseur δ,
R_{dc} = la résistance équivalente à la diffusion convective dans la couche δ,
R_m = la résistance équivalente à la migration dans la couche δ.

La diffusion de l'hydrogène en Pd devient prépondérante dans la réaction globale d'électrode si la condition:

$$R_d \gg \Sigma R_j \qquad (j = t, \delta) \tag{2}$$

est satisfaite.

Pratiquement cette condition est accomplie si:

(a). Le courant de maximum voltamétrique, I_p, ne dépasse pas la valeur du courant limite de migration[4]. De cette manière l'entier flux de protons à travers l'interface peut être pris; dans la solution, par la migration, il n'y a pas de modifications de concentration autour de l'électrode et, par conséquent, la couche de transfert de substance n'apparaît plus, $\delta = 0$. Dans ces conditions, $R_\delta = 0$[2-4]. Ayant en vue que $I_p \sim C_1^{0n}$, on peut réaliser aisément $\delta = 0$ en travaillant avec des petites concentrations, C_1^0, d'hydrogène en Pd.

L'utilisation des petites concentrations d'hydrogène en Pd a aussi un effet direct sur la résistance équivalente de diffusion, R_d; en augmentant sa valeur[6], on augmente encore d'avantage le poids de la diffusion dans la réaction globale d'électrode.

(b). On réduit l'effet de la résistance équivalente de transfert au moyen d'une activation convenable de la surface de l'électrode, par dépôt de noir de Pd. Pour réduire l'effet de barrière de la couche de noir de Pd[7,8], on n'en a déposé que 3 mg cm^{-2}, provenant d'une solution $PdCl_2$ 2% en HCl 1 *M*. Le courant de déposition était 3 mA. On a constaté que des dépôts plus épais que ceux correspondants à 3 mg cm^{-2} conduisent à une plus grande[8] résistance équivalente de transfert.

3. RÉSULTATS ET DISCUSSIONS

Dans la première partie de ce travail[1] on a montré qu'il est impossible de résoudre analytiquement l'équation de diffusion, dans les conditions imposées par la voltamétrie à tension linéairement variable pour l'oxydation quasi-réversible $\{[I(t)/nFSk_sC_1^{0(1-\alpha)}C_2^{0(\alpha)}] \approx 1\}$ de l'hydrogène dissous dans une électrode mince de Pd. C'est pourquoi, on a en recouru à "l'expérimentation" du processus d'électrode sur un calculateur analogique électronique.

A cause de la variation caractéristique du courant, $I(t)$, pendant le balayage du potentiel, le rapport cité ci-dessus varie dans de larges limites, ayant des valeurs beaucoup plus petites que l'unité au commencement et à la fin du processus. Pour le

courant de maximum ce rapport prend des valeurs voisines de l'unité; cependant, la valeur I_p reste pratiquement indépendante des constantes cinétiques, k_s et α[1]. C'est pourquoi, dans le domaine choisi pour l'expérimentation sur le modèle analogique, on peut constater que le processus d'électrode se déroule réversiblement. Ce fait permet d'aborder l'étude du mécanisme de la réaction globale d'électrode selon une cinétique réversible, ce qui rend possible la résolution analytique de l'équation de diffusion et donc, le calcul de la courbe courant–temps, $I(t)$.

Dans ces conditions, l'équation de la courbe $I(t)$ obtenue pour la réaction d'oxydation contrôlée par la diffusion de l'hydrogène en Pd, peut être écrite sous la forme

$$I(t) = 2\frac{nFSDC_1^0}{l}\beta\sum_{m=0}^{\infty}\frac{\exp(-\beta t)-\exp\{-[\frac{1}{2}(2m+1)\pi]^2 wt\}}{[\frac{1}{2}(2m+1)\pi]^2 w-\beta} \tag{3}$$

où

n —nombre d'électrons qui participent dans la réaction d'électrode,
F —constante de Faraday,
S —l'aire de l'électrode,
C_1^0—concentration de l'hydrogène en Pd,
D —coefficient de diffusion de l'hydrogène en Pd,
l —l'épaisseur de l'électrode mince de Pd,
v —vitesse de balayage du potentiel,
R —constante des gaz,
T —température absolue, et

$$\beta = (nF/RT)v \qquad w = D/l^2 \tag{4}$$

La relation (3) est déduite à partir de la solution de l'équation différentielle pour le problème analogue à la diffusion de la chaleur, obtenue par la méthode de Fourier[9], en effectuant les substitutions correspondantes. Cette relation présente une bonne convergence pour des grandes valeurs de t—comparables aux valeurs expérimentales—ce qui rend avantageuse son utilisation dans la vérification expérimentale.

Dans le domaine de convergence rapide et pour la condition

$$\beta \neq w[\tfrac{1}{2}(2m+1)\pi]^2 \qquad (m=0, 1, 2, \ldots,) \tag{5}$$

la relation (3) peut être simplifiée, en retenant seulement le premier terme de la série. On obtient alors (à une approximation suffisante) la relation

$$I(t) \approx (nFSDC_1^0/l)\left(\sqrt{\beta_0}\,\mathrm{tg}\,\sqrt{\beta_0}\cdot e^{-\beta t} - \frac{2\exp(-\frac{1}{4}\pi^2 wt)}{(\pi^2/4\beta_0)-1}\right) \tag{6}$$

où

$$\beta_0 = (nF/RT)(vl^2/D) \tag{6'}$$

De la relation (6) on peut calculer, d'une manière simple, la valeur du courant de maximum voltamétrique, I_p, en obtenant

$$I_p = 2(nFSDC_1^0/l)\,P(\beta_0) \tag{7}$$

où on a noté $P(\beta_0)$ la fonction independante de C_1^0

$$P(\beta_0) = \left[\tfrac{1}{2} \left(1 - \frac{4}{\pi^2} \beta_0 \right) \sqrt{\beta_0} \operatorname{tg} \sqrt{\beta_0} \right]^{\{1-(4/\pi^2)\beta_0\}^{-1}} \tag{8}$$

La relation (7) est valable seulement si deux conditions expérimentales sont satisfaites : $t > t_{min}$ et $\beta_0 < (\pi^2/4)$. La valeur t_{min} résulte du fait qu'on a négligé les termes correspondants à $m > 1$ dans la relation (3) et sa valeur numérique dépend de la valeur maximale admise pour l'erreur relative qui résulte pour la série en négligeant ces termes.

Cette relation est identique à celle obtenue par Schmidt et Gygax pour la voltamétrie à tension linéairement variable dans de petits volumes de solution[10]. On constate qu'en dépit de la différence qualitative entre la nature des processus pour aborder à l'électrode (diffusion de l'hydrogène en Pd, et diffusion des ions en solution) on obtient des résultats identiques.

La relation (7) est en état d'exprimer qualitativement la dépendance du courant maximal, I_p, en fonction des paramètres expérimentaux caractéristiques et elle peut être employée dans l'étude de la cinétique de la réaction d'oxydation des électrodes minces (Pd–H) à contrôle exclusif par diffusion. Mais, à cause des simplifications introduites pendant sa déduction, la relation (7) ne permet pas d'obtenir des résultats numériques rigoureux ; elle peut être pourtant employée pour faire des comparaisons qualitatives parce que les approximations faites n'altèrent pas la qualité de cette relation.

3.1. *La dépendance du courant de maximum, I_p, en fonction de l'épaisseur de l'électrode, l, et de la vitesse de balayage, v*

La dépendance du courant de maximum, I_p, de l'épaisseur de l'électrode, l, et de la vitesse de balayage du potentiel, v, peut être exprimée à l'aide du paramètre nondimensionel, β_0, défini par la relation (6′).

Selon la grandeur de ce paramètre, on peut définir deux domaines de variation :

(a). $\beta_0 > (\pi^2/4)$ respectivement $vl^2/D > 6.4 \cdot 10^{-4}$ où le courant de maximum est donné par la relation (7) et la dépendance, I_p *vs.* β_0, est caractéristique au contrôle exclusif de diffusion.

(b). $\beta_0 < (\pi^2/4)$ respectivement $vl^2/D < 6.4 \cdot 10^{-4}$ où le courant de maximum est donné par la relation simplifiée[11]

$$I_{p\lim} = (n^2 F^2 C_1^0 Slv/RT) \tag{9}$$

Le courant de maximum limite, $I_{p\lim}$ est indépendant du coefficient de diffusion de l'hydrogène en Pd.

La relation (9) ressemble à la relation déduite par Hubbard et Anson, pour une réaction d'oxydation réversible en couche mince de solution sans contrôle de diffusion ; elle diffère de leur relation par un facteur 4 au dénominateur[12]. Elle est en concordance, également, avec la relation empirique de de Vries et van Dalen pour des films d'amalgame, en ce qui concerne la dépendance du courant de maximum en fonction des paramètres expérimentaux[13].

Le courant $I_{p\lim}$ représente la plus grande valeur qui peut être obtenue pendant l'oxydation d'une quantité constante de substance ($C_1^0 Sl = \text{const.}$) dissoute dans un film mince (Pd, Hg ou solution).

La dépendance, I_p *vs.* l, pour trois valeurs différentes de la vitesse de balayage,

v, conformément à la relation (7) est portée dans la Fig. 1a. Les calculs ont été effectués en utilisant les valeurs numériques suivantes pour les constantes qui interviennent dans la relation (7):

$n = 1$
$F = 9.65 \cdot 10^4$ C mole^{-1}
$D = 2.48 \cdot 10^{-7}$ cm^2 sec^{-1} [14]
$T = 298.2°$K
$R = 8.315$ J grad^{-1} mole^{-1}

Dans la Figure on a représenté la grandeur $P(\beta_0)/l^2$ proportionnelle à I_p, pour une quantité constante d'hydrogène en Pd.

La variation, I_p *vs.* l, est pareille à celle donnée par de Vries[15] pour une électrode couche mince d'amalgame de Cd: avec la diminution de l'épaisseur, le courant de maximum croît vers la valeur limite pour laquelle la réaction globale se déroule rapidement, sans contrôle de diffusion. Au fur et à mesure que la vitesse de balayage

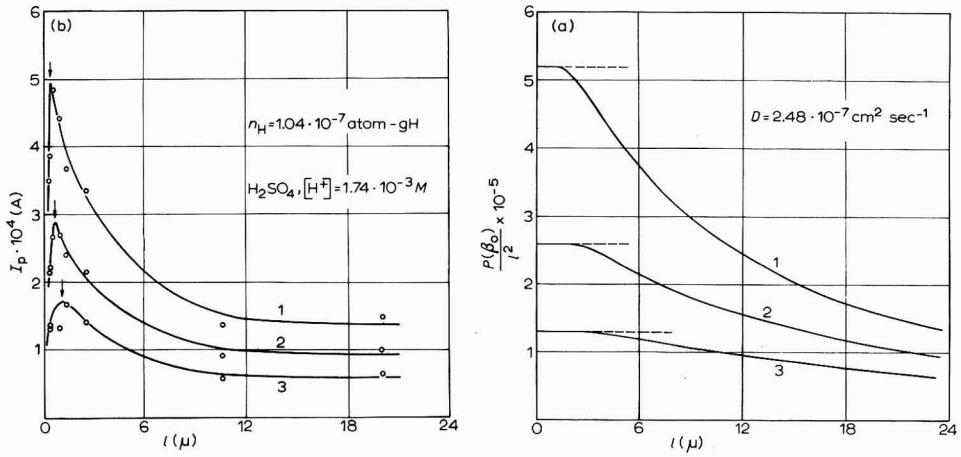

Fig. 1. L'effet de l'épaisseur, l, de la couche de Pd sur le courant de maximum, I_p: (a), calculé selon la relation (7); (b), déterminé expérimentalement. v: (1), 0.4; (2), 0.2; (3), 0.1 V min^{-1}; H_2SO_4, 25°.

décroît, $I_{p\,lim}$ diminue, mais la valeur de l'épaisseur à partir de laquelle l'effet de freinage de diffusion cesse, s'agrandit.

Dans la Fig. 1b on a représenté les résultats expérimentaux pour des électrodes minces (Pd–H) d'épaisseur variable, obtenus en solution H_2SO_4 à 25°. On y remarque que l'allure générale des courbes, I_p *vs.* l, ressemble à celle des courbes calculées, à l'exception du domaine des petites valeurs, ($l \leqslant 1\mu$), où le courant de maximum décroît brusquement. La limite où cette diminution apparaît, déduite de la Figure, est donnée par l'inégalité, $l^2 v \leqslant 1.66 \cdot 10^{-11}$ V cm^2 sec^{-1}.

Comme on a déjà précisé, on ne doit pas attendre une concordance quantitative entre les données expérimentales et celles calculées, à cause des erreurs qui proviennent des approximations de calcul. Mais, en aucun cas, ces erreurs ne peuvent être la cause de la discordance qualitative chez les couches minces. Le changement du sens de variation de I_p peut être mis, plutôt, sur le compte d'une modification du mécanisme de transport de l'hydrogène en Pd. Il paraît que, chez les électrodes très minces, des

interactions puissantes apparaissent entre l'hydrogène dissous et le réseau du Pd, ce qui peut mener à l'apparition d'un freinage puissant dans le développement de la réaction globale d'électrode.

Un effet pareil a été remarqué, également, dans la variation de l'exposant, α, avec l'épaisseur, l; l'exposant, α, est défini par la relation, $I_p \sim v^{\alpha}$. Les résultats calculés (courbe a) et déterminés expérimentalement (courbe b) sont montrés dans la Fig. 2. Les valeurs α ont été calculées de la pente des droites log $[P(\beta_0)/l^2]$ *vs.* log v pour différentes valeurs de l prises de la Fig. 1a. Les valeurs expérimentales ont été calculées d'une représentation log I_p *vs.* log v pour $v=0.1$, 0.2, et 0.4 V min^{-1} à partir des droites expérimentales $I_p \sim$ const. C_1^0, pour une valeur donnée, C_1^0.

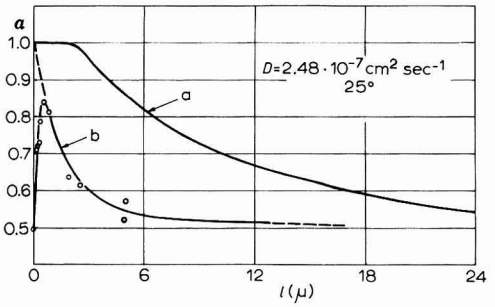

Fig. 2. L'effet de l'épaisseur, l, de la couche de Pd sur l'exposant, α ($I_p \sim v^{\alpha}$): (a), calculé; (b), déterminé expérimentalement; H_2SO_4, 25°.

Les différences entre les valeurs calculées et celles expérimentales y sont plus accentuées, mais l'aspect général de la courbe reste le même: l'exposant α varie entre 1 et 0.5 mais chez les couches très minces il s'écarte brusquement de la manière de variation théorique.

3.2. *Dépendance du courant de maximum, I_p, en fonction de la température*

Dans les conditions expérimentales d'un contrôle exclusif de diffusion dans la réaction globale d'oxydation des électrodes minces (Pd–H), on pourrait déterminer l'énergie d'activation du processus lent, à partir de la variation du courant de maximum avec la température.

En groupant les termes qui dépendent de la température, la relation (7) peut être écrite

$$I_p = knFSC_1^0 \tag{10}$$

où le coefficient de transfert de substance, k, est donné par

$$k=2(DP(\beta_0)/l) \text{ cm sec}^{-1} \tag{11}$$

Le coefficient de transfert de substance est le produit de deux fonctions de température, qui varient de façon opposée avec la température (Fig. 3): la droite (1) représente le coefficient de diffusion calculé selon l'expression donnée par Simons et Flanagan, $D=6.1\cdot10^{-3}$ (exp $(-5990/RT)$[14] et la droite (2), la fonction $P(\beta_0)$ calculée avec la relation (8), et elle a l'expression log $P(\beta_0) = -3.239+852/T$.

Si on écrit les équations de ces deux droites dans une forme générale

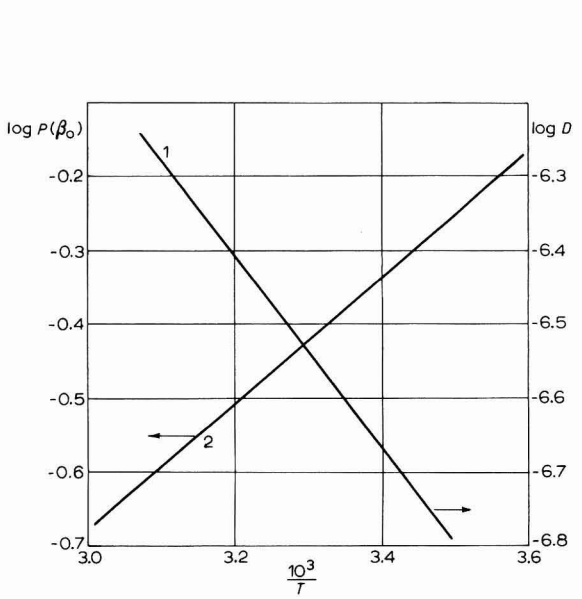

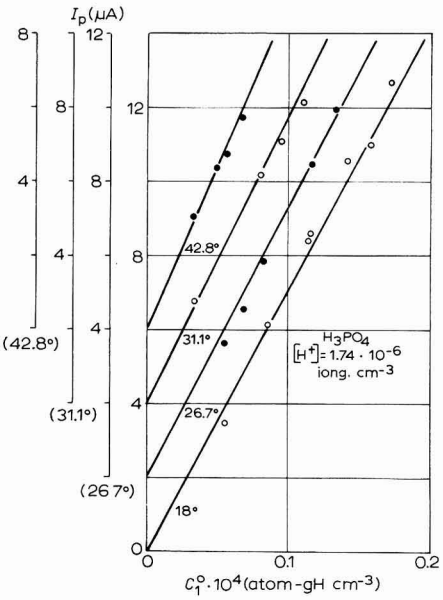

Fig. 3. La dépendance du coefficient de diffusion de l'hydrogène en Pd (1)[14], et de la fonction $P(\beta_0)$ (2), calculée à l'aide de la relation (8), en fonction de la temp.

Fig. 4. La dépendance du courant de maximum, I_p, en fonction de la concn. de l'hydrogène en Pd, C_1^0, dans le domaine du contrôle de diffusion H_3PO_4.

$$\ln D = \ln D_0 - E/RT \tag{12}$$

et

$$\ln P(\beta_0) = \ln P_0 + A/RT \tag{13}$$

où D_0, P_0 et A sont des constantes indépendantes de la température et de E, l'énergie d'activation effective de la diffusion de l'hydrogène en Pd ; si on calcule, à leur aide, la dépendance, log k *vs.* T^{-1}, on obtient

$$\ln k = \ln D_0 P_0 - (E - A)/RT \tag{14}$$

Tenant compte de ce que la constante A est positive, il résulte que l'énergie d'activation calculée à partir du coefficient de transfert de substance devrait être plus petite que l'énergie d'activation effective de diffusion. Notons cette différence, E_a. Elle représente l'énergie d'activation apparente, $E_a = E - A$.

En utilisant les données présentées dans la Fig. 4, on a calculé conformément à l'éqn. (10) le coefficient de transfert de substance pour $C_1^0 = 5.18 \cdot 10^{-6}$ atom g H cm^{-3}, à quatre différentes valeurs de température. Les résultats sont présentés dans le Tableau 1.

TABLEAU 1

°C	$k \cdot 10^5$ ($cm\ sec^{-1}$)	°C	$k \cdot 10^5$ ($cm\ sec^{-1}$)
18	7.32	31.1	8.20
26.7	7.80	42.8	9.20

La fonction, $\log k$ *vs.* T^{-1}, déterminée expérimentalement et calculée théoriquement à l'aide de la relation (14) est présentée dans la Fig. 5.

Les équations des droites sont:

$$\log k_{calc} = -2.454 - 457/T \tag{15}$$

pour la droite calculée et

$$\log k_{exp} = -2.688 - 430/T \tag{16}$$

pour la droite expérimentale. On obtient de la pente de ces droites les énergies apparentes d'activation

$$E_a^{calc} = 2.09 \text{ kcal mole}^{-1} \tag{17}$$

$$E_a^{exp} = 1.97 \text{ kcal mole}^{-1} \tag{18}$$

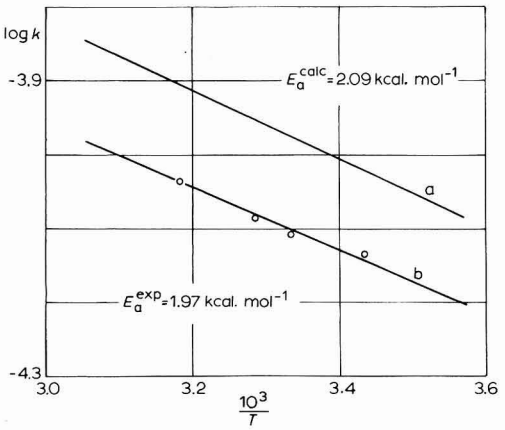

Fig. 5. La fonction, $\log k$ *vs.* T^{-1}, calculée (a), à l'aide de la relation (14); (b), déterminée expérimentalement en solution H_3PO_4.

L'énergie d'activation effective déterminée expérimentalement est alors (la constante $A = 3900$)

$$E^{exp} = 5.87 \text{ kcal mole}^{-1} \tag{19}$$

en bonne concordance avec celle déterminée dans des évaluations directes par diffusion, $E = 5.99$ kcal mole^{-1}.

La bonne concordance entre les valeurs de l'énergie d'activation déterminée dans des expériences voltamétriques et celles obtenues en mesurant directement de diffusion est un indice clair et certain du fait que, dans ces conditions expérimentales, la diffusion est le seul processus déterminant de la vitesse.

Si la valeur de l'énergie effective d'activation est indépendante de la concentration de l'hydrogène en Pd, la valeur de l'énergie apparente en dépend sensiblement. Il en est bien ainsi, car, si la concentration C_1^0 croît, le mécanisme de la réaction globale d'électrode devient plus compliqué, les autres processus partiels entrant en jeu: la réaction de transfert de charges et le transfert de substance à travers la couche limite de transfert de substance. Au delà de toute prévision, l'apparition des autres

processus partiels ne conduit pas à l'augmentation de l'énergie apparente d'activation, parce que, avec l'augmentation de la concentration, le poids de la diffusion d'hydrogène en Pd decroît puissamment[6], et les autres processus partiels ont des énergies d'activations plus petites.

Les résultats de deux séries de déterminations de l'énergie apparente d'activation en H_2SO_4 et H_3PO_4, pour des différentes concentrations, C_1^0, sont présentés dans la Fig. 6: (a) H_2SO_4 et (b) H_3PO_4. On y constate qu'au fur et à mesure que la concentration croît, la pente des droites, log I_p *vs.* T^{-1}, décroît, en indiquant une diminution de l'énergie apparente d'activation.

Les valeurs plus petites de l'énergie apparente d'activation déterminées aux grandes concentrations, indiquent que les processus déterminants de vitesse deviennent les processus hydrodynamiques autour de l'électrode, probablement la convection libre dont l'énergie d'activation doit être du même ordre que l'énergie d'activation

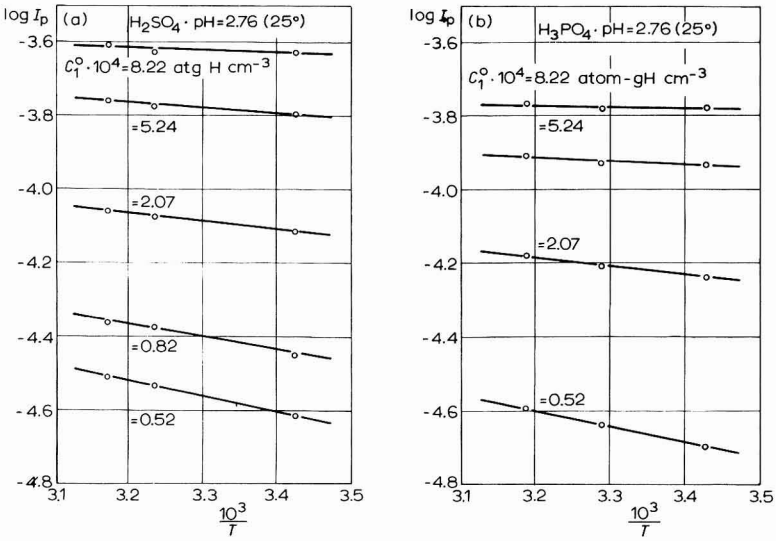

Fig. 6. La variation log I_p *vs.* T^{-1} avec la concn. de l'hydrogène en Pd, C_1^0, en solution: (a), H_2SO_4; (b), H_3PO_4.

de l'écoulement visqueux[16]. Cette supposition est confirmée par le fait que l'amoindrissement de l'énergie apparente d'activation dépend de la nature de la solution, comme on peut voir dans la Fig. 7.

D'autre part, la valeur limite de l'énergie apparente d'activation pour $C_1^0 \rightarrow 0$ est indépendante de la nature de la solution, comme c'était à prévoir, et, pratiquement, égale à celle déterminée directement pour le contrôle exclusif de la diffusion. Les valeurs sont données dans le Tableau 2.

La moyenne des valeurs déterminées expérimentalement, $E_a = 2.04$ kcal mole^{-1}, conduit à une énergie d'activation effective pour la diffusion, $E = 5.94$ kcal mole^{-1}.

4. CONCLUSIONS

(a). Le transport de l'hydrogène en Pd dans les conditions de l'oxydation anodi-

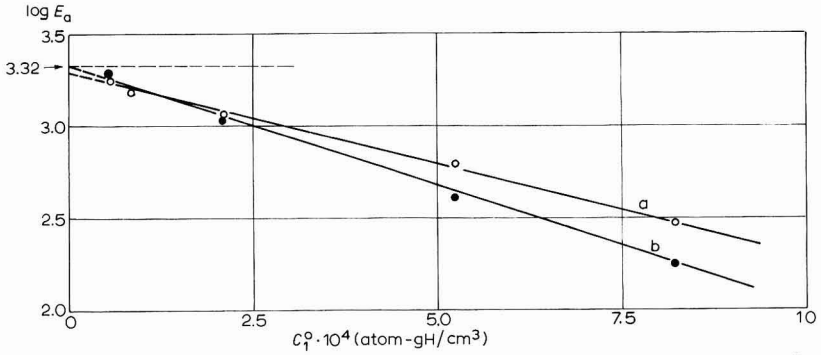

Fig. 7. La dépendance de l'énergie apparente d'activation, E_a, en fonction de la concn., C_1^0, de l'hydrogène en Pd, en: (a), H_2SO_4; (b), H_3PO_4.

TABLEAU 2

E_a (*kcal mole*$^{-1}$)	*La manière d'obtention*
2.09	calcul
1.97	expérimentalement, de k
1.95	expérimentalement, $C_1^0 \rightarrow 0$, H_2SO_4
2.14	expérimentalement, $C_1^0 \rightarrow 0$, H_3PO_4

que à tension linéairement variable peut être abordé analytiquement, selon une cinétique d'électrode réversible.

(b). Jusqu'à l'épaisseur $l \cong 1\mu$ la dépendance du courant de maximum I_p, soit calculée soit déterminée expérimentalement, en fonction de l'épaisseur de l'électrode, l, et de la vitesse de balayage, v, suit qualitativement la même allure. Pour $l < 1\mu$, la valeur I_p s'écarte brusquement du comportement prévu théoriquement, probablement à cause de la modification de la nature du processus de transport de l'hydrogène en Pd.

(c). La dépendance, I_p *vs.* C_1^0, est linéaire dans le domaine des petites concentrations d'hydrogène en Pd et à différentes températures. Selon la variation avec la température des pentes de ces droites, on peut déterminer l'énergie d'activation apparente, E_a, de la diffusion de l'hydrogène en Pd. La valeur déterminée expérimentalement, $E_a^{exp} = 2.04$ kcal mole^{-1}, est en bon accord avec la valeur calculée sur la base de la cinétique réversible d'électrode, $E_a^{calc} = 2.09$ kcal mole^{-1}.

L'énergie effective d'activation, E, calculée est $E = 5.94$ kcal mole^{-1} en bonne concordance avec les données de la littérature.

(d). L'énergie apparente d'activation décroît avec l'augmentation de la concentration, C_1^0, de l'hydrogène en Pd, parce que, si la concentration C_1^0 croît, l'effet de freinage de la diffusion décroît puissamment et l'effet de freinage de l'écoulement visqueux croît, lié à la convection libre autour de l'électrode. Dans ces conditions E_a dépend de la nature de la solution.

(e). Dans la relation, $I_p \sim C_1^{0n}$, $n = 1$ est une condition nécessaire et suffisante pour assurer un contrôle exclusif de diffusion dans la réaction globale d'oxydation de l'hydrogène dissous dans une électrode mince de Pd.

REMERCIEMENTS

Je tiens à remercier M. Covaci I. de sa contribution à la partie mathématique de ce travail.

RÉSUMÉ

À l'aide des résultats obtenus à l'expérimentation sur le modèle électronique analogique, on étudie la diffusion de l'hydrogène dans une couche mince de Pd, dans les conditions de la voltamétrie à tension linéairement variable, selon une cinétique d'électrode réversible. On en fait la vérification expérimentale, en utilisant la valeur du courant de maximum $I_p = 2\,nFSDC_1^0 P(\beta_0)/l$, $P(\beta_0)$ étant une fonction du paramètre non-dimensionel, $\beta_0 = nFvl^2/RTD$. La dépendance, I_p *vs.* l et v, calculée et celle déterminée expérimentalement, concordent qualitativement jusqu'à l'épaisseur, $l = 1\,\mu$. Au dessous de cette valeur, I_p décroît brusquement, probablement à cause de la modification de la nature du processus de transport de l'hydrogène en Pd. La dépendance, I_p *vs.* C_1^0, dans le domaine des petites concentrations et pour des températures différentes, est linéaire. A partir de la variation avec la température de la pente de ces droites, on a déterminé l'énergie apparente d'activation, E_a, de la diffusion de l'hydrogène en Pd. La valeur déterminée expérimentalement, $E_a^{exp} = 2.04$ kcal mole^{-1}, est en bonne concordance avec la valeur calculée selon la cinétique réversible d'électrode, $E_a^{calc} = 2.09$ kcal mole^{-1}. D'ici, on a calculé l'énergie effective d'activation, $E = 5.94$ kcal mole^{-1}, en bonne concordance avec les données de la littérature.

L'énergie apparente d'activation décroît avec l'augmentation de la concentration C_1^0, parce que si la concentration C_1^0 croît, l'effet de freinage de la diffusion décroît puissamment et l'effet de l'écoulement visqueux croît, lié à la convection libre autour de l'électrode. Dans ces conditions, E_a dépend de la nature de la solution.

SUMMARY

On the basis of the results obtained in the experiment on an electronic analogue model, the problem of hydrogen diffusion through a thin palladium layer, under linear sweep voltammetry has been studied. This result was verified experimentally by using the peak current value, $I_p = 2\,nFSDC_1^0 P(\beta_0)/l$ where $P(\beta_0)$ is a function of the dimensionless parameter, $\beta_0 = nFvl^2/RTD$. The calculated dependence of I_p on l and v corresponds qualitatively to that determined experimentally down to thickness $l = 1\,\mu$. I_p decreases suddenly below this value, probably because of changes in the hydrogen transport process through Pd. The dependence of I_p on C_1^0 is linear at low concentrations for different temperatures. It was used to determine the apparent activation energy, E_a, of the hydrogen diffusion through Pd. The experimental values ($E_a^{exp} = 2.04$ kcal mole^{-1}) are in a good agreement with the value calculated on the basis of the assumption of reversible electrode kinetics; $E_a^{calc} = 2.09$ kcal mole^{-1}. The effective activation energy, $E = 5.94$ kcal mole^{-1}, calculated from this is in a good agreement with the literature data.

The apparent activation energy decreases with increase of the concentration, C_1^0, because simultaneously with the increase of this concentration, the diffusion rate decreases strongly and the effect of the viscous flow increases, as a result of the

free convection in the neighbourhood of the electrode. Under these conditions E_a depends on the nature of the solution.

BIBLIOGRAPHIE

1 R. V. BUCUR, I. COVACI ET C. MIRON, *J. Electroanal. Chem.*, 13 (1967) 263.
2 R. V. BUCUR ET J. MERCEA, *J. Electroanal. Chem.*, 16 (1968) 111.
3 R. V. BUCUR ET J. MERCEA, *Rev. Roum. Phys.*, 13 (1968) 601.
4 R. V. BUCUR ET V. V. MORARIU, *J. Electroanal. Chem.*, 20 (1969) 61.
5 V. V. OSTROUMOV, *Zh. Fiz. Khim.*, 31 (1957) 1812.
6 R. V. BUCUR, *J. Electroanal. Chem.*, 17 (1968) 241.
7 R. V. BUCUR, *J. Electroanal. Chem.*, 10 (1965) 8.
8 R. V. BUCUR ET V. V. MORARIU, *Electrochim. Acta*, sous presse.
9 H. S. CARSLAW ET J. C. JAEGER, *Conduction of Heat in Solids*, Oxford Univ. Press, London, 2nd Ed., 1959, p. 102.
10 E. SCHMIDT ET H. R. GYGAX, *Chimia (Aarau)*, 16 (1962) 165.
11 R. V. BUCUR ET V. V. MORARIU, *Electrochim. Acta*, sous presse.
12 A. T. HUBBARD ET F. C. ANSON, *Anal. Chem.*, 38 (1966) 58.
13 W. T. DE VRIES ET E. VAN DALEN, *J. Electroanal. Chem.*, 14 (1967) 315.
14 J. W. SIMONS ET T. B. FLANAGAN, *J. Phys. Chem.*, 69 (1965) 3581.
15 W. T. DE VRIES, *J. Electroanal. Chem.*, 9 (1965) 448.
16 S. V. GORBACHEV, *Zh. Fiz. Khim.*, 24 (1950) 888.

ELECTROANALYTICAL CHEMISTRY AND INTERFACIAL ELECTROCHEMISTRY
Elsevier Sequoia S.A., Lausanne – Printed in The Netherlands

VOLTAMMETRIC BEHAVIOUR OF Ag(I)– AND Ag(II)–2,2′-BIPYRIDINE COMPLEXES IN AQUEOUS SOLUTION

G. RASPI AND L. NUCCI

VI Gruppo di Ricerca "Elettroliti e processi elettrochimici" del C.N.R., presso Istituto di Chimica Analitica dell'Università di Pisa (Italy)

(Received February 12th, 1969)

INTRODUCTION

It is known that Ag(I) reacts with 2,2′-bipyridine (Bip) to yield the complex $AgBip_2^+$ the nitric, sulphuric and perchloric salts of which are very slightly soluble in water[1,2]. Cabani and Scrocco[3], by potentiometric measurements, found evidence of the formation of $AgBip^+$ and $AgBip_2^+$ complexes in aqueous alcoholic medium (in the presence of KNO_3) and determined their stability constants ($\log \beta_1 = 3.7$; $\log \beta_2 = 7.2$). The complex $AgBip_2^{2+}$ is easily obtained by chemical[2] or electrochemical[4] oxidation, Ag(II) being strongly stabilized through coordination with the heterocyclic ligand; as a consequence of complex formation, the formal redox potential of Ag(II)/Ag(I) (1.928 V *vs.* NHE in 1–4 *M* NHO_3[5]) is greatly reduced. By potentiometric measurements, Scrocco and coworkers[6] found a value of 1.453 V (*vs.* NHE) in $0.5–2 \cdot 10^{-2}$ *M* H_2SO_4 and $0.5–2 \cdot 10^{-3}$ *M* 2,2′-bipyridine solutions at extrapolated zero ionic strength. The free energy change accompanying $AgBip_2^{2+}$ complex formation has been calculated (– 26.36 kcal/mole[7]) and the kinetics of decomposition and the reduction process were also studied[8]; in the pH-range 3–5 the complex $AgBip_2^{2+}$ is fairly stable[9] and its salts are more soluble in water than those of the $AgBip_2^+$ complex[2].

This paper deals with the voltammetric behaviour of the complexes of silver with 2,2′-bipyridine in the pH range 0–5.5 by means of the platinum microelectrode with periodic renewal of the diffusion layer[10], taking into account the protophilic characteristics of the organic ligand.

REAGENTS AND INSTRUMENTATION

2,2′-bipyridine was purified by distillation at reduced pressure over KOH which frees ligand from products that are electroactive at tensions near to the oxygen discharge. The salt $AgBip_2(NO_3)_2$, was prepared and analyzed as described by Barbieri[4]. Stock solutions were titrated by standard methods. The ionic concentration was unity and constant throughout all experiments. Polarographic measurements were carried out at 25 ± 0.1°C with a Polarecord model E261 modified to allow a slow tension scanning. The polarograph was joined to a Metrohm IR compensator model E446. The platinum microelectrode was activated by alternate successions of three anodic and three cathodic polarisations in 1 *M* H_2SO_4 (c.d. = 1.0 A/cm^2), each of 20 sec duration. A saturated mercurous sulphate electrode was used as reference; this electrode was joined to the polarographic cell through a bridge filled with a

mixture of silica gel and potassium sulphate in the ratio 3/2. All potential values are referred to the saturated calomel electrode. The current/time measurements were carried out with the aid of a double-beam Tektronix 502A cathode-ray oscilloscope. The solutions were deaerated, when necessary, by nitrogen bubbling.

RESULTS AND DISCUSSION

Figure 1a shows the current–voltage curve obtained for $1 \cdot 10^{-4}$ *M* $AgNO_3$ in 1 *N* HNO_3 solution. The cathodic wave, which appears at a potential lower than 0.295 V, is due to the reduction process: $Ag^+ + e^- \rightarrow Ag$. The anodic current peak between +0.295 and +0.395 V, is due, however, to the dissolution of silver previously deposited on the electrode surface. At potentials above 1.4 V, oxygen is discharged and the current–voltage curve is identical with that obtained with the supporting electrolyte alone. The height of the cathodic wave increases linearly with the silver concentration, and the temperature coefficient is 1.6%/°C. The electrode process is therefore controlled by diffusion and the variation of the instantaneous current with the electrolysis time at controlled potential supports this assumption. It has already been shown that[10] when the electrode process is controlled by diffusion the current intensity at time, *t*, is given by the expression:

$$i_t = a + bt^{-\frac{1}{2}} \tag{1}$$

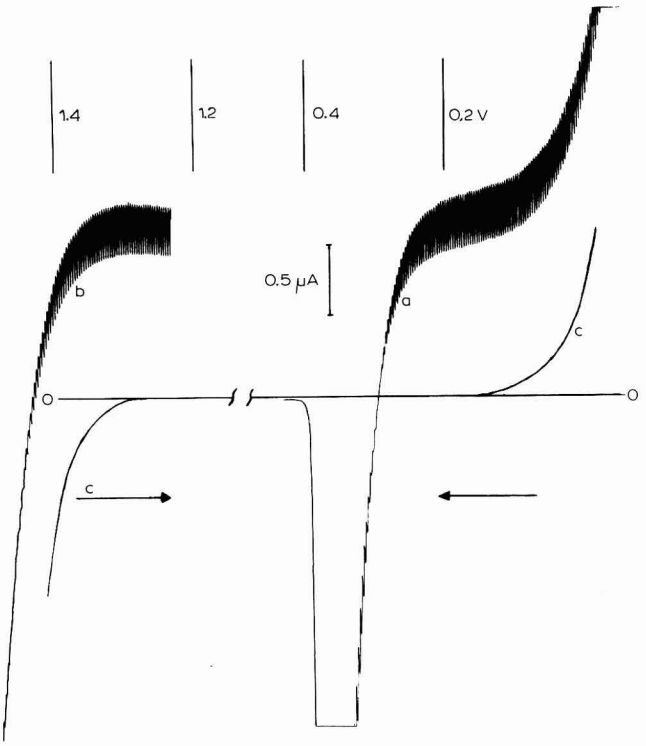

Fig. 1. (a), Reduction wave of $1 \cdot 10^{-4}$ *M* Ag(I) in 1 *M* HNO_3; (b), reduction wave of $1 \cdot 10^{-4}$ *M* Ag(II) to Ag(I) in 3 *M* HNO_3; (c), curve obtained with 1 *M* HNO_3 alone.

where $a = nFADC/r$, $b = nFAD^{\frac{1}{2}}C/\pi^{\frac{1}{2}}$ and n,r,F,A,D,C have their usual meaning. A typical plot of log i *vs.* log t, at a potential corresponding to the limiting current, is practically a straight line with a slope of -0.5 which is in agreement with the previous relation (1), the contribution of the first term, a, being negligible.

The reduction process, $Ag^+ + e^- \rightleftharpoons Ag$, is reversible and the polarographic curve is described in every point by the relation, $E = E^0 + 0.0591 \log(i_d - i)$ assuming that the activity of the deposit is constant and independent of the current density. The intersection potential (E_{int}) is in good agreement with that calculated ($+0.299$ V) from the $AgNO_3$ mean activity coefficient (0.429[11]) at unit ionic strength. E_{int} shifts by about 60 mV for unit change of log $[Ag^+]$ at constant ionic strength.

When Ag(II) is present in the solution as a consequence of AgO dissolution or of Ag(I) chemical oxidation by persulphate, the reduction process, $Ag(II) + e^- \rightarrow Ag(I)$, already gives rise to a cathodic limit current intensity at $+1.4$ V (Fig. 1b): this limiting current is obtained only if the HNO_3 concentration is $\geqslant 3$ *M*. At potentials above 1.4

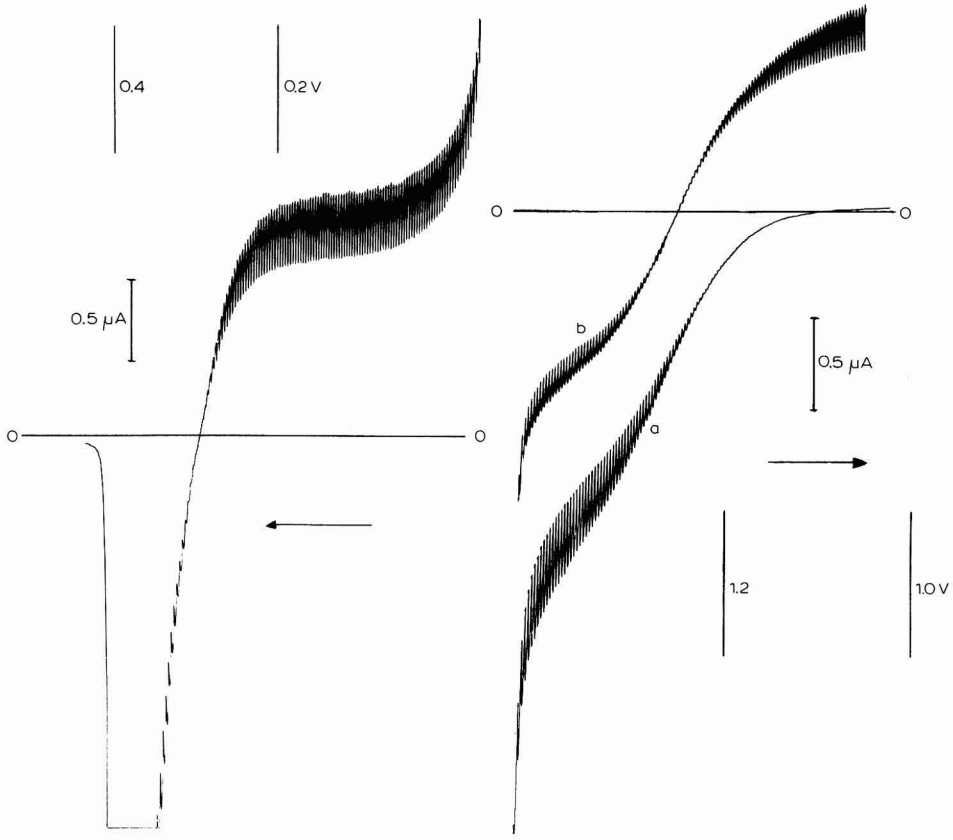

Fig. 2. Reduction wave of $1 \cdot 10^{-4}$ *M* Ag(I) in 1 *M* $HNO_3 + 5 \cdot 10^{-2}$ *M* 2,2′-bipyridine.

Fig. 3. (a), Oxidation wave of $1 \cdot 10^{-4}$ *M* Ag(I) in 1 *M* $HNO_3 + 5 \cdot 10^{-2}$ *M* 2,2′-bipyridine soln.; (b), cathanodic wave obtained in 1 *M* $HNO_3 + 5 \cdot 10^{-2}$ *M* 2,2′-bipyridine after partial electrochemical oxidation of Ag(I) to Ag(II).

V this current is added to the oxygen discharge. Analogous results are obtained in concentrated sulphuric, phosphoric (in presence of $HClO_4$) solutions. The limiting current of the process, $Ag(II)+e^- \rightarrow Ag(I)$, gradually decreases with time as a consequence of the low stability of Ag(II) solutions[12].

When the 1 M HNO_3 and $1 \cdot 10^{-4}$ M Ag^+ solution contains also $5 \cdot 10^{-2}$ M 2,2′-bipyridine, the voltammetric curve reveals two waves, a cathodic wave (Fig. 2) and an anodic wave (Fig. 3a). The cathodic wave, which is identical with that shown in Fig. 1, is again ascribed to the reduction of Ag(I) to metallic silver. The anodic wave is due to the process, $Ag(I) \rightarrow Ag(II)+e^-$, and its height is the same as for the cathodic wave; this wave is well developed if the electrode is previously oxidized at 3 V for a period of 2 min and if the polarogram is recorded by scanning gradually decreasing potentials. This charge transfer process is reversible on the activated platinum electrode but it is characterized by overvoltage on smooth platinum. Logarithmic analysis of the anodic and cathodic waves obtained with a solution of Ag(I) (Fig. 3a) and with a mixture of Ag(I) and Ag(II) (Fig. 3b) respectively, gives a straight line with a slope of 59 mV, as would be expected with a one-electron reversible process. The proportionality of the anodic wave height with the Ag(I) concentration is verified. The temperature coefficient was 1.6% per degree: the process, $Ag(I) \rightleftharpoons Ag(II)+e^-$, is therefore controlled by diffusion and oscillographic measurements on the basis of eqn. (1) give further evidence of this.

The half-wave potential of the anodic step is a function of the 2,2′-bipyridine concentration, being shifted to more positive values as the latter is decreased. Since the system, $Ag(I) \rightleftharpoons Ag(II)+e^-$, is characterized by a high redox potential, the corresponding wave is wholly masked by the oxygen discharge as the ligand concentration is decreased to below $1.5 \cdot 10^{-2}$ M. Figure 4 shows that the E_{int}-values (line a) are not a function of 2,2′-bipyridine concentration, which means that in 1 M HNO_3Ag^+ is not appreciably complexed by the ligand. Line b, the slope of which is about 120 mV

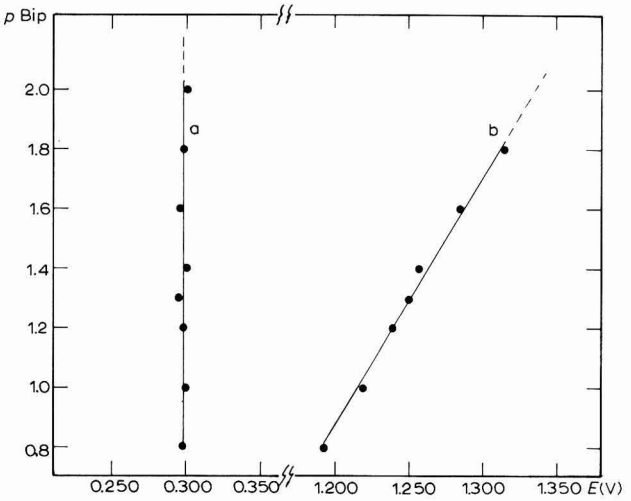

Fig. 4. (a), E_{int} of the reduction wave obtained with $1 \cdot 10^{-4}$ M Ag(I) in 1 M HNO_3 as a function of 2,2′-bipyridine concn.; (b), $E_{\frac{1}{4}}$ of the oxidation wave obtained with $1 \cdot 10^{-4}$ M Ag(I) in 1 M HNO_3 as a function of 2,2′-bipyridine concn.

TABLE 1

VARIATION OF $E_{\frac{1}{2}}$ AND E_{int} OF THE Ag(I) OXIDATION AND REDUCTION WAVES, AND CORRESPONDING CALCULATED VALUES OF LOG β_2 [Ag(II)] AND LOG β_2 [Ag(I)] WITH 2,2′-BIPYRIDINE CONCENTRATION, AT UNIT AND CONSTANT IONIC STRENGTH

Section	*pH*	*pBip*	*Ag(II)/Ag(I) system*		*Ag(I)/Ag system*	
			$E_{\frac{1}{2}}(V)$	*log* β_2	$E_{int}(V)$	*log* β_2
A	0.15	—	(1.686)*	–	0.295	–
		1.8	1.316	9.85	0.298	—
		1.6	1.285	10.00	0.295	—
		1.4	1.257	10.05	0.300	—
		1.3	1.251	9.95	0.295	—
		1.2	1.240	9.95	0.298	—
		1.0	1.219	9.90	0.300	—
		0.8	1.192	9.95	0.298	—
			mean value	9.95 ± 0.1		
B	5.0	—	—	—	0.288	—
		3.6	1.051	18.30	0.268	6.22
		3.4	1.029	18.40	0.260	6.18
		3.2	1.011	18.45	0.250	6.22
		3.0	1.001	18.50	0.239	6.16
		2.8	0.991	18.45	0.223	6.28
		2.6	0.985	18.38	0.205	6.35
		2.5	0.982	18.37	0.199	6.20
		2.3	0.976	18.40	0.184	6.15
		2.2	0.978	18.35	0.171	6.23
		2.0	0.973	18.40	0.147	6.30
			mean value	18.40 ± 0.1	mean value	6.23 ± 0.1

* Refs. 5 and 13.

for unit logarithmic ligand concentration change, reproduces the anodic half-wave potential variation. In such acidic conditions, the Ag^+ oxidation process takes place at the electrode surface according to the following scheme:

$$Ag^+ + 2\,[HBip]^+ \rightleftharpoons [AgBip_2]^{2+} + 2\,H^+ + e^- \qquad (2)$$

The logarithmic mean value of the $[AgBip_2]^{2+}$ complex conditional overall stability constant is log β_2[Ag(II)] = 9.95 ± 0.1 (Table 1, section A); this value is calculated assuming for the Ag(II)/Ag(I) formal potential in 1 *M* HNO_3 the value given by Noyes and coworkers[5,13] ($E^{0\prime} = 1.686$ V *vs.* SCE). The change of log β_2[Ag(II)] in the pH-range 0–6 at constant ionic strength (Fig. 5a) is calculated assuming that 2,2′-bipyridine in 1 *M* HNO_3 is completely protonated and (as a first-order approximation) that the $[HBip]^+$ dissociation constant value is $3.00 \cdot 10^{-5}$[14] at unit ionic strength. The experimental verification of this behaviour evidently implies a knowledge of the conditional stability constant values, at unit ionic strength, of the $[AgBip]^+$ and $[AgBip_2]^+$ complexes.

Since the nitric, sulphuric, perchloric and acetic salts of these complexes are very slightly soluble in water, phosphoric buffers in the pH-range 1.5–5.0, and

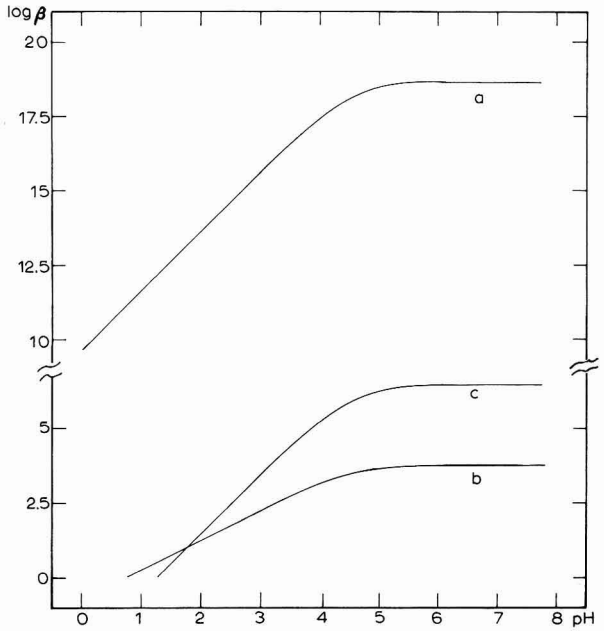

Fig. 5. (a), Log β_2[Ag(II)]; (b), log β_1[Ag(I)]; (c), log β_2[Ag(I)] as a function of pH at unit ionic strength.

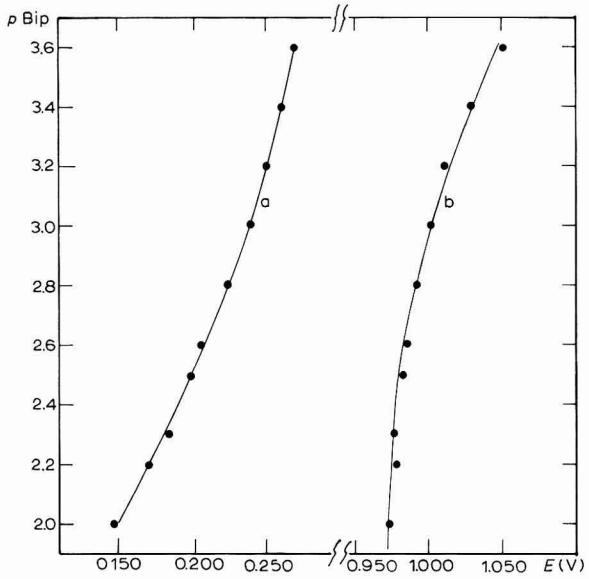

Fig. 6. (a), E_{int} of the reduction wave obtained with $1 \cdot 10^{-4}$ M Ag(I) in buffer soln. at pH 5.0 ($\mu = 1$) as a function of 2,2′-bipyridine concn.; (b), $E_{\frac{1}{2}}$ of the oxidation wave obtained with $1 \cdot 10^{-4}$ M Ag(I) in buffer soln. at pH 5.0 ($\mu = 1$) as a function of 2,2′-bipyridine concn.

succinic buffers for higher pH-values, were used. Under these conditions $AgNO_3$ and 2,2′-bipyridine concentrations, present together in solution, reach the values, $1 \cdot 10^{-4}$ M and $1 \cdot 10^{-2}$ M, respectively.

When the solution at pH 5.0 (in the absence of ligand) contains $1 \cdot 10^{-4}$ *M* $AgNO_3$, a reversible cathodic wave controlled by diffusion is obtained. The experimental value of E_{int} (0.288 V), both in phosphoric and succinic medium, is in good agreement with that found in 1 *M* HNO_3 (0.295 V). When 2,2′-bipyridine is present in solution in addition to the cathodic wave, the oxidation of Ag(I) to Ag(II) takes place. The cathodic wave is shifted towards decreasing positive potentials as the ligand concentration is increased (Fig. 6a), as a consequence the formation of $[AgBip]^+$ and $[AgBip_2]^+$ complexes. The reduction processes of both complexes are reversible and diffusion-controlled and can be represented as:

$$[AgBip]^+ + e^- \rightleftharpoons Ag + Bip$$

$$[AgBip_2]^+ + e^- \leftrightharpoons Ag + 2\ Bip$$

At pH 5.0, the logarithmic values of the conditional overall stability constant of the complexes $[AgBip]^+$ and $[AgBip_2]^+$ were calculated by the use of the DeFord–Hume method[15] on the basis of the E_{int}-value (0.288 V) obtained in a solution free from ligand, and of the E_{int}-values at various ligand concentrations (Table 1, section B): $\log \beta_1[Ag(I)] = 3.64 \pm 0.1$, $\log \beta_2[Ag(I)] = 6.23 \pm 0.1$. Figure 5, b and c, shows the changes of these constants as a function of pH.

When the 2,2′-bipyridine concentration is increased in the range $0.25–5 \cdot 10^{-3}$ *M*, the half-wave potential of the anodic step obtained at pH 5.0 is shifted by about 60 mV towards less positive values for unit pBip change (Fig. 6b). As the ligand concentration is increased above $5 \cdot 10^{-3}$ *M*, the half-wave potential tends to become constant. The corresponding oxidation processes of Ag(I) can therefore be expressed as:

$$[AgBip]^+ + Bip \rightleftharpoons [AgBip_2]^{2+} + e^-$$

$$[AgBip_2]^+ \rightleftharpoons [AgBip_2]^{2+} + e^-$$

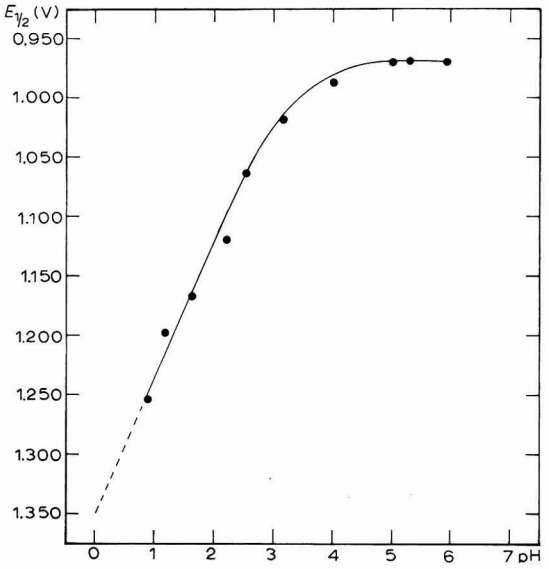

Fig. 7. Variation with pH of $E_{\frac{1}{2}}$ of the reversible wave (Ag(II)/Ag(I)) obtained with $1 \cdot 10^{-4}$ *M* Ag(I) or $1 \cdot 10^{-4}$ *M* Ag(II) in buffer solns. at $\mu = 1$ containing $1 \cdot 10^{-2}$ *M* 2,2′-bipyridine.

Both processes are reversible and controlled by diffusion.

The logarithmic mean value of the conditional stability constant for th $[AgBip_2]^{2+}$ complex was calculated from the half-wave potentials at various 2,2 bipyridine concentrations (Table 1, section B) and from the values of log β_1[Ag(I) and log β_2[Ag(I)], assuming that the Ag(II)/Ag(I) formal potential (1.686 V) obtaine in 1 M HNO_3 solution is valid in the phosphoric mixture (at $\mu = 1$). The resulting valu of log β_2[Ag(II)] is in a good agreement with that calculated in Fig. 5a.

The solid line of Fig. 7 represents the calculated behaviour of the half-wav potential of the Ag(II)/Ag(I) couple in the pH-range 0–6.0 at analytic ligand concen tration of $1 \cdot 10^{-2}$ M on the basis of the log β_1[Ag(I)], log β_2[Ag(I)], log β_2[Ag(II) values at various concentrations of non-protonated 2,2′-bipyridine in the same pH range. The experimental values, obtained with Ag(I) and Ag(II) solutions, fit in we with the calculated curve.

ACKNOWLEDGEMENT

This work was carried out with the financial support of the "Consiglio Nazionale del Ricerche" of Italy.

SUMMARY

Aqueous Ag(I)–2,2′-bipyridine complexes are oxidized at the platinum m croelectrode with periodic renewal of the diffusion layer, to give well-developed an reversible waves the limiting currents of which are diffusion-controlled. The effect c pH and ligand concentration on the polarographic behaviour was examined, and th conditional stability constants of the complexes, at unit ionic strength, were calculate

REFERENCES

1 G. A. Barbieri and A. Malaguti, *Atti Accad. Nazl. Lincei Rend. Classe Sci. Fis. Mat. Nat.*, 8 (195 619.
2 A. Malaguti, *Atti Accad. Nazl. Lincei Rend. Classe Sci. Fis. Mat. Nat.*, 9 (1950) 349;
3 S. Cabani and E. Scrocco, *Ann. Chim. (Rome)*, 48 (1958) 85.
4 A. Barbieri, *Atti Accad. Nazl. Lincei Rend. Classe Sci. Fis. Mat. Nat.*, [16] 6, II (1932) 44.
5 A. A. Noyes, D. De Vault, C. D. Coryell and T. J. Deahl, *J. Am. Chem. Soc.*, 59 (1937) 1326.
6 E. Scrocco, G. Marmani and P. Mirone, *Boll. Sci. Fac. Chim. Ind. Bologna*, 8 (1950) 119.
7 E. Scrocco and O. Salvetti, *Boll. Sci. Fac. Chim. Ind. Bologna*, 12 (1954) 98.
8 V. Balzani, A. Bertoluzza, V. Carassiti and A. Malaguti, *Ann. Chim. (Rome)*, 52 (1962) 105
9 E. Gagliardi and P. Presinger, *Mikrochim. Acta*, 6 (1964) 1175.
10 D. Cozzi, G. Raspi and L. Nucci, *J. Electroanal. Chem.*, 12 (1966) 36.
11 R. A. Robinson and R. H. Stokes, *Electrolytic Solutions*, Butterworths, London, 1955.
12 A. A. Noyes, C. D. Coryell, F. Stitt and A. Kossiakoff, *J. Am. Chem. Soc.*, 59 (1937) 1316.
13 A. A. Noyes and A. Kossiakoff, *J. Am. Chem. Soc.*, 57 (1935) 1238.
14 P. Krumholz, *J. Am. Chem. Soc.*, 71 (1949) 3654.
15 D. D. DeFord and D. N. Hume, *J. Am. Chem. Soc.*, 73 (1951) 5321.

ELECTROANALYTICAL CHEMISTRY AND INTERFACIAL ELECTROCHEMISTRY
Elsevier Sequoia S.A., Lausanne – Printed in The Netherlands

SHORT COMMUNICATIONS

Acidité des ions argent dans l'acétamide fondu à 98°

Au cours de l'étude que nous avons effectuée sur les propriétés acides–bases dans l'acétamide fondu à 98°[1], des essais pour réaliser une électrode de comparaison utilisant le système Ag/Ag^+ nous ont montré qu'une solution neutre de nitrate d'argent n'est pas stable. Il apparaît en effet immédiatement après la dissolution une coloration brune puis, peu à peu, un précipité noirâtre.

Par titrage conductimétrique du nitrate d'argent par l'acétamidure de sodium, Grüttner et Jander[2] ont montré la formation de deux composés: l'acétamidure d'argent, $Ag(CH_3CONH)$, précipité brun noir, puis le complexe incolore, $Ag(CH_3CONH)_2^-$. Ces réactions correspondent à un caractère acide de l'ion Ag^+ solvaté en solution dans l'acétamide fondu—analogue au caractère acide des cations métalliques hydratés en solution aqueuse par formation d'hydroxydes; le précipité qui apparaît lors de la dissolution du nitrate d'argent dans l'acétamide neutre est par conséquent l'acétamidure d'argent résultant de la solvolyse:

$$Ag^+ + CH_3CONH_2 \rightleftharpoons Ag(CH_3CONH)\downarrow + H^+$$

Pour préciser ces phénomènes, nous avons effectué l'étude électrochimique des réactions entre l'acétamidure et Ag^+.

La technique instrumentale utilisée est classique. Pour ce qui concerne l'emploi de l'acétamide fondu comme solvant, on pourra consulter le mémoire principal[1]. Toutefois, nous avons ici utilisé de l'acétamide U.C.B. pour analyse, plus parfaitement exempt de traces d'halogènures. L'obtention d'acétamidure de sodium et d'acide fort (HNO_3, CH_3CONH_2) a déjà été également décrite, ainsi que l'électrode de comparaison.

Toute les mesures ont été effectuées en présence de nitrate de sodium 1 *m* (1 mole/kg de solvant), donc à la force ionique constante, $\mu = 1$.

Résultats et interprétation

1. *Détermination du potentiel normal apparent du système Ag/Ag^+.* Le trouble d'acétamidure d'argent disparaît dès l'addition d'un peu d'acide fort. Nous avons donc admis que l'électrode d'argent fonctionne alors selon le système, $Ag^+ + e = Ag$. Effectivement, en présence de nitrate d'argent 10^{-2} *m*, le potentiel d'une électrode d'argent reste invariable pour pH compris entre 3 et 0.3 environ; en-dessous de pH = 0.3, l'argent est oxydé par l'acide nitrique.

A pH = 1, nous avons mesuré les différentes valeurs du potentiel d'équilibre pris par une électrode d'argent en présence d'ions Ag^+, de concentration variant entre 10^{-2} *m* et 0.2 *m*. La fonction $E = f[\log(C_{Ag^+})]$ est représentée par une droite dont les coefficients de régression (probabilité de 95%, 9 mesures) sont: pente 79 ± 2.5 mV par unité de log *C* (coefficient théorique à 98°: 74 mV); potentiel normal apparent (par extrapolation à $C_{Ag^+} = 1$ *m*, $\mu = 1$):

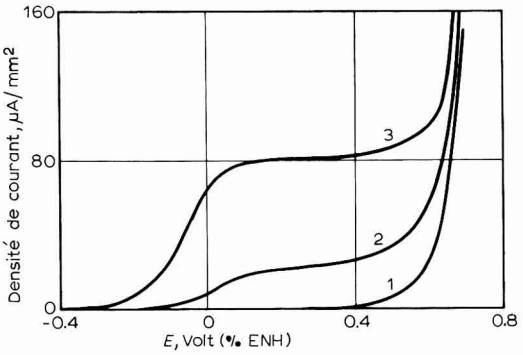

Fig. 1. Courbes intensité–potentiel à une micro-électrode tournante à disque d'argent (0.5 mm^2, 600 t/min). (1), Oxydation de l'argent en présence de nitrate de sodium 1 m; (2) et (3), après addition d'acétamidure de sodium dilué.

$E^0_{Ag} = 0.759$ (± 0.003) V (par rapport à l'électrode normale à hydrogène dans l'acétamide à 98°)

2. *Identification du complexe* $Ag(CH_3CONH)_2^-$. L'oxydation électrochimique d'un disque d'argent (obtenu par dépôt électrolytique d'argent sur un disque de platine poli), en présence d'une solution diluée d'acétamidure, permet de déterminer les courbes intensité–potentiel représentées Fig. 1. Il apparaît une vague d'oxydation dont la hauteur, i_l, augmente avec la concentration de l'acétamidure. Aucun indice de précipitation du produit d'oxydation ne se manifeste. En outre, la forme des vagues d'oxydation est en accord avec l'équation théorique établie en supposant la formation du complexe $Ag(CH_3CONH)_2^-$:

$$E_{an} = \text{cte.} + (2.3RT/F) \log \{i/(i_l - i)^2\}$$

Par ailleurs, nous avons mesuré les valeurs du potentiel d'équilibre pris par

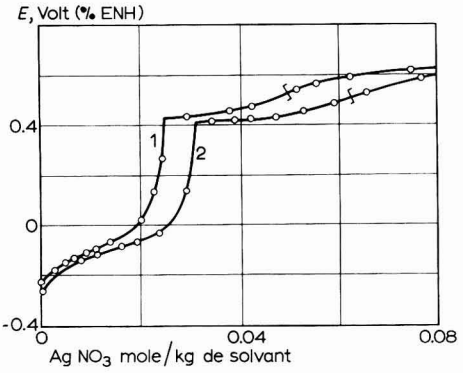

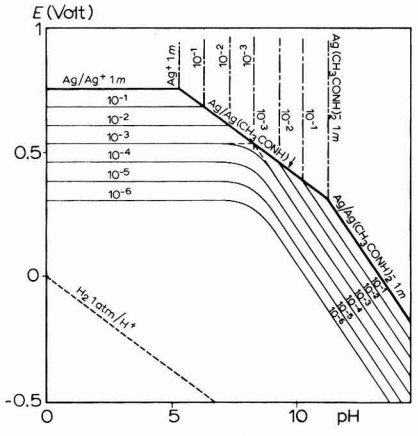

Fig. 2. Courbes de titrage potentiométrique d'acétamidure de sodium par les ions Ag^+. (1), CH_3CONH^- $4.95 \cdot 10^{-2}$ m; (2), $6.25 \cdot 10^{-2}$ m.

Fig. 3. Diagramme potentiel–pH de l'argent dans l'acétamide fondu à 98° ($\mu = 1$).

une électrode d'argent en présence d'ions Ag^+ 10^{-2} *m* et d'acétamidure de sodium $8 \cdot 10^{-2}$–0.2 *m* (7 mesures). La fonction $E = f[\log(C_{CH_3CONH^-})]$ est représentée par une droite dont les coefficients de régression sont: pente 134 ± 5 mV par unité de log *C*; potentiel apparent extrapolé à $C_{CH_3CONH^-} = 1$ *m*: -0.310 (± 0.005) V.

On déduit de la valeur de la pente que l'argent(I) existe bien alors sous la forme du complexe $Ag(CH_3CONH)_2^-$ et de la valeur du potentiel apparent extrapolé à $C_{CH_3CONH^-} = 1$ *m* que la constante de stabilité de ce complexe est:

$$\log(\beta_2/\mathrm{kg^2\,mole^{-2}}) = \log\frac{[Ag(CH_3CONH)_2^-]}{[Ag^+][CH_3CONH^-]^2} = 12.4\ (\pm 0.15)\ (\text{à } \mu = 1)$$

3. *Titrage potentiométrique de CH_3CONH^- par Ag^+. Détermination du produit de solubilité de l'acétamidure d'argent.* Deux courbes de titrage expérimentales sont représentées Fig. 2. Au premier point équivalent, correspondant à la formation du complexe $Ag(CH_3CONH)_2^-$, le point anguleux correspond à l'apparition du précipité d'acétamidure d'argent, $Ag(CH_3CONH)$. Un second point équivalent peu prononcé apparaît ensuite pour une quantité de Ag^+ double de celle au 1er point équivalent.

Les points expérimentaux de chacune des deux parties des courbes de titrage permettent de déterminer:

$$\log(\beta_2/\mathrm{kg^2\,mole^{-2}}) = 12.6\ (\pm 0.05)$$

$$-\log(K_s/\mathrm{mole^2\,kg^{-2}}\varepsilon = -\log[Ag^+][CH_3CONH^-] = 9.3\ (\pm 0.05)\ (\text{à } \mu = 1)$$

Conclusion

Ces deux constantes permettent de calculer les constantes d'acidité de l'ion Ag^+ dans l'acétamide fondu à 98° (et $\mu = 1$):

$$Ag^+ + CH_3CONH_2 \rightleftharpoons Ag(CH_3CONH)\downarrow + H^+, K_{a_1} = [H^+]/[Ag^+] = K_i/K_s$$

$$Ag(CH_3CONH)\downarrow + CH_3CONH_2 \rightleftharpoons Ag(CH_3CONH)_2^- + H^+,$$

$$K_{a_2} = [Ag(CH_3CONH_2^-][H^+] = \beta_2 K_s K_i$$

On obtient $pK_{a_1} = 5.3$ (± 0.15) et $pK_{a_2} = 11.3$ (± 0.15).

En conclusion, ces propriétés du couple Ag/Ag^+ peuvent être traduites sous la forme d'un diagramme potentiel–pH représenté Fig. 3. Il y apparaît bien qu'en milieu initialement neutre (pH = 7.3), la concentration des ions Ag^+ en solution ne peut dépasser 10^{-2} *m*, une précipitation de l'acétamidure d'argent survenant à ce moment.

Pour $[Ag^I] < 10^{-3}$ *M*, il ne peut plus y avoir précipitation de $Ag(CH_3CONH)$, ce qui explique la vague d'oxydation unique de la Fig. 1.

Faculté des Sciences de Paris,
Laboratoire de Recherches de Chimie Analytique
(associé au CNRS),
Paris (France)

Sylviane Guiot

Bernard Trémillon

1 S. GUIOT ET B. TRÉMILLON, *J. Electroanal. Chem.*, 18 (1968) 261.
2 B. GRÜTTNER ET G. JANDER, *Z. Anorg. Allgem. Chem.*, 268 (1952) 229.

Reçu le 3 février, 1969

Elsevier Sequoia S.A., Lausanne – Printed in The Netherlands

A reversible 2*e* redox couple. Anodic oxidation of tetraanisylethylene

During the course of a study of the anodic electrochemistry of aryl-olefins[1], tetra-*p*-anisylethylene (TAE) was examined. Buckles and coworkers[2a] have shown that the chemical oxidation of TAE produces salts of the stable di-cation. While the voltammetric behaviour of several compounds that give stable cation-radicals[3,4] has been reported, the only previous electrochemical study of stable di-cations is the polarographic investigation of tetrakis(dimethylamino)ethylene which was found to undergo two successive 1*e* transfers[5]. Sioda reported the anodic hydroxylation of the unstable di-cation of 9,10-diphenylanthracene to form the diol[6]. It is obvious from Sioda's cyclic voltammogram of 9,10-DPA that the di-cation reacts as it is formed, since no reduction current is observed for the di-cation. The primary electrode process for the oxidation of polynuclear hydrocarbons has been shown to involve the transfer of one electron to form the cation-radical[7] and this has been cited as evidence against two-electron oxidations during anodic substitution[4]. A direct two-electron transfer has been proposed for the anodic acetoxylation of 4,4′-dimethoxystilbene[8]. The present study reveals that TAE undergoes a reversible 2*e* transfer to the di-cation which is stable in acetonitrile for several hours.

Experimental

A Heath EUW 19A operational amplifier with polarography module EUA-19-2 was used for both conventional polarography and cyclic voltammetry. Single sweep polarograms were obtained at a rotating platinum electrode (RPE) or a Beckman platinum button (No. 39273) and the latter was employed for cyclic voltammetry. A saturated calomel electrode (SCE) was used as the reference electrode and the counter electrode was a carbon rod. Controlled potential coulometry was conducted at a platinum gauze electrode in a two-compartment cell employing an Amel (Model 555) potentiostat.

The supporting electrolyte was lithium perchlorate (0.1 *M*) and the solvent was acetonitrile which was purified by two distillations from phosphorus pentoxide in which only the middle 60% was collected. TAE was prepared by a modification of a published procedure[2b].

Results and discussion

The cyclic polarogram shown in Fig. 1 is that of TAE in acetonitrile. The oxidation peak is at +0.78 V and the corresponding peak for reduction of the di-cation is at +0.75 V. The potential difference between anodic and cathodic peaks in a reversible couple is given by the equation[9,10],

$$E_{p_a} - E_{p_c} = 0.058/n \text{ V}$$

or for a two-electron transfer, a peak separation of 0.029 V may be calculated. The oxidation of TAE (Fig. 1) fits these criteria for reversibility. Some deviation from reversibility is indicated by the fact that $E_p - E_{p/2}$ has a value of 0.050 V rather than 0.029 V predicted by the equation[8,9]:

$$(E_p - E_{p/2})_{REV} = 0.057/n \text{ V}$$

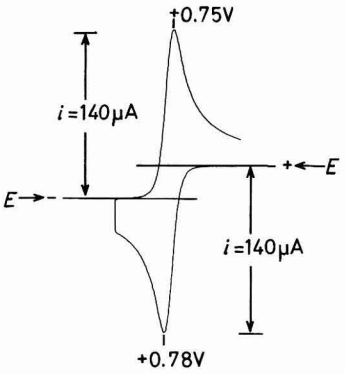

Fig. 1. Cyclic polarogram for oxidation of TAE. Anode potential was held for 20 sec at +0.90 V before initiating cathodic sweep.

The foregoing criteria of reversibility have been applied to the dimethylphenazine system by Adams and coworkers in establishing this compound as a model electrochemical system[11]. Linear scan polarograms over a range of scan rates were recorded and the $i_p/V^{\frac{1}{2}}$ data are summarized in Table 1. A reasonably constant value for $i_p/V^{\frac{1}{2}}$ is observed, as predicted by the Randles–Sevčik equation[11].

TABLE 1
PEAK CURRENTS FOR OXIDATION OF TAE AS A FUNCTION OF SCAN-RATE

Scan rate	$V^{\frac{1}{2}}$	i_p	$i_p/V^{\frac{1}{2}}$
10	3.16	150	47.5
5	2.24	110	49.1
2.5	1.58	79	50.0
1.0	1.00	51	51.0
0.5	0.71	35	49.5

Controlled potential coulometry for the anodic oxidation of TAE in acetonitrile verifies that 2.0 electrons/molecule are transferred during the oxidation. The cyclic polarogram of a solution of the di-cation of TAE, which was prepared during the coulometric experiment mentioned above, was recorded in the following manner. Starting the scan at +1.2 V in the cathodic direction a reduction peak is observed at +0.75 V, and reversing the direction of the scan gives a corresponding anodic peak at +0.78 V.

For a reversible system, the ratio of anodic to cathodic peak heights is equal to unity[10,11]. This was found to be the case with the oxidation of TAE over the range of scan rates employed, 2.5–10 V/min. The method of Adams and coworkers was used for establishing the proper base line for evaluating i_{p_c}[11]. The anodic sweep was carried out to +1.2 V, and the potential held at +1.2 V until the current decayed to a steady value before initiating the cathodic sweep. This procedure was carried out for each of the scan rates given in Table 1 and a value of 1.0 was observed for the ratio of anodic to cathodic peaks in each case.

Our results clearly show that TAE is oxidized by a direct two-electron transfer. This indicates the multiplicity of mechanisms for anodic reactions of hydrocarbons, which are now generally believed to oxidize by a one-electron transfer to the cation-radical[12]. It appears necessary to examine the individual system in question before one can say with certainty which mechanism is followed.

Acknowledgement

The authors gratefully acknowledge financial support from the Swedish Natural Science Research Council and are indebted to Professor R. N. Adams for use of voltammetric equipment.

Division of Organic Chemistry,
University of Lund, Chemical Centre,
P.O. Box 740, S-22007, Lund (Sweden)

Vernon D. Parker
Klas Nyberg
Lennart Eberson *

1 V. D. PARKER AND L. EBERSON, to be published.
2 a.N. C. BAENZIGER, R. E. BUCKLES AND T. D. SIMPSON, *J. Am. Chem. Soc.*, 89 (1967) 3405.
b. R. E. BUCKLES AND W. D. WOMER, *ibid.*, 80 (1958) 5055.
3 A. ZWEIG, W. G. HODGSON AND W. H. JURA, *J. Am. Chem. Soc.*, 86 (1964) 4124.
4 N. L. WEINBERG AND H. R. WEINBERG, *Chem. Rev.*, 68 (1968) 449.
5 K. KUWATA AND D. H. GESKE, *J. Am. Chem. Soc.*, 86 (1964) 2101.
6 R. E. SIODA, *J. Phys. Chem.*, 72 (1968) 2322.
7 M. E. PEOVER AND B. S. WHITE, *J. Electroanal. Chem.*, 13 (1967) 93.
8 V. D. PARKER AND L. EBERSON, *Chem. Comm.*, in press.
9 H. MATSUDA AND Y. AYABE, *Z. Elektrochem.*, 59 (1955) 494.
10 R. S. NICHOLSON AND I. SHAIN, *Anal. Chem.*, 36 (1964) 706.
11 R. F. NELSON, D. W. LEEDY, E. T. SEO AND R. N. ADAMS, *Z. Anal. Chem.*, 224 (1967) 184.
12 R. N. ADAMS, *Accounts of Chemical Research*, in press.

Received February 10th, 1969

J. Electroanal. Chem., 22 (1969) 152

Eine Methode zur Bestimmung der Redoxpotentiale empfindlicher Hydrochinonsulfone und Hydrochinonsulfonamide

Chinone mit Substituenten, die das Redoxpotential erhöhen (SO_2R, NO_2, CN), sind als charakterisierte Substanzen bisher nur in wenigen Beispielen beschrieben worden[1]. Eine experimentelle Bestimmung der reversiblen Redoxpotentiale durch kontinuierliche potentiometrische Titration gelingt nur, wenn Reversibilität des Redoxsystems an den Messelektroden und gute Reproduzierbarkeit der Messwerte durch ein genau definiertes und leicht kontrollierbares System aus Lösungsmittel und Titriermittel gegeben sind. Da während der Titration von Sulfon- oder Sulfonamid-substituierten Redoxsystemen eine Chinonform entsteht, die äusserst leicht (z.B. mit Wasser) reagiert, so erhält man bei einer Titration derartiger Systeme in wasserhalti-

* To whom correspondence should be addressed.

gen Medien ein ständig fallendes Potential, was auf die laufende Verringerung der Chinonform im Gleichgewicht zurückgeführt wird.

In den einzigen systematischen Arbeiten[2] werden bei allen vermessenen Hydrochinonsulfonen nicht die theoretischen Werte (bei 20°C 13.9 mV[3]) der Indexpotentiale erreicht; im übrigen werden je nach Anwesenheit weiterer Substituenten stark unterschiedliche Werte für die Potentialerhöhung durch den SO_2R-Substituenten (43–132 mV in 80%ig. Essigsäure) gefunden.

Daher kann bei allen derartig vermessenen Hydrochinonen eine Zersetzung der oxydierten Form auch bei der von den Autoren angewandten diskontinuierlichen Titrationstechnik eine Rolle spielen. Eine kontinuierliche potentiometrische Titration gelang bisher nur in Fällen, bei denen im Hydrochinonkern zusätzliche Substituenten, die das Potential stark senken ($-OCH_3$, $-CH_3$), enthalten waren.

Wir fanden nun in wasserfreiem Eisessig (Merck, p.a.) ein Medium, in dem die Zersetzung der unbeständigen Chinon-Form so langsam verläuft, dass unter der Bedingung rascher Einstellgeschwindigkeit an der Messelektrode eine kontinuierliche Titration möglich ist. Die gut reproduzierbaren Messwerte erlaubten selbst die Bestimmung kleiner Unterschiede der Mittelpunktspotentiale von verschiedenen substituierten Chinonen. Als Oxydationsmittel erwies sich Bleitetraacetat in Eisessig als hervorragend geeignet, da es rasche Einstellgeschwindigkeit und grosse Titerbeständigkeit mit einem hohen Redoxpotential verbindet. Die geringe Eigenleitfähigkeit von reinem Eisessig wurde durch den Zusatz eines Leitsalzes erhöht. Die besten Ergebnisse erzielten wir mit Eisessig, der 0.2 *m* an Ammoniumacetat war. Wie zu erwarten war, lagen bei Sulfon- oder Sulfonamid-substituierten Chinon/Hydrochinon-Systemen die Redoxpotentiale im Vergleich zum unsubstituierten Chinon/Hydrochinon-System deutlich höher (Abb. 1).

Die Mittelpunktspotentiale (jetzt bezogen auf die Normalwasserstoffelektrode) der Sulfone II und III sind mit 697.5 mV und 717.5 mV um 116.5 mV bzw. 136.5 mV höher als das des auf gleiche Weise im gleichen Medium gemessene Potential des unsubstituierten Hydrochinons ($E'_0 = 581$ mV). Es ist bekannt, dass 2,6-Dichlorhydrochinon ein um etwa 25 mV höheres Mittelpunktspotential aufzeigt als das unter gleichen Bedingungen gemessene Hydrochinon[8,9]. Auch bei dem Hydrochinonsulfon III erhöht sich das Mittelpunktspotential im Vergleich zum nicht chlorierten 2,5-Dihydroxy-4′-methyl-diphenylsulfon auf Grund der zweifachen Chlorsubstitution um 22.5 mV.

Die Anilide der Hydrochinonmono- und -2,6-disulfonsäure I und IV wiesen Mittelpunktspotentiale von 687.5 und 763.5 mV auf.

Die Indexpotentiale lagen bei allen Verbindungen um 14.5 mV. Dieser Wert weicht nur wenig von dem bei bivalenten Systemen ohne univalente Zwischenstufe zu erwartenden Wert von 13.9 mV[3] ab.

Die Messung (jeweils gegen die gesättigte Kalomelelektrode) erfolgte mit einem Präzisionsvoltmeter (Typ 35, Firma Knick, Berlin), bzw. sie wurde mit Hilfe einer automatischen Titriervorrichtung[10] von einem Polymetron-Schreiber registriert.

Aus der Form der Kurven und ihrer guten Reproduzierbarkeit und aus den vernünftigen oben aufgeführten Potentialwerten ergibt sich demnach, dass nach der hier geschilderten Methode eine kontinuierliche Titration der in der oxydierten Form instabilen Hydrochinonsulfone und -sulfonamide in einfacher Weise erfolgreich durchführbar ist.

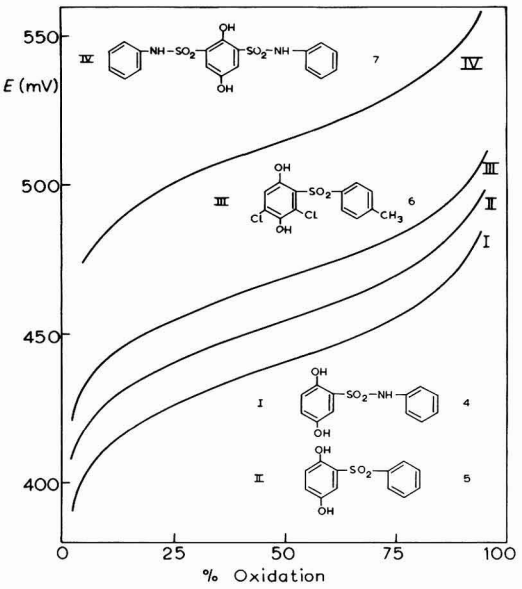

Abb. 1. Potentiometrische Titrationskurven von Hydrochinonsulfonen und -sulfonaniliden in wasserfreiem Eisessig (0.2 *m* an CH_3COONH_4) mit *ca.* 0.05 *N* $Pb(CH_3COO)_4$ in wasserfreiem Eisessig (0.2 *m* an CH_3COONH_4) bei 20°C (gemessen gegen gesättigte Kalomelelektrode); Messelektroden: Graphitelektroden (aus Graphit höchster Reinheit) oder blanke Platinelektroden.

Die Methode ist zu einer quantitativen Bestimmung geeignet.

Fritz-Haber-Institut der Max-Plank-Gesellschaft, Berlin–Dahlem — Georg Manecke, Hans-Jürgen Beyer

Institut für Organische Chemie der Freien Universität, Berlin — Reiner Mölleken

1 R. M. SCRIBNER, *J. Org. Chem.*, 31 (1966) 3671.
2 I. H. SPINNER, W. D. RAPER UND W. METANOMSKI, *Can. J. Chem.*, 41 (1963) 483; I. H. SPINNER, H. P. KASSERA UND U. METANOMSKI, *Can. J. Chem.*, 42 (1964) 554.
3 W. M. CLARK, *Oxidation-Reduction Potentials of Organic Systems*, Williams and Wilkins, Baltimore, 1960.
4 G. MANECKE UND R. MÖLLEKEN, *Makromol. Chem.*, in Vorbereitung.
5 O. HINSBERG, *Ber. Deut. Chem. Ges.*, 27 (1894) 3259.
6 G. MANECKE UND H.-J. BEYER, *Makromol. Chem.*, 116 (1968) 26.
7 O. LITVAY, E. RIESZ UND L. LANDAU, *Chem. Ber.*, 62 (1929) 1867.
8 G. MANECKE UND H. J. PANOCH, *Makromol. Chem.*, 96 (1966) 1.
9 J. B. CONANT UND L. F. FIESER, *J. Am. Chem. Soc.*, 45 (1923) 2194.
10 G. MANECKE, G. WALENTOWITZ, W. STORCK UND H.-J. BEYER, unveröffentlicht.

Eingegangen den 18. Februar 1969

J. Electroanal. Chem., 22 (1969) 152–154

Elsevier Sequoia S.A., Lausanne – Printed in The Netherlands

BOOK REVIEW

Introduction aux Méthodes Electrochimiques, No. 1 of the *Monographies du centre d'actualisation scientifique et technique*, edited by J. Robin, Masson et Cie., Paris, 1967, 360 pages, 65 F.

This volume is a record of the lectures delivered during advanced courses in 1964 and 1965 in the Institut National des Sciences Appliquées de Lyon. They are primarily designed for analysts and it would have been preferable to have used a title which made this clear. In such a collective volume it is almost inevitable that the contributions are uneven. This is most evident in the first half of nine chapters under the general title of *Voltampèrométrie*. This begins with a very elementary account of current–voltages curves, sometimes misleading, as in the equations on p. 29 (where i_0 is not the exchange current) and on p. 36 where the discovery that the system H^+/H_2, is rapid on platinized-platinum is ascribed to Mme. Courtot in 1960. A much better and more systematic introduction to irreversible reactions is, in fact, given in the ninth chapter on corrosion.

The later chapters in this section are more systematic and better referenced. The accounts of fuel cells, corrosion and melts form a useful introduction. In contrast to the melts chapter, the one on non-aqueous solution is rather qualitative and vague; for example, the use of ferrocene and rubidium reference scales is given without any mention of Strehlow or Pleskov.

The second half entitled *Polarographie*, of seven chapters, is more even in standard. Chapters 10, 11 and 15 discuss clearly material which is the staple of many well-established texts on polarography. Chapters 13 and 14 summarize inorganic and organic polarography, respectively, in 5 or 6 pages each, although the former gives more references than any other chapter in the book. Chapter 12 gives a useful elementary account of some of the newer polarographic methods including square-wave and pulse-polarography. This material is not yet so well worked over. The final chapter is on electrochemical applications of electron spin resonance. The origin of ESR spectra and electrochemical applications are briefly but clearly discussed.

From the evidence of this book, the course on which it was based seems to have been of a good standard and particularly useful to modern analytical chemists. However, it seems doubtful in view of the many other books covering similar ground, whether this course should have been given the permanence of print. The answer to this doubt may depend on the language of the reader. English-speaking readers will find most of the material readily available elsewhere. The price is high for a paperback.

Roger Parsons, University of Bristol

Elsevier Sequoia S.A., Lausanne – Printed in The Netherlands

ANNOUNCEMENT

Under the auspices of the Euchem Conference Committee the second conference on

CHEMISTRY OF INTERFACES

is to be held in Lunteren, Netherlands from April 7–10, 1970. This conference will be organized along the lines of the American Gordon Conferences with ample discussion time, a limited audience and a limited number of invited speakers. The main part of the programme will be centered around the subjects:

Electrical aspects and the structure of phase boundaries,
Polymers at interfaces,
Monolayers.

Information and application forms can be obtained from Mr. J. W. Th. Lichtenbelt, Van 't Hoff Laboratory, Sterrenbos 19, Utrecht, Netherlands.

ERRATUM

R. De Levie and J. C. Kreuser, On the measurement of small photo-currents on a dropping mercury electrode, *J. Electroanal. Chem.*, 21 (1969) 221–236.
p. 233, line 9, 45° should be replaced by 450°.

ELECTROANALYTICAL CHEMISTRY AND INTERFACIAL ELECTROCHEMISTRY
Elsevier Sequoia S.A., Lausanne – Printed in The Netherlands

PRELIMINARY NOTE

THE REST POTENTIAL AT INERT ELECTRODES IN CONTACT WITH OXYGEN: PRESSURE DEPENDENCE

It appears that there is discrepancy in the reported facts on the dependence on oxygen partial pressure of the electrode potential at platinum at rest in oxygen saturated solutions. Thus, Hoare[1,2] gives $\partial V/\partial \log p_{O_2} = 15$ mV/decade. Schuldiner and Roe[3], Wroblowa *et al.*,[4] and Damjanovic and Brusic[5] report, however, a value for the same dependence of 60 mV/decade. These data influence *settling* the controversy concerning the nature of the often-observed "0.98 V" rest potential at Pt electrodes in oxygen saturated solutions. Consequently, we wish to report the following new experimental finding.

A platinum electrode pre-reduced either by heating in an inert atmosphere or by potentiostatting at 0.3 V (*vs.* h.e.) establishes in one minute in oxygen-saturated acid solutions a potential close to 0.98 V. Then, $\partial V/\partial \log p_{O_2} = 60$ mV. However, if the same electrode is kept in an oxygen-saturated solution longer, over 10 h, $\partial V/\partial \log p_{O_2}$ becomes < 60 mV. Data of two such experiments are illustrated in Figure 1. Whereas the rest potential at 1 atm oxygen pressure changes only insignificantly during the standing period, the $\partial V/\partial \log p_{O_2}$ dependence changes considerably, tending toward lower values. This behavior is perhaps due to a slow oxidation of the electrode surface and a change of the mechanism(s) by which the 0.98 V potential is controlled. The adsorption of impurities, and the oxidation of residual organics and possible formation of a skeleton of polymers over some parts of the electrode surface, cannot, however, be ruled out as a cause for the observed change in the $\partial V/\partial \log p_{O_2}$ dependence.

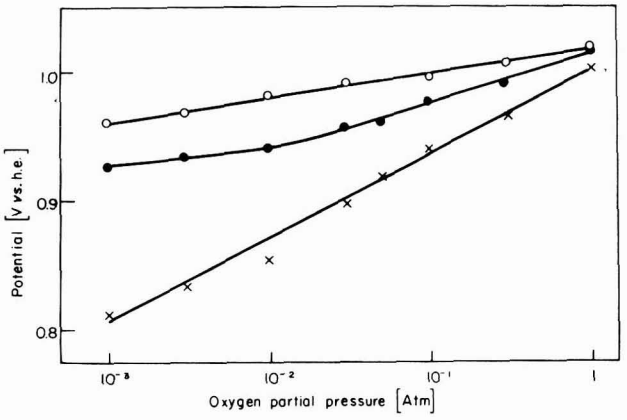

Fig.1. Dependence of rest potential at platinum electrode on partial pressure of oxygen. (X), freshly pre-reduced, oxide-free electrode; (●), after the electrode has been exposed for 14 h to oxygen saturated solution; and (O), after the exposure of 17 h to oxygen saturated solution.

Now, Hoare obtained the $\partial V/\partial \log p_{O_2}$ dependence of 15 mV/decade after keeping platinum electrodes in oxygen-saturated solutions for 24 h, and hence his data have a different relevance from those obtained at freshly pre-reduced electrodes.

The financial support of this work by the U.S. Army Electronics Command, Power Sources Division, Fort Monmouth, N.J., is here acknowledged. We thank Professor J.O'M. Bockris for discussions and reading of the manuscript.

Electrochemistry Laboratory,
University of Pennsylvania,
Philadelphia, Pa. 19104, (U.S.A.)

A. DAMJANOVIC
V. BRUSIĆ

REFERENCES

1 J.P. Hoare, *J. Electrochem. Soc.*, 109 (1962) 858
2 J.P. Hoare, *J. Res. Inst. Catalysis, Hokkaido Univ.*, 16 (1968) 19.
3 S. Schuldiner and M.R. Roe, *J. Electrochem. Soc.*, 110 (1963) 1142.
4 H. Wroblowa, M.L.B. Rao, A. Damjanovic and J.O'M. Bockris, *J. Electroanal. Chem.*, 15 (1967) 139.
5 A. Damjanovic and V. Brusić, *Electrochim. Acta*, 12 (1967) 615.

Received April 18th, 1969.

Vol. 22 No. 1 JOURNAL OF ELECTROANALYTICAL CHEMISTRY AND INTERFACIAL ELECTROCHEMISTRY JULY 1969

CONTENTS

A New Important Encyclopaedic Work of Reference

COMPREHENSIVE CHEMICAL KINETICS

edited by C.H. BAMFORD F.R.S., and C.F.H. TIPPER

The aim of this series is to cover in a critical way the practice and theory of kinetics and the kinetics of inorganic and organic reactions in the gas and condensed phases or at interfaces.
Each chapter is written by an expert in the field so that the series as a whole will serve as a direct source of reference and information over the whole range of kinetics.
The vast amount of material scattered through the literature has never before been gathered together and presented in this accessible form.

Subscribers who place a standing order for the whole series before December 15, 1969 will be entitled to an overall 15% discount.

Elsevier Publishing Company

P.O. BOX 211,
AMSTERDAM, THE NETHERLANDS
402E

Volume 1. The Practice of Kinetics

1. Experimental methods for the study of slow reactions (L. Batt)
2. Experimental methods for the study of fast reactions (D.N. Hague)
3. Experimental methods for the study of heterogeneous reactions (D. Shooter)
4. The detection and estimation of intermediates (R.P. Wayne)
5. The treatment of experimental data (D. Margerison)

7 x 10″, xiii + 450 pages, 32 tables, 161 illus., 1174 lit. refs., 1969, Dfl. 95.00, £10.15.0
SBN 444-40673-5

Volume 2. The Theory of Kinetics

1. Kinetic characterization of complex reaction systems (Z.G. Szabó)
2. Chain reactions (V.N. Kondratiev)
3. Theory of the kinetics of elementary gas phase reactions (R.P. Wayne)
4. Theory of elementary reactions in solution (I.D. Clark and R.P. Wayne)
5. Theory of solid phase kinetics (L.G. Harrison)

7 x 10″, xiii + 462 pages + index, 16 tables, 77 illus., 794 lit. refs., 1969
SBN 444-40674-3

Volume 3. Formation and Decay of Excited Species

1. Effect of low energy radiation (C.S. Burton and W.A. Noyes, Jr.)
2. Effect of high energy radiation (G. Hughes)
3. The chemical production of excited states (T. Carrington and D. Garvin)
4. The transfer of energy between chemical species (A.B. Callear and J.D. Lambert)

7 x 10″, 1969, in preparation
SBN 444-40676-x

The series as a whole will comprise about 25 volumes divided into a number of sections:

Section 1. The practice and theory of kinetics (3 volumes)
Section 2. Decomposition and isomerisation reactions (2 volumes)
Section 3. Inorganic reactions (2 volumes)
Section 4. Organic reactions (6 volumes)
Section 5. Polymerization reactions (2 volumes)
Section 6. Oxidation and combustion reactions (2 volumes)
Section 7. Selected elementary reactions (2 volumes)

Other sections are planned on heterogeneous reactions, solid state reactions, and kinetics and technological processes.